Universitat Politècnica de València
Departamento de Máquinas y Motores Térmicos

DUAL-MODE DUAL-FUEL COMBUSTION: IMPLEMENTATION ON A REAL MEDIUM DUTY ENGINE PLATFORM

Doctoral Thesis

Presented by:
Rafael Lago Sari
Supervised by:
Dr. Antonio García Martínez

València, January 2021

Doctoral Thesis

DUAL-MODE DUAL-FUEL COMBUSTION: IMPLEMENTATION ON A REAL MEDIUM DUTY ENGINE PLATFORM

Presented by: Rafael Lago Sari
Supervised by: Dr. Antonio García Martínez

Examining Board:

President: Prof. Raúl Payri Marín
Secretary: Prof. Jacobo Porteiro Fresco
Examiner: Dr. Christopher Paul Kolodziej

Reviewing Board:

Dr. Christopher Paul Kolodziej
Prof. Juan José Adrover Hernández
Prof. Lambertus Marinus Theodorus Somers

València, January 2021

Abstract

The medium and heavy-duty transport sector was historically challenged by the emissions regulations that were imposed along the years, requiring to step up the research effort aiming at advancing the product development to deliver a normative compliant option at similar price to the owner. Nonetheless, the recent introduction of EUVI normative have required the addition of a complex aftertreatment system, adding new fixed costs to the product as well as operational costs with the urea consumption. This breakthrough was required due to the limitation of the conventional diesel combustion which cannot decouple high NOx emissions and efficiency.

This technological limitation has boosted the investigation on different combustion concepts that could maintain similar efficiency levels than the diesel combustion while controlling the emission formation during the combustion process. Among the different solutions that have appeared along the years, Reactivity Controlled Compression Ignition (RCCI) was demonstrated to have a competitive edge due to its better controllability, high efficiency and low soot and NOx emissions. Despite the benefits, the extension of RCCI to full map operation has presented significant limitations, as excessive pressure gradients at high load and high combustion instability and unburned products at low engine load. Recently, Dual-Mode Dual-Fuel (DMDF) combustion concept was introduced as an attempt of solving the drawbacks of the RCCI combustion while maintaining its advantages. The preliminary results obtained in single cylinder engine (SCE) have evidenced that DMDF can achieves similar efficiency levels than those from conventional diesel combustion while promoting ultra-low levels of soot and NOx. Albeit, the boundary condition requirements are hard to fit in the operating range of commercial air management system as well as drawbacks like excessive HC and CO that still persists from low to medium load, which can be a challenge for the aftertreatment system. Moreover, short-term future regulations will demand a 15 % reduction of CO_2 emissions in 2025 which was proven in the literature to not be easily achieved only by combustion process optimization.

In this sense, this thesis has as general objective the implementation of the DMDF combustion concept in a multi-cylinder engine (MCE) under the restrictions of real applications to realize clean and efficient combustion in the complete map while providing alternatives to reduce the HC and CO concentration and accomplish CO_2 savings.

This objective is accomplished by means of a first extensive experimental calibration procedure aiming to translate the guidelines of the DMDF combustion from the SCE to the MCE while respecting the operating limits of the stock hardware, assessing its impacts on combustion, performance, and emission results under steady and driving cycle conditions. Next, dedicated studies are performed to address the issue related with the excessive concentration of unburned products by means of experimental investigations and numerical simulations, to understand the consequences of using fuels with different reactivity in the stock oxidation catalyst conversion efficiency and its ability in achieving EUVI tailpipe emissions. Finally, CO_2 reduction is explored through fuel modification, investigating both combustion process improvement and well-to-wheel balance as paths to realize CO_2 abatement.

Resumen

Históricamente, el sector del transporte de servicio mediano y pesado ha sido desafiado por las regulaciones de emisiones que se han impuesto a lo largo de los años, lo que requirió intensificar el esfuerzo de investigación con el objetivo de avanzar en el desarrollo tecnológico para ofrecer una opción que cumpla con las normas a un precio similar para el propietario. No obstante, la reciente introducción de la normativa EUVI ha requerido la adición de un complejo sistema de postratamiento, agregando nuevos costes fijos al producto, así como costes operativos con el consumo de urea. Este avance fue necesario debido a la limitación de la combustión diésel convencional que no puede desacoplar las altas emisiones de NOx y la eficiencia.

Esta limitación tecnológica ha impulsado la investigación sobre diferentes conceptos de combustión que podrían mantener niveles de eficiencia similares a los de la combustión diésel controlando la formación de emisiones durante el proceso de combustión. Entre las diferentes soluciones que han ido apareciendo a lo largo de los años, se demostró que la Ignición por Compresión Controlada por Reactividad (RCCI por sus siglas en inglés) tiene una ventaja competitiva debido a su mejor controlabilidad, alta eficiencia y bajas emisiones de hollín y NOx. A pesar de sus beneficios, la extensión de RCCI a la operación de mapa completo ha indicado limitaciones importantes como gradientes de presión excesivos a alta carga, o alta inestabilidad de combustión y productos no quemados a baja carga del motor. Recientemente, se introdujo el concepto de combustión Dual-Mode Dual-Fuel (DMDF) como un intento de resolver los inconvenientes de la combustión RCCI manteniendo sus ventajas. Los resultados preliminares obtenidos en un motor mono cilíndrico (SCE por sus siglas en inglés) han demostrado que el DMDF puede alcanzar niveles de eficiencia similares a los de la combustión diésel convencional al mismo tiempo que favorece niveles ultra bajos de hollín y NOx. Si bien, los requisitos de la condición límite son difíciles de encajar en el rango operativo de sistema de gestión de aire, así como inconvenientes como el exceso de HC y CO que aún persiste en la zona de baja y media

carga, lo que puede ser un desafío para el sistema de postratamiento. Además, las futuras regulaciones a corto plazo exigirán una reducción del 15 % de las emisiones de CO_2 en 2025, reto que la literatura sugiere que no se logrará fácilmente solo mediante la optimización del proceso de combustión.

En este sentido, esta tesis tiene como objetivo general la implementación del concepto de combustión DMDF en un motor multicilindro (MCE por sus siglas en inglés) bajo las restricciones de las aplicaciones reales para realizar una combustión limpia y eficiente en el mapa completo a la vez que brinda alternativas para reducir la concentración de HC y CO y lograr un ahorro de CO_2.

Este objetivo se logra mediante un primer extenso procedimiento de calibración experimental que tiene como objetivo trasladar las pautas de la combustión DMDF del SCE al MCE respetando los límites operativos del hardware original, evaluando su impacto en los resultados de combustión, rendimiento y emisiones en condiciones estacionarias y condiciones de ciclo de conducción. A continuación, se realizan estudios específicos para abordar el problema relacionado con la concentración excesiva de productos no quemados mediante investigaciones experimentales y simulaciones numéricas para comprender las consecuencias del uso de combustibles con diferente reactividad en la eficiencia de conversión del catalizador de oxidación original y su capacidad para lograr emisiones en el escape menores que el límite EUVI. Finalmente, se busca la reducción de CO_2 a través de la modificación del combustible, investigando tanto la mejora del proceso de combustión como el equilibrio entre el ciclo de vida del combustible.

Resum

Històricament, el sector del transport de servei mitjà i pesat ha sigut desafiat per les regulacions d'emissions que s'han imposat al llarg dels anys, la qual cosa va requerir intensificar l'esforç d'investigació amb l'objectiu d'avançar en el desenvolupament tecnològic per a oferir una opció que complisca amb les normes a un preu similar per al propietari. No obstant això, la recent introducció de la normativa EUVI ha requerit l'addició d'un complex sistema de postractament, agregant nous costos fixos al producte, així com costos operatius amb el consum d'urea. Aquest avanç va ser necessari a causa de la limitació de la combustió dièsel convencional que no pot desacoblar les altes emissions de NOx i l'eficiència.

Aquesta limitació tecnològica ha impulsat la investigació sobre diferents conceptes de combustió que podrien mantindre nivells d'eficiència similars als de la combustió dièsel controlant la formació d'emissions durant el procés de combustió. Entre les diferents solucions que han anat apareixent al llarg dels anys, es va demostrar que la Ignició per Compressió Controlada per Reactivitat (RCCI per les seues sigles en anglés) té un avantatge competitiu a causa de la seua millor controlabilitat, alta eficiència i baixes emissions de sutge i NOx. Malgrat els seus beneficis, l'extensió del RCCI a l'operació de mapa complet ha indicat limitacions importants com a gradients de pressió excessius a alta càrrega, o alta inestabilitat de combustió i productes no cremats a baixa càrrega del motor. Recentment, es va introduir el concepte de combustió Dual-Mode Dual-Fuel (DMDF) com un intent de resoldre els inconvenients de la combustió RCCI mantenint els seus avantatges. Els resultats preliminars obtinguts en un motor mono-cilíndric (SCE per les seues sigles en anglés) han demostrat que el DMDF pot aconseguir nivells d'eficiència similars als de la combustió dièsel convencional al mateix temps que afavoreix nivells ultra baixos de sutge i NOx. Si bé, els requisits de la condició límit són difícils d'encaixar en el rang operatiu de sistema de gestió d'aire, així com inconvenients com l'excés de HC i CO que encara persisteix en la zona de baixa i mitja càrrega, la qual cosa pot ser un desafiament per al sistema de postractament. A més, les futures regulacions a curt termini

exigiran una reducció del 15% de les emissions de CO_2 en 2025, repte que la literatura suggereix que no s'aconseguirà fàcilment només mitjançant l'optimització del procés de combustió.

En aquest sentit, aquesta tesi té com a objectiu general la implementació del concepte de combustió DMDF en un motor multi-cilindre (MCE per les seues sigles en anglés) sota les restriccions de les aplicacions reals per a realitzar una combustió neta i eficient en el mapa complet alhora que brinda alternatives per a reduir la concentració de HC i CO i aconseguir un estalvi de CO_2.

Aquest objectiu s'aconsegueix mitjançant un primer extens procediment de calibratge experimental que té com a objectiu traslladar les pautes de la combustió DMDF del SCE al MCE respectant els límits operatius del motor original, avaluant el seu impacte en els resultats de combustió, rendiment i emissions en condicions estacionàries i condicions de cicle de conducció. A continuació, es realitzen estudis específics per a abordar el problema relacionat amb la concentració excessiva de productes no cremats mitjançant investigacions experimentals i simulacions numèriques per a comprendre les conseqüències de l'ús de combustibles amb diferent reactivitat en l'eficiència de conversió del catalitzador d'oxidació original i la seua capacitat per a aconseguir emissions al tub d'escapament menors que el límit EUVI. Finalment, es busca la reducció de CO2 a través de la modificació del combustible, investigant tant la millora del procés de combustió com l'equilibri entre el cicle de vida del combustible.

A Bianca
A mis padres

Agradecimientos - Acknowledgements

This work was done with the aid and support from several people whose I would like to express my gratitude.

First, I would like to thank Francisco Payri and the director of CMT-Motores Térmicos *José María Desantes* for the opportunity of joining this outstanding research group and providing me the tools to perform my investigation along these years. I would like to be grateful particularly to *Jesús Benajes* for welcoming me in the combustion group and supporting me during this investigation.

Second, to my advisor and friend *Antonio García*. I am certainly learned innumerous lessons during these years together. I would like to express my gratitude for the formal education, timeless discussions, and teachings in the engine area. But, also, to the friendship, the personal help and support during the tough times. I am really lucky to have found you in my path. Thank you for the professional and personal growth that you provide me.

I would like to also express my gratitude to the combustion department, especially to *José Vicente Pastor, José María García*, *Javier López*, *Jaime Martín*, *Santiago Molina, Ricardo Novella* y *Pablo Olmeda* for their support and help along these years. My special thanks to *Javier Monsalve Serrano* that was always available to me, one of the major responsible in the development of this work.

My acknowledgement also to my office colleagues *David Villalta, Santiago Martinez Boggio, Álvaro Fogués Robles y Maria Gabriela Guzmán.* You guys always stand by my side, helping in all moments. Thank you for the good times together working and discussing as well as enjoying the time. I would like also to thanks my colleagues from the combustion group which contributed for the development of the work and made the life easy with the talks and time spent together during this journey *Vicent Boronat, Leonardo*

Pachano, *Daniel Estepa y Alba Andreína.* Your help has been fundamental to this work.

I would like also to thank all the technical group *Vicente Esteve, Daniel Lérida, José Galvez, Toni Peris and Ivan Garrido.* My most sincere gratitude to *Gabriel Alcantarilla* for all the time spent together in front of the engine, solving issues and measuring points. Thank you for your talks and for easing the path. My many thanks also to *Amparo Cutillas, Juan Antonio Yustas*, *Norma Molina*, *José Enrique del Rey*, *Omar Huerta* and to the administrative department for opening their door as always as I needed.

My gratitude to Aramco Overseas® and Volvo Group Trucks Technology® for funding the work in this thesis. Thanks to *Patrick Gaillard* and *Oliver Poussin* for following closely the different projects that we have developed together during all these years. It was a pleasure to be part of this investigation together with you.

I would like to express my gratitude to the Institute for Combustion Engines of the Lund University for welcoming me in their laboratories and giving me all the support during my research internship. Especially, I sincerely appreciate the advices of *Dr. Martin Tuner* as well as the reception and technical conversations from *Dr. Öivind Andersson, Dr. Per Tunestål, Dr. Sebastian Verhelstand* and *Dr Marcus Lundgren* during my stay in Lund. Thank you also to *Nika Alehmadi* and *Amir Amiz* for the reception, friendship and technical discussions.

I would like also to thanks my friends that have been supporting me in this time. Thank you for the talks, the time spent together, the barbecues and the company, you are amazing. I would like to thank specially *Felipe De Vargas Lewiski* for being so supportive during these years and for being a friend, best man and for sharing all these experiences together.

My last words in this section were saved for my family. During this academic journey their support and unconditional love have kept me in the path. My eternal gratitude to my parents, *Valnei and Ivanilde*, you are my

heroes and examples. I would like to thank my sister, *Vanessa*, to make life easier connecting the worlds in our family and being so dedicated and worried with me during the life. Words are not enough to thank my wife *Bianca.* Thank you for always believing in me and supporting me, unconditionally and undoubtedly. This work is as yours as is mine. I love you.

This doctoral thesis has been partially supported Spanish ministry of science innovation and universities under the grant ‘‘Ayudas para contratos predoctorales para la formación de doctores” (PRE2018-085043).

Table of Contents

Index of Figures

Index of Tables

Nomenclature

Latin

A/F - Air Fuel Ratio

C - Carbon

C_p - Specific heat capacity at constant pressure

CO - Carbon Monoxide

CO_2 - Carbon Dioxide

C_3H_6 - Propylene

C_2H_4 - Ethylene

C_2H_6 - Ethane

1,3-C_4H_6 - 1,3-Butadiene

C_6H_6 - Benzene

C_7H_8 -Toluene

C_7H_{16} -Heptane

C_8H_{18} - Octane

m - Mass

$\dot{m}$ - Mass flow

h - Hours

$\bar{h}$ - Enthalpy

H - Unimolecular Hydrogen

HC - Hydrocarbon

H_2O - Water

N_2 – Nitrogen

NO - Nitrogen monoxide

NO_2 - Nitrogen dioxide

NOx - Nitrogen oxides (NO and NO2)

O_2 - Oxygen

OMEx - Oxymethylene Dimethyl Ethers

OH - Hydroxyl radical

p - Pressure

Qw - Heat transfer to the walls

t - Time

T - Temperature

u - Internal energy

V - Volume

X - Molar fraction

Y - Mass Fraction

Z - Zeolite

Greck

γ - Density

Δ - Variation

η – Efficiency

μ – Micro

ρ – Density

ϕ - Equivalence Ratio

Superscripts

$^{\circ}$ – Standard conditions

Subscripts

a - relative to air

b - relative to brake power

bb - Relative to blow-by

cyl - Relative to in-cylinder conditions

exh - relative to exhaust conditions

evap - Relative to evaporation conditions

f - relative to fuel

g - grams

i - relative to indicated power

in - relative to intake conditions

inj - relative to injection

out - relative to outlet conditions

O_2 - relative to oxygen

Initials and Acronyms

ASC - Ammonia Slip Catalyst

ATS - Aftertreatment System

BMEP - Brake Mean Effective Pressure

BSFC - Brake Specific Fuel Consumption

CA50 - Crank Angle at 50% mass fraction burned

CAD - Crank angle degree

CFD - Computational Fluid Dynamics

CI - Compression Ignition

CDC - Conventional Diesel Combustion

COV - Covariance

CR - Compression Ratio

D - Diesel

DAC - Direct Air Capture

CFR - Cooperative Fuel Research

CN - Cetane Number

DF- Diesel Fuel

DI - Direct-Injection

DMDF- Dual-Mode Dual-Fuel

DOC - Diesel Oxidation Catalyst

DPF - Diesel Particulate Filter

Ea - Energy of activation

ECU - Electronic Control Unity

EGR - Exhaust Gases Recirculation

ES - Engine Speed

EU - European

FCEC - Fuel Consumption Equivalent Cycle

FID - Flame Ionization Detector

FIS - Fuel Injection System

FSN - Filter Smoke Number

FTIR - Fourier Transformed Infrared Spectroscopy

G - Gasoline

GIE - Gross Indicated Efficiency

GF - Gasoline Fraction

GHG - Greenhouse gases

HCCI - Homogeneous Charge Compression Ignition

HP - High Pressure

HRF - High Reactivity Fuel

HRR - Heat Release Rate

HTHR - High Temperature Heat Release

ICE - Internal Combustion Engines

IMEP - Indicated Mean Effective Pressure

ISC - In-Service Conformity

ISFC - Indicated Specific Fuel Consumption

J - Joule

Kde - Kernel Density Estimation

K - Kelvin

L - Liters

LCA - Life Cycle Analysis

LRF - Low Reactivity Fuel

LHV - Lower Heating Value

LP - Low Pressure

LTC - Low Temperature Combustion

LTHR - Low Temperature Heat Release

MFB - Mass Fraction Burned

MCE - Multi-Cylinder Engine

MON - Motor Octane Number

NDA - Non – Disclosure Agreement

NTC - Negative Temperature Coefficient

NVH - Noise Vibration and Harshness

OEM - Original Equipment Manufacturers

PEF - Pre-Exponential factor

PFI - Port Fuel Injection

PLIF - Planar Laser Induced Fluorescence

PM - Particulate matter

PMEP - Pumping Mean Effective Pressure

PN - Particulate number

PPC - Partially Premixed Combustion

PPCI - Partially Premixed Compression Ignition

PRR - Pressure Rise Rate

PRR - Primary Reference Fuel

PT - Pressure Temperature

RCCI - Reactivity Controlled Compression Ignition

RWGS - Reverse Water-Gas Shift

RON - Research Octane Number

S - Sensitivity

SCE - Single Cylinder Engine

SCR - Selective Reduction Catalysts

SET - Supplementary Engine Test

SI - Spark Ignition

SoI - Start of Injection

PDF - Probability Density Function

TCO - Total Cost of Ownership

TDC - Top Dead Center

ToI - Time of Injection

TRF- Toluene Reference Fuel

VGT - Variable Geometry Turbine

TRL - Time readiness levels

TTW - Tank - to - Wheel

WHSC - World Harmonized Stationary Cycle

WHTC - World Harmonized Transient Cycle

WHVC - World Harmonized Vehicle Cycle

WTW - Well-To-Wheel

Chapter 1

Introduction

Content

1.1 Introduction

This first chapter intends to draw the actual scenario within which the present work is found. Firstly, an overview of the current energy sources applied for transportation followed by a contextualization of the different sources of CO_2 in the actual economy are presented, elucidating the relevance of this sector. Followed, the recent advances on combustion process are discussed revealing the advantages, disadvantages, and potential of each concept. Finally, the organization of the document is described, providing a summary of the different studies developed during this thesis.

1.2 Energy matrix and transport sector relevance

Since the development of the firsts engines concepts relying on internal combustion during the 1870s, their importance has readily grown becoming a key device in the today's society. Indeed, they stand as the most used energy source for road and goods transportation as depicted in Figure 1.1, which is a graphical representation of the data provided by [1]. As it is shown, most of the energy that is used on the transport relies on converting oil derived fuel to propel the powertrains. Additional energy sources, such as biofuels and electricity, still play a secondary role considering the whole energy matrix.

Internal combustion engines (ICE) have been the most used power source in road and maritime transportation. This is justified by the operation flexibility and the wide range of primary energy sources that can be used by them [2]. Different concepts were successfully developed, but undoubtedly, the ones developed by Nikolaus Otto and Rudolf Diesel were the responsible for the definitive success of these devices. While the first conceptualized a constant pressure combustion cycle, the second relied on the assumption of an ideal constant volume combustion process to obtain the maximum

efficiency of the engine. These ideal cycles are the basis of the well-known spark ignition engines and diesel engines [3].

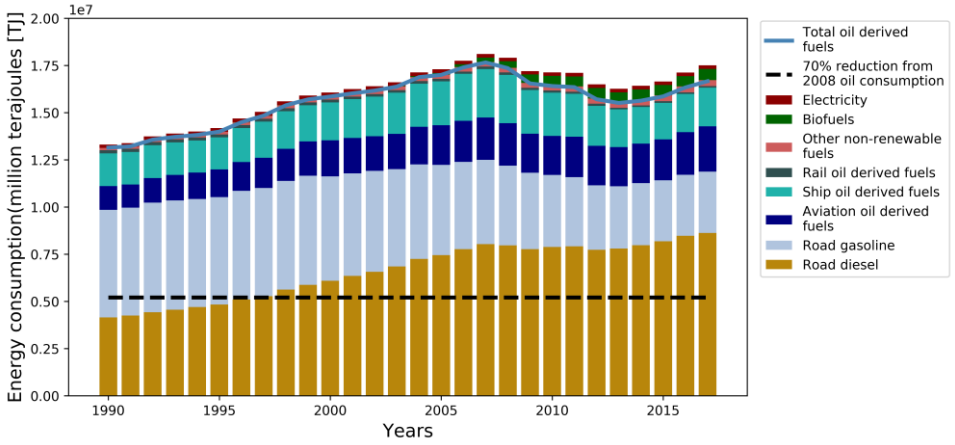

Figure 1.1. Energy consumption in transport considering the most significant energy sources available [1].

For several years, ICEs were carelessly used, regardless of their exhaust pollutants. But early in 1896, the scientific society would become aware of the risks and concerns that should be accounted for regarding greenhouse gases (GHG) emissions in the combustion process. The findings of Svante Arrhenius [4] stablished a proportional relation between the CO_2 concentration in the atmosphere and the increase of the average temperature. Based on this statement, the accelerated growth of vehicles sales worldwide that has proceeded in the 20th century, became a subject of attention due to direct increase in the CO_2 emissions it caused, as a function of the low efficiency of the current engines. Moreover, different issues start to be correlated with those pollutants emitted by internal combustion engines as nitrogen oxides (NOx), particulate matter (PM) and the particulate number (PN), unburned hydrocarbons (HC), and carbon monoxide (CO). Nitrogen oxides are known to form ground level ozone (which can worsen respiratory issues as bronchitis, emphysema, and asthma), acid rain and impact the water and soil quality [5]. Particulate matter is also a hazardous pollutant as it

affects both respiratory and cardiovascular systems facilitating lung cancer [6]. Both CO and HC are also harmful for both health and environment as they may cause coma, heart failure (long exposure to CO), cancer and photochemical smog (HC) [7].

In this sense, later, in 1992, the first emission regulation appeared pushing the original equipment manufacturers (OEMs) to obtain lower emissions levels. As a derivative effect, this action boosted the research with the aim of understanding the combustion process and how to optimize the current engines. Each normative phase brought relevant advances in the combustion process and peripherals of the engine. In which regards the diesel engines, the early normative phases introduced the common rail injection system, allowing to increase to thousands of bar the diesel injection pressure, improving the mixture and combustion process, resulting in consequent benefits on efficiency and emissions [8][9]. Additionally, the so called aftertreatment systems were also established and applied to the vehicle powertrain to reduce the final emissions [10][11]. These ATS system are composed by a diesel oxidation catalyst (DOC) that oxidizes both HC and CO and assist the formation of NO_2. This specie is the responsible for the passive regeneration of the diesel particulate filter (DPF) which filters the particulate matter prior reaching the environment. Finally, a selective catalytic reduction (SCR) system reduces the NOx emissions by means of a chemical reaction with urea. However, these systems promoted an increase in the vehicle cost and introduced maintenance and utilization costs as those from urea consumption [12]. These advances were fundamental to fulfil regulations that became more stringent during the years. From the first values of the European regulation (EU) EU I to the nowadays regulation, the emissions levels were reduced by factors higher than 36 in the case of PM and 20 for NOx emissions. The evolution of the steady-state targets for each pollutant is presented in Figure 1.2. It is also interesting to note that from EUII, transient normative cycles were introduced in the legislation with specific emission requirements.

Even with improvements on efficiency and the reduction of pollutant emissions, the global scenario for CO_2 and consequent global temperature increase was not improved as it was thought it would be. Figure 1.3 illustrates the global average near surface temperature evolution since the first measurements compared to the preindustrial age considering different measurement stations [13]. As it can be seen, the recent period from 2000 up to 2018 presented an increase from 0.6 °C to 1.14 °C approximately. This temperature increase is not only attributed to the transport sector itself, but to the set of the individual process that produce CO_2, some of them intangibles.

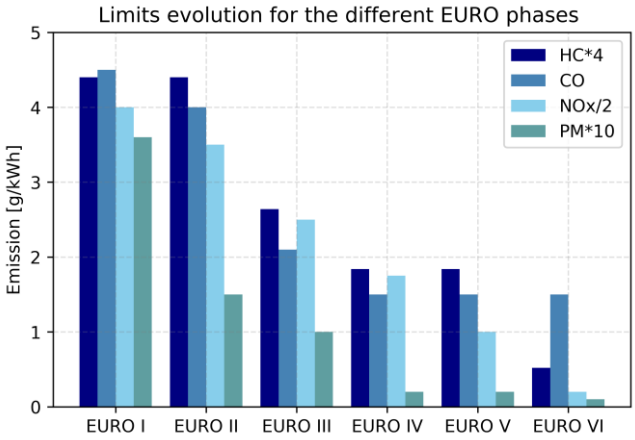

Figure 1.2. Evolution of EURO normative since its introduction for steady state homologation for medium and heavy-duty vehicles.

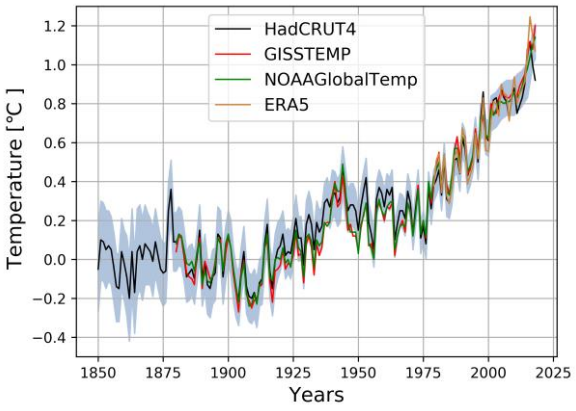

Figure 1.3. Average global temperature variation along the years from different measurement locations.

Regarding Europe, the efforts in reducing the CO_2 footprint were being effective up to 2014 as it is depicted in Figure 1.4 (a). The period from 1990 to 2014 presented a reduction rounding 23% in the total CO_2 production, which seems to be a direct impact of the CO_2 reduction in the energy sector [14]. Nonetheless, starting from 2014, the CO_2 levels started to increase again, turning on the red flag on the policies that had been employed until this moment. The main question that should be raised is: what is happening in the energy sector that could be causing this increase? Figure 1.4 (b) allows to identify some key points to understand this phenomenon. From 2007, both energy industry and transport sector have experienced a drastic decrease in the CO_2 production which can be correlated to the financial crisis that started that year and was followed by a recession period [15]. From 2012, both transport and construction sector started to accelerate again, reverting its downtrend in CO_2 emissions.

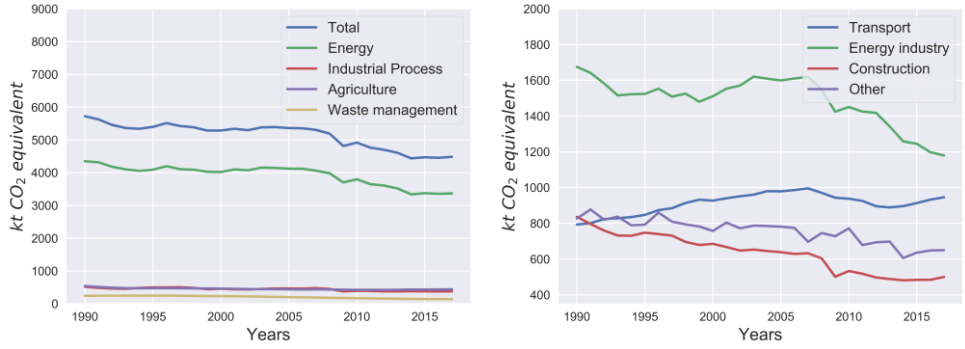

(a) (b)

Figure 1.4. Graphical representation of the total equivalent CO_2 from (a) the different macro sectors of economy and (b) the most significant subsectors that composes the energy sector.

Contrary to the construction sector that represents a small percentage of the total CO_2 from the energy sector, in 2017 transportation represented more than 30% of the CO_2 emitted in the atmosphere from the energy sector, comprehending land, air and marine transportation. Its relevance on the greenhouse gases production is clear, which justifies the stringent policies that will be introduced as the targets for CO_2 reduction to 2025 (15%) and 2030 (30%) [16]. In this sense, the understanding of the major CO_2 contributors in this sector is fundamental to develop technologies and measures to reduce the GHG footprint. Figure 1.5 illustrates the most relevant transport media in terms of CO_2 production. As shown, both cars and trucks stand to more than 80% of the total CO_2 production. While alternatives as fleet electrification coupled to renewable energy generation are prone to provide a significant reduction on CO_2 emissions for cars and light duty trucks [17], the direct use of electrification on heavy duty transportation is a difficult path to tread, as factors as charging times, truck utilization, battery size and total cost of ownership drive the purchase decisions [18].

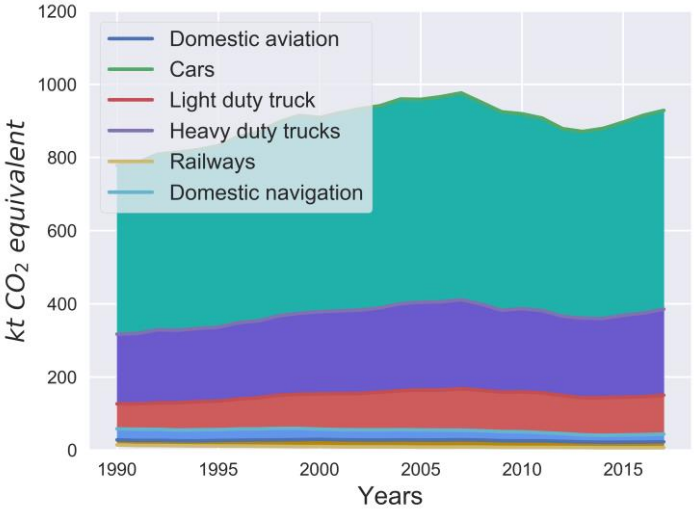

Figure 1.5. Share of the total equivalent CO_2 in the transportation sector by each one of the transport types.

Therefore, research on developing advanced combustion processes, that can provide CO_2 savings as well as alternatives to introduce renewable fuels on heavy duty transportation, is urgent. At the same time, the former normative emissions (NOx, soot, HC and CO) are still a challenge to be addressed to deliver a cleaner and cheaper powertrain option to the consumer. Recent advances have introduced the so-called low temperature combustion (LTC) process as a path to realize improvements in conversion efficiency while providing ultra-low-NOx and soot emissions [19]. Among the different combustion approaches, Reactivity-Controlled Compression Ignition (RCCI) has presented competitive advantages, like active control of combustion phasing through tailoring the in-cylinder reactivity, and a wider operating range compared to most of the LTC concepts [20][21]. Despite these benefits, the extension of the concept to real applications has been a challenge due to high pressure gradients at high load, combustion instability and excessive unburned products at low load operation [22][23]. Different attempts have been made to extend the operating limits of the RCCI combustion towards the full map calibration. The Dual-mode Dual-Fuel (DMDF) combustion has

emerged as a potential solution. Single cylinder engine (SCE) results demonstrated that it allows to overcome the major drawbacks of RCCI by modifying the gasoline fraction (GF) and switching the combustion strategy according to the engine load requirements while providing ultra-low NOx and soot in the complete map [24].

In spite of the promising SCE results, the extension of the concept to real platforms often introduces additional phenomena to consider as the air management system and engine safety operation that may prevent the replication of the settings from SCE engine. Moreover, the concept stills incorporate the fully premixed combustion at low and medium engine load, which provides excessive amounts of engine-out HC and CO with very low exhaust temperatures [25]. Last, but not least, previous results have demonstrated that the CO_2 reduction are still far from those of short-term horizons as H2025.

Having the aforementioned points in consideration, the work proposed in this thesis aims to extend the DMDF combustion process to a multi-cylinder engine targeting higher time readiness levels (TRLs) while dealing with the different challenges that should be faced in the process. Moreover, it also intends to assess the impact of the concept on the aftertreatment system and to propose new fuel solutions able to deliver well-to-wheel CO_2 reductions. In this sense, a deep characterization of the concept concerning current and future normative can be done. To do this, an experimental-numerical approach is proposed, combining multi-cylinder engine testing (with its stock hardware) coupled to 0-D/1-D simulations.

1.3 Document content and structure

This thesis is structured in seven chapters starting from this introduction chapter. The main contents of each subsequent chapters can be outlined as follows:

Chapter 2 details the literature review addressing the most relevant advancements considering novel combustion strategies for internal combustion engines as well as their benefits, drawbacks, and challenges. This first discussion will enlighten which should be the gaps to be filled by this research, justifying it, and defining the main objectives to be pursued.

Chapter 3 presents the experimental and numerical tools that were used. First, the multi-cylinder engine and its subsystems are discussed in detail. Next, the experimental facility in which the engine was installed is described, evidencing the most relevant measurement devices, instrumentation, and test cell characteristics. At the numerical side, both 0-D and 1-D numerical fundamentals are presented, including a description of the most relevant aspects of each software. To conclude, both experimental calibration and numerical evaluation methodologies are presented in detail.

Chapter 4 describes the implementation of the calibration methodology proposed in chapter 3 to obtain optimized operating maps in terms of fuel consumption, respecting a set of emissions constraints. These open loop maps describe the engine settings to implement the DMDF concept on a multi-cylinder engine application. In a second step, the steady-state maps are used as input data during driving cycle simulations addressing representative driving conditions and payloads. In this sense, the results from the proposed calibration can be also compared directly with those from transient normative. Finally, the main drawbacks of the concept are identified, and the potential solutions are the basis of the next chapters.

Chapter 5 aims to assess the impact of the different engine-out pollutants on the performance of the stock aftertreatment system. First, the diesel oxidation catalyst is evaluated in terms of conversion efficiency for both HC and CO under steady and transient conditions. Moreover, the chapter discuss the application of hydrocarbon speciation to understand the impact of having two different fuels on the engine out hydrocarbon composition. Still, the first part of chapter 5 presents a detailed investigation of the DPF accumulation and regeneration processes (passive and active)

under steady DMDF conditions. Next, both DOC and DPF numerical models are calibrated based on the experimental results and driving cycle simulations are employed to assess the potential of having EUVI tailpipe emissions for these pollutants.

Chapter 6 proposes the modification of both low reactivity and high reactivity fuels as an attempt to address short term future fuels aiming at CO_2 reduction and future legislation fulfillment. The first part of the chapter presents a detailed analysis on the research octane number and motor octane number influence on the combustion, performance, and emissions by means of experimental and numerical assessment. The optimum fuel is then selected through a merit function approach based on an eight points-based driving cycle. In the second part, the evaluation focuses on assessing advanced high reactivity fuels with lower well-to-wheel CO_2 footprint and lower soot production as an alternative to realize cleaner and efficient operation compared to the previous diesel-gasoline calibration. The select fuel is then combined with that from the low reactivity fuel evaluation and a new calibration is proposed and evaluated in the same driving cycles than that presented in chapter 4.

Chapter 7 summarizes the contributions of the investigation and draws the most significant conclusions of this work. Moreover, enhancements and additional investigations for this topic are proposed as future works.

Figure 1.6 depicts the argument line that was followed from the thesis definition to the conclusions.

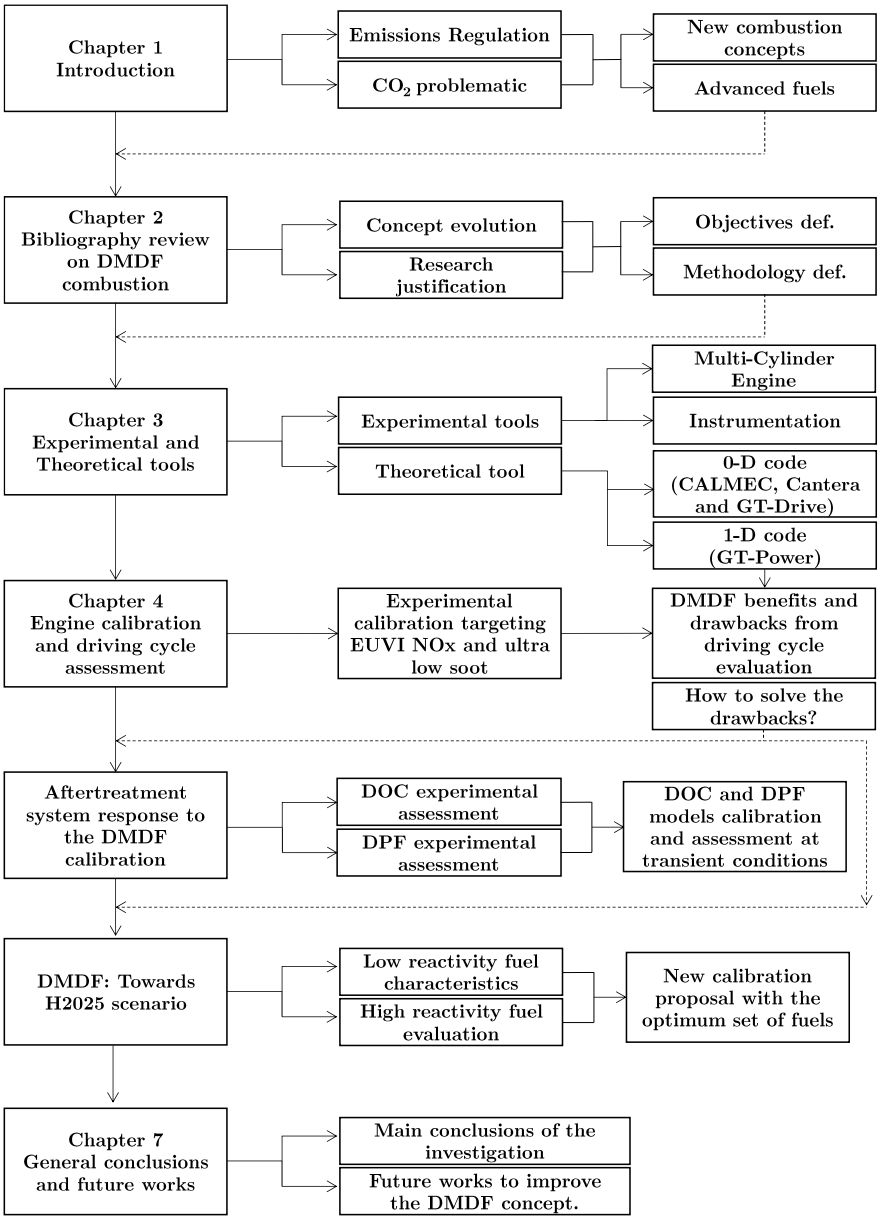

Figure 1.6. Graphical representation of the argument line followed in the investigation.

1.4 Bibliography

[1] Statistical Office of the European Union (Eurostat). "Energy statistics-Energy balances." Available in https://www.iea.org/subscribe-to-data-services/world-energy-balances-and-statistics, accessed in June, 2020.

[2] Kalghatgi, G. "Is it really the end of internal combustion engines and petroleum in transport?" *Applied Energy*, Vol. 225, pp. 965-974, 2018.

[3] Heywood J B. "Internal Combustion Engine Fundamentals". McGraw-Hill, 2018, Second edition.

[4] Arrhenius, S. "On the influence of carbonic acid in the air upon the temperature of the ground". *Philosophical magazine and journal of science*, Vol. 41, pp. 237–276, 1896.

[5] Environmental Protection Agency. "Nitrogen Oxides (NOx), Why and How They Are Controlled". *Technical report*, 1999.

[6] World health organization. "Health-effects-of-particulate-matter". Available in http://www.euro.who.int/___data/assets/pdf_file/0006/189051/Health-effects-of-particulate-matter-final-Eng.pdf, accessed in June, 2020.

[7] Ioannis M., Elisavet S., Agathangelos S., Eugenia B. "Environmental and Health Impacts of Air Pollution: A Review". *Frontiers in Public Health*, Vol. 8, 2020.

[8] Yamaki Y., Mori K, Kamikubo H, Kohketsu S, Mori K, Kato T. "Application of Common Rail Fuel Injection System to a Heavy Duty Diesel Engine". *SAE Technical Paper,* n° 942294, 1996.

[9] Verlag Des Verein Deutscher Ingenieure GmbH. "Common-Rail Injection System for Di-Diesel Engines". *SAE Technical Paper,* n° 967009, 1996.

[10] Russell A, Epling W S. "Diesel Oxidation Catalysts". *Catalysis Reviews: Science and Engineering*. Vol. 53, pp. 337-423, 2011.

[11] Hori M., Oguchi M. "Feasibility Study of Urea SCR Systems on Heavy Duty Commercial Vehicles". *SAE Technical paper*, n° 2004-01-1944, 2004.

[12] Posada F., Chambliss S. and Blumberg K. "Costs of emission reduction technologies for heavy-duty diesel vehicles". *ICCT White paper*, 2016.

[13] European Environment Agency. "Global average near surface temperatures relative to the pre-industrial period". June, 2019. Available at https://www.eea.europa.eu/data-and-maps/daviz/global-average-air-temperature-anomalies-5#tab-dashboard-02, accessed in June, 2020.

[14] European Environment Agency. "EEA greenhouse gas-data viewer". Available at https://www.eea.europa.eu/data-and-maps/data/data-viewers/greenhouse-gases-viewer , accessed in June, 2020.

[15] Sadorsky P. "Energy Related CO2 Emissions before and after the Financial Crisis". *Sustainability*, Vol. 12, 2020.

[16] European union. Reducing CO2 emissions from heavy-duty vehicles Available at https://ec.europa.eu/clima/policies/transport/vehicles/heavy_en, accessed in June 2020.

[17] Luján J.M., García A., Monsalve-Serrano J., Martínez-Boggio S. "Effectiveness of hybrid powertrains to reduce the fuel consumption and NOx emissions of a Euro 6d-temp diesel engine under real-life driving conditions". *Energy Conversion and Management*, Vol. 199, 2019.

[18] U.S department of energy. "Medium- and Heavy-Duty Vehicle Electrification: An Assessment of Technology and Knowledge Gaps". December, 2019, available at https://info.ornl.gov/sites/publications/Files/Pub136575.pdf.

[19] Pachiannan T., Zhong W, Rajkumar S, He Z, Leng X, Wang Q. "A literature review of fuel effects on performance and emission characteristics of low-temperature combustion strategies". *Applied Energy*, Vol. 251, 2019.

[20] Kokjohn S L, Hanson R M, Splitter D A, Reitz R D. "Fuel reactivity-controlled compression ignition (RCCI): a pathway to controlled high-efficiency clean combustion". *International Journal of Engine Research*, Vol. 12, pp. 209-226, 2011.

[21] Benajes J, Molina S, García A, Monsalve-Serrano J. "Effects of direct injection timing and blending ratio on RCCI combustion with different low reactivity fuels". *Energy Conversion and Management*, Vol. 99, pp 193-209, 2015.

[22] Reitz, R.D., Duraisamy, F. Review of high efficiency and clean reactivity-controlled compression ignition (RCCI) combustion in internal combustion engines. *Progress in Energy and Combustion Science*. Vol. 46, pp. 12-71, 2014.

[23] Benajes J, García A, Monsalve-Serrano J, Villalta D. Exploring the limits of the RCCI combustion concept in a light-duty diesel engine and the influence of the direct-injected fuel properties. *Energy Conversion and Management*, Vol. 157, pp. 277-287, 2018.

[24] Benajes, J., García, A., Monsalve-Serrano, J., Boronat, V. "Dual-Fuel Combustion for Future Clean and Efficient Compression Ignition Engines". *Applied Sciences*, Vol. 7, 2017.

[25] Benajes J, García A, Monsalve-Serrano J, Boronat V. "Achieving clean and efficient engine operation up to full load by combining optimized RCCI and dual-fuel diesel-gasoline combustion strategies". *Energy Conversion and Management*, Vol. 136, pp 142-151, 2017.

Chapter 2

Alternative combustion modes for medium duty applications

Content

2.1 Introduction

This second chapter intends to set the fundamentals of the research scope by evidencing the different challenges that have been faced during the last years in which regards medium duty powertrains. Moreover, it also aims to establish a detailed description of the research approach.

To accomplish this, a comprehensive literature review is presented, addressing the issues that are currently faced by conventional diesel combustion (CDC). Next, some of the most promising alternative combustion concepts that have been proposed to tackle the CDC issues are discussed, enlightening their advantages and drawbacks. Moreover, the implications related to the extension of these concepts to real applications are also highlighted. This justifies the introduction of new combustion concepts to be able to extend the benefits of LTC combustion while covering the full engine map. Such characteristics are fully addressed by the Dual-Mode Dual-Fuel (DMDF) combustion concept, which is then described in detail, allowing to emphasize its governing parameters, advantages and the most critical drawbacks that are still needed to be solved.

Lastly, the chapter is closed by establishing the thesis approach, comprehending the motivation of the study, the detailed objectives of the thesis and a general description of the methodology that will be employed to achieve the proposed objectives.

2.2 Problematic of conventional diesel combustion

Conventional diesel combustion can be phenomenologically described as a sequence of processes from the fuel injection at the end of compression stroke to the well-controlled diffusion combustion during the expansion stroke. Briefly, the injection process takes place on a high-density flow, originated by the compression of the fresh air plus residuals during the

compression stroke [1]. The liquid fuel is injected with high velocity into this environment to allow a proper spray penetration [2]. During this injection process a variety of simultaneous phenomena can be found, like gas-liquid phase interaction [3], spray atomization [4], evaporation [5][6], and droplet-wall interaction [7]. The evolution of the mixing process coupled to the high pressure and temperatures inside of the combustion chamber enables the spontaneous ignition of the mixture, burning part of the already premixed fuel [8]. The period from the start of the injection process to the ignition of the mixture is defined as the ignition delay and generally last a few crank angle degrees. Once the combustion is stablished, the fuel continues to be injected into a more reactive environment, reducing the vaporization and ignition delay time. This sequence of steps is generally known as the mixing-controlled part of the diesel combustion or, also, the diffusive part once the fuel and air must diffuse into each other to realize flammable mixtures [9]. Dec [10] has proposed the most accepted conceptual description of the diesel combustion, defining characteristics zone in terms of the fuel state, flame, and pollutant formation. His well-known conceptual description is presented in Figure 2.1.

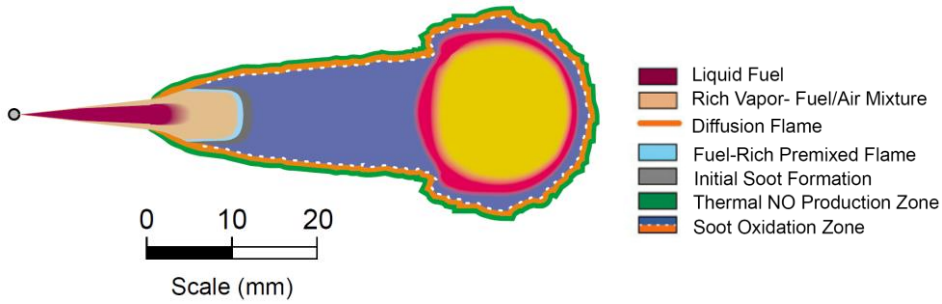

Figure 2.1. Conceptual description of DI diesel combustion during the mixing-controlled burn phase illustrating the different zones and process that occurs in the diffusive combustion. Adapted from [10].

As it can be observed, once the combustion is stablished, the injected fuel is progressively vaporized and mixed by diffusion from the rich fuel zone near to the spray to the leaner mixture near to the thin reaction sheet. This

rich zone is prone to agglomerate polycyclic aromatic compounds and therefore, initiate the soot formation [11]. In the outer side of the flame, the high temperature with the excess oxygen and nitrogen environment give space to the thermal NOx formation mechanism which consists of the decomposition of N_2 by unimolecular oxygen and its subsequent reactions, producing nitrogen oxides [12].

As discussed in Chapter 1, both pollutants are actual concerns due to the diversity of issues that may be caused by them. Despite the intensive research on reducing the conventional diesel combustion hazardous products, it was concluded that soot and NOx emissions coexists and strategies to reduce one of them penalizes the other, which is called the NOx-soot trade off [13][14]. In this sense, the technological answer to the current normative was the introduction of aftertreatment systems, to reduce the emissions levels after leaving the combustion chamber. Nonetheless, these devices have increased the vehicle price and the total cost of ownership (TCO) [15].

This scenario has supported the development of new combustion concepts, aiming at the active reduction of the combustion pollutants while maintaining similar efficiency levels than those found on conventional diesel combustion. The next section provides a brief description of the recent advances on the alternative combustion field which can promote the aforementioned benefits. This discussion will act as an argument line on which the objectives of the thesis will be defined.

2.3 Potential of low temperature combustion strategies

This subsection intends to describe some of the most relevant low temperature combustion approaches that have been developed along the years. As discussed, these combustion concepts aim to mitigate both NOx and soot emissions by means of avoiding the trade-off between them. This means that they should be able to operate at leaner mixtures than those

found at CDC (to avoid the soot formation) and with high levels of charge dilution to decrease the in-cylinder temperatures (mitigate NOx). Figure 2.2 illustrate the conventional operation zone of some of these concepts compared to the conventional diesel combustion on a Φ-T diagram based on the work performed by Neely et al. [16].

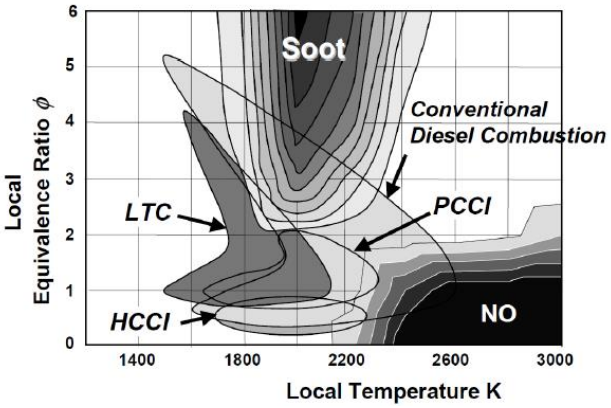

Figure 2.2. NO and soot formation zones as function of the local equivalence ratio and local temperature with the operating zone illustration of conventional diesel combustion, LTC, PCCI and HCCI. Adapted from [16].

Two different low temperature strategies have been proposed in the literature, being classified as: mixing controlled low temperature combustion [17] and premixed low temperature combustion [18]. The difference between them can be evidenced from Figure 2.2. It can be observed that the mixing controlled low temperature combustion (defined as LTC in the figure) operates in a narrow range regarding both local temperature and equivalence ratio compared to the conventional diesel combustion. This allows to avoid, almost completely, the soot and NOx formation islands [19]. Nonetheless, the shape of the Φ-T island in which it occurs still presents the characteristics of the diesel combustion [20]. By contrast, premixed low temperature combustion relies on early fuel injections, allowing to obtain a more homogeneous fuel mixing, avoiding rich zones which allows to mitigate the

soot formation. Some of the most conventional premixed low temperature combustion modes are homogeneous charge compression ignition (HCCI), premixed charge compression ignition (PCCI), partially premixed combustion (PPC), and reactivity-controlled compression ignition (RCCI). Despite having similar operating zones inside the Φ-T diagram, these concepts rely on different techniques to achieve this [21]. The next subsections describe some of the most studied premixed low temperature concepts: HCCI and RCCI. Detailed discussion of concepts as PCCI and PPC was not included for brevity sakes.

2.3.1 Homogeneous charge compression ignition

Homogeneous charge compression ignition was a pioneer premixed LTC technique, incorporating the theoretical characteristics of a fully homogenous combustion. It was frequently defined as a merging of the benefits from the conventional SI and CI combustion [22]. The HCCI combustion concept consists of an early fuel injection allowing to obtain a complete air fuel mixing during the compression stroke. This homogeneous charge is then compressed towards the top dead center, increasing its temperature and pressure. In a certain point, the environment inside the combustion chamber will provide enough energy to activate the initiation reactions in several sites that will depend on the thermal stratification of the combustion chamber. Once the reactions initiate, a chain reaction will occur, burning rapidly the mixture inside the cylinder. This fast combustion process has several benefits such as the low heat transfer losses combined with low in-cylinder temperature and the volumetric combustion, close to an ideal cycle [23]. Originally, this concept was proposed considering the combustion of diesel [24]. Nonetheless, the versatility of the concept allowed to introduce a wide range of fuels as alcohols, gasoline, ethers, etc. [25][26]. In spite of that, HCCI is restricted to narrow zones inside the engine map [27]. The high load operation extension is a challenge in terms of mechanical limitations, since the increase of the energy delivered in short periods has as consequence pressure gradients that cannot be supported by conventional engines [28]. On the other side, low load

conditions are a challenge scenario for Kinect controlled combustion concepts as they may not be able to provide the required activation energy for a proper fuel oxidation, reducing the fuel conversion efficiency and presenting excessive cycle-to-cycle variability [29]. The Kinects controlled nature of this combustion concept is indeed a hurdle, independent of the engine load, since the combustion process can be significantly affected by small variations of temperature and composition, which reduces the control over the combustion progress [30]. Figure 2.3 depicts a conventional operating map for an HCCI engine illustrating the restrict operating zones considering engine speed and load.

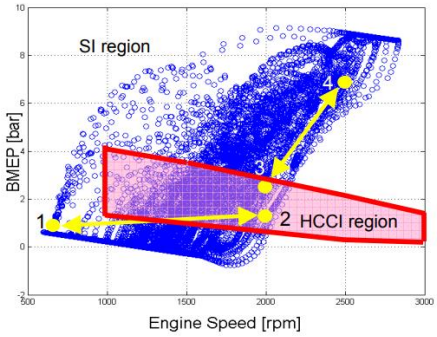

Figure 2.3. HCCI operating zone for a light duty naturally aspirated engine (red). The blue dots stand to the operating points for the FTP 75 driving cycle. Adapted from [31].

Several authors have tried to extend the HCCI operating range and improve the combustion controllability by different means, such as charge preparation, air heating control, fuel additives and reactivity modification. Both charge preparation and air heating control demonstrated to be effective means to extend the lower limit of the HCCI combustion. Ganesh et al. [32] have proposed the use of a dedicated fuel vaporizer to avoid conventional issues of liquid fuel injection as wall wetting and fuel impingement. In addition, the high temperature stratification and its consequent reduction by the fuel vaporization could also be mitigated, allowing to reduce the exhaust unburned products concentration. Regarding high load operation, studies

have been focused on using high research octane number (RON) fuels, compression ratio (CR) variation and high heat capacity substances to lower the in-cylinder temperature. This last has been deeply addressed by the works of Christensen et al. [33], Mack et al. [34] and Saxena et al. [35]. They have investigated in detail the effects of the water addition or blends of water in ethanol to realize higher engine load, concluding that the increase of mixture heat capacity can be a path to extend the HCCI upper limit. The works performed by Kalghatgi [36][37] and Bessonette [38] have followed a similar research line, concluding that the use of low cetane or high-octane fuels are an alternative to realize engine loads as higher as 16 bar of $IMEP_{gross}$. Although, these levels of power output were achieved at the cost of excessive pressure gradients (↑30 bar/CAD). Moreover, the use of low reactivity fuels has as side effect the worsening of low load operation, increasing the unburned products and deteriorating the combustion stability, suggesting that the a proper HCCI operation would infer the use of a high reactivity fuel at low load and a low reactivity fuel at high load operation.

Despite the promising results, the HCCI combustion implementation was still challenging in terms of the combustion controllability since most of the control techniques rely on low dynamic parameters such as inlet temperature. Moreover, the short combustion duration found at high load, even if it is well adjusted, is a limiting condition concerning pressure rise rate (PRR) and noise, vibration, and harshness (NVH). In this sense, several authors have suggested that a controlled energy release at high load should be introduced to successfully extend the upper limit operation and improve the control over the combustion process [39]. Promising results were obtained by introducing controlled degrees of thermal and/or fuel stratification. Sjöberg et al. [40] have evaluated the potential of including different thermal stratification degrees as an alternative to reducing pressure rise rate at high engine load. To do this, a multizone Kinects based simulation model was built in the software Chemkin, allowing to define the number of zones temperatures and specific thermal stratification widths. The results have demonstrated that the increase of thermal stratification is an effective way to enlarge the combustion process and therefore to reduce the pressure

gradient, allowing to extend, in theory, the upper limit of the HCCI combustion up to 16 bar of $IMEP_{gross}$. Herold et al. [41] has continued the work from Sjöberg by inducing both thermal and compositional stratification through different heating rates and air-fuel-argon composition for each intake valve. The results have demonstrated that there is an inverse correlation between both stratifications, i.e., the increase of the compositional stratification compensates the higher thermal stratification.

The work presented by Inagaki et al. [42] is considered a breakthrough on solving the issues related with the HCCI combustion. They have demonstrated that the creation of a reactivity stratification inside the cylinder is a mean to achieve a mild combustion progress. To realize such stratification, they have proposed two different injection systems. A port fuel injection system to supply iso-octane (which will be herein defined as low reactivity fuel - LRF), representing a high-octane fuel and a direct injection system to inject diesel (which will be herein defined as low reactivity fuel-HRF). In this sense, the reactivity of the cylinder mixtures could be tailored according to the injected mass ratio of the fuels. This combustion system proposal demonstrated to be capable of extending the operating map of conventional HCCI combustion in both directions with ultra-low soot and NOx emissions while maintaining the pressure gradient values under reasonable levels. Later, this concept was further investigated by Kokjohn et al. [43] reinforcing the promising results. They have also renamed the concept as Reactivity Controlled Compression Ignition (RCCI) as a reference to the combustion control by the reactivity modification.

2.3.2 Reactivity controlled compression ignition combustion

The promising results achieved by Inagaki et al. have promoted the interest on understanding the fundamentals of this combustion concept to allow the optimization for current applications. Kokjohn [43] and Hanson [44] were pioneers in optimizing the work from Inagaki through experimental evaluation and numerical simulations. The combination of in-cylinder planar

laser induced fluorescence (PLIF) and emissions spectroscopy have supported that the combustion progress is dominated by the sequential ignition of zones with different reactivity, from the most reactive to the least. These zones with non-uniform reactive were found to be a consequence of the blending process of both high reactivity and low reactivity fuels [45]. As previously said, this originated the name reactivity controlled compression ignition [46].

Since its introduction, RCCI combustion was extensively investigated with different aims, e.g. determination of the concept dependence with respect to the fuel characteristics [47] and operating parameters [48], piston and combustion chamber geometry optimization [49], assessing its potential on different engine platforms (light duty and heavy duty) [50] [51], understanding the major source of efficiency improvements [52], quantification of its operating limits [53], etc. The different studies have stablished the basics to realize the benefits from the RCCI mode as the dependence with parameters as gasoline fraction, high reactivity fuel injection and dilution levels [54]. These different parameters allow to obtain a better control on the combustion onset, where the HRF injection timing can dictate the combustion start [55]. Moreover, the investigations have demonstrated that the RCCI concept can be successfully implemented on both light duty and heavy duty engine platforms as a partial load combustion concept by modifications in the engine injection system like the addition of a port fuel injector and low pressure pump and a separated fuel tank for the low reactivity fuel.

The use of the RCCI combustion in large displacement engines (medium and heavy-duty platform) was proven to be an interesting technological application of the concept. Investigations performed by Splitter et al. have experimentally demonstrated that the RCCI concept can be extended to engine loads as high as 18 bar of IMEP, i.e., full load operation [56]. As opposed to the earliest LTC concepts, RCCI allowed to extend the benefits of LTC combustion in high load zones, which have a significant weight on the final emissions for this type of application. Similar results were also obtained in a heavy-duty SCE engine by Benajes et al. [57]. The authors

proposed a full map calibration in a SCE engine, representative of a 13L commercial engine to demonstrate the potential of the RCCI application to realize ultra-low NOx and soot emissions and efficient combustion. The original engine compression ratio was decreased from 17.5:1 to 11:1 as an attempt to reduce the excessive pressure gradients and extend the RCCI combustion towards full load operation. Figure 2.4 presents the values of gross indicated efficiency (GIE), SNOx, dry soot and PRR obtained by the authors.

As it can be seen, the use of RCCI combustion with a lower compression ratio enabled the achievement of almost full load operation. Moreover, it provided EUVI NOx (≤0.4 g/kWh) and soot (≤0.01 g/kWh) engine out emissions while maintaining similar to higher values of gross indicated efficiency compared to typical conventional diesel combustion engines considering medium to high loads. Although this is a promising result within the heavy-duty area, the concept still presents some concerns about its applicability. First, it is not possible to avoid the excessive pressure gradients at high engine load, as depicted in Figure 2.4 (d). The PRR results at low to medium engine speeds can be as high as 26 bar/CAD, much higher than the current limits that are used by OEMs (15bar/CAD). If this threshold is considered, the proposed calibration should be able to reach only 50 % of engine load, even in the case of having a CR of 11:1. In addition, the use of these low compression ratios are detrimental to low load operation, resulting in CO and HC emissions higher than 80 g/kWh and 22 g/kWh, respectively [58].

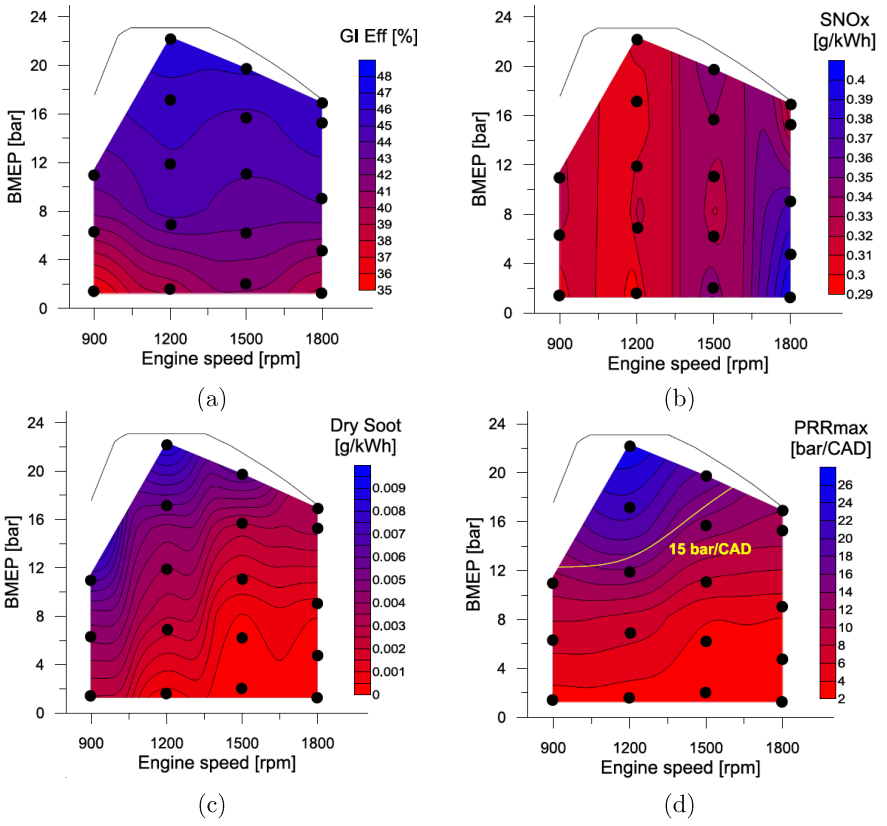

Figure 2.4. Iso surface representation of (a) gross indicated efficiency, (b) nitrogen oxides emissions, (c) dry soot emissions and (d) pressure rise rate for a single cylinder engine calibration with RCCI combustion. Adapted from [58].

From this brief review on RCCI combustion, it can be concluded that the concept is indeed a breakthrough in alternative combustion concepts, allowing to explore the benefits of the LTC combustion while promoting degrees of combustion controllability. Nonetheless, the trials to extend the combustion concept to full map operation have faced recurrent issues from the LTC combustion as excessive pressure gradient at high engine load and low combustion efficiency with high cycle-to-cycle variation at low load. These results have pushed the investigation efforts on answering the question:

how can the combustion process be managed to allow exploring the benefits of RCCI combustion while enabling a full map operation?

2.4 Dual-Mode Dual-Fuel concept: potential and challenges

Dual-Mode Dual-Fuel (DMDF) combustion has emerged as an attempt to answer the previous questions. It incorporates the benefits of the RCCI combustion while the pressure gradients allow it and progressively switch the operating parameters to obtain a mixed controlled dual fuel combustion as the engine load is increased towards higher values. The next subsections intend to describe in detail the fundamentals of this combustion concept, as well as to evidence its advantages, drawbacks and the points that still need to be addressed to extend its application on real powertrains.

2.4.1 Conceptual description of the DMDF combustion

The Dual-Mode Dual-Fuel combustion (DMDF) combustion concept proposed by Boronat [59] has its roots on the previous experimental works presented by Monsalve [58], considering the issues that were found to extend the engine load to low and high limits. Considering the previous conclusions from Monsalve, modifications of the combustion process were suggested according to the different restrictions found at each operating zone (low, medium, or high load). Figure 2.5 depicts a conceptual description of the DMDF concept. As it is shown, the concept is composed by two main combustion modes, a fully premixed combustion and a dual-mode diffusive combustion. Between both, a highly premixed zone is included which is a consequence of the progressive switch between both combustion modes (premixed and diffusive). To obtain this, different constraints in terms of mechanical abuse as well as NOx and soot emissions were set prior to the calibration. The information about each one of these constraints can be visualized in the left-hand side of Figure 2.5.

As it is depicted, the mechanical stress was limited by setting the maximum in-cylinder pressure and PRR to 190 bar and 15 bar/CAD respectively. Moreover, the emissions constraints were set as NOx<0.4 g/kWh and soot <0.01 g/kWh. These constraints could be achieved from low load up to medium load by implementing a conventional RCCI combustion. Nonetheless, as the load was increased the pressure gradients started to be a limitation in extending the RCCI mode. In this sense, modifications of the injection settings were proposed, including decreasing the relevance of the energy provided by the gasoline and the shifting of the diesel injections towards the top dead center as it is shown in Figure 2.5.

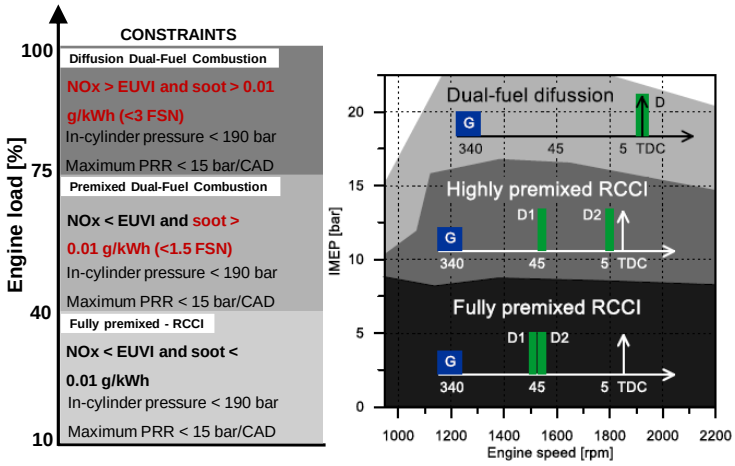

Figure 2.5. Conceptual description of the Dual-Mode Dual-Fuel combustion and the respective constraints that are generally used for each one of the operating zones. Adapted from [59].

Although this strategy is effective in reducing the pressure gradients, the increase of the diesel quantity with delayed start of injection (SoIs) enhances the formation of rich zones, which increases the soot formation. In this sense, this highly premixed zone requires a relaxation of the soot constraints to values up to 1.5 filter smoke number (FSN). In the last part of the operating map, even highly premixed strategies result in excessive mechanical requirements. Then, a dual fuel diffusive combustion mode was

proposed as an alternative to enlarge the heat release rate and smooth the combustion process. This diffusive combustion is enabled by an early gasoline injection (340 CAD bTDC) coupled with a single diesel injection near to the TDC. Therefore, once the diesel is injected, the high temperature and pressure that are found in the combustion chamber allows to have a small ignition delay, which initiates the combustion of the gasoline that was fully premixed in a highly diluted by exhaust gases recirculation (EGR) environment. Nonetheless, this first heat release is not high enough to exceeds the mechanical limitations.

Once the combustion is stablished, the diesel injection remains, providing the energy by means of a well-controlled conventional diffusive combustion. As the diffusive combustion is recalled, the drawbacks of its usage are again introduced. At these conditions, both NOx and soot emissions must be relaxed to 2 g/kWh and 3 FSN, respectively. Despite the relaxation, these values are still much lower than those verified at conventional diesel combustion since part of the energy is provided by the gasoline and the fuel premixing is maximized to avoid soot formation. In addition, the high levels of EGR at low load, an order of magnitude higher than those from CDC, allow to inhibit to a certain degree the formation of NOx emissions by the Zeldovich mechanism.

Boronat [59] remarked that the width of the zones inside of the operating map are highly dependent on the engine compression ratio and the fuel characteristics. As the RCCI combustion and most of the transition zone are still kinetically controlled combustion, the variation of the in-cylinder state parameters as well as the fuel reactivity would impact the development of the combustion process. The effects of the compression ratio modification have been extensively discussed by Boronat while the fuel impact was still not addressed in the literature and will be later presented in this thesis.

2.4.2 Hardware influence on DMDF combustion

Boronat [59] has evaluated the benefits that could be achieved by modifying the transition zone locations by using different compression ratios. To accomplish this, the same approach proposed by Monsalve [60] was used, reducing the compression ratio by means of piston machining. The bowl templates were also based on the CFD optimized pistons proposed by Monsalve and depicted in Figure 2.6. As it can be seen, compression ratios of 15.3:1 and 12.75:1 were achieved by removing the material from the piston bowl, moving from a reentrant bowl (original piston) to a non-reentrant (15.3:1) and finally to a bathtub bowl (12.75:1). The details of each bowl template are presented in Table 2.1.

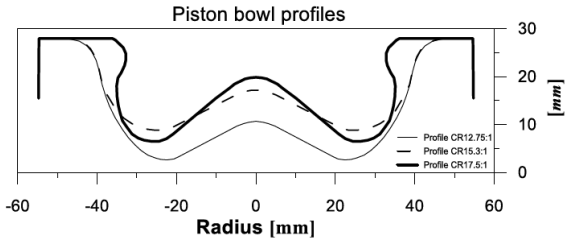

Figure 2.6. Optimized piston bowl templates to reduce the compression ratio while maximizing gross indicated efficiency. Adapted from [60].

The results of both compression ratios are presented as absolute difference maps considering the percentage variation for each parameter as CR 15.3 - CR 12.75. This means that positive values indicate a higher value for CR 15.3 while a negative value means the opposite. As it is demonstrated in Figure 2.7, it was concluded that the use of the lower compression ratio has a negative impact on the gross indicated efficiency. In general, CR 15.3 was able to deliver higher efficiencies (2-4 %) for most of the engine map with the exception of isolated conditions at high load operation in low engine speeds [61].

Table 2.1. Characteristics of the original piston bowl template as well as the two optimized bowls for CR 15:3 and CR 12.75 [60].

Production bowl (CR 17.5:1)	**Non re-entrant bowl (CR 15.3:1)**	**Bathtub bowl (CR 12.75:1)**
Area/Volume:8.18 cm^2/63.51 cm^2=0.128	Area/Volume: 9.05 cm^2/77.8 cm^2=0.116	Area/Volume: 9.78 cm^2/97.8 cm^2=0.1
Depth: 20.8 mm	Depth: 20.8 mm	Depth: 24.35 mm
Min. distance to oil gallery	Min. distance to oil gallery: 5.35 mm >3.9 mm (used in bathtub design)	Min. distance to oil gallery: 4.5 mm >3.9 mm (used in bathtub design)
In distance in center: 19.3 mm	In distance in center: 16.79 mm	In distance in center: 10.37 mm

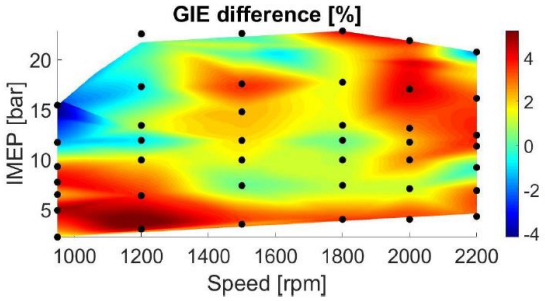

Figure 2.7. Gross indicate efficiency percentage difference between compression ratio of 15.3:1 and CR 12.75:1. Adapted from [61].

The authors have also assessed the impact of the compression ratio modification on the different regulated emissions. It was concluded that the higher compression ratio demands an early transition due to the dual fuel diffusive combustion. Consequently, both NOx and soot emissions are worsened at high loads, exceeding values of 1g/kWh (NOx) and 1 FSN (soot) in a wide part of the operating map as shown in Figure 2.8. These results suggested that higher compression ratios should require the use of dedicated after treatment systems since the use of these higher engine loads could have a significant weight during normative evaluations.

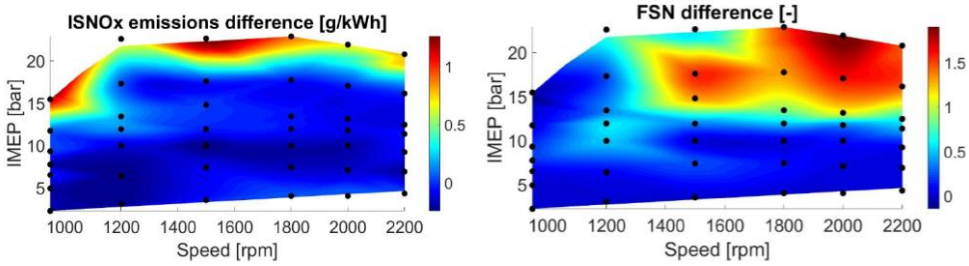

(a) (b)

Figure 2.8. Iso surface map depicting the percentage absolute differences of (a) indicated specific nitrogen oxides emissions and (b) filter smoke number (FSN) between compression ratio of 15.3:1 and CR 12.75:1. Adapted from [61].

Moreover, the same analysis has been extended to the HC and CO emissions (Figure 2.9). It was remarked that the most affected zone is the low load region which reflects the effect of using higher intake temperatures in the case of CR 12.75. Moreover, it is suggested that both excessive HC and CO emissions at low load operation are an additional challenge to the diesel oxidation catalyst due to the low exhaust temperature that is found on these conditions.

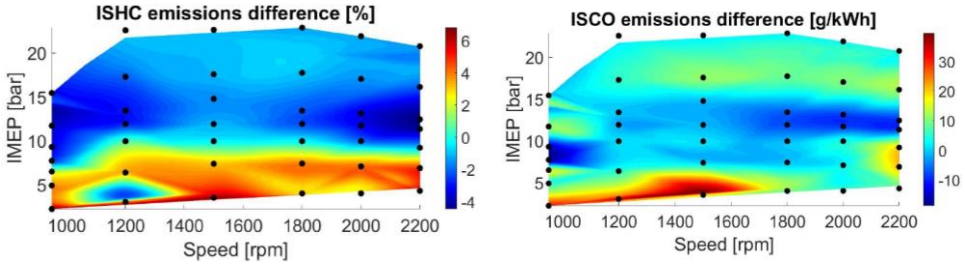

(a) (b)

Figure 2.9. Iso surface map depicting the percentage absolute differences of (a) indicated specific unburned hydrocarbons and (b) indicated specific carbon monoxide between compression ratio of 15.3:1 and CR 12.75:1. Adapted from [61].

The contrasting behavior between emissions and efficiency has required the use of comparative assessment by means of a World Harmonized Stationary Cycle (WHSC). The calibration operating conditions were assumed close enough from those proposed by the normative cycle as presented in Figure 2.10. In this sense, both compression ratios were evaluated targeting the achievement of EUVI engine-out NOx and Soot.

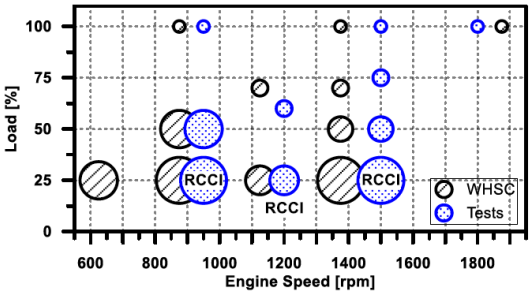

Figure 2.10. Schematic description of the normative WHSC steady cycle points and those operating conditions from the DMDF calibration. Adapted from [59].

The results of the analysis can be evidenced in Table 2.2. In spite of the high efficiency obtained compression ratio of 15.3:1, the early switch to the dual fuel diffusive combustion impairs both NOx and soot emission. This last exceeds the limits imposed by the normative, which in the authors judgement, prohibits the use of this hardware setup. Therefore, the compression ratio of 12.75:1 was suggested as the best alternative as it provides reasonable levels of conversion efficiency while fulfilling EUVI engine out emissions in terms of NOx and soot.

Table 2.2. Characteristics of the original piston bowl template as well as the two optimized bowls for CR 15:3 and 12.75 [61].

Emissions	EUVI limits	WHSC [CR 15.3:1]	WHSC [CR 15.3:1]
NOx	0.4	0.223	0.138
Soot	0.01	0.016	$7.4x10^{-4}$

2.4.3 DMDF: benefits and challenges

This subsection intends to detail the benefits that can be achieved by using the DMDF with the previously selected hardware as well as the challenges to obtain those benefits in multi-cylinder engine platforms. Starting with the benefits, the results from Boronat [59] have suggested that the use of the DMDF combustion, even with low CR, is able to provide diesel like indicated specific fuel consumption (ISFC). As it is demonstrated in Figure 2.11, it was possible to obtain ISFC values as low as 180 g/kWh in a wide zone of the map, comparable to modern heavy duty diesel engines. This should be summed up to the EUVI NOx and soot emissions that are realized by means of the successful implementation of an LTC combustion in the complete engine map (premixed and mixed controlled LTCs). As it is shown in Figure 2.12, all the evaluated experimental conditions are able to remain under the EUVI normative limits.

The detailed analysis of the unburned products presents a less favorable scenario. Despite having lower CO and HC emissions at low load compared to CR 15.3:1, the specific emission of these pollutants exceeds by order of magnitudes those from CDC, which may be a challenge even for optimized oxidation catalyst materials.

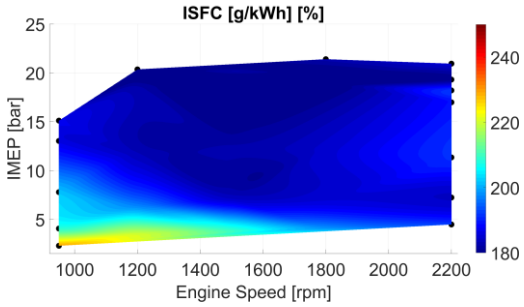

Figure 2.11. Indicated specific fuel consumption for the DMDF calibration with compression ratio of 12.75:1. Adapted from [59].

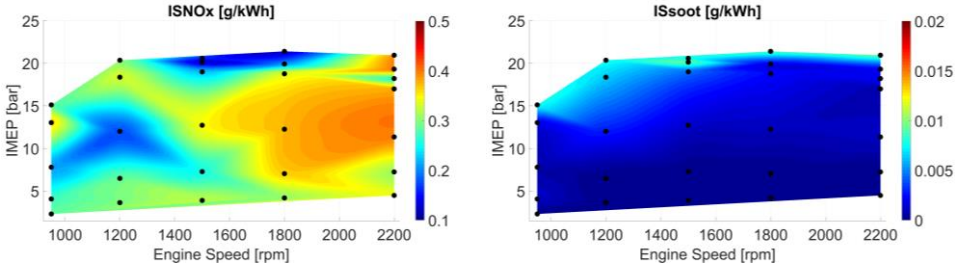

(a) (b)

Figure 2.12. Iso surface representation of (a) indicated specific nitrogen oxides emissions and (b) indicated specific soot emissions for the DMDF calibration with compression ratio of 12.75:1. Adapted from [59].

In addition, the high concentration of hydrocarbons in the exhaust competes at low temperatures with the formation of NO_2 which is an important specie to guarantee a proper passive regeneration of the DPF [62]. This may be an important question to be addressed if the DMDF concept is intended to be used in real powertrains.

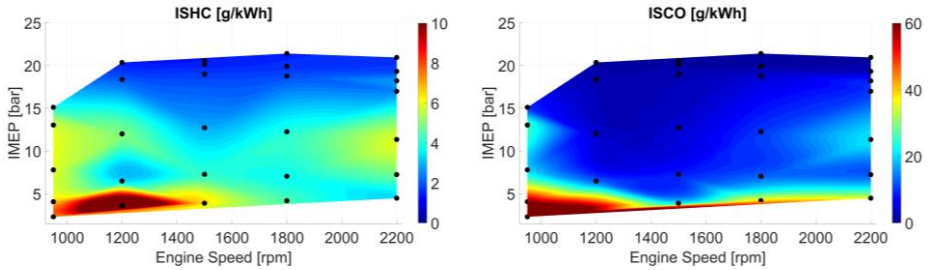

(a) (b)

Figure 2.13. Iso surface representation of (a) indicated specific unburned hydrocarbon emissions and (b) indicated specific carbon monoxide emissions for the DMDF calibration with compression ratio of 12.75:1. Adapted from [59].

The detailed analysis of the air management system also provides a challenging scenario to be faced. As it is shown in Figure 2.14 and Figure 2.16, the values of intake and exhaust pressure coupled with the higher EGR levels and low exhaust temperature seems not be easily reproduced with a real turbocharger. In which regards the pressure targets, it is demonstrated that a minimal backpressure is added to the system since the difference between the intake and exhaust pressure is very low. This scenario is commonly achieved in well matched turbocharged diesel engines where the turbo group is operating at their optimum point [63]. Generally, this zone is very narrow which limits the optimum points that can be founded in the map. From the figure analysis, it can be concluded that to obtain the same conditions than those from the experiments, the turbocharger should be working always close to its best efficiency point. This could be true if the reduced mass flow and pressure ratio were maintained during the operation. Nonetheless, the wide range of intake and exhaust pressures depicts that this is not accomplished in the concept.

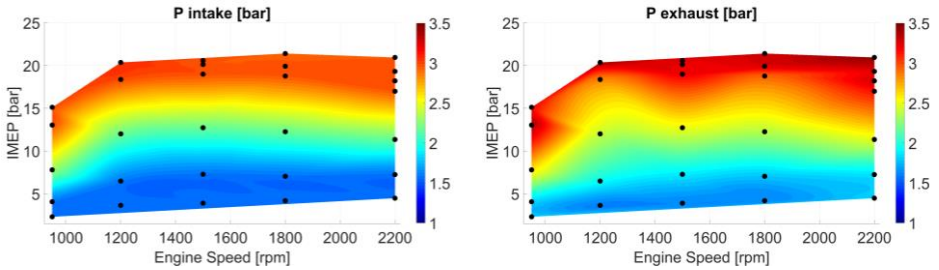

(a) (b)

Figure 2.14. Iso surface representation of (a) manifold inlet pressure (b) manifold exhaust pressure for the DMDF calibration with compression ratio of 12.75:1. Adapted from [59].

This can be better visualized by placing the operating conditions inside the compressor map from the stock air management system as depicted in Figure 2.15. As it is shown, the DMDF use requires a mass flow and an intake pressure that cannot be addressed by the original compressor map from 75 % of the engine load. The higher mass flows and intake pressure place the operating points outside the compressor, which in real applications leads to compressor overheating and choke, reducing its lifetime. The solution for this situation could be the modification of the compressor to a higher capacity one. Nonetheless, this modification could impair the low engine speed operating conditions since they are already found close to the surge line of the compressor.

Moreover, the intake pressure values are higher than 2 bar for almost the complete operating map. This means that the turbocharger should be fed by a high energy flow, allowing to extract this energy and provide it again as dynamic pressure. Nonetheless, the results from Figure 2.16 demonstrate the opposite. Most of the flow that leaves the engine is recirculated as EGR while the temperature is lower than 400 °C in most of the map. The compensation of the low mass flow can be made using a variable geometry turbine, modifying the impeller angle as the mass flow is reduced. Nonetheless, such approach may result in higher back pressures, impairing the efficiency results. In addition, even a closed impeller could still be not able to deliver the

required energy if the energy flow is lower than the required. Finally, the high EGR rates are also a challenge to be matched in the air management system. Considering that the system is equipped with a high pressure (HP) EGR only, this lack of energy could lead to a compressor surge. By contrast, the use of low pressure (LP) EGR would mean a significant mass flow flowing through the compressor which could elevate its working temperature and cause issues as over speeding and mechanical fatigue. The use of both systems could be a feasible alternative to be applied at the cost of increasing the overall complexity.

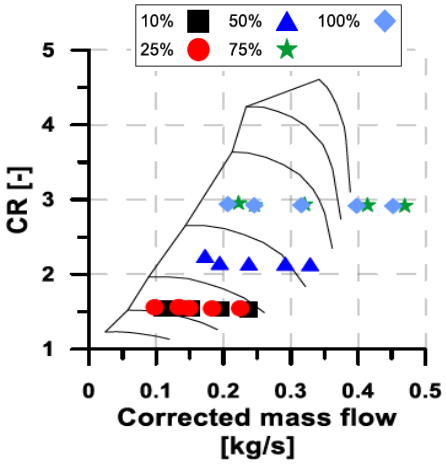

Figure 2.15. Measured operating conditions inside the stock compressor map illustrating the exceeding of the operating range of the device. Adapted from [59].

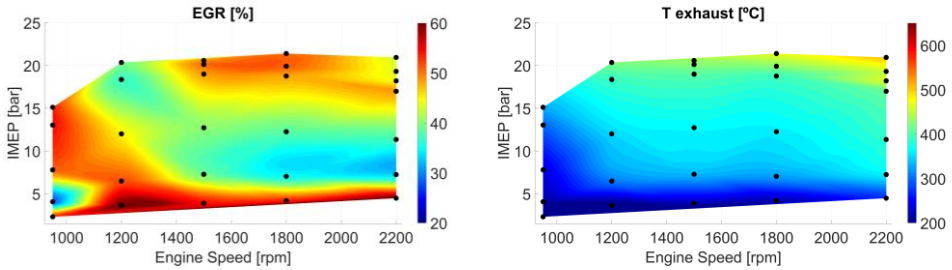

Figure 2.16. Iso surface representation of (a) exhaust gas recirculation rate (b) exhaust temperature for the DMDF calibration with compression ratio of 12.75:1. Adapted from [59].

In this sense, it can be concluded that the DMDF concept is a promising combustion concept to face the actual and the upcoming scenarios in the transportation sector. Nonetheless, there are still significant points to be addressed as the issues with the high concentration of unburned products and the challenges in translating the concept to real applications. Lastly, the short-term future will require a significant reduction of the total CO_2 emitted by medium and heavy-duty transportation. In spited of having similar to higher efficiency than conventional diesel engines, the concept is still not able to provide the required reductions of 15 % and 30 % on the 2025 and 2030 horizons, respectively, which requires additional investigations on techniques or fuels that could help the concept to fulfill these requirements.

2.5 Approach of the study

2.5.1 Motivation of the study

Solutions to the diesel combustion *dilemma* have been proposed along the years. Within the combustion area, low temperature combustion concepts have demonstrated a major potential to avoid the NOx-soot trade-off while providing superior conversion efficiencies.

The introduction of homogeneous charge compression ignition was a breakthrough in the engine combustion area due to its promising results and the simplicity of the engine hardware. Nonetheless, several problems were identified as excessive HC and CO at low load, limited operating range and low combustion controllability. Extensive investigations on mixture preparation, fuel ignition quality, etc., have been made as an attempt to solve these issues. Compositional and reactivity stratification by the introduction of a second fuel have proven to be a path to obtain a higher degree of control over the combustion while maintaining the benefits of the LTC, introducing the reactivity controlled compression ignition combustion concept. In addition to the better combustion control, RCCI also allowed to extend the operating range inside the engine map. Nonetheless, the issues of the premixed low temperature combustion persist, avoiding working in high load conditions due to the pressure gradients and low load due to the excessive unburned products and combustion instability.

Dual-Mode Dual-Fuel combustion has been introduced as a pathway to realize full load operation while maintaining the benefits from the premixed LTC. For this, the combustion concept is based on a progressive modification from a fully premixed combustion to a dual-fuel diffusive combustion as the engine load is increased. Literature results demonstrated that the application of the concept in a medium duty SCE with compression ratio of 12.75:1 can achieve full load operation while fulfilling the EUVI NOx and soot normative in all the operating conditions evaluated with diesel-like efficiency. Nonetheless, the extension of these results to a real platform are challenging due to the air management and ATS requirements. Hence, the literature review suggests that there are still specific research areas that require deeper investigation to extend this concept to real applications:

- The technological development of the combustion concept was made on a SCE platform with external air management system to provide the required boost pressure, EGR rate and backpressure to the engine. The engine settings extension to real multi-cylinder engine may be a challenge in which refers to the higher intake pressures and massive

EGR amounts that are simultaneously required. In this sense, the calibration of a real engine is recommended to assess the impact of translating the engine settings from SCE in the overall engine performance.

- The previous results from Boronat [59] have demonstrated an excessive concentration of unburned products (HC and CO) at low load operating coupled to low exhaust temperatures. These combinations can be a hurdle on the performance of ATS devices. Moreover, high load operation still produces significant amounts of soot due to the change from premixed LTC to mixing controlled LTC. This should be added to the fact that the use of a dual EGR system (LP+HP) requires the filtering of the exhaust gases prior to reinserting them in the intake system. This means a dedicated DPF would still play a significant role on the DMDF combustion. In this sense, a complete evaluation of the DMDF impact on the performance of the DOC and the DPF is required.

- Finally, despite the benefits in NOx and soot emissions, the tank to wheel CO_2 emissions are only slightly reduced by the DMDF combustion, being far from the targets imposed to 2025 and 2030. In this sense, the improvement of the efficiency of the concept as well as the use of alternative fuels that may promote a reduction in the CO_2 footprint in its lifecycle should be assessed.

2.5.2 Objectives of the study

Considering the detailed literature review and the investigation gaps that were identified, the general objective of this work is *to adapt the DMDF combustion concept under the restrictions of real applications to realize clean and efficient combustion in the complete map while providing alternatives to realize CO_2 savings in a medium duty multi-cylinder engine, representative of on-road applications.*

Specific objectives were defined to accomplish the general objective that was proposed:

- *Understand the feasibility of extending the DMDF concept on real engine platforms and its potential with respect to normative under driving cycle evaluations.* The extension of the previous calibration settings from literature on real applications will be explored. Moreover, a full map calibration for the real engine platform will be proposed considering the restrictions that may be faced during the process.
- *Assess the impact of the DMDF combustion on the oxidation catalyst and particulate filter in both steady and transient conditions.* Experimental and numerical evaluations will be performed aiming to identify the overall impact of the DMDF combustion on the DOC and DPF as well as to characterize the critical operating conditions for these devices.
- *Identify solutions in terms of fuel characteristics to realize ultra-low emissions, high efficiency, and life cycle CO_2 savings.* Both low reactivity fuel and high reactivity fuel properties will be explored as an attempt to identify the most suitable fuel to the concept. First, several low reactivity fuels will be assessed by means of bi and tri component blends, allowing to sweep both research octane and motor octane number. Lastly, different advanced reactivity e-fuels and their blends with diesel will be evaluated aiming to combine both CO_2 reduction potentials with efficiency and emissions improvements.

2.5.3 General methodology and research development

An experimental-numerical methodology approach is proposed to address the different objectives that were defined as it can be evidenced in Figure 2.17. The experimental results obtained in the fully instrumented multi-cylinder engine are processed by means of CALMEC (an in-house

combustion diagnostic tool). The processed results are then ready to be analyzed or to be used as boundary conditions in different evaluations. The instantaneous pressure and temperature profiles as well as the in-cylinder composition are fundamental to Kinects evaluation. Moreover, the GT-drive simulations are based on the interpolations of the experimental maps for performance and emissions. Finally, the engine-out results analysis is needed to understand the impact of operating parameters on the performance, combustion, and emission results.

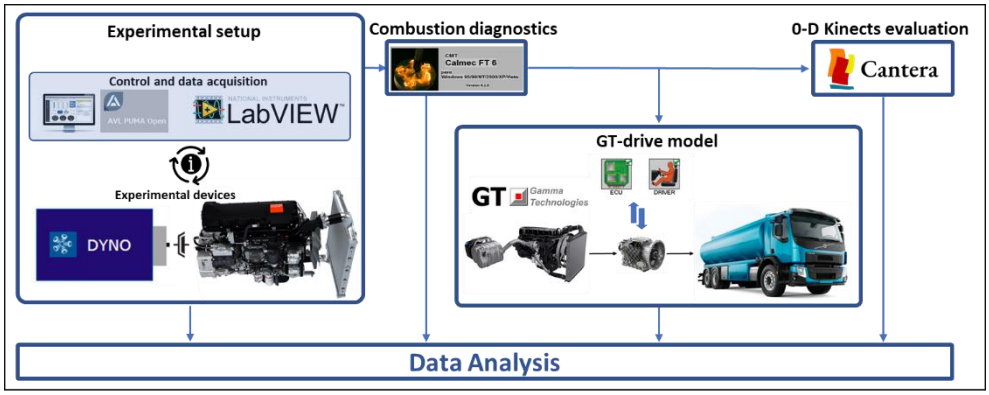

Figure 2.17. Conceptual description of the different sources of information and workflow followed during the investigation.

The research was developed in a connected way, trying to bring the results from the SCE development to a real-world application while solving the already known issues and those that would appear. Hence, chapter 4 describes the implementation of the DMDF concept following the guidelines provided by Boronat [59] in a multi-cylinder engine. The chapter 4 answers if the proposed boundary conditions can be achieved in a stock platform, identifies possible solutions and proposes an adaptation of the calibration to deal with the restrictions imposed by the system. Finally, it assesses the potential of the DMDF calibration in achieving normative NOx and soot emissions and highlights the main drawbacks of the concept.

Chapter 5 responds the second particular objective of this investigation by analyzing the dominant parameters on the DOC conversion efficiency. To do this, a steady-state methodology is proposed measuring the calibration points from low to medium load, since these are the most challenging operating conditions. Speciation, conversion efficiency and temperature evolution are measured for each one of the calibration points allowing to understand the effect of the fuel composition variation on the exhaust emissions. Then, transient measurements are proposed to understand the DMDF influence on light off time under specific transient steps. Finally, two models representing the DOC and DPF are calibrated and used in driving cycle simulations allowing to assess the DMDF performance on different normative, in-service conformity and real driving conditions. This provides an overview of the DMDF impact on the ATS as well as the capabilities of the stock system in realizing tailpipe EUVI emissions.

The last objective (achieve reductions on CO_2 emissions by means of fuel optimization) is accomplished through an extensive test matrix. First, PRFs from 100 to 80 are evaluated, isolating the effect of RON on the DMDF combustion. Then, the most promising candidates for short-term future and midterm future are selected by a merit function. Then, the sensitivity effect is introduced on the RON by means of ternary blends with toluene, assessing the impact of increased aromatic content from real fuels on the combustion and emissions process. This analysis is aided by means of 0-D Kinects simulations in Cantera. In a second step, OMEx and e - Fischer Tropsch are considered in their net form of blended with diesel as potential high reactivity fuels enabling the reduction of CO_2 in the lifecycle while providing an alternative to reduce the soot emissions. Lastly, a new calibration is proposed considering the best set of low reactivity fuel and high reactivity fuel and then compared with the previous calibration in a driving cycle evaluation.

2.6 Bibliography

[1] Benajes J., Novella R., García A., Arthozoul S. "The role of in-cylinder gas density and oxygen concentration on late spray mixing and soot oxidation processes". *Energy*, Vol. 36, pp. 1599–1611, 2011.

[2] Desantes J.M., Payri R., Salvador F.J., Gil A. "Development and validation of a theoretical model for diesel spray penetration". *Fuel*, Vol. 85, pp. 910–917, 2005.

[3] Siebers D.L. "Liquid-phase fuel penetration in diesel sprays". *SAE Technical Papers,* n° 980809, 1998.

[4] Xin J., Ricart L., Reitz R.D. "Computer Modeling of Diesel Spray Atomization and Combustion". *Combustion Science and Technology*, Vol. 137, pp. 171–194, 1998.

[5] Bertoli C., Migliaccio M.N. "A finite conductivity model for diesel spray evaporation computations". I*nternational Journal of Heat Fluid Flow.* Vol. 20, pp. 552–561, 1999.

[6] Pastor J. V., Javier López J., García J.M., Pastor J.M. "A 1D model for the description of mixing-controlled inert diesel sprays". *Fuel*, Vol. 87, pp. 2871–2885, 2008.

[7] Andreassi L., Ubertini S., Allocca L. "Experimental and numerical analysis of high pressure diesel spray-wall interaction". *International Journal of Multiphase Flow.* Vol. 33, pp. 742–765, 2007.

[8] Higgins B., Siebers D., Aradi A., *SAE Technical Papers,* Diesel-Spray Ignition and Premixed-Burn Behavior, (2014).

[9] Chmela F.G., Orthaber G.C., Rate of heat release prediction for direct injection diesel engines based on purely mixing controlled combustion, *SAE Technical Papers,* (1999). doi:10.4271/1999-01-0186.

[10] Dec J.E., A conceptual model of di diesel combustion based on laser-sheet imaging, *SAE Technical Papers,* n° 970873, 1997.

[11] Arrègle J., Pastor J. V., López J.J., García A. "Insights on postinjection-associated soot emissions in direct injection diesel engines". *Combustion and Flame*, Vol. 154, pp. 448–461, 2008.

[12] Turns S.R. "Understanding NOx formation in nonpremixed flames: Experiments and modeling". *Progress in Energy and Combustion Sciences*, Vol. 21, pp. 361–385, 1995

[13] Desantes J.M., Arrègle J., López J.J., García A. "A comprehensive study of diesel combustion and emissions with post-injection". *SAE Technical Papers* , n° 2007-01-0915, 2007.

[14]Li T., Ogawa H. "Analysis of the trade-off between soot and nitrogen oxides in diesel-Like combustion by chemical kinetic calculation". *SAE International Journal of Engines*. Vol. 5, pp. 94–101, 2012.

[15] Posada F., Chambliss S., Blumberg K. "Costs of emission reduction technologies for heavy-duty diesel vehicles". *ICCT White Pap*er, 2016.

[16] Neely G.D., Sasaki S., Huang Y., Leet J.A., Stewart D.W. "New diesel emission control strategy to meet US tier 2 emissions regulations", *SAE Technical Papers*, n°2005-01-1091, 2005.

[17] Pickett L.M., Siebers D.L. "Non-sooting, low flame temperature mixing-controlled di diesel combustion". *SAE Technical Papers,* n° 2004-01-1399, 2004.

[18] Kimura S., Aoki O., Kitahara Y., Aiyoshizawa E. "Ultra-clean combustion technology combining a low-temperature and premixed combustion concept for meeting future emission standards". *SAE Technical Papers,* n° 2001-01-0200, 2001.

[19] Benajes J., Molina S., Novella R., Belarte E. "Evaluation of massive exhaust gas recirculation and Miller cycle strategies for mixing-controlled low temperature combustion in a heavy duty diesel engine". *Energy,* Vol. 71, pp. 355–366, 2014.

[20] Kook S., Bae C., Miles P.C., Choi D., Pickett L.M. "The influence of charge dilution and injection timing on low-temperature diesel

combustion and emissions". *SAE Technical Papers,* n° 2005-01-3837, 2005.

[21] Agarwal A.K., Singh A.P., Maurya R.K. "Evolution, challenges and path forward for low temperature combustion engines". *Progress in Energy and Combustion Sciences*, Vol. 61, pp. 1–56, 2017.

[22] Stanglmaier R.H., Roberts C.E. "Homogeneous Charge Compression Ignition (HCCI): Benefits, Compromises, and Future Engine Applications". *SAE Technical Papers,* n° 1999-01-3682, 1999.

[23] Jin C., Zheng Z. "A Review on Homogeneous Charge Compression Ignition and Low Temperature Combustion by Optical Diagnostics". *Journal of Chemistry*, Vol. 2015, 2015.

[24] Gray A.W., Ryan T.W. "Homogeneous charge compression ignition (HCCI) of diesel fuel". *SAE Technical Papers,* n° 971676, 1997.

[25] Christensen M., Hultqvist A., Johansson B. "Demonstrating the multi fuel capability of a homogeneous charge compression ignition engine with variable compression ratio". *SAE Technical Papers,* n° 1999-01-3679, 1999.

[26] Martins M., Fischer I., Gusberti F., Sari R., Nora M.D. "HCCI of Wet Ethanol on a Dedicated Cylinder of a Diesel Engine". *SAE Technical Papers,* n° 2017-01-0733, 2017.

[27] Yao M., Zheng Z., Liu H. "Progress and recent trends in homogeneous charge compression ignition (HCCI) engines". *Progress in Energy and Combustion Sciences*, Vol 35 pp. 398–437, 2009.

[28] Hyvönen J., Haraldsson G., Johansson B. "Supercharging HCCI to extend the operating range in a multi-cylinder VCR-HCCI engine". *SAE Technical Papers,* n° 2003-01-3214, 2003.

[29] Song H.H., Edwards C.F. "Understanding chemical effects in low-load-limit extension of homogeneous charge compression ignition engines via recompression reaction". *International Journal of Engine Research*, Vol. 10, pp. 231–250, 2009.

[30] Tanaka S., Ayala F., Keck J.C., Heywood J.B. "Two-stage ignition in HCCI combustion and HCCI control by fuels and additives". *Combustion and Flame. Vol.* 132, pp. 219–239, 2003.

[31] Chang K., Babajimopoulos A., Lavoie G.A., Filipi Z.S. "Assanis D.N., Analysis of load and speed transitions in an HCCI engine using 1-D cycle simulation and thermal networks". *SAE Technical Papers,* n° 2006-01-1087, 2006.

[32] Ganesh D., Nagarajan G., Mohamed Ibrahim M. "Study of performance, combustion and emission characteristics of diesel homogeneous charge compression ignition (HCCI) combustion with external mixture formation". *Fuel* Vol. 87 pp. 3497–3503, 2008.

[33] Christensen M., Johansson B. "Homogeneous Charge Compression Ignition with Water Injection". *SAE Technical Papers,* n° 1999-01-0182, 1999.

[34] Mack J.H., Aceves S.M., Dibble R.W. "Demonstrating direct use of wet ethanol in a homogeneous charge compression ignition (HCCI) engine". *Energy.* Vol. 34, pp. 782–787, 2009.

[35] Saxena S., Schneider S., Aceves S., Dibble R. "Wet ethanol in HCCI engines with exhaust heat recovery to improve the energy balance of ethanol fuels". *Applied Energy*, Vol. 98, pp. 448–457, 2012.

[36] Kalghatgi G.T. "Auto-ignition quality of practical fuels and implications for fuel requirements of future SI and HCCI engines". *SAE Technical Papers,* n° 2005-01-0239, 2005.

[37] Kalghatgi G.T., Risberg P., Ångström H. "Advantages of Fuels with High Resistance Auto-ignition in Late-injection, Low-temperature, Compression Ignition Combustion". *SAE Technical Papers,* n° 2006-01-3385, 2006.

[38] Bessonette P.W., Schleyer C.H., Duffy K.P., Hardy W.L., Liechty M.P. "Effects of fuel property changes on heavy-duty HCCI combustion". *SAE Technical Papers,* n° 2007-01-0191, 2007.

[39] Shibata G., Urushihara T. "Realization of dual phase high temperature heat release combustion of base gasoline blends from oil refineries and a study of HCCI combustion processes". *SAE Technical Papers,* n° 2009-01-0298, 2009.

[40] Sjöberg M., Dec J.E., Cernansky N.P. "Potential of thermal stratification and combustion retard for reducing pressure-rise rates in HCCI engines, based on multi-zone modeling and experiments". *SAE Technical Papers* n°, 2005-01-0113, 2005.

[41] Krasselt J., Foster D., Ghandhi J., Herold R., Reuss D., Najt P. "Investigations into the effects of thermal and compositional stratification on HCCI combustion - Part I: Metal engine results". *SAE Technical Papers,* n° 2009-01-1105, 2009.

[42] Inagaki K., Fuyuto T., Nishikawa K., Nakakita K., Sakata I. "Dual-fuel PCI combustion controlled by in-cylinder stratification of ignitabilit". *SAE Technical Papers,* n° 2006-01-0028, 2006.

[43] Kokjohn S.L., Hanson R.M., Splitter D.A., Reitz R.D. "Experiments and modeling of dual-fuel HCCI and PCCI combustion using in-cylinder fuel blending". *SAE International Journal of Engines,* Vol. 2, pp. 24–39, 2009.

[44] Kokjohn S., Reitz R.D., Splitter D., Musculus M. "Investigation of Fuel Reactivity Stratification for Controlling PCI Heat-Release Rates Using High-Speed Chemiluminescence Imaging and Fuel Tracer Fluorescence". *SAE International Journal of Engines,* Vol. 5, 2012.

[45] Splitter D., Kokjohn S., Rein K., Hanson R., Sanders S., Reitz R. "An optical investigation of ignition processes in fuel reactivity controlled PCCI combustion". *SAE Technical Papers,* n° 2010-01-0345, 2010.

[46] Kokjohn S.L., Hanson R.M., Splitter D.A., Reitz R.D. "Fuel reactivity controlled compression ignition (RCCI): a pathway to controlled high-efficiency clean combustion". *International Journal of Engine Research*, Vol. 12 pp. 209–226, 2011.

[47] Benajes J., Molina S., García A., Monsalve-Serrano J. "Effects of low reactivity fuel characteristics and blending ratio on low load RCCI (reactivity controlled compression ignition) performance and emissions in a heavy-duty diesel engine". *Energy,* Vol. 90, pp. 1261–1271, 2015.

[48] Benajes J., Molina S., García A., Monsalve-Serrano J. "Effects of direct injection timing and blending ratio on RCCI combustion with different low reactivity fuels". *Energy Conversion and Management,* Vol. 99, pp. 193–209, 2015.

[49] Benajes J., García A., Pastor J.M., Monsalve-Serrano J. "Effects of piston bowl geometry on reactivity controlled compression ignition heat transfer and combustion losses at different engine loads". *Energy*, Vol. 98, pp. 64–77, 2016.

[50] Benajes J., García A., Monsalve-Serrano J., Villalta D. "Exploring the limits of the reactivity controlled compression ignition combustion concept in a light-duty diesel engine and the influence of the direct-injected fuel properties". *Energy Conversion and Management,* Vol. 157, pp. 277–287, 2017.

[51] Benajes J., Molina S., García A., Belarte E., Vanvolsem M., An investigation on RCCI combustion in a heavy duty diesel engine using in-cylinder blending of diesel and gasoline fuels, *Applied. Thermal. Engineering,* Vol. 63 pp. 66–76, 2014.

[52] Olmeda P., García A., Monsalve-Serrano J., Lago Sari R. Experimental investigation on RCCI heat transfer in a light-duty diesel engine with different fuels: Comparison versus conventional diesel combustion". *Applied Thermal Engineering,* Vol. 144, pp. 424–436, 2018.

[53] Benajes J., A. García, J. Monsalve-Serrano, I. Balloul, G. Pradel. "An assessment of the dual-mode reactivity controlled compression ignition/conventional diesel combustion capabilities in a EURO VI medium-duty diesel engine fueled with an intermediate ethanol-gasoline blend and biodiesel". *Energy Conversion and Management,* Vol. 123, pp. 381–391, 2016.

[54] Reitz R.D., Duraisamy G. "Review of high efficiency and clean reactivity controlled compression ignition (RCCI) combustion in internal combustion engines". *Progress in Energy and Combustion Sciences*, Vol. 46, pp. 12–71, 2014.

[55] Li J., Yang W., Zhou D. "Review on the management of RCCI engines". *Renewable and Sustainable Energy Reviews*, Vol. 69, pp. 65–79, 2017.

[56] Splitter D., Hanson R., Kokjohn S., Reitz R. "Reactivity controlled compression ignition (RCCI) heavy-duty engine operation at mid-and high-loads with conventional and alternative fuels." *SAE Technical Papers,* n° 2011-01-0363, 2011.

[57] Benajes J., V J.. Pastor, García A., Monsalve-Serrano J. "The potential of RCCI concept to meet EURO VI NOx limitation and ultra-low soot emissions in a heavy-duty engine over the whole engine map". *Fuel,* Vol. 159, pp. 952–961, 2015.

[58] Monsalve J., *Dual-fuel compression ignition: towards clean, highly efficient combustion.* Doctoral Thesis, Universitat Politécnica de València, Departamento de Máquinas y Motores Térmicos, 2016.

[59] Boronat Colomer V. *Dual-Fuel Dual-Mode combustion strategy to achieve high thermal efficiency, low NOx and smoke emissions in compression ignition engines.* Doctoral Thesis, Universitat Politécnica de València, Departamento de Máquinas y Motores Térmicos, 2018.

[60] Benajes J., Pastor J. V., García A., Monsalve-Serrano J. "An experimental investigation on the influence of piston bowl geometry on RCCI performance and emissions in a heavy-duty engine". *Energy Conversion and Management,* Vol. 103, pp. 1019–1030, 2015.

[61] Benajes J., García A., Monsalve-Serrano J., Boronat V. "Achieving clean and efficient engine operation up to full load by combining optimized RCCI and dual-fuel diesel-gasoline combustion strategies". *Energy Conversion and Management,* Vol. 136, pp. 142–1511, 2017.

[62] Katare S.R., Patterson J.E., Laing P.M. "Aged DOC is a Net Consumer of NO_2: Analyses of Vehicle, Engine-dynamometer and Reactor Data". *SAE Technical Papers,* n° 2007-01-3984, 2007.

[63] Alshammari M., Alshammari F., Pesyridis A. "Electric boosting and energy recovery systems for engine downsizing". *Energies,* Vol. 12, 2019.

Chapter 3

Tools and methodology

Content

3.1 Introduction

This work intends to implement the DMDF combustion concept on a multi-cylinder commercial engine and assess its potential and challenges. Moreover, dedicated studies are aimed at identifying the aftertreatment response to the DMDF combustion and the fuel optimization to realize CO_2 reductions. To do this, experimental and numerical tools and methodologies will be employed. This allows to extend the capabilities regarding the evaluation of the DMDF implementation on real applications. Therefore, this section will be divided in different subsections. First, the experimental devices, working principles and important considerations are presented. Next, the different 0-D and 1-D simulation and analysis tools are described. Finally, the methodologies that will be employed in both numerical and simulation campaign will be explained in detail.

3.2 Experimental facilities

This section intends to describe the different devices that compose the experimental facilities that were used in this research in terms of their main characteristics, working principle and operation.

3.2.1 Multi-cylinder engine description

The main object of study is a multi-cylinder commercial engine, 8L, that is originally provided by VOLVO trucks®. This engine is equipped with devices that allow to extract the maximum engine efficiency while fulfilling the current normative. Modifications were done in the original engine platform to accommodate the DMDF combustion concept. In this sense, this subsection intends to describe the engine itself as well as its auxiliary devices and the modifications that were made in the original platform to enable DMDF combustion.

3.2.1.1 Engine description

As previously discussed, this research has as aim at the implementation of the DMDF concept in a real engine platform. For this, a multi-cylinder engine (MCE) with the same unitary displaced volume than the one used in the initial single cylinder evaluations [1] it was selected. The engine in discussion is a VOLVO D8K 350, 8L, with a configuration of six cylinders in-line. This engine equips a wide range of commercial trucks, and is presented in different power versions (250-350 hp) by modifying the injection and air management system as well as the calibration maps, as it is depicted in Figure 3.1. Its commercial version is compliant with the last normative (EUVI) at the cost of using a complex aftertreatment system for each one of the engine-out pollutants: DOC (HC and CO), DPF (Soot) and SCR (NOx) [2].

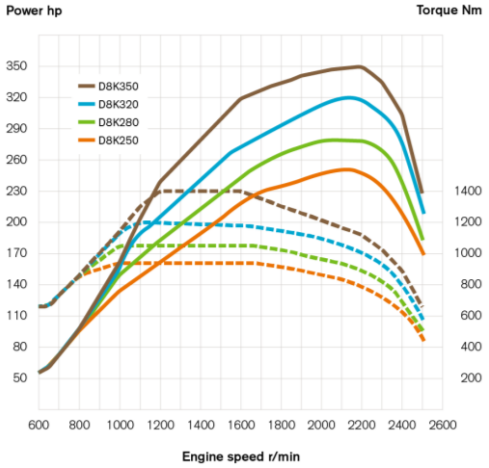

Figure 3.1. Maximum torque and power curve for the same 8L engine considering different calibration setups [2].

Geometrical modifications were made in the engine to enable the implementation of the Dual-Mode Dual-Fuel combustion concept based on the result from previous works [59]. First, the compression ratio was reduced from 17.75 to 12.75 by decreasing the piston height. Moreover, the piston geometry was optimized by means of CFD aiming to realize low emission and

improved fuel consumption. Both modifications were based on the previous work from Boronat [59]. The main characteristics of the engine are presented in Table 2.1.

Table 3.1. Main characteristics of the modified engine D8k 350.

Engine Type	4 stroke, 4 valves, direct injection
Number of cylinders [-]	6
Displaced volume [cm^3]	7700
Stroke [mm]	135
Bore [mm]	110
Piston bowl geometry [-]	Bathtub
Compression ratio [-]	12.75:1
Rated power [kW]	235 @ 2100 rpm
Rated torque [Nm]	1200 @ 1050-1600 rpm

3.2.1.2 Fuel injection systems

As presented in the literature review, the DMDF combustion concept relies on using two different fuels with contrasting reactivities, generally diesel and gasoline. To do this, an additional fuel injection system (FIS) was included. Therefore, a port fuel injection (PFI) system was added, composed by six PFI injectors (described in Table 3.2) as well as a low-pressure pump. In addition, a fuel conditioning system was developed to control the temperature of the fuel, mitigating the influence of the test cell environment temperature on the fuel properties.

The high reactivity fuel is injected by means of the stock engine high-pressure piezoelectric injector whose characteristics are presented in Table 3.2. The injection system is composed by a fuel lubricated high-pressure pump (which allows to achieve injection pressures up to 2000 bar), pressure regulator and common rail.

Table 3.2. Fuel injection system characteristics for both direct injection and port fuel injection subsystems.

Direct injector		Port fuel injector	
Actuation Type [-]	Solenoid	Injector Style [-]	Saturated
Steady flow rate @ 100 bar [cm^3/min]	1300	Steady flow rate @ 3 bar [cm^3/min]	980
Included spray angle [°]	150	Included Spray Angle [°]	30
Number of holes [-]	7	Injection Strategy [-]	single
Hole diameter [µm]	177	Start of Injection [CAD aTDC]	340
Maximum injection pressure [bar]	2500	Maximum injection pressure [bar]	5.5

3.2.1.3 Dual route exhaust gas recirculation system

The detailed analysis done in the literature review on the air management requirements that should be faced in a real engine application considering the EGR amounts and the aimed manifold pressures has led to the decision of including a low pressure EGR (LP EGR) system to be summed with the original high pressure EGR (HP EGR) system. Since higher EGR levels are needed, the use of only one route would difficult the implementation on a real platform. The use of only HP EGR would difficult the implementation on a real platform due to a lack of energy in the turbine inlet. Consequently, the turbocharger would be not able to provide the required boost pressure. By contrast, the use of only LP EGR would result in an excessive mass flow flowing through the compressor. In this case, the stock turbocharger would be not able to deal with this mass, exceeding the temperature restraint at the compressor. In this sense, the dual route EGR was chosen allowing to control the energy and mass flow balances at the turbine and compressor. Moreover, the dual route approach also enables a way to control the temperature at the intake manifold, becoming an additional path to tailor the mixture reactivity.

As said, the original engine was equipped with only HP EGR since the EGR amounts in conventional diesel applications rarely exceed 10 %. In this respect, a LP EGR system, composed of pipes, control valves, intercooler, particulate filter, and water filter, was designed to be included in the engine, as depicted in Figure 3.2. The last two devices are responsible of cleaning and to drying the EGR flow, eliminating both particulates and water condensates prior to entering the compressor, which could damage the compressor blades, reducing the compressor efficiency and lifetime [4].

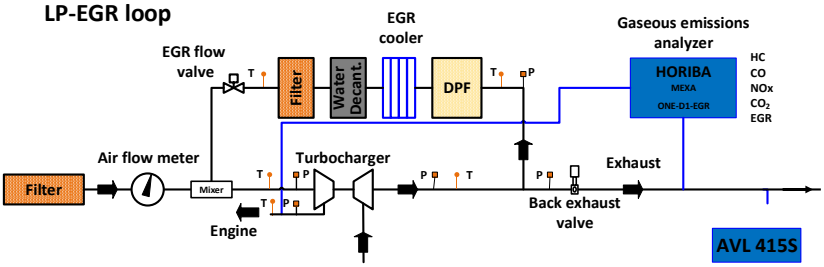

Figure 3.2. Low pressure exhaust gas recirculation system illustrating the different that are included to remove the moisture and particles from the exhaust gases.

3.2.1.4 Aftertreatment system

The commercial engine platform enables the achievement of EUVI emissions limits by means of a complete aftertreatment system as that illustrated in Figure 3.3. It consists of a diesel oxidation catalyst (DOC), diesel particulate filter (DPF), selective catalytic reduction (SCR) and an ammonia slip catalyst (ASC) [5]. Based on the previous results presented by Boronat [59], the DMDF concept should be able to realize engine out EUVI NOx emissions. Therefore, the SCR and ASC system were disabled on the ATS package and only the DOC and DPF were operative during the aftertreatment system evaluation proposed in chapter 6. The characteristics of both DOC and DPF are presented in Table 3.3.

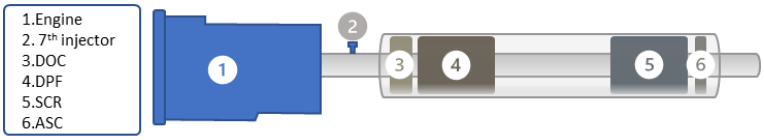

Figure 3.3. Scheme of the aftertreatment layout in the commercial truck. Adapted from [5].

Table 3.3. Diesel oxidation catalyst and diesel particulate filter characteristics of the stock after treatment system.

DOC	
Diameter [m]	0.266
Length [m]	0.102
Cell density [cpsi]	400
Total volume [dm^3]	5.7
DPF	
Substrate	Cordierite NGK
Diameter [m]	0.266
Length [m]	0.254
Cell density [cpsi]	200
Volume [dm^3]	14.2

3.2.1.5 Air management system

An important feature present in the commercial engine platform is its air management system. This comprehends a turbocharger with variable geometry turbine and a fixed geometry compressor. The operating map in terms of pressure ratio and corrected mass flow are presented in Figure 3.4. As it can be seen, the compressor map presents the optimum efficiency point at pressure ratios of 2.5 bar and corrected mass flow 0.22 kg/s (Figure 3.4 (a)). Moreover, the variable geometry turbine allows an efficient operation in

a wide range of mass flows according to its vane position (Figure 3.4 (b)). This provides an additional degree of flexibility which is beneficial in the case of having huge mass flow variations and EGR concentrations.

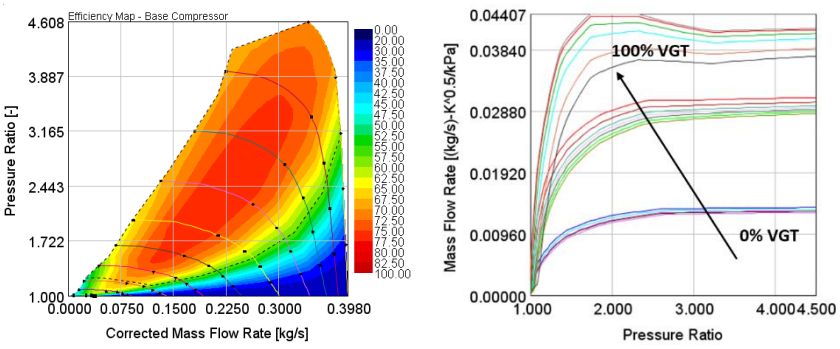

(a) (b)

Figure 3.4. Compressor (a) and turbine (b) operation map of the turbocharger.

3.2.2 Test cell characteristics

Experimental facilities for engine testing are generally complex and costly as they must be provided with reliable measurement systems as well as robust control to guarantee precise and steady boundary conditions during each test. Figure 3.5 depicts the standard test cell configuration used during this investigation, which is composed by a dynamometer (that will be presented in detail in the next subsections), an AVL 415S Smoke meter, a Horiba Mexa 7100 D-EGR, two AVL 733S gravimetric fuel flow balances (one for HRF and one for LRF), controls and acquisition systems. Additional devices are added to the standard configuration depending on the investigation that is performed and will be introduced in the corresponding chapters.

In addition, the test cell scheme allows also to visualize the different systems that were included to the conventional engine configuration. The LP EGR system can be found at the center of the figure, with the filters that

were previously discussed. Moreover, a backpressure valve is introduced right before the LP EGR split, which aims for the introduction of a pressure loss to create a positive pressure gradient from the exhaust and intake manifold and, therefore, extend the quantities of LP EGR that can be done. Finally, the six PFI injectors are located at the intake manifold, after the HP-EGR mixer.

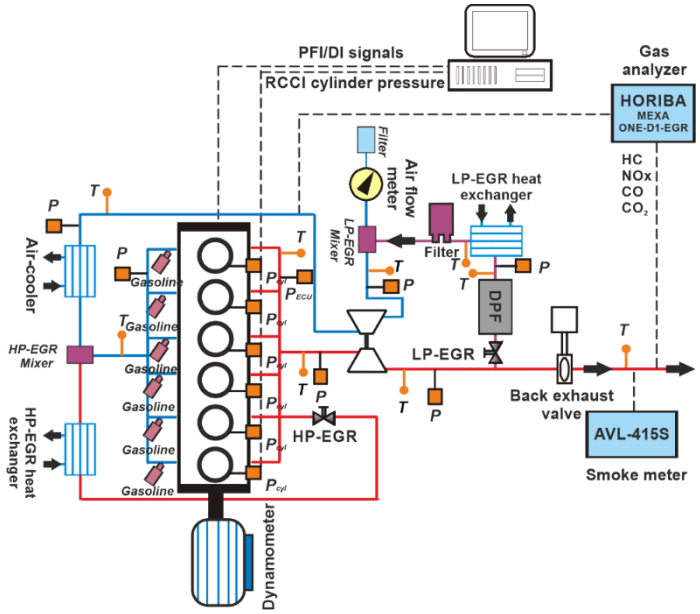

Figure 3.5. Test cell facility scheme presenting the different subsystem as well as the measurement devices that were used to assess the DMDF concept on the multi-cylinder engine.

Instantaneous pressure transducers are also employed at both intake and exhaust manifold to capture pressure wave interactions and flow pulsation caused by the engine operation, which can provide valuable information for modelling applications. In addition to this, average pressure and temperature sensors are included in different locations of interest to capture important phenomena like pressure drop and flow expansion in specific devices as well as to track the heat transfer that occurs along the

exhaust and intake lines. The main pressure and temperature measurement locations are depicted in Figure 3.5.

As it can be seen, all the six cylinders contains instantaneous in-cylinder pressure transducers which are introduced to monitor the in-cylinder dispersion that could occur from different sources as differences in the emptying-filling process, air distribution or even injection differences. Moreover, the individual monitoring allows to guarantee that none of the cylinders are operating over the mechanical limitations that are imposed during the evaluations.

3.2.2.1 Engine speed and torque regulation

Each engine operating condition is defined by a combination of a unique engine speed and torque. The control of these variables must be accurate enough to guarantee no variation over the time. The engine size is an additional challenge since its power output at full load can achieve up to 260 kW (350 hp) and the dynamometer system must be capable of to absorb this power and its fluctuations.

The engine was installed in a test cell facility containing an AVL DYNOEXACT dynamometer. This equipment can support engines with power outputs up to 400 kW. Moreover, its working principle allows to load and to motor the engine, assisting the engine start and the evaluation conditions near to misfire operation. The dynamometer control was carried out by means of the AVL PUMA interface, allowing to select different operating modes as well as to acquire the most important parameters during the evaluations. The system also enables a complete integration of the gas analyzers, fuel measurement balances, air flow meter, etc., allowing to have online visualization of the most important metrics. During the engine tests, the speed/alpha mode was selected, where the dynamometer control is responsible to maintain the engine speed, independently of the disturbances caused by the user. Alpha here stands for engine load, which is modified by

the user according to the desired operating condition by means of the injected fuel.

3.2.3 Instrumentation and measuring equipment

This subsection intends to describe the variety of sensors that have been employed during the experimental campaign. Their working range, measurement uncertainties and principles are discussed to provide insights about the reliability of the measurements. Moreover, the different correlations and signal processing devices are also presented.

3.2.3.1 Torque and engine speed measurements

Torque and speed measurement systems are part of the dynamometer, allowing to measure the reactive force of the device and, consequently, the engine power output present since the first friction band dynamometers [6]. Nowadays, different measurement devices can be found for torque measurement, for example, torque flanges as well as load cells. The latter is frequently found at steady-state applications; it consists of a strain-gauge inside a specific metal shape, designed to provide the highest sensibility to load variations. Prior to its application, a calibration curve should be provided to the acquisition software which relates the voltage output (post load cell amplification circuit) to a calibrated weight. The AVL DYNOEXACT used in this research is equipped with load cell measurement, calibrated prior to starting the experimental campaign, and frequently checked by the specific AVL PUMA® routine which consists in using calibrated weights to verify the corresponding torque.

Regarding engine speed measurements, a variety of type of sensors can be also found. Hall and inductive effect sensors placed near to a teethed well can deliver precise engine speed measurements. Nonetheless, due to the teethed well limitations, they generally provide 60-2 pulses/stroke, which is not suitable for heat release analysis applications. In this sense, an additional

optical encoder AVL 364 was installed on the crankshaft of the engine which has an interpolated resolution of 0.2 CAD. The common three band signals (A, B and C) are also present in this encoder where A allows to acquire the pulses per stroke, B is a phased A, which allows to determine the direction of rotation, and C the trigger that is used to reference the start of acquisition with respect to the piston position.

3.2.3.2 Average pressure and temperature measurement

Despite not having a temporal discretization, the time-averaged quantification is still useful to monitor and control boundary conditions at sites where the signal dynamics are low. Generally, their cost is order of magnitude lower than instantaneous instrumentation, which allows to use several sensors in a same experimental facility.

The test bench was instrumented with both average pressure and temperature sensors. Average pressure was measured by means of a PMA P40 model piezoresistive pressure transducer with a measurement range from 0 to 10 bar and an accuracy of 25 mbar. On the other hand, temperature was acquired by means of both thermocouple and thermo resistive sensors. Thermocouples type k were used with a measurement range from 0 to 1100 °C, and a precision of 2.5 °C. Pt100 thermo resistances have been used to measure the oil and water temperatures with a measuring range from -200 to +850 °C, and precision of 0.3 °C.

3.2.3.3 Instantaneous pressure transducers

Instantaneous pressure measurement is one of the most critical tasks to be performed,, since it requires special instrumentation that must be able to provide signals with low thermal shock and to support high pressure values. In this sense, the piezoelectric Kistler 6125C sensor was chosen as it fulfills all these previous requirements, allowing to measure pressure ranges from 0 to 300 bar (higher than the maximum pressure limit imposed during the

evaluations) with low thermal impact on its sensibility [7]. The 6125C pressure transducer presents an uncertainty of ±1 % at maximum pressure and a linearity of ±0.4 % of the full-scale output. Moreover, this sensor does not require any additional cooling system which simplifies its mounting and reduces the required space for its assembling in the engine. A Kistler 5011B10 charge amplifier was used to pre-condition the signal before its acquisition. It should be stated that instantaneous pressure measurements were also performed at the intake and exhaust manifold. Nonetheless, the pressure and temperatures found at these locations are far inferior to those in the in-cylinder, allowing to use Kistler 4045A10 piezoresistive sensors.

3.2.3.4 Mass flow measurement

Mass flow measurements can be divided according to the state of the fluid in discussion. First, the gas phase is considered addressing the measurement of the intake air that flows to the engine per unit of time. This is accomplished by means of a positive displacement flow meter Elster RVG G100 rotary meter, located at the intake runner, before any heat transfer device. The device allows to measure flows ranging from 0.05 m^3/h to 160 m^3/h with a precision of 0.1 %. The conversion from volumetric to mass flow basis is done considering the state properties of the air, measured by thermocouple and pressure sensors.

On the other hand, the main liquid phase fluids of interest are the fuel flow of both low reactivity and high reactivity fuel. Their measurement is performed by means of two AVL 733S balances based on the gravimetric measurement principle, allowing to measure flows from 0 to 160 kg/h with a precision of 0.2 % [8].

3.2.3.5 Data acquisition systems

The diversity of signals that can be found on the experimental facility represents a puzzle concerning the data acquisition system. A reliable system

must be able to address the contrasting frequencies, protocols, and output signals. The logical simplification seems to be the use of a high frequency acquisition for all the signals of interest. Nonetheless, this would produce files with excessive sizes and the system to overflow. In addition, according to the Nyquist's principle, there is no need to acquire average signals at the same frequency than the instantaneous ones since no additional information would be gathered [9]. In this sense, the measurement system was divided in two main blocks: a low frequency and a high frequency acquisition system.

Low frequency signals address the average pressure sensors as well as the temperature and flow measurements. These signals are then connected to a native AVL FEM-A board from the PUMA® system which allows the acquisition at 10 HZ of frequency. These signals are them available to the PUMA interface allowing to monitor their behavior as well as to set safety operation limits based on temperature and pressure outputs. Once an operating condition is set, the signals of interest are described in a DST (data storage table) and are recorded during 40s. Finally, their average value is written at the output file.

By contrast, high frequency signals are dealt by a dedicated high frequency system consisting of a NI PXIe 1071 board with an in-house interface built in LabView. The high-frequency signals comprehend instantaneous pressures as well as encoder position and injection profiles. The same routine can use these signals as inputs to an online heat release analysis routine, which allows to monitor the effect of settings variation on the main combustion metrics as well as the HRR profile.

3.2.3.6 Emission measurement

As deeply discussed in chapter 2, most of the investigations on internal combustion engines aim to achieve fuel consumption improvement and reductions on the main hazardous pollutants at engine-out. In this sense, the experimental instrumentation must be able to deliver precise quantification of these magnitudes. In which concerns emissions measurements, different

measurement principles and devices are found on the market with specific capabilities. This subsection intends to provide light on the devices that were used during the experimental campaign as well their measurement principles and specificities.

Horiba Mexa 7100 D-EGR

The Horiba Mexa 7100 D-EGR is a compact solution in terms of a measurement system for different components: CO, CO_2, THC, O_2, NOx, NO and NO_2. Each specie is determined by specific measurement principles that are extensively addressed in the literature. Table 3.4 relates the specie in discussion with the respective measurement principle, range and uncertainty associated with the measurement.

Table 3.4. Horiba MEXA 7100 D-EGR components, measurement principles range and associated uncertainty.

Component	Model	Principle	Range	Uncertainty
CO	AIA-31	NDIR	0-12 vol %	4 %
CO_2	AlA-32	NDIR	0-20 vol %	4 %
THC	FIA-01	FID	0-10000 ppmC	4 %
O_2	MPA-01	MPD	0-25 vol %	4 %
NO/NOx	CLA-01	HCLD	0-10000 ppm	4 %
NO, NOx, NO_2	CLA-02HV	DH-CLD	0-10000 ppm	4 %

As it can be seen in Table 3.4, four measurement principles are employed in determining the different engine-out species. The Non-Dispersive InfraRed detector (NDIR) is based on the separation of the broadband light into suitable wavelength that can be absorbed by the gas of interest. This signal is compared to a reference signal in a neutral environment and the respective intensity reduction is proportional to the concentration values [10]. A magneto-pneumatic detector (MPD) measurement system is employed exclusively for O_2 measurement. This specie is known to have extremely strong paramagnetism which produces a modification of a dumbbell position

as it flows. A feedback system applies a force to return the dumbbell to its original position which can be measured and translated into oxygen concentration [11].

Heated chemiluminescence detector (HCLD) consist of producing a high energy state of the NO_2 molecule through the reaction of NO and ozone. Once the reaction stops, the NO_2 returns to its ground state emitting light which is then correlated to the concentration of NOx [12]. Finally, HC is measured by means of flame ionization detection (FID). The measurement principle consists of burning a sample of the exhaust gas with a mixture of hydrogen, helium and synthetic air. The oxidation process produces ions that are submitted to an electric field. The ionization current produced by this process is then correlated to the quantity of carbon atoms [13].

It should be noted that the emissions measurement system is composed by sensors that deliver their result in molar concentration and different basis (wet or dry). Since mandates are expressed in mass basis and at wet basis, the conversion of the raw emissions is required. The regulation 49 from UNECE is widely accepted as an emission measurement guide providing guidance to attain the aforementioned conversion and it was herein employed [14]. It determines that once the raw emissions are obtained, they can be converted to mass by employing the general equation presented in equation 3.1. The units of each parameter are introduced at the first time usage.

$$m\_emission\,[g/s] = y_i[-] \cdot \dot{q}_{exhaust}[g/s] \qquad 3.1$$

Where $\dot{q}_{exhaust}$ is the exhaust mass flow rate in g/s and y_i stands for the mass fraction of each component which can be obtained by:

$$y_i[-] = x_i\,[-] \cdot \frac{MW_i[kg/mol]}{MW_{exhaust}[kg/mol]} \qquad 3.2$$

The equation 3.1 can be particularized for each component of interest and their measurement basis. In addition, the values can be converted to power specific units dividing by the power delivered in each operating

condition. This last parameter can be given in both brake (BS) or indicated basis (IS) depending on the power (P) used in the denominator (indicated or brake power).

$$SCO = \frac{\dot{m}_{CO}[g/s]}{P[kW]} = \frac{x_{CO} \cdot \frac{MW_{CO}}{MW_{exhaust}} \cdot \dot{q}_{exhaust} \cdot k_{w,r}[-]}{P} \quad 3.3$$

$$SNO_x = \frac{\dot{m}_{NO_x}}{P} = \frac{x_{NO_x} \cdot \frac{MW_{NO_x}}{MW_{exhaust}} \cdot \dot{q}_{exhaust} \cdot k_{w,r} \cdot k_{h,D}[-]}{P} \quad 3.4$$

$$SHC = \frac{\dot{m}_{HC}}{P} = \frac{x_{HC} \cdot \frac{MW_{HC}}{MW_{exhaust}} \cdot \dot{q}_{exhaust}}{P \cdot k_{FID}} \quad 3.5$$

In the previous equation $k_{w,r}$ stands for the dry to wet correction factor while $k_{h,D}$ is the humidity correction factor (both are dimensionless factors). It is also worth to be stated that the D-EGR in the Horiba measurement system, previously introduced, stands for an additional CO_2 measurement line which enables the online measurement of the EGR quantity by a simple equation:

$$EGR\ [\%] = \frac{CO_2 intake_{dry}[ppm] - CO_2 ambient[ppm]}{CO_2 exhaust_{dry}[ppm] - CO_2 ambient[ppm]} * 100 \quad 3.6$$

A last remark should be done considering the A/F calculation. The equipment allows to obtain the online output of the A/F values during the measurement considering the routine proposed by Silvis [15]. Nonetheless, the fuel composition is an input for this method. As the gasoline fraction is frequently changed during the investigations, the same occurs with the composition. Therefore, any A/F reported in this investigation is a result of an offline application of the Silvis [15] method considering the real composition of the fuel blend.

Horiba Mexa ONE-FT

Specific studies performed during the experimental campaign required the measurement of additional species which the traditional measurement principles from HORIBA Mexa 7100 cannot deal with. For these cases, a Horiba Mexa ONE FT was included, since its measurement principles are based on Fourier transformed infrared spectroscopy (FTIR) which allows to obtain information about a variety of species and their respective concentration in the exhaust gases.

FTIR fundaments are based on the fact that each substance interacts with a characteristic wavelength which depends on its chemical bonds and mass of each element that compose it. Once the molecule is excited by this specific wavelength, it absorbs energy, jumping from its ground state to a high energy one. Consequently, this energy difference is observed in the infrared detector. Table 3.5 summarizes the species and the ranges that could be measured by the Horiba Mexa FTIR used in the investigations for hydrocarbon speciation that are presented in chapter 5.

Table 3.5. Horiba Mexa ONE FT components, measurement principles range and associated uncertainty.

Component	Range	Component	Range
CO	0-5000 ppm	NH_3	0-1000 ppm
CO_2	0-20 vol%	SO_2	0-200 ppm
NO	0-5000 ppm	C_2H_6	0-200 ppm
NO_2	0-200 ppm	C_3H_6	0-200 ppm
N_2O	0-200 ppm	1,3-C_4H_6	0-200 ppm
H_2O	0-24 vol%	Iso-C_4H_8	0-200 ppm
C_6H_6	0-500ppm	C_7H_8	0-500ppm
C_2H_4	0-500ppm	CH_4	0-500ppm

It should be remarked that both monoatomic and homonuclear diatomic molecules cannot be measured by this principle as they present no vibration (first case) and symmetrical vibration (second case) [16].

AVL smoke meter

Last, but not least, an AVL 415S smoke meter was employed to quantify the soot production for the different operating conditions assessed. A specific volume of exhaust gases is forwarded to the smoke meter passing through a clean paper filter. The blackening of the paper filter is measured by means of a reflectometer and then correlated to FSN (Filter smoke Number) that can range from 0 to 10. The AVL 415 S has a resolution of 0.001 FSN with a minim detectable limit of 0.002 FSN [17]. Since the normative values are generally specified in g/kWh, the correlation presented in equation 3.7 proposed by Christian et al. [18] was employed to determine the volumetric soot mass (mg/m^3). Following, a constant exhaust gas density is used to convert it to mass basis ($mg_{soot}/kg_{exhaust\ gas}$). Next, the total soot mass is obtained by multiplying the mass fraction by the total exhaust mass and dividing it by the engine power allowing the subsequent conversion to g/kWh.

$$Soot = \frac{1}{0.405} \cdot 4.95 \cdot FSN \cdot e^{(0.38 \cdot FSN)} \qquad 3.7$$

It should be stated the smoke meter measurements are not able to quantify the totality of particulate matter mass presented in the exhaust gases. Its optical measurement system is not accurate to account condensable organics, underestimating the real particulate matter mass in the exhaust. Moreover, the DMDF particulate matter composition has shown to deviate on that from that of the CDC because the condensable organic hydrocarbons are the dominant PM mode on RCCI, affecting the accuracy of the soot estimation for this combustion concept [19]. Despite, AVL 415 S has been widely used for estimating the particulate matter values, being a good and fast indicator of the total soot mass produced by the engine.

3.3 Fuels properties and characteristics

Throughout this work, different fuels for both low reactivity and high reactivity application were evaluated aiming to precise the fuel characteristics to deliver the best results in terms of both performance and emissions. Therefore, this subsection intends to describe the net fuel characteristics as well as the blending process that were used to derive the different blends to be assessed.

3.3.1 Low reactivity fuels

Considering LRF, mostly of the investigation relied on using commercial gasoline. Nonetheless, dedicated studies were performed using surrogate fuels obtained by binary and ternary blends of iso-octane, n-heptane and toluene allowing to attain different octane numbers as well as fuel sensitivities. Table 3.6 presents the characteristics of each one of them. In the table RON stands for research octane number while MON stands for motor octane number. Both are metrics to report the reactivity quality of a fuel.

Table 3.6. Characteristics of commercial gasoline as well as the different net components that are used to emulated different research octane numbers and sensitivities.

	Gasoline	N-heptane	Iso-octane	Toluene
Density [kg/m^3] (T= 15 °C)	720	645	658	866
Carbon content [%m/m]	83	91.3	84	84.2
Hydrogen content [%m/m]	13.5	8.7	16	15.8
Oxygen content [%m/m]	3.5	0	0	0
RON [-]	95.6	0	100	121
MON [-]	85.7	0	100	107
Lower heating value [MJ/kg]	42	44.5	44.4	40.5

The volumetric proportion of n-heptane and iso-octane in binary blends dictates the RON of the fuel. RON 100 fuels stands for net iso-octane while RON 0 is obtained when only n-heptane is employed. Any intermediate RON can be achieved by mixing both components, being the iso-octane volume, the reference for the RON value. However, the blend of ternary components requires a more methodological step to assure the reliability of the fuel blends in which refers to the research octane number and sensitivity. To do this, the method proposed by Morgan et. al. [20] was employed, which consist of a two-step iteration to determine the volume fraction of each component from a diagram analysis. Figure 3.6 (a) depicts the sensitivity (RON-MON) versus toluene diagram for several RONs while Figure 3.6 (b) illustrates the dependence of the primary reference fuel (PRF) strength for a given toluene volumetric percentage for different RONs.

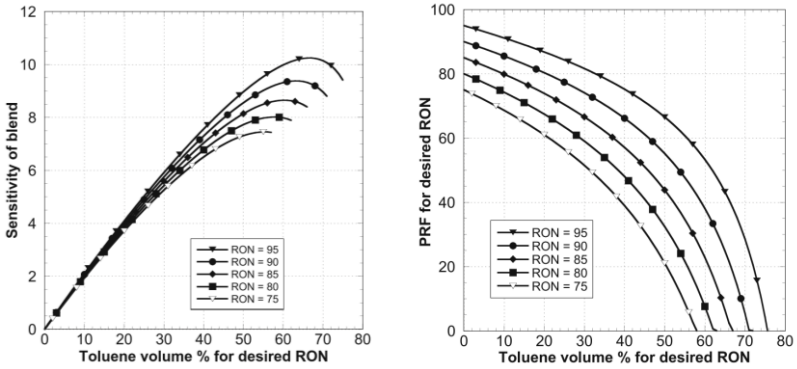

(a) (b)

Figure 3.6. Diagram representation of the (a) sensitivity- toluene dependence in a ternary blend of iso-octane, n-heptane and toluene and (b) the PFR for desired RON (PRF strength) with respect to the toluene fraction on the mixture for different RON [20].

The first step in the methodology is to define the aimed sensitivity for the blend, the target RON for the mixture and the total blend volume. Then, one should find in the first diagram what should be the toluene volume percentage to accomplish the first two target values. Once this value is defined, the PRF strength, i.e., the iso-octane and n-heptane blending ratio

is defined by means of identifying the point where the toluene volumetric percentage crosses the RON line and looking at y-axis the resultant value. With this set of results, the volume of both iso-octane and n-heptane can be finally calculated by equation 3.8 and equation 3.9.

$$Vol_{C_8H_{18}}[L] = PRF_{strength}[-] \cdot (Vol_{total}[L] - Vol_{toluene}[L]) \quad 3.8$$

$$Vol_{C_7H_{16}}[L] = (Vol_{total}[L] - Vol_{toluene}[L]) - Vol_{C_8H_{18}}[L] \quad 3.9$$

3.3.2 High reactivity fuels

Commercial diesel was used extensively during the investigations as a drop-in fuel to DMDF combustion. Despite this, additional high reactivity fuels were also evaluated as alternatives to push the combustion concept towards lower CO_2 emissions. Specifically, e-Fischer Tropsch (e-FT) and oxymethylene ethers (OMEx) were used as both can achieve a significant reduction of the CO_2 footprint during their production process.

E-Fischer-Tropsch diesel (e-FT) can be obtained from syngas (mix of CO and H_2) processing at specific temperature and pressure ranges. From this process a highly paraffinic fuel is obtained, with qualities similar to those found in hydrogenated vegetable oils (HVO). Like in HVO, the absence of polyaromatic compounds and the low sulfur reduce the soot formation during the combustion process. Additionally, the absence of aromatics together with highly paraffinic contents results in a high cetane number for this fuel. Hydrocarbon-based feedstock is generally used as source for CO and H_2 co-production using processes like gasification or steam reforming. They can also be produced via separated processes like water electrolysis, using renewable electricity for H_2, and reverse water-gas shift (RWGS) of CO_2 captured from ambient air for CO. Then, they can be mixed in the desired proportions. These last routes enable substantial CO_2 savings since hydrogen is produced from a non-hydrocarbon source and CO_2 is extracted from direct air capture (DAC). Moreover, both processes can consume renewable energy supporting the CO_2 reduction [21].

The production process of Oxymethylene dimethyl ethers (OMEx) involves a few conversion steps from CO_2 and H_2 to methanol and finally to OMEx. Once CO_2 is used as raw material, this fuel presents a substantial potential on CO_2 abatement. Nonetheless, if the electrical energy demand and the electrolysis efficiency are considered, OMEx still ranks lower than other e-fuels as dimethyl ether (DME) and methanol. This means that the CO_2 abatement will be real only when low carbon intensity energy sources are employed in the production process. Regarding the combustion process, OMEx allows for a drastic reduction of soot formation. Nonetheless, it has a low value of lower heating value (LHV), which increases its volumetric fuel consumption. The low LHV is a direct consequence of the low carbon and hydrogen content in the molecule, as almost half of it is composed by oxygen [22]. Table 3.7 summarizes chemical-physical properties of the high reactivity fuels used.

Table 3.7. Physical chemical properties of the high reactivity fuels that are evaluated during the investigation.

	EN 590 diesel	e-FT	OMEx
Density [kg/m^3] (T= 15 °C)	842	832	1067
Viscosity [mm^2/s] (T= 40 °C)	2.9	3.2	1.2
Cetane number [-]	55.7	75.5	72.9
Carbon content [% m/m]	86.2	85.7	43.6
Hydrogen content [% m/m]	13.8	14.3	8.82
Oxygen content [% m/m]	0	0	47.1
Lower heating value [MJ/kg]	42.4	44.2	19.0

It should be remarked that both LRF and HRF fuels present a significant dispersion on the lower heating values. In this sense, the brake specific fuel consumption can be seen affected by these LHV differences. Therefore, an equivalent brake specific fuel consumption premise was included whenever the fuel is modified to account these differences by normalizing the LHV (MJ/kg) of the given fuel with respect to diesel as a

way to create a comparable metric to the engine running only with diesel as presented in equation 3.10.

$$BSFC_{eq}[g/kWh] = \frac{\dot{m}_{HRF} \cdot \left(\frac{LHV_{HRF}}{LHV_{diesel}}\right) + \dot{m}_{LRF} \cdot \left(\frac{LHV_{LRF}}{LHV_{diesel}}\right)}{P_b} \qquad 3.10$$

3.4 Theoretical tools

This section intends to briefly describe the theoretical tools used during the post-process of the experimental data. Moreover, the different software interfaces used in the simulation part of the work, as well as the main governing equations of them, are herein discussed.

3.4.1 0 - dimensional models

In spite of the simplifications that can be found in 0-D calculations, it is a powerful approach to investigate phenomena under specific assumptions and well controlled conditions. Moreover, it allows to obtain a general overview of a process in a much fast time order than 1-D and multi-dimensional approaches. This investigation uses different 0-D routines for post-processing and to investigate specific phenomena of interest, which will be described in this subsection.

3.4.1.1 CALMEC

CALMEC is a 0-D package developed in CMT-motores térmicos with the aim of allowing an organized and user-friendly process to perform heat release calculations. It consists of using experimental boundary conditions, as the instantaneous in-cylinder pressure and averaged values of mass flow consumption (air and fuel), as well as temperatures and pressures to accomplish an accurate heat release analysis. This analysis is based on a closed cycle calculation considering the first law of thermodynamics with the

fuel energy as the energy added to the system and different energy outcomes that leaves the control volume (inefficiencies, blow-by, heat transfer, etc.) [23].

As expected, this 0-D approach does not provide spatial resolution, assuming homogeneity of the in-cylinder pressure and composition during the analysis. Moreover, the in-cylinder gas is considered a homogenous mixture off air, fuel and burned products that are governed by ideal gas law. The effect of using ideal and real gas to represent the in-cylinder mixture were deeply addressed in previous investigations which concluded that the differences are minimal, allowing to accept this approach during the calculations [24].

The energy balance solved during the closed cycle is presented in equation 3.11. As it can be seen, different terms are accounted, representing the most important phenomena that occurs during the engine operation.

$$\Delta HRL = m_{cyl} \cdot \Delta u_{cyl} + \Delta Q_w + p \cdot \Delta V - \left(\bar{h}_{f,inj} - u_{f,g}\right) \cdot \Delta m_{f,evap} + R_{cyl} \cdot T_{cyl} \cdot \Delta m_{bb} \tag{3.11}$$

Equation 3.11 states that the total energy released during the combustion of the fuel injected at a given CAD interval ($\Delta HRL\,[J/CAD]$) is equal to the sum of the internal energy variation of the mass trapped ($\mathrm{d}m_{cyl} \cdot \Delta u_{cyl}$), the heat transfer ΔQ_w, total work produced by the gas on the piston area ($p \cdot \Delta V$), the energy balance in the injection process ($\left(\bar{h}_{f,inj} - u_{f,g}\right) \cdot \Delta m_{f,evap}$) and the term referent to the mass loss due to blowby ($R_{cyl} \cdot T_{cyl} \cdot \Delta m_{bb}$). Each term comprehends detailed submodels which address the dominating parameters of each process; for example, the piston velocity and pressure included in the Woschni model. The detailed description of them can be found in [25].

The heat release analysis allows to obtain insights about the burning process in the cylinder, which is fundamental to reach an efficient energy conversion. From the instantaneous heat release, an accumulated profile can be generated and them normalized by the total energy provided to the

system, resulting in the mass fraction burned (MFB) curve. This approach allows to define different combustion metrics such as the ignition delay (0-2 % of MFB), CA 10, CA50 and CA 90 (crank angle degrees where 10, 50 and 90 % of the mass fraction is burned) or the combustion duration, generally defined as CA90-CA10.

Combustion efficiency

One important source of energy loss in an engine is caused by the part of the fuel that is not properly burned. This can be originated by different mechanisms as the trapping of fuel between the gaps of the cylinder or partial oxidation of the hydrocarbon molecule. Once this information is obtained through the exhaust emissions measurement, the combustion efficiency can be calculated by means of an energy balance. This is done by considering the total fuel energy that enters the cylinder subtracted by the energy from the unburned species that are present in the exhaust and can be calculated by:

$$\eta_c = 1 - \frac{\sum y_i \cdot LHV_i}{\left[\dot{m}_f/\left(\dot{m}_a + \dot{m}_f\right)\right] \cdot LHV_f} \qquad 3.12$$

Where y_i stands for the mass fractions of the different exhaust species that contains heating value greater than zero. During the calculations, only the most common species where used: HC, CO and H_2. This last was approximated as 1/3 of the carbon monoxide molar fraction [26]. The heating value of each specie was obtained from the literature as: CO=10.1 MJ/kg, HC=42.5 MJ/kg, H_2=120 MJ/kg

3.4.1.2 Cantera

Cantera is a 0-D /1-D open source code to perform different Kinects evaluations as the solution of reactive systems as well as the determination of laminar burning velocities, etc. In this investigation Cantera has been applied to solve chemical reaction systems in its simplest form, which are generally known as 0-D reactors. These systems are 0-D domains where the

different conservation equations are solved for the state parameters as well as the chemical species giving a set of boundary conditions. The use of this approach allows to exclude the interaction from flow, wall shear and heat transfer from the Kinects problem itself, allowing to investigate the composition effect of a specific fuel on a reactivity basis and over the dominant reaction paths that governs the oxidation of a fuel molecule. The closed ideal constant volume reactor was chosen to evaluate different situations found during the experimental campaign. Its formulation is mainly based on solving the mass conservation equation for each species and the energy equation which are presented in equation 3.13 and equation 3.14, respectively [27].

$$m\frac{dY_k}{dt} = \sum_{in} \dot{m}_{in}\left(Y_{k,in} - Y_k\right) + \dot{m}_{k,gen} - Y_k\,\dot{m}_{wall} \tag{3.13}$$

$$mc_v\frac{dT}{dt} = -p\frac{dV}{dt} - \dot{Q} + \sum_{in} \dot{m}_{in}\left(h_{in} - \sum_k u_k Y_{k,in}\right) - \frac{pV}{m}\sum_{out}\dot{m}_{out} - \sum_k \dot{m}_{k,gen}u_k \tag{3.14}$$

Where, m stands for the reactor mass, V is the reactor volume, p is the reactor pressure, t is the time, T stands for temperature, Y_k is the mass fraction of each specie, u is the internal energy, h is enthalpy and $\dot{Q}$ is the total heat transfer through an wall. These equations are presented in the expanded form and simplifications are done in the convenient way during the problem setup.

3.4.1.3 Particulate filter submodels

Diesel particulate filter models can be found in different degrees of complexity. Once the DPF evaluation performed in this work aimed to evaluate global effects of DMDF combustion on the DPF performance, a 0-D model proposed by Piqueras el al. [28] was employed. This routine has shown to be able of modelling the different phenomena that takes place on the DPF as filtration, accumulation and regeneration under different steady-state and transient conditions [29]. Because the routine is presented in an in-house code, the simulations were done by means of using the results from GT-Drive as boundary conditions to the model.

3.4.2 GT-suite description

GT-Suite is a simulation tool from Gamma technologies® which addresses the variety of problems found in transportation (road, maritime and aerial). During this research, the packages GT-Power and GT-drive were used to develop flow, chemical simulations and driving cycle evaluations, respectively. In this sense, the following subsections intend to describe each one of them to elucidate the specificities of each package as well as the most significant points to be remarked.

3.4.2.1 GT-Power

This package consists in multi domain approach combining the 1-D discretization of the conservation equations by finite volumes method with 0-D phenomenological model and experimental data to properly describe the engine operation [30]. Generally, these equations are solved explicitly in the time, i.e., considering the solution field from the last iteration during the integration and specifying a proper time step to guarantee solver stability calling the Courant condition [31]. It also allows the modelling of several subsystem as cooling circuits and after treatment by including dedicated submodels. This last was the focus of the simulation campaign performed in

GT-Power, aiming to calibrate a Diesel oxidation catalyst to the proposed combustion concept [32]. The submodels and validation of the DOC are deeply discussed in chapter 5, were the after treatment is discussed in detail.

3.4.2.2 GT-Drive

GT Drive is a dedicated tool for vehicle simulation aiding the development phases by enabling the assessment of multi subsystem as powertrain, vehicle cooling, etc. in driving cycle conditions by means of 0D formulation. This means that there is no space discretization of the differential equations, i.e., they are integrated only with respect to time in an explicit manner. In this work, GT-drive is applied to determine the performance of the proposed engine calibration by assuming that the instantaneous values of performance and emissions values can be assumed as an interpolation of steady-state maps. Different driving conditions as normative, in-service conformity and real driving cycles are assessed. For each condition, an energy balance equation is solved as that presented in equation 3.15 [33].

$$\begin{aligned}\tau_{vehicle} = &\left[I_{trans1} + \frac{I_{trans2}}{R_t^2} + \frac{I_{dsh}}{R_t^2} + \frac{I_{axl}}{(R_d^2)(R_t^2)} + \frac{(M_{veh})(r_{whl}^2)}{(R_d^2)(R_t^2)}\right]\frac{d\omega_{drv}}{dt} \\ &- \left[\frac{I_{trans2}}{R_t^3} + \frac{I_{dsh}}{R_t^3} + \frac{I_{axl}}{(R_d^2)(R_t^3)} + \frac{(M_{veh})(r_{whl}^2)}{(R_d^2)(R_t^3)}\right]\omega_{drv}\frac{dR_t}{dt} \\ &+ \left[\frac{F_{aer} + F_{rol} + F_{grd}}{R_d R_t}\right] r_{whl}\end{aligned} \qquad 3.15$$

In Equation 3.15, I_{trans1} and I_{trans2} accounts for the inertia in the input and output of the transmission while I_{dsh} and I_{axl} represents the driveshaft and axle moment of inertia. Next, R_d and R_t comprehends the final drive and transmission ratio for each gear. Wheel speed, herein defined as ω, is directly related to the wheel radius (r_{whl}) and vehicle mass (M_{veh}) for each instant of time (t). Finally, aerodynamic forces (F_{aer}), rolling resistance forces (F_{rol}) and gravity forces (F_{grd}) are included in the last part of the equation.

3.5 Experimental and numerical methodologies

This last section has as aim to present the different methodologies that are used in both experimental evaluation and simulation. More specific methodologies that are used only in short campaigns are described in the correspondent chapters.

3.5.1 Calibration Methodology

Through the years, with the development of the electronic devices, the adjustment of settings to obtain the required output of the engine (i.e., calibration) become more complex. In the beginning, a few parameters could be adjusted, like the injection timing in diesel engines or carburetor nozzles and spark advance for SI engines. Nowadays, besides the ignition and injection maps, the electronic control units have a vast number of correction maps to deal with the different situations that can be found during the engine operation.

In the DMDF combustion concept, the use of two different fuels injected separately requires two independent injection maps for each one of them. The air management settings like inlet and exhaust pressure and the injection pressures should be also determined. Nonetheless, from the formal definition of the word calibration, a target/output should exist to justify the calibration process. In the case of an engine calibration, one desires always to obtain the maximum efficiency while minimizing the emissions under determined constraint, e.g., mechanical limitations. In this context, a calibration procedure was defined to obtain the final operating maps in the multi-cylinder engine platform. It should be bore in mind that nowadays automated calibration processes in platforms are a more effective way of obtaining the best calibration settings. The calibration process here presented tries to approximate to the best settings solution, nonetheless, it has limitations regarding the number of settings combinations that should be tested. Despite of its limitations, it is worth to remind that manual

calibration can be also safer for this novelty combustion concept as calibration rules needs to be developed.

The calibration methodology employed is based on an iterative method where different settings are adjusted under determined constraints. The first step of this routine is presented in Figure 3.7 and has as aim to obtain the desired engine load at dual fuel combustion fulfilling the mechanical constraints of the engine: 15 bar/CAD of PRR, 185 bar of in-cylinder pressure. In addition, a maximum COV_{IMEP} of 4 % is respected for all operating conditions.

First, the engine is started in a CDC operating condition at a low load. Gasoline is steeply increased aiming the target load (as there is no strict rule regarding the best gasoline fraction to be used, the calibration assumes that the higher the GF value, better should be the results since higher GF means high premixing which delivers lower NOx and soot emissions. This assumption is retested during the calibration). If the pressure and/or pressure gradient are exceeded, the SoI of both injections is delayed. In the case of not being enough, the premixing degree is reduced. This premixing degree reduction is here defined as the SoI delay coupled with the reduction of the gasoline fraction. Once the load is achieved, the combustion variability is assessed. If the value is higher than 4 %, a low GF value is used, and the routine is performed again until fulfilling all the constraints.

The next step has as goal to obtain EUVI compliant emissions in which regards NOx with soot values lower than 0.01g/kWh by adjusting injection and air management settings. As it is presented in Figure 3.8, four different scenarios can be achieved during the first calibration steps: (1) EUVI fulfillment of NOx and Soot lower than 0.01g/kWh, (2) higher NOx than EUVI, (3) soot exceeding the 0.01g/kWh threshold and (4) both emissions exceeding the targets (NOx higher than EUVI and soot higher than 0.01g/kWh). Different strategies are developed according to each one of these scenarios except in the case of already fulfilling NOx and soot targets. For the first non-compliant scenario strategies that allow to reduce NOx should

be employed. Therefore, both higher EGR levels as well as delayed SoI can be employed to reduce the in-cylinder temperature and decrease the NOx formation.

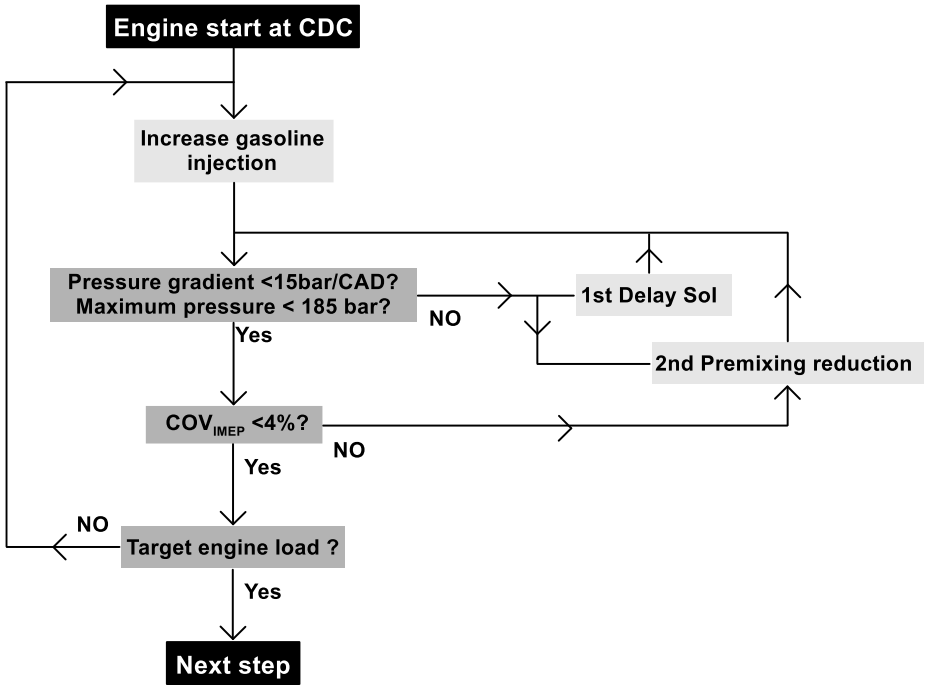

Figure 3.7. Schematic description of the first stage of the calibration methodology which aims to achieve the desired engine load under Dual-Mode Dual-Fuel combustion.

The second non-compliant scenario requires strategies that aim to increase both the oxygen content and the premixing time of the high reactivity fuel. The main strategies are: decrease the EGR concentration, increase oxygen content by means of higher boost pressure and using early SoIs. In addition to this, higher injection pressure can be also used to improve the fuel mixing. Last, both NOx and soot can be higher than the defined constraints. In this case, generally, the strategies employed have a negative impact on fuel consumption. For example, the increase of the injection pressure and closed VGT position can increase the auxiliary and the pumping

losses respectively. Nonetheless, this is required to reduce the soot at levels in which higher EGR can be used to reduce the NOx emissions. It is important to remark that despite the strategies previously defined, there are conditions where it is not possible to achieve the proposed constraints. These conditions are generally found at high load operation where a triplet exists: excessive NOx and soot coupled with high pressure gradients. In these cases, the second step of the optimization routine aims to reduce the emission levels as much as possible. Detailed description of these cases will be provided in the calibration results chapter.

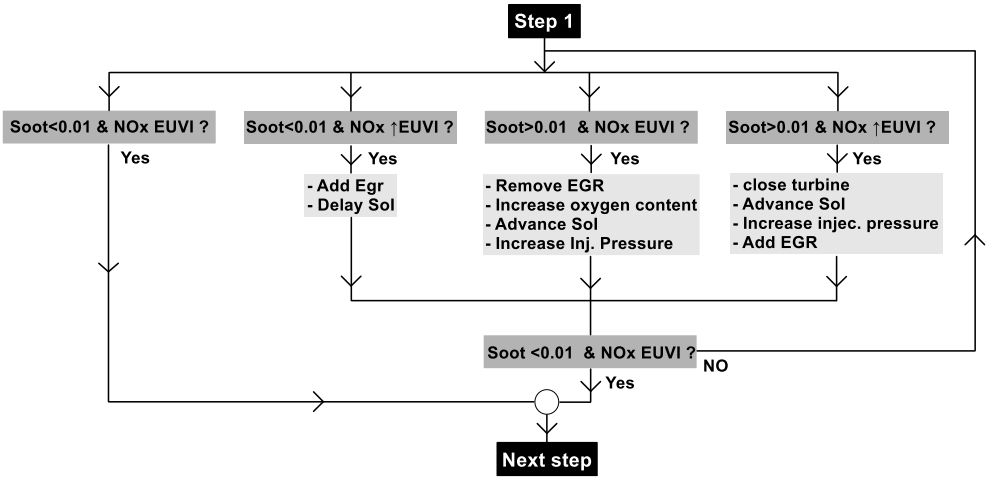

Figure 3.8. Schematic description of the second stage of the calibration methodology which aims to minimize the emissions of NOx and soot under specific constraints.

Finally, the last phase intents to optimize the fuel consumption values by adjusting the injection settings and the EGR levels. Figure 3.9 depicts a scheme of the different optimization subroutines that are employed. The application of each subroutine is straightforward. Different sweeps are made in each one of the subroutines and the final impact of each iteration on torque is assessed. The loop is exited if the torque does not show any benefit compared to the previous steps. It should be bear in mind that the modifications in each one of the settings are in a narrow range since the NOx

and soot emissions should be maintained under the constraints defined in step 2 while optimizing the BSFC.

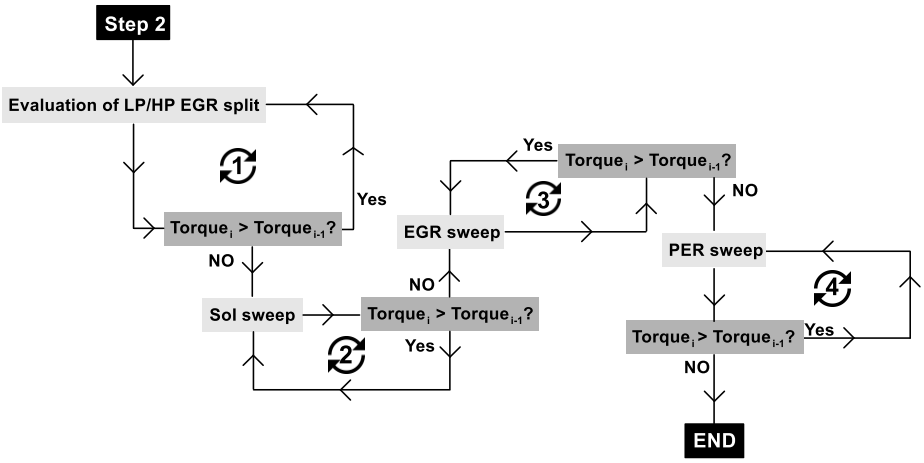

Figure 3.9. Schematic description of the third stage of the calibration methodology intending to realize the optimum fuel consumption values for each operating condition.

Figure 3.10 summarizes the main steps of the optimization routine previously described. It is interesting to note that an additional step is present here: at the final of the three steps a new starting GF is proposed. This is recommended to avoid choosing a local optimum as the final calibration set. In addition, this is also required to confirm the assumption used in step 1 that higher GF should provide better results in terms of efficiency and emissions.

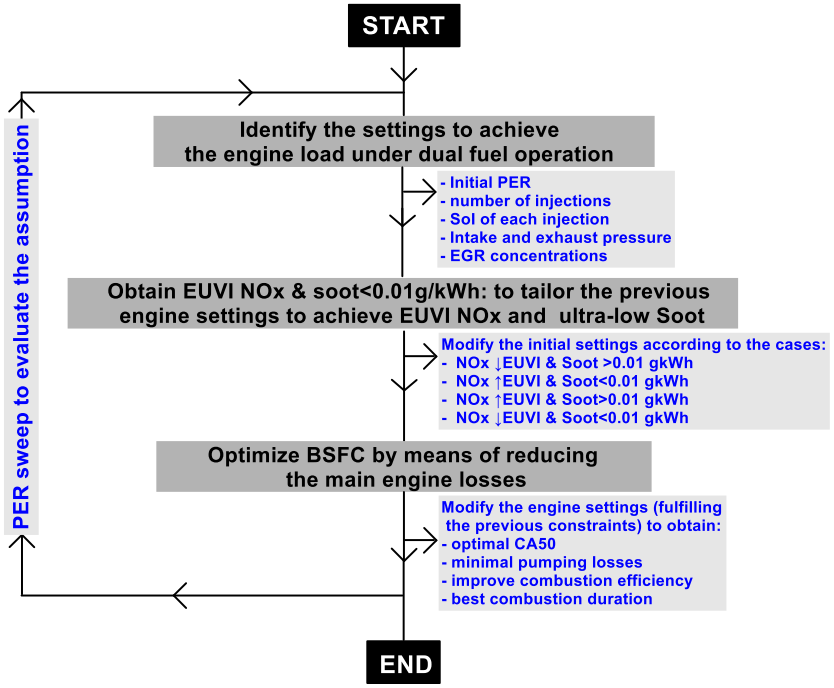

Figure 3.10. Summary of the steps followed during the calibration methodology.

3.5.2 Vehicle model and driving cycle assessment methodology

The implementation of a new technology in a real platform requires a TRL 9. This means that the subsystems, controls, sensors and trials are already done. Unfortunately, reaching this level of readiness is time and money consuming. Nonetheless, despite of being in lower TRL, the potential of the concept can be proved to some extent by means of the technology emulation in a virtual platform. Among the different software to perform this task, GT-drive stands as a leading market option. The vast number of tools and templates ready to be used together with the user-friendly interface allows to model complex systems in a reduced time. Therefore, this software was employed to perform the evaluation of the developed concept and asses

the advantages and drawbacks of using the DMDF combustion mode in a truck application. The section that follows describes the characteristics of the truck used during the evaluation, its configuration in GT-drive and the map-based evaluation methodology.

3.5.2.1 Truck characteristics

As discussed in the beginning of the chapter, the engine evaluated in this research equips a wide range of trucks from different OEMs (VOLVO and Renault). Each model has its peculiarities regarding structure, geometry and assembling. As the modelling and validation of all trucks is time consuming and there is no significant contribution to the archival nature of the study, a single model was chosen based in the experimental data provided by the OEM. Table 3.8 summarizes the characteristics of the VOLVO FE 350 truck. Additional details can be also evidenced in Figure 3.11.

Table 3.8. Aerodynamic and geometric characteristics of the VOLVO FE 350 truck.

Truck characteristics	
Engine	MD8 350K
Vehicle weight [kg]	7035
Max. payload [kg]	17965
vehicle frontal Area [m^2]	6.9
Vehicle Wheelbase [m]	4.4
Rolling friction [-]	0.0155
Drag coefficient [-]	0.65
Tires specification	295/80R/22.5”
Gear box models	ZF 6AP1400B SP4[1]
	AMT 2412f[2]
Differential drive ratio	5.29 for ZF
	3.36 for AMT

The truck is commercialized in different versions which differ in terms of the truck applicability. One of the most significant variations is the gear box model used in each model. Some of the cycles used for model calibration are based on the manual gearbox while others use the automatic one. In this sense, both gearboxes were introduced in the model allowing to modify it as always as needed. The characteristics of each one are presented in Table 3.9.

Table 3.9. Characteristics of the automatic gearbox AT2412F and the manual ZF 6AP1400B SP4.

AT2412F		ZF 6AP1400B SP4	
Gear	Gear ratio	Gear	Gear ratio
F1	14.94	1H	7.80
F2	11.73	1	3.36
F3	9.04	2	1.91
F4	7.10	3	1.42
F5	5.54	4	1.00
F6	4.35	5	0.72
F7	3.44	6	0.62
F8	2.70	R	9.86
F9	2.08		
F10	1.63		
F11	1.27		
F12	1.00		
R	17.48		

The data herein identified is of utmost importance to represent the real truck behavior in GT-drive. The characterization of the different templates according to these data is detailed in the next subsection.

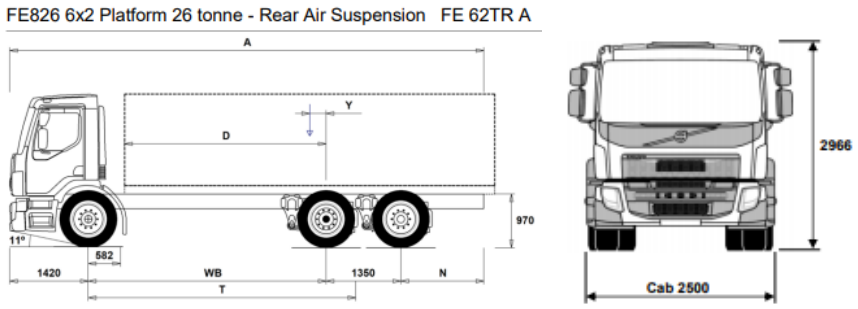

Figure 3.11. Geometrical characteristics of VOLVO FE 350K, illustrating the wheelbase (WB), disposition of the different axis as well as the cabin dimensions.

3.5.2.2 Final model and evaluation methodology

Based on the previous discussion and using the data that was detailed, a complete GT drive model of the truck to be investigated was developed. Figure 3.12 represents the final model with the respective general subassemblies.

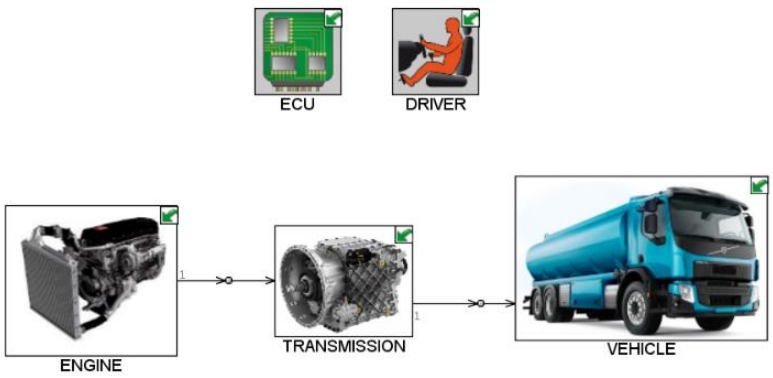

Figure 3.12. Overview of the final model developed in GT-drive to enable the simulation of the FE350K truck.

Each one of them are a set of submodels that are coupled allowing to realize different configurations. To exemplify, the transmission subassembly will be analyzed. As it can be seen in Figure 3.13, this subassembly is composed by the gear box, clutch and inertia axes models. This set of objects can describe the different phenomena that occurs at the transmission during the vehicle operation as slip, inertial resistance, gear transition time, etc.

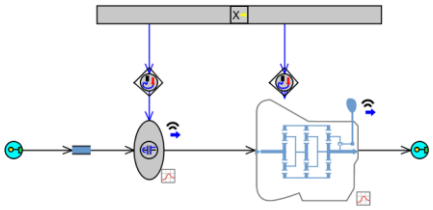

Figure 3.13. Transmission subassembly illustrating the different components that constitutes the transmission setup as clutch, gearbox and signal connections.

Another important subassembly is the vehicle part in which the information about the truck geometry is inserted, for example, cabin, axle, chassis and tires. The aerodynamic factors are also included in this subassembly as well as the main axle properties. Finally, environment as wind velocity and the road properties, like elevation are set in this subassembly. Figure 3.14 presents the configuration of the truck used in this work.

The last subassembly comprehends the engine modelling being depicted in Figure 3.15. This subassembly requires the complete characterization of geometrical characteristics like engine displacement as well as the description of idle conditions, engine starter speed, etc. Moreover, it includes the complete description of the performance, operation and emissions characteristics of the steady-state maps. Operation maps here are defined as the maps of friction mean effective power and brake mean effective power that are required to calculate the friction losses and the total power that can be delivered by the engine given a specific engine speed.

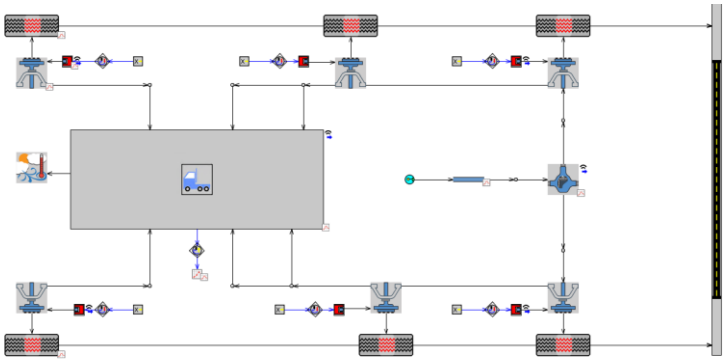

Figure 3.14. Vehicle subassembly depicting the different subsystem that are included in the simulation as tires, axles, environment, etc.

The calculation routine is based on solving equation 3.15, allowing to specify what should be the required engine torque to move the vehicle at a given velocity. Moreover, this velocity will dictate the required engine speed once it passes through the transmission and differential. This pair reaches the engine subassembly where torque is converted to BMEP by means of the displaced volume, while engine speed has its units in rpm.

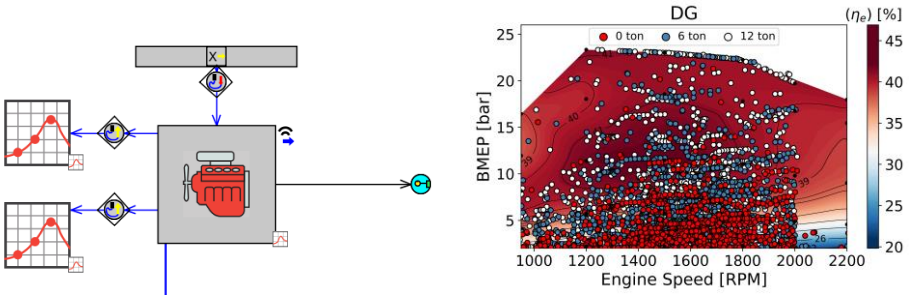

(a) (b)

Figure 3.15. Illustration of (a) engine subassembly (b) operating points distribution inside the efficiency map for the world harmonized vehicle cycle (WHVC).

With these values, the solver searches on the brake specific fuel consumption and emission maps what should be the interpolated values of

each one of the parameters. This will provide a rate of production for them that can be integrated over time to realize a cumulative profile. Figure 3.15 (b) illustrates the scatter operating points distribution on a WHVC driving cycle. Each of these points has its own production rates for the aforementioned parameters which at the end of the cycle will be integrated and normalized to deliver different metrics to assess the driving cycle performance.

3.6 Summary and conclusions

In this chapter the different experimental and numerical tools that are used to develop this investigation were detailed. At a first instance, the experimental setup was described evidencing the characteristics of the multi-cylinder engine, test cell facility and the instrumentation that is used to obtain the required information to assess the combustion process as well as the performance and emissions. Then, the numerical tools were introduced divided in 0-D simulation codes and 1-D routines that complement the study in both fundamental understanding of the chemical processes involved and the overview of the proposed calibration applied to a commercial truck. Finally, the most recurrent methodologies that were applied in the investigation are detailed focusing on the calibration methodology that was developed and on the driving cycle assessment approach.

3.7 Bibliography

[1] Benajes J., García A., Monsalve-Serrano J., Boronat V. "Achieving clean and efficient engine operation up to full load by combining optimized RCCI and dual-fuel diesel-gasoline combustion strategies". *Energy Conversion and Management,* Vol. 136, pp. 142–151, 2017.

[2] VOLVO trucks. Powertrain specification of VOLVO FE truck. Available in https://www.volvotrucks.es/es-es/trucks/trucks/volvo-fe/specifications/powertrain.html.

[3] Boronat Colomer V. *Dual-Fuel Dual-Mode combustion strategy to achieve high thermal efficiency, low NOx and smoke emissions in compression ignition engines.* Doctoral Thesis, Universitat Politécnica de València, Departamento de Máquinas y Motores Térmicos, 2018.

[4] Serrano J.R., Piqueras P., Angiolini E., Meano C., De La Morena J.. "On Cooler and Mixing Condensation Phenomena in the Long-Route Exhaust Gas Recirculation Line". *SAE Technical Papers,* n° 2015-24-2521, 2015.

[5] VOLVO trucks. VOLVO D8K Engine. https://www.volvo trucks.com.au/en-au/trucks/volvo-fe/features/d8k- engine. html#, acessed in July 2020.

[6] Payri F. and Desantes J.M. Motores de combustion interna alternativos. *Editorial Reverté*, 2011.

[7] KISTLER, PiezoStar ® Pressure Sensor kistler 6125C, Datasheet. (2013) 1–4.

[8] AVL 733S fuel balance. Technical information available at http://www.avl.com.

[9] Landau H.J. "Sampling, Data Transmission, and the Nyquist Rate". *Proceedings of IEEE*, Vol. 55, pp. 1701–1706, 1967.

[10] Dinh T.V., Choi I.Y., Son Y.S., Kim J.C. "A review on non-dispersive infrared gas sensors: Improvement of sensor detection limit and

interference correction". *Sensors and Actuators B: Chemical,* Vol. 231, pp- 529–538, 2016.

[11] Tsai C.L., Fann C.S., Wang S.H., Fung R.F. "Paramagnetic oxygen measurement using an optical-fiber microphone". *Sensors and Actuators B: Chemical,* Vol. 73 pp. 211–215, 2001.

[12] Collier T., Gregory D., Rushton M., Hands T. "Investigation into the performance of an ultra-fast response NO analyser equipped with a NO2 to NO converter for gasoline and diesel exhaust NOx measurements". *SAE Technical Papers,* n° 2000-01-2954, 2000.

[13] Holm T. "Aspects of the mechanism of the flame ionization detector". *Journal of Chromatography A*, Vol. 842, pp. 221–227, 1999.

[14] U. Nations, UNECE Regulation 49, 2013.

[15] Silvis W.M. "An algorithm for calculating the air/fuel ratio from exhaust emissions". *SAE Technical Papers,* n° 970514, 1997.

[16] Smith B.C., Fundamentals of Fourier Transform Infrared Spectroscopy, 2011.

[17] AVL. *Smoke Value Measurements with the Filter-Paper-Method*, 2005.

[18] Northrop W.F., Bohac S. V., Chin J.Y., Assanis D.N. "Comparison of filter smoke number and elemental carbon mass from partially premixed low temperature combustion in a direct-injection diesel engine". *Journal of Engineering for Gas Turbines Power,* Vol. 133, 2011.

[19] Benajes J., García A., Monsalve-Serrano J., Boronat V. "Gaseous emissions and particle size distribution of dual-mode dual-fuel diesel-gasoline concept from low to full load". *Applied. Thermal. Engineering,* Vol. 120, pp. 138–149, 2016.

[20] Morgan N., Smallbone A., Bhave A., Kraft M., Cracknell R., Kalghatgi G. "Mapping surrogate gasoline compositions into RON/MON space". *Combustion and Flame,* Vol. 157, pp. 1122–1131, 2010.

[21] Liu C.M., Sandhu N.K., McCoy S.T., Bergerson J.A. "A life cycle assessment of greenhouse gas emissions from direct air capture and Fischer-Tropsch fuel production". *Sustainable Energy and Fuels*, Vol. 4, pp. 3129–3142, 2020.

[22] Burre J., Bongartz D., Mitsos A. "Production of Oxymethylene Dimethyl Ethers from Hydrogen and Carbon Dioxide - Part II: Modeling and Analysis for OME3-5". *Industrial and Engineering Chemistry Research,* Vol. 58, pp. 5567–5578, 2019.

[23] Payri F., Olmeda P., Martín J., García., A. "A complete 0D thermodynamic predictive model for direct injection diesel engines". *Applied Energy,* Vol. 88 pp. 4632–4641, 2011.

[24] Lapuerta M., Ballesteros R., Agudelo J.R. "Effect of the gas state equation on the thermodynamic diagnostic of diesel combustion". *Applied Thermal Engineering,* Vol. 26, pp. 1492–1499, 2006.

[25] Martín J. *Aportación al diagnóstico de la combustión en motores Diesel de inyección directa.* Docctoral Thesis, Universitat Politécnica de València, Departamento de Máquinas y Motores Térmicos, 2007.

[26] Heywood J. B. *Internal Combustion Engine Fundamentals.* New York: McGraw-Hill, 1988.

[27] Cantera userguide. Available at https://cantera.org/ science/reactors. Html.

[28] Payri F., Arnau F.J., Piqueras P., Ruiz M.J., Lumped Approach for Flow-Through and Wall-Flow Monolithic Reactors Modelling for Real-Time Automotive Applications, *SAE Technical Papers,* n° 2018-01-0954, 2018.

[29] Macián V., Serrano J.R., Piqueras P., Sanchis E.J. "Internal pore diffusion and adsorption impact on the soot oxidation in wall-flow particulate filters". *Energy*, Vol. 179, pp. 407–421, 2019

[30] Gamma Technologies. *Engine Performance Application Manual*, 2016.

[31] Gamma Technologies. *Flow Theory Manual*, 2016.

[32] Gamma Technologies. *Aftertreatment manual*, 2016.

[33] Gamma Technologies, Vehicle Driveline and HEV application manual, 2016.

Chapter 4

Engine calibration under DMDF combustion and driving cycle assessment

Content

4.1 Introduction

From the previous literature review, it could be inferred that the Dual-Mode Dual-Fuel combustion is a pathway to realize ultra-low NOx and soot emissions while achieving diesel like conversion efficiencies. Despite these clear benefits, some possible hurdles that could be found in applying this concept in real platforms were identified. Since the SCE facilities rely on external devices to emulate the effects of real devices (e.g. turbocharger) and provide the required amount of air and EGR, those boundary conditions seem to be not easy to be obtained with real air management devices. The extension of those boundary conditions to real applications can be limited by the mechanical and thermodynamic constraints as maximum pressure and the limiting amount of the energy in the flow. In this sense, the results from both platforms (SCE and MCE) can differ, requiring a proper assessment of the potential of the concept considering the use of a stock hardware.

Therefore, this chapter aims to describe the calibration process of a stock multi-cylinder engine operating under DMDF combustion concept employing commercial gasoline and diesel as LRF and HRF, respectively. As described in previous chapters, a few modifications of the original setup of the engine were made to enable the operation in this combustion regime. The combustion, performance and emissions maps obtained in the calibration process are presented and discussed. Next, these results are used as inputs in a truck model developed in GT-Drive to evaluate the potential of this concept in replacing the original diesel engine under normative and real driving conditions. Finally, the main conclusions from both steady-state and transient analysis are drawn allowing to evidence the benefits and drawbacks that are found when the DMDF concept is extended to a real engine platform.

4.2 Steady-state engine calibration under DMDF combustion

The aim of this subsection is to present the calibration settings and the final performance and emission maps resultant from applying the methodology described in section 3.5.1. Initially, the calibration was intended to be performed at 30 different operating conditions (6 engine speeds and 5 engine loads) as depicted in Figure 4.1. As it can be seen, the brake power output of the engine was translated to engine load percentage, which is an indicative of the pedal position. Next, this pedal position was refereed to BMEP as this is a more direct measure of the engine load to target at the calibration. For each operating condition, the optimization routine was applied aiming at optimizing the engine settings for the DMDF combustion concept under the pre-defined constraints. Eventually, additional operating conditions are included in transition zones to refine the limit definition of each combustion mode.

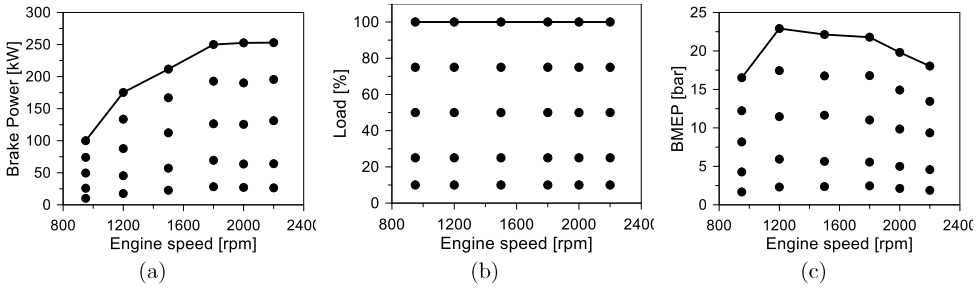

Figure 4.1. Operating conditions to be calibrated inside the power output maps in terms of (a) engine brake power, (b) engine load and (c) brake mean effective pressure.

First, the maps containing the most relevant engine settings are presented. Second, the performance maps such as brake specific fuel consumption (SFC), gross indicated efficiency (GIE) combustion efficiency (η_C) as well as combustion metrics (combustion duration, CA50, etc.) are depicted and discussed. Finally, the different pollutant results are presented followed by an analysis of the main findings. From now on, the dark dots are

representations of the experimental conditions while the surface maps are a spline interpolation of the experimental results.

4.2.1. Engine settings: injection and air management

As previously described in the calibration methodology, the main settings that were adjusted during the process can be summarized as EGR, GF and injection settings (SOI and TOI). In addition to this, air management settings were also adjusted to obtain the minimum pumping losses for each operating condition while providing the required air and EGR. The results for each one of these parameters are presented in the next subsections.

4.2.1.1. Injection settings: SoI, ToI, GF and injection pressure

The reactivity stratification inside the cylinder is one of the most important features of the DMDF combustion that allows it to operate in a fully premixed combustion while having smoother heat release rates than conventional single fuel LTCs [1]. This is accomplished by injecting two fuels with different reactivity (LRF and HRF) at different timings. The low reactivity fuel is always injected at -340 CAD aTDC which was demonstrated to be the optimum timing in previous researches in this platform [2]. By contrast, the injection of the high reactivity fuel needs to be calibrated to obtain the best values of fuel consumption while maintaining the emissions values under the desired constraints. Figure 1 presents the values of injection timing (a) and duration (b) obtained for the pilot injection.

The pilot injection is generally set to early times during the compression stroke and has as main role the creation of a first reactivity stratification, conditioning the mixture near to the squish zone to assure a proper oxidation at this region. By crossing the information of the two graphs (Figure 4.2 (a) and Figure 4.2 (b)) it is possible to verify that the pilot injection is not used at high loads, medium to high speed conditions in the final calibration. This will be furtherly discussed in the next subsections. Nonetheless, it can be

advanced that the main justification relies on the mechanical (↑ in-cylinder pressure) and emissions constraints (↑soot) that cannot be fulfilled when double injection strategy is used at these conditions. It can also be inferred that the pilot injection durations do not exceed 1000 µs and generally happens from -15 to -50 CAD aTDC. At low engine speeds, the pilot injection is also used for high load conditions to improve combustion stability and reduce the amount of unburned HC and CO.

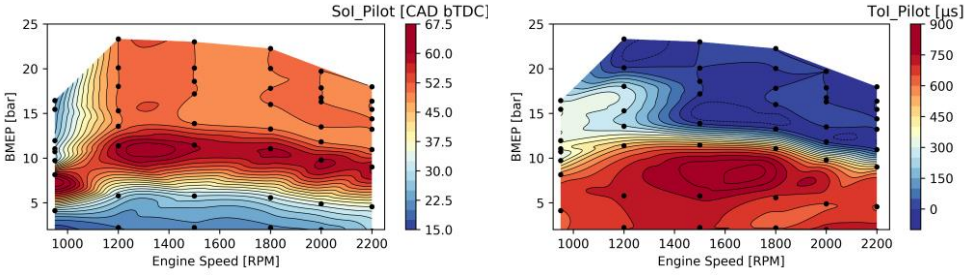

(a) (b)

Figure 4.2. Iso-surface maps depicting the (a) Start of injection and (b) injection duration of the pilot injection for the complete engine map.

From low to medium load, the pilot and main injections (Figure 4.3) are present at the same time to enable a fully premixed combustion. The analysis of the injection timing of the main injection allows to understand the strategy that should be used at each zone of the calibration map. Starting from low loads, both pilot and main injections are placed in the last 40 degrees of the compression stroke. This allows to inject the fuel in conditions with higher pressure and temperature, reducing the unburned components at the exhaust. Moreover, at 10 % of the engine load (first row of black dots), the combustion relies on only diesel combustion (GF=0, see Figure 4.4 (a)) as any gasoline injection is directly converted to unburned products due to the improper conditions to the oxidation of a low reactivity fuel (poor ignition quality). As the load is increased, and so is the pressure and temperature, early injection timings can be employed (≈-60 aTDC). This produces a fully premixed combustion which supports high gasoline fraction levels. From medium to high load, the use of premixed combustion results in excessive

pressure gradients because of the high amount of energy released in a short period of time. Therefore, the injection strategy must be modified aiming a higher compositional stratification which allows to increase the engine load towards full load operation. This modification was accomplished by delaying the injection timing towards the expansion stroke and removing the pilot injection resulting in a dual fuel diffusive combustion. Moreover, the GF values were consistently decreased to reduce mechanical demand (pressure gradients).

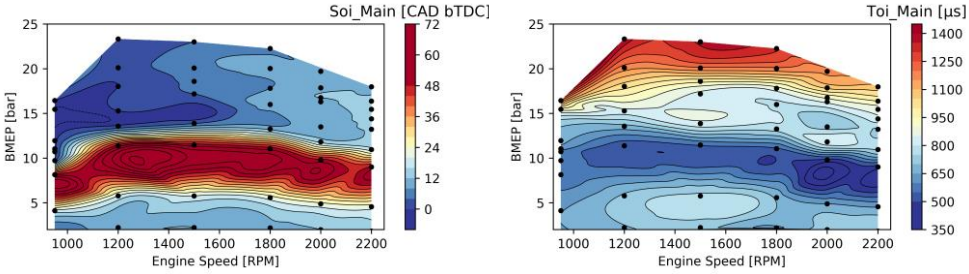

(a) (b)

Figure 4.3. Iso-surface maps depicting (a) start of injection and (b) injection duration of the main injection for the complete engine map.

The reduction of the GF required an energy compensation by the DI system. Therefore, the injection durations have been extended reaching values up to 1400 µs. Unfortunately, these long injections are prone to produce soot as the amount of locally rich mixtures is increased. In addition, the high EGR levels decrease the oxygen availability contributing to the soot production. To minimize this, high injection pressures were employed at the cost of increasing the parasite power losses. Even in this case, the air management system configuration was not able to provide the required amount of oxygen to achieve EUVI limits in all the operating map. Some of the main operating parameters of the air system will be discussed in the next subsection, together with the problems that were verified during the calibration process.

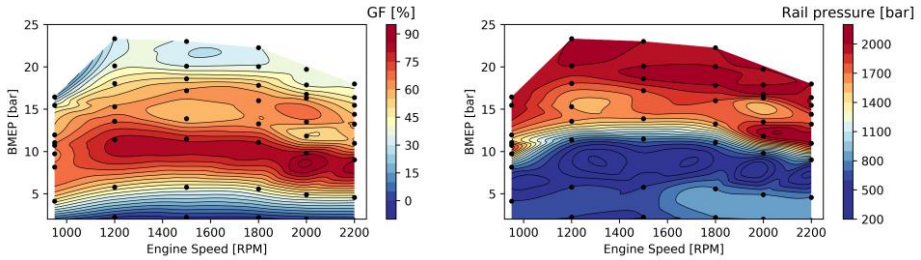

(a) (b)

Figure 4.4. Iso-surface maps depicting (a) gasoline fraction and (b) rail pressure values employed in the calibration map.

4.2.1.2. Air management settings

Low temperature combustion techniques are generally based on high dilution levels as a path to control the reaction rates and consequently the rate of heat released during the combustion [3]. The SCE results from Boronat [2] have suggested that a proper DMDF combustion should be obtained if both oxygen content and EGR rates are maintained over the full calibration map. This was pointed as a challenge for the air management system and the implications of trying to replicate this approach in a multi-cylinder engine are herein discussed. As it can be seen in Figure 4.5 (a), from low to medium load the EGR levels are always higher than 30 %, independently on the engine speed. Therefore, a proper premixed combustion can be achieved by combining the early injections and high GF presented in section 4.2.1.1 with high EGR levels. Nonetheless, this strategy cannot be extended as the load is increased, since the pressure gradients exceeds the proposed mechanical constraint. Therefore, the GF starts to be steeply decreased and the diesel energy starts to be more relevant. In addition to this, the injection timings are modified to values closer to the TDC. By doing this, the pressure gradient problem can be solved. As a side effect, the strategy now is prone to produce soot as the combustion tends to be less premixed (i.e., more diffusive) and the A/F ratios are close to the stoichiometric as presented in Figure 4.5 (b). In this sense, the air management settings must be modified to increase the fresh air mass in the

cylinder. The most important modifications rely on the decrease of the EGR levels (Figure 4.5a) and increase of boost pressure (Figure 4.6a).

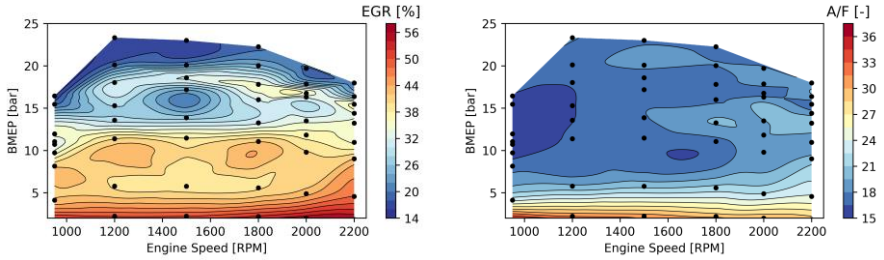

(a) (b)

Figure 4.5. Iso-surface maps depicting (a) EGR concentration and (b) air-to-fuel ratio for the complete engine map.

With these modifications, the oxygen concentration can be maintained at levels where the partial soot oxidation is achieved. Nonetheless, the increase of boost pressure demonstrated in Figure 4.6 (a) means that the VGT should be closed, increasing the pumping losses. Moreover, the low temperatures from the LTC combustion and the requirements of boost pressure imply critical conditions at the VGT inlet, where the turbine inlet pressure values start to be higher than 3.5 bar as it can be seen in Figure 4.6 (b) (the maximum recommended value is 3.8 bar at turbine inlet due mechanical reasons). Once this condition is achieved, the VGT exploration was limited, requiring a new strategy to continue increasing the load.

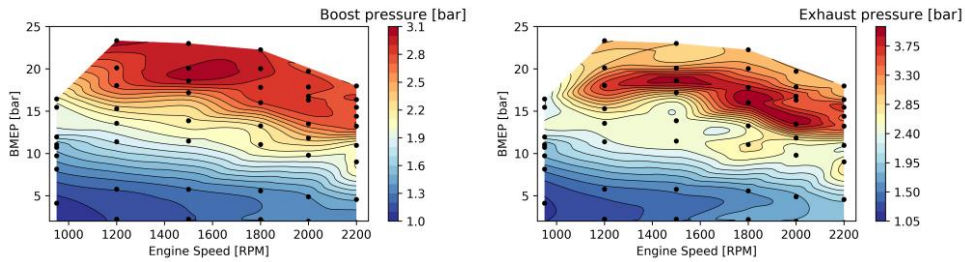

(a) (b)

Figure 4.6. Iso-surface maps depicting (a) Boost pressure and (b) exhaust pressure/turbine inlet pressure for the complete engine map.

At this point, the combustion strategy is based on a partially premixed combustion and the turbine is working at its maximum allowable inlet pressure, with almost stoichiometric conditions and excessive pressure rise rates. To continue increasing the load under partially premixed combustion, both EGR and oxygen should be increased. Nonetheless, higher HP EGR should reduce the mass flow through the turbine, decreasing the inlet pressure. An option should be the increase of LP EGR, which could maintain the energy in the turbine. However, as it is depicted in Figure 4.7, the compressor is also operating at its maximum allowable temperature (≈200°C) which prevents the increase of the low pressure EGR amounts as well as the fresh air flow. Consequently, the direct conclusion is that the engine hardware is at its limiting conditions. To solve this, the combustion strategy should be modified to a dual fuel diffusive combustion with low GF levels, single injection and delayed SoI, close to or after the TDC fire as previously discussed. It is implicit that, in these cases, the air management system is not able to provide the required amount of EGR and air to achieve EUVI limits. Therefore, the calibration limits were relaxed to values higher than the EUVI normative to allow obtaining full load operation.

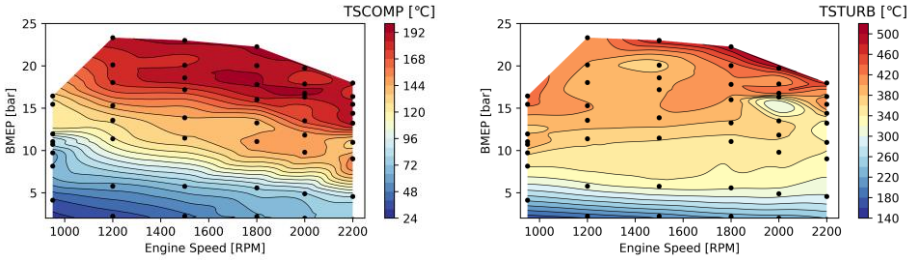

(a) (b)

Figure 4.7. Iso-surface maps depicting (a) compressor outlet and (b) turbine outlet (b) temperature for the whole calibration map.

As it was demonstrated by these two first subsections, the implementation of the DMDF concept on a real platform presented significant hurdles. Unfortunately, at high engine loads, the air management system was not able to provide the required boundary conditions that were proposed from the SCE evaluations. Therefore, the full load operation was

achieved by low GF (around 30 %) and low EGR levels (around 20 %). This may have significant influence in the performance and emissions values of the final calibration. The next subsection will detail the final calibration results of some of the most relevant performance, emission, and combustion parameters.

4.2.2. Performance analysis: efficiency, combustion, and main energy losses of the DMDF calibration

The conversion of the fuel energy into work under determined constraints is the task that one wants to optimize during a calibration process. The quantitative evaluation of this can be done by the fuel consumption and efficiency parameters. As discussed, they can be presented in both indicated and brake basis, having as difference that the brake values consider the losses that are presented up to the work deliver output. In this sense, this section describes the indicated results obtained, the losses that result from the different sources and the final brake parameters in which regards the engine performance.

Figure 4.8 (a) presents the indicated fuel consumption and indicated efficiency results obtained for the final calibration settings. As it can be seen, most of the fuel consumption values are lower than 200 g/kWh. Moreover, the medium load zone presents the best ISFC values. In these operating range, a fully premixed combustion can be used, resulting in a fast combustion process as it can be verified in Figure 4.9 (a), decreasing the heat losses [4]. This volumetric combustion is highly efficient as it can provide most of the fuel energy in a short period of time and at the best phasing (see Figure 4.9 (b)), even though, most of the calibration map presents indicated efficiency higher than 40 %.

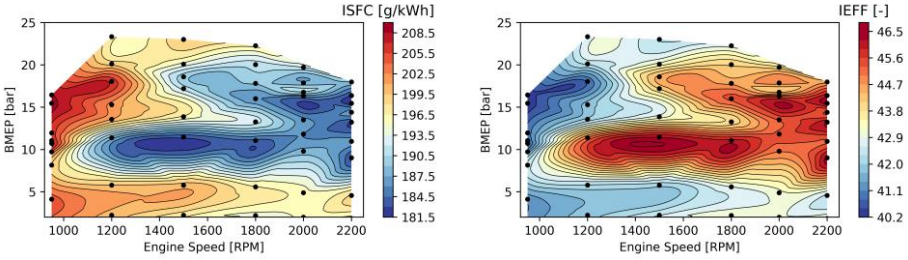

(a) (b)

Figure 4.8. Iso-surface maps depicting (a) gross indicated specific fuel consumption and (b) gross indicated efficiency obtained for the complete engine map.

Once the combustion mode is modified to a diffusive one, the combustion duration starts to increase, providing more time for heat transfer losses. This can be visualized in Figure 4.9 (a) where the values of combustion duration for medium to high load increases by a factor of three. Generally, the diffusive conditions (80 % to full load) present combustion duration up to 30 CAD enhancing the heat transfer process. In addition, the combustion phasing must be delayed maintaining the pressure gradients levels under the limiting value of 15 bar/CAD. This constraint is one of the most difficult to realize as the fast heat release has as consequence a rapid increase in the in-cylinder pressure. As it can be seen in Figure 4.10 (a), most of the medium to high load zone presents cycle average pressure gradients higher than 10 bar/CAD.

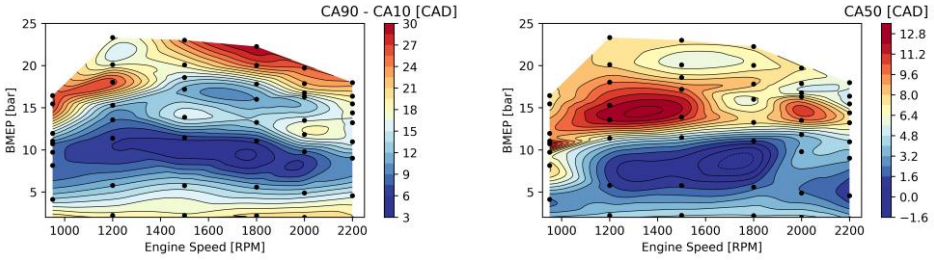

(a) (b)

Figure 4.9. Iso-surface maps depicting (a) combustion duration and (b) combustion phasing obtained for the complete engine map.

It is interesting to note that the maximum pressure gradient values do not happen at full load operation. As it is depicted, they are found mainly at medium to high load, where the combustion presents high gasoline fraction values and consequently a high degree of premixing. In the case of high to full loads, the use of lower GF and the diffusive combustion enlarges the combustion duration reducing the maximum pressure gradients. Figure 4.10 (b) depicts the maximum in-cylinder pressure values. This parameter is an additional mechanical constraint employed during the calibration as discussed in the methodology section. As it can be seen, the maximum pressures achieved at the fully premixed zone do not exceed the limiting value of 185 bar. Nonetheless, as the load is increased, the in-cylinder pressure is steeply increased to around 160 bar. At these conditions, small modifications in the engine settings as SoI modifications can result in surpassing the maximum pressure values.

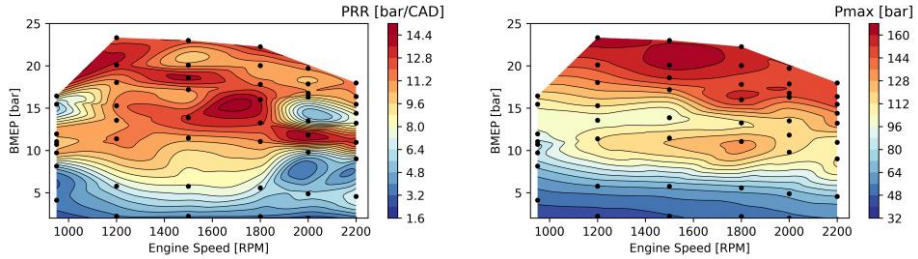

(a) (b)

Figure 4.10. Iso-surface maps depicting Pressure rise rate (a) and maximum in-cylinder pressure for the complete engine map.

During the calibration process, different settings should be adjusted to guarantee the minimum losses for each operating condition, maximizing the work output. Different mechanisms are responsible to impair the fuel conversion and work delivery. For example, the fuel can be only partially burned because of the reaction inhibitions due to low temperatures or cold walls. This means a direct reduction in the combustion efficiency. In addition, the work delivery is affected by different losses that can be related to the heat transfer, pumping losses and additional energy requirements to run

auxiliary devices (e.g. the injection system). For these reasons, a complete evaluation of each one of these sources of losses is next presented.

First, the combustion efficiency was assessed by employing equation 3.12 that accounts the unburned products that have lower heating value greater than 0. The most important ones are the unburned hydrocarbons, carbon monoxide and hydrogen. As it can be seen in Figure 4.11, the major losses by combustion inefficiency are verified at conditions where a fully premixed combustion is employed. It can be also stated that low engine loads (<5 bar) are the most impacted. This is justified by the low pressure and temperature values resultant from the low compression ratio. As the engine load is increased, so is the combustion efficiency, achieving similar levels to those verified from current diesel engines that run on diffusive combustion.

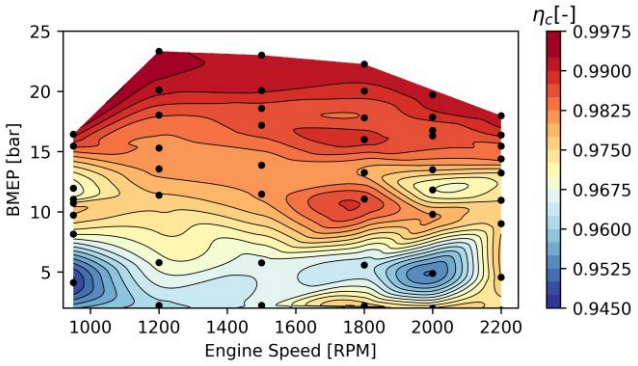

Figure 4.11. Combustion efficiency results for the different operating conditions.

Considering the four engine strokes, usually, the expansion is the only that provides positive work while the others are accounted as negative work (compression, exhaust, and intake). Sometimes, the pumping work (exhaust and intake lace) can provide a positive balance if the manifold intake pressure overcomes the exhaust pressure. Nonetheless, this is difficult to obtain, and generally, one desires to minimize the pumping losses. For this, the difference between the intake and exhaust pressure should be minimized as described

in the calibration methodology [5]. A common parameter to evaluate the total pumping losses is the pumping mean effective pressure. Figure 4.12 depicts the results obtained for this parameter in the final calibration. It is interesting to state that the engine has an air throttle at the inlet manifold that was kept fully open during all the tests. Two different trends can be observed in the PMEP map. First, a horizontal one, correlated with the engine speed, demonstrates the impact of increasing the flow velocity through pipes and consequently the pressure losses due to the wall interaction. Second, a vertical trend, correlated with the air management requirements at each condition.

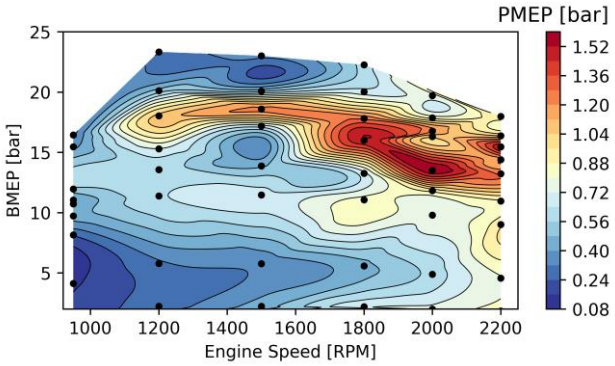

Figure 4.12. Pumping mean effective pressure for the complete engine map.

As previously discussed, at low engine loads, the air management system can deal properly with the demanded EGR amount while providing the air mass to the combustion process. Nonetheless, as the load is increased and the combustion is modified to a diffusive one, the air requirements are stricter, demanding an increment in the intake pressure. As the EGR amounts are also higher, the VGT should be closed to increase the gas flow velocity in the stator to reach the desired pressures. As a side effect, the exhaust pressure increases in a higher proportion than the intake pressure, increasing the pumping losses. In addition, in these conditions the backpressure valve should be closed to provide the required amount of LP EGR. This also contributes to increase the back pressure since low

modifications in the turbine exhaust affects the inlet turbine pressure by a factor that depends on the pressure ratio of the operating condition.

All these losses have fundamental impact on the final brake fuel consumption results. Figure 4.13 presents the results of brake specific fuel consumption and brake thermal efficiency for the final calibration. As it can be seen, some of the best zones verified in the indicated efficiency and fuel consumption are not maintained in the brake values. In addition, the values are considerably decreased, mainly at low load conditions. This is justified by the importance of the friction losses compared to the indicated work delivered at these conditions. As the load is increased, the ratio between IMEP/FMEP increases, reducing the importance of the friction losses.

The previous analysis of the indicated efficiency demonstrated that an optimum zone was achieved at medium load, medium to high speed. As depicted in Figure 4.13 (b), this zone is not presented in the brake values. This can be attributed to the pumping losses presented at this region (see Figure 4.12) due to the high engine speeds combined with a closed turbine to provide enough air. Even with this scenario, it is interesting to note that the BSFC achieved values lower than 200 g/kWh (minimum value of 192 g/kWh). These values are comparable to those of modern EUVI diesel engines, i.e., to those of the original engine calibration. Therefore, it can be stated that the proposed DMDF calibration is able to obtain similar fuel consumption to the original engine.

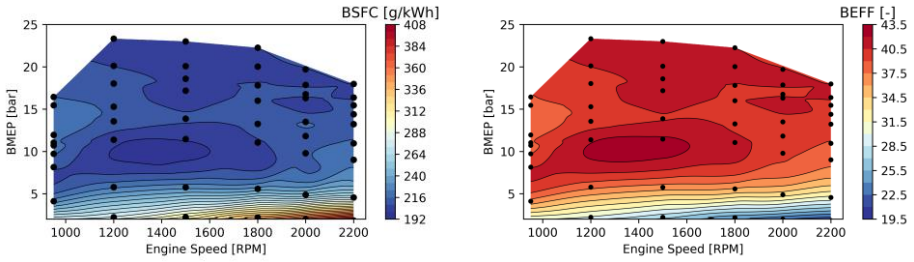

(a) (b)

Figure 4.13. Iso-surface maps depicting (a) brake specific fuel consumption and (b) brake efficiency for the complete calibration map.

4.2.3. Emissions: NOx, CO, HC, Soot and CO_2

The emissions maps obtained in the calibration process are presented from Figure 4.14 to Figure 4.16. From their analysis, it is possible to verify the impact of the calibration strategy in the different zones. Figure 4.14 depicts the results of NOx (a) and soot (b) for the whole operating map. As it can be seen, most of the NOx emissions are lower than 0.4 g/kWh, i.e., under the EUVI steady normative limits. This was accomplished by using highly diluted strategies as frequent as possible. Therefore, the low bulk temperature achieved during the combustion with its small duration inhibits the formation of this pollutant by the Zeldovich's mechanism. Unfortunately, as previously stated, the high-pressure gradients found from medium to full load required the progressive modification to a dual fuel diffusive combustion at the cost of increasing the combustion duration and soot production. The soot increase is a consequence of the major dependence of the HRF as the energy source (i.e., lower GF values).

Therefore, the increase of the diesel injection times produces richer zones where the fuel cannot be properly oxidized, resulting in soot production. This drawback is even more pronounced as the engine approaches to full load operation. As it was previously discussed, in these conditions, the turbocharger operation was limited by the turbine inlet pressure as well as the temperature at the compressor outlet that are close to the limiting mechanical constraints provided by the manufacturer. In this case, the NOx/soot trade-off could not be avoided resulting in penalties of both emissions. As the soot values could not exceed 2 FSN (defined in the calibration methodology), it was chosen to reduce the EGR rates, promoting higher engine out NOx. As it can be seen, the NOx emissions reached 2.2 g/kWh as maximum values. Even in this case, the raw emissions are considerably lower than conventional EUVI diesel engines. The same cannot be said for the soot emissions. The limit of 2 FSN at high load conditions results in a specific soot emission of 0.3 g/kWh that is one order of magnitude higher than the values obtained for conventional diesel combustion in this engine platform.

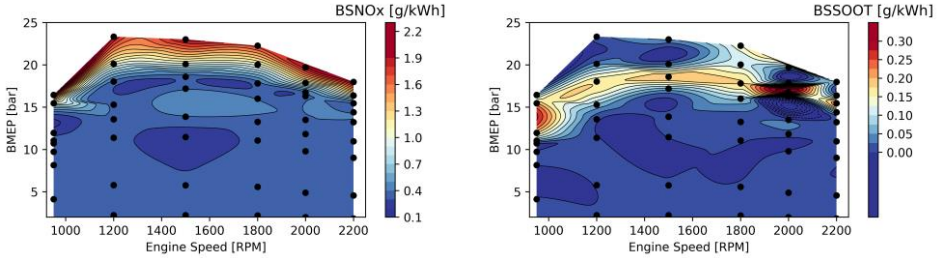

(a) (b)

Figure 4.14. Iso-surface maps depicting (a) brake specific NO_x and (b) brake specific soot emissions for the complete engine map.

The chosen strategy (premixed to diffusive) also impacts the unburned products as was previously discussed in the combustion efficiency results. The results of the total unburned hydrocarbons and the carbon monoxide are depicted in Figure 4.15 (a) and Figure 4.15 (b). The major concern on these emissions is found at low load to medium load conditions, where a fully premixed combustion is employed. The high GF in very diluted environment, low in-cylinder temperature and the amount of the fuel that enter in the piston gaps during the compression stroke are the major reasons to obtain the excessive unburned HC values [6]. Both pollutants are usually controlled by adding a DOC at the exhaust line. Nonetheless, the particularity of having two different fuels burning under low temperature conditions modifies the common reaction paths, resulting in a different composition at the exhaust line. In addition, the low exhaust temperatures can difficult the proper operation of the after-treatment system that relies on the oxidation of the major pollutants in specific devices. Therefore, the impact of having these composition modifications on the efficiency of commercial after treatment system should be assessed.

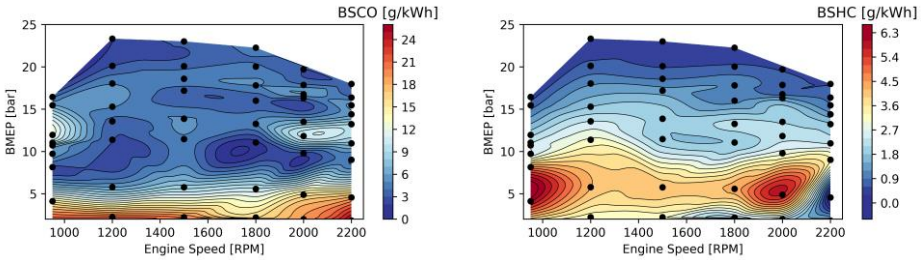

(a) (b)

Figure 4.15. Iso-surface maps depicting (a) brake specific CO and (b) brake specific HC emissions for the complete engine map.

Considering the new regulations regarding the CO_2 emissions, that should start in the upcoming normative updates (H2025, H2030), the engine-out values of this pollutant were also quantified [7]. The raw values of the CO_2 are depicted in Figure 4.16. It should be bore in mind that the results at low to medium load conditions are masked by the low combustion efficiency values. This means that once the CO and HC emissions are converted in the after treatment system, the final emissions of CO_2 should increase. Nonetheless, this accounts for a small portion of the total. Once diesel and gasoline present a similar CO_2 to fuel carbon molar mass ratio (CO_2 mass divided by the carbon mass of the fuel) the benefits in the final CO_2 emissions can be only obtained by reducing the exhaust flow or improving the fuel conversion efficiency. The point to point comparison with conventional diesel combustion could be done. However, it was preferred to evaluate the differences on transient conditions that will be addressed in the next sections. Nonetheless, it can be seen that the CO_2 is scaled proportionally to the fuel consumption in a ratio of nearly 3.06, which is almost the aforementioned mass ratio (3.09 for gasoline and 3.17 for diesel). In this sense, it can be stated that neither the total mass nor the CO_2 molar concentration is modified to a level where the CO_2 is reduced.

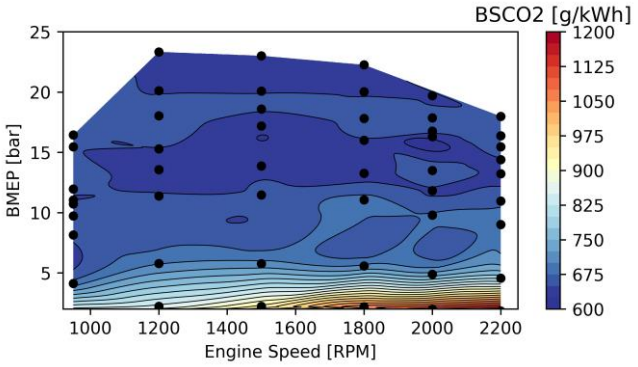

Figure 4.16. Brake specific engine-out CO_2 emissions for the complete engine map.

4.2.4. Summary of the DMDF calibration

The different issues faced during the calibration process that were previously discussed required setting new limits for NOx and soot emissions according to the zone in which the operating condition is included. First, the EUVI limit was aimed at NOx while maintaining soot levels lower than 0.01g/kWh. When the pressure gradients started to be a problem, the GF started to be decreased and the soot emissions were relaxed to 1 FSN. The following reduction of the GF values and the delayed SoI required an even more pronounced relaxation of the soot emissions to FSN 2. In the cases where the FSN 2 started to be exceed, the EGR amount was reduced. This resulted in a continuous increase in NOx emissions, first to 1 g/kWh and finally to 2 g/kWh. These boundaries can be easily verified at Figure 4.17 (a) and Figure 4.17 (b) where the whole engine map is presented. As it can be seen, EUVI limits are fulfilled in most parts of the calibration map, reaching values up to 60 % of engine load independently on the engine speed. Only 1/3 of the engine map is not able to fulfil soot emissions while only a small part of it exceeds the EUVI limits for NOx emissions. It is believed that depending on the truck operation (payload and driving cycle), transient normative limits can be achieved.

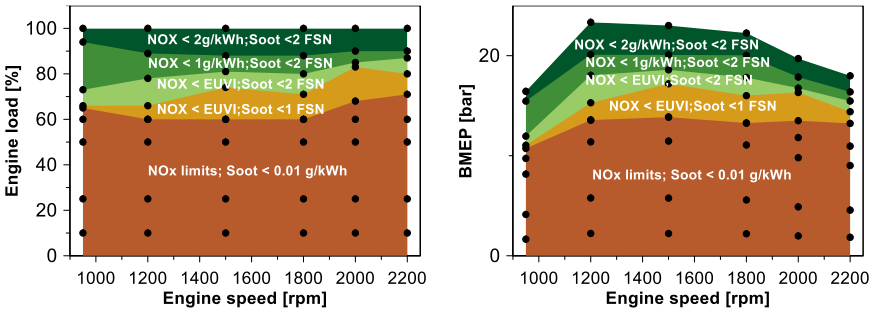

Figure 4.17. Calibration constraints obtained for the DMDF with respect to the (a) engine load and (b) BMEP.

It is clear that the engine application and the load requirement can shift the operating conditions in a fashion that penalizes the soot and NOx emissions. Moreover, despite not being directly compared, the DMDF combustion have demonstrated to achieve similar BSFC values than those of the original CDC calibration, which are also dependent on the engine zone that the truck operates. In this sense, the evaluation of different scenarios to address these possibilities is of utmost importance. This will allow deeper insights into the potential of the concept. In the next sections, these results will be confronted against the original OEM engine calibration by employing driving cycle analysis.

4.3 Driving cycle assessment: CDC *versus* DMDF

Single operating conditions are useful to investigate the effect of isolated parameters on the combustion process of an engine. However, homologation phases require the assessment on a set of operating conditions, which have different weights, representing the time usage on real applications. Both stationary and transient tests are considered according to the engine application. As the present work intends to assess the DMDF potential in truck applications, it must be evaluated on transient driving cycles. The actual homologation process requires the evaluation under the

World Harmonized Vehicle Cycle (WHVC). Nonetheless, recently, in-service conformity tests (ISC) were also included to guarantee that the vehicle still fulfills specific emissions targets (broader than the WHVC) [8] during its daily application. In this sense, this section aims to detail the evaluation of the previous engine calibration under the WHVC, ISC and real driving conditions, allowing to compare the engine out emissions with those values from the normative. The results of the stock engine (with conventional diesel combustion) are also included as reference for some of the parameters evaluated, e.g., fuel consumption. The original diesel calibration maps will be omitted as they are part of a non-disclosure agreement (NDA). However, the cumulative and cycle average results obtained from them will be used as references to the comparison with the DMDF calibration.

4.3.1. Driving cycles

Since the introduction of regulations in the transport market, driving cycles were continuously enhanced by increasing their complexity (e.g. speed profile) to better represent the real usage of the vehicle and to avoid the possibility of having frauds in the verification procedure, as occurred in the past. Currently, the homologation procedure of a new engine in Europe is composed by different stages of verification. Both steady and transient tests are employed for homologation purposes. In the first case, the engine is submitted to the WHSC (World Harmonized Stationary Cycle). This cycle is a weighted average of thirteen modes (speed and loads) that represents real drive conditions from Europe, USA, Japan and Australia. In sequence, the transient phase is employed. In EUVI, transient tests are composed by two types of evaluation. First, the World Harmonized Transient Cycle (WHTC) test is employed which is representative of the different real-world heavy commercial vehicle on typical driving conditions found in United States, Europe, etc. Lately, the evaluation of tailpipe emissions under in-service conditions was also introduced as a way of guarantee that the vehicle can maintain the emission levels below the normative ones during its lifetime. The frequency of evaluation is dependent of the vehicle class and a relaxing

factor of 1.5, which multiplies the EUVI constraints, is allotted for each emission to account for the differences of real operation from the controlled ones verified in laboratory testing.

In light of this, a set of driving cycles representing both normative and in-service conformity were chosen to perform the evaluations in this work. First, the WHVC will be used to compare the results to those from normative. Despite not being identical to the WHTC, the chassis dynamometer cycle WHVC is generally accepted for comparison purposes with the values of the normative. In sequence, three different driving cycles comprehending an ISC, an urban real driving condition and a fuel consumption evaluation cycle are used to assess the truck performance. Figure 4.18 (a) to Figure 4.18 (d) represent the driving cycles that will be employed in the transient evaluations. First, the WHVC driving cycle is presented, followed by an ISC full cycle. Next, an urban real driving condition is depicted, being characterized by low maximum velocities and frequent start-stops and acceleration. Finally, a fuel consumption evaluation cycle (FCEC) is employed to compare the truck performance with those of the original truck operating in CDC.

It is interesting to note that the WHVC presents significant differences compared to the remaining full cycles. First, the duration of the ISC (FC1) is almost 4.5 times higher than the normative cycle. Second, the number of acceleration and deceleration is more representative of the real conditions than the smooth WHVC. Finally, the idle times are reduced, being able to reproduce fuel consumption values closer to the reality. Table 3.2 summarizes some of the relevant parameters of each driving cycle, evidencing the differences in terms of speed and driving cycle phases.

Table 4.1. summary of statistic parameters for the driving cycles evaluated.

Parameter	WHVC	ISC_FC	Urban	FCEC
Time [s]	1800.0	9489.4	8688.2	2592.0
Distance [km]	20.1	118.6	119.0	85.3
Maximum speed [km/h]	87.2	95.8	75.3	90.3
Average speed [km/h]	39.3	66.8	35.4	43.6
Idle phases [%]	16.4	3.8	11.3	18.4
Acceleration phases [%]	32.7	19.7	28.7	16.8
Deceleration phases [%]	28.3	15.6	21.4	11.3
Cruising phases [%]	25.0	60.9	38.7	53.6

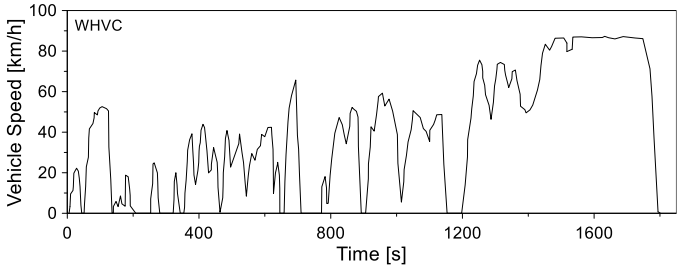

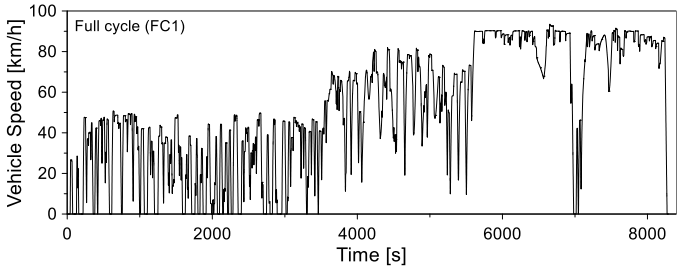

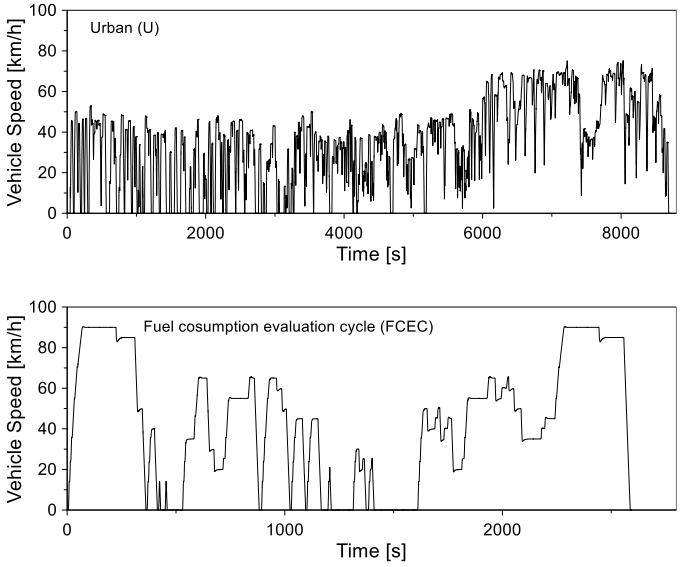

Figure 4.18. Different driving cycle used for the trainset evaluation (a) WHVC, (b) ISC-full cycle (c) urban and (d) fuel consumption evaluation cycle.

4.3.2. GT-power model validation

Prior to the evaluation of the developed model described in section 3.5.2 under DMDF combustion mode, it should be calibrated with experimental results from the original truck. To do this, experimental data from real truck tests were provided by the OEM in an ISC cycle. Measurements were made at different locations during the driving cycle to obtain values of torque and speed at the engine, before transmission, after transmission and at the axle. In addition to those values, the instantaneous and average fuel consumption values were also recorded.

Initially, the engine was isolated by means of a simplified model (Figure 4.19) in which the experimental engine torque and speed were used as demands. As previously explained, it can emulate the different operating conditions achieved during the driving cycle, resulting in the instantaneous

values of emission and fuel consumption. This approach allows to isolate any effects from the adjacent parts as clutch and truck characteristics. As it can be seen in Figure 4.20 and Figure 4.21, both engine speed and torque demands are exactly those from the experimental measurements. This means that, if the calibration map used in the simulation model is the same one employed in the real truck (without ECU corrections for temperature, etc.), the results of fuel consumption should be similar.

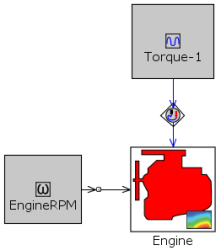

Figure 4.19. Simplified model used to evaluate the engine maps by imposing the experimental engine torque and speed.

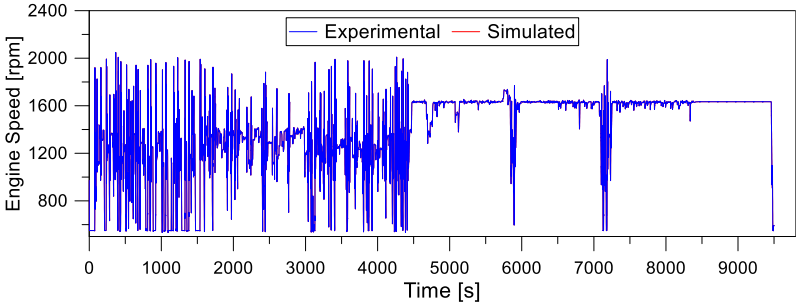

Figure 4.20. Imposed engine speed profile from the experimental driving cycle.

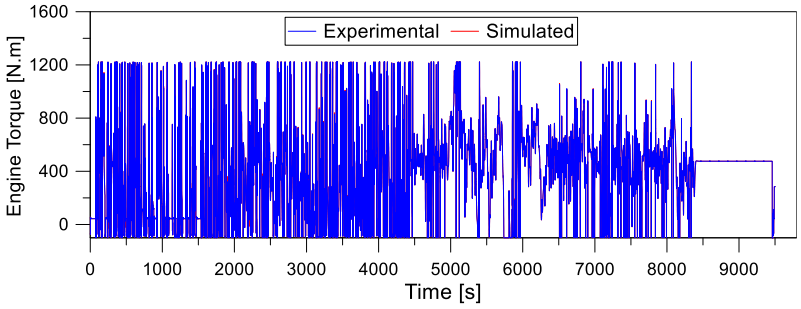

Figure 4.21. Imposed engine torque profile from the experimental driving cycle.

Indeed, as it can be seen in Figure 4.22 similar values of instantaneous fuel consumption are obtained. This confirms that once similar maps of fuel consumption are used as boundary conditions the engine model can emulates the real instantaneous behavior of the engine. Moreover, as presented in Figure 4.23, this can also be stated for the cumulative fuel consumption results, which provides differences lower than 5 % in the final value. The differences can be attributes to different ambient conditions and measurements discrepancies.

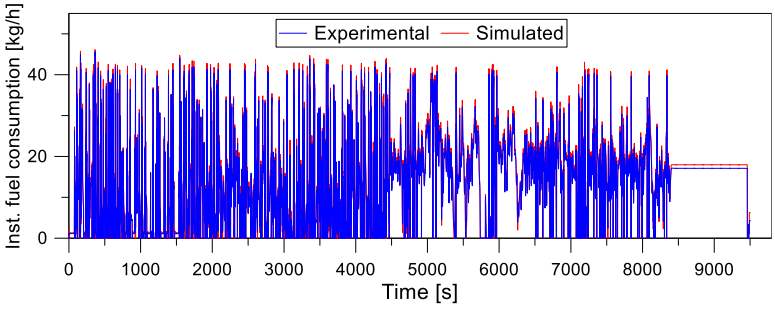

Figure 4.22. Instantaneous fuel consumption results: experimental versus simulated.

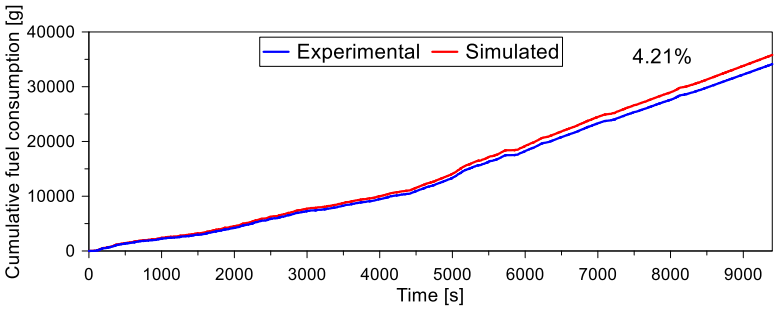

Figure 4.23. Cumulative fuel consumption results for the engine map comparison: experimental versus simulated.

In a second step, the clutch and gearbox from the original truck were added to the model to assess the impact of the transmission ratios, inertias, slip and shifting times on the axle speed profiles. The resultant model is presented in Figure 4.24. The axle torque values cannot be accessed in this phase since there is no load in the right-hand side of the driveshaft. Therefore, during the simulation the value is zero after the driveshaft.

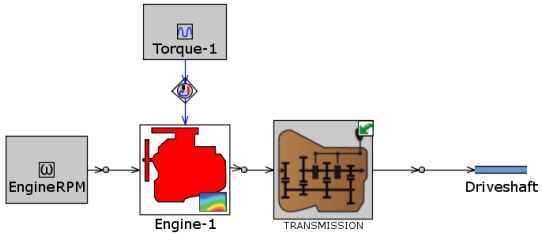

Figure 4.24. GT-Drive model of the powertrain system up to the gearbox output.

Figure 4.25 presents the instantaneous values of speed at the driveshaft. Slight differences appear between the measured and simulated values in different simulation times. This can be attributed to the input characteristics of the transmission where different properties are not described in the literature. Therefore, they were adjusted aiming to minimize the differences

in respect to the measured values. The results presented in Figure 4.25 are achieved considering the optimized set of constants.

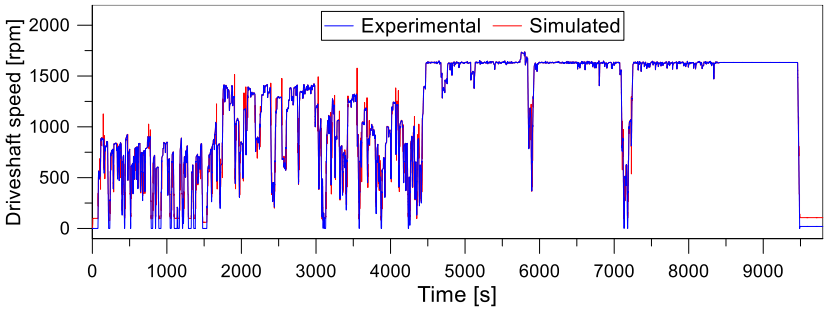

Figure 4.25. Driveshaft speed comparison between experimental and simulated results.

Finally, the remaining parts of the truck as tires, axles and vehicle geometry were added to the model (Figure 4.26). Parameters as the rolling resistance factor were iteratively adjusted during the simulations aiming to minimize the differences with the experimental values. It is interesting to note that, differently to the previous analysis, the engine torque and speed are not imposed anymore. This means that all the longitudinal vehicle model is simulated considering the speed profile imposed by the driving cycle. This assumes that if any part of the model is not properly set, discrepancies will be apparent in the instantaneous and cumulative results. The results of the complete model comparison with those from the real measurements are presented from Figure 4.27 to Figure 4.32.

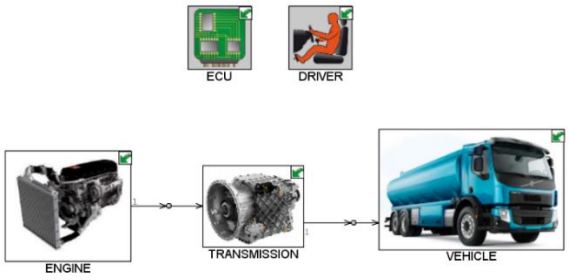

Figure 4.26. Complete GT-Drive model for the FE 350 truck.

First, the results at the engine are discussed. As it can be seen in Figure 4.27 and Figure 4.28, generally, there is a good correlation between the experimental and simulated results for both engine torque and speed. Some discrepancies can be verified mainly in conditions were the engine is at idle presenting higher velocities than the experimental. Moreover, the signal is noisier than the experimental which can be related to the clutch slip and different inertias that are difficult to be properly adjust without dedicated transmission experimental test. However, considering the purpose of this work, the adjustments seems to be enough for the comparative evaluation between CDC and DMDF.

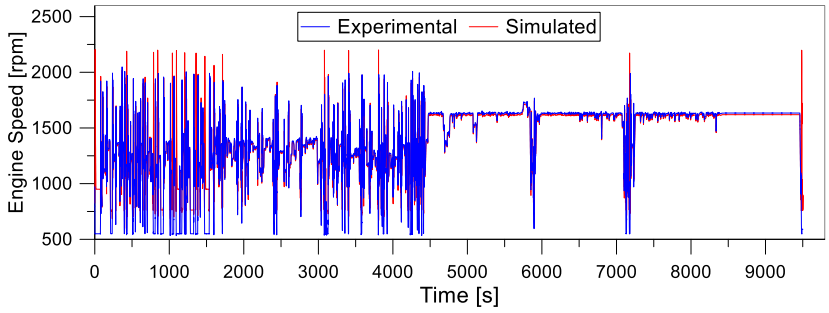

Figure 4.27. Simulated versus experimental engine speed for ISC FC3 driving cycle.

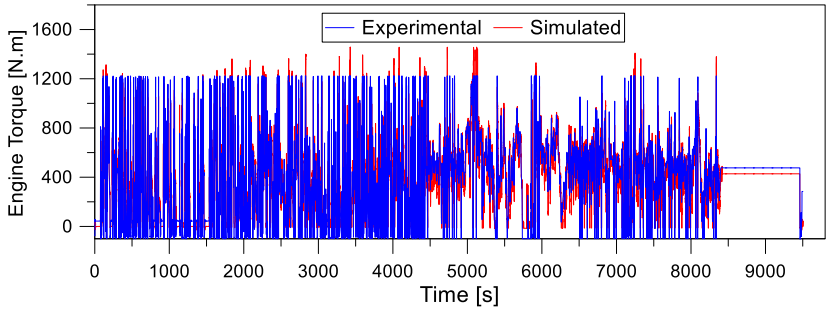

Figure 4.28. Simulated versus experimental engine torque for ISC FC3 driving cycle.

Since all the truck is modelled and the driving cycle and truck load are imposed, the values of axle torque are now available and can be compared together with the speed of the measured ones. Figure 4.29 depicts the values of the instantaneous axle speed for both simulated and experimental cases. It is possible to verify that there is an excellent agreement between the experimental and simulated results. The analysis of both Figure 4.29 and Figure 4.30 together allows to get important information about the transmission system. As the ratio between the speed before and after the transmission for both experimental and numerical results is the same, it can be inferred that the transmission is correctly modelled, with the same gear ratios than those from experiments.

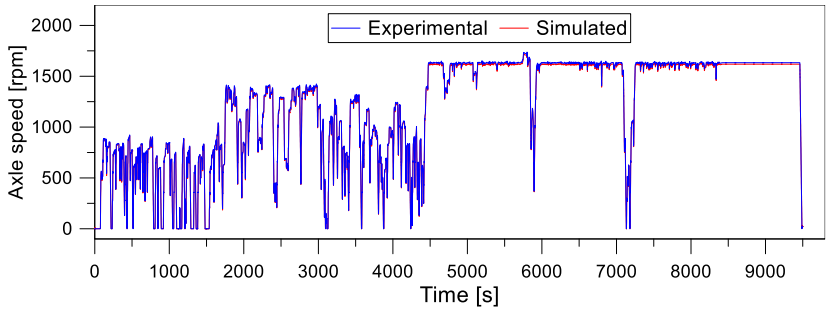

Figure 4.29. Simulated versus experimental axle speed for ISC FC3 driving cycle.

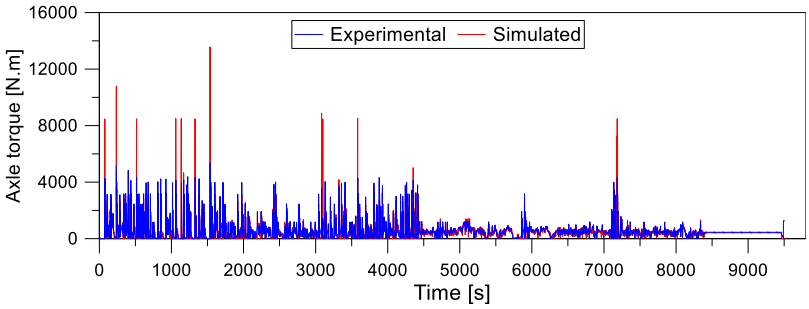

Figure 4.30. Simulated versus experimental axle torque for ISC FC3 driving cycle.

Figure 4.31 and Figure 4.32 present the results for the instantaneous and cumulative fuel consumption, respectively. Some discrepancies can be verified mainly in conditions were the engine is at idle conditions and in some transients where the interpolation of steady-state maps is not enough to reproduce mixture enrichment or any other modification that can exist in the ECU strategy. Even with these slight deviations, the results of cumulative fuel consumption have differences lower than 1.48 %. Based on this, it can be concluded that the model is able to represent the real truck in which regards fuel consumption.

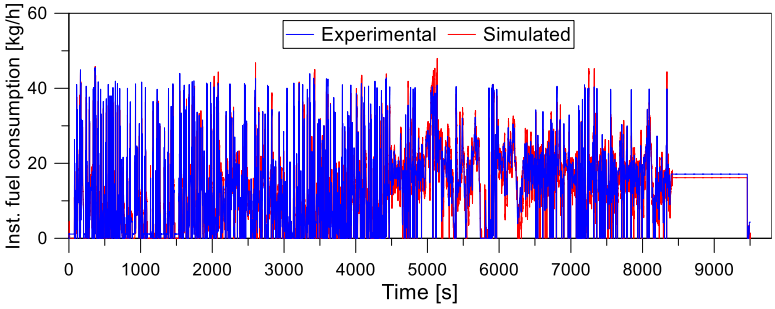

Figure 4.31. Experimental versus simulated instantaneous fuel consumption for the FC3 ISC driving cycle.

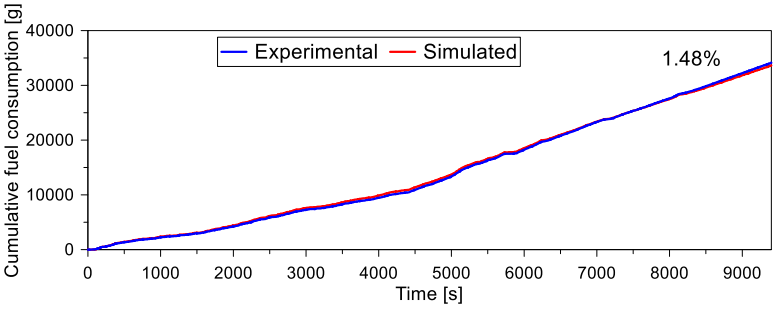

Figure 4.32. Experimental versus simulated cumulative fuel consumption for the FC3 ISC driving cycle.

The same verification procedure could not be applied to the emissions since the truck was not equipped with portable gas analyzers. In this sense,

a specific methodology was developed to perform the assessment of the evaluation strategy (map-based) considering transient measurements in the engine test bench. Once the truck characteristics are validated, it is suggested that the isolation of the engine to compare the map-based approach with those from transient engine measurements should be valid. To do this, a simplified engine load and engine speed step was proposed, following the recommendations from conventional supplementary engine steps (transition time, evaluation limits, etc.) with the engine operating at DMDF mode. Figure 4.33 presents the step used for the emission evaluations. As it can be seen, the evaluation step considers engine loads from 0 % to 25 %, representative of fully premixed operating conditions. At the same time, the engine speed was modified from 1200 to 1800 following different combinations with the engine load. A heating step was included in the first 200 s to assure warm conditions, since the calibration maps do not account warming phases. Once the heating phase is done, the measurements can be started, inhibiting the effect of the engine heating on the raw emissions.

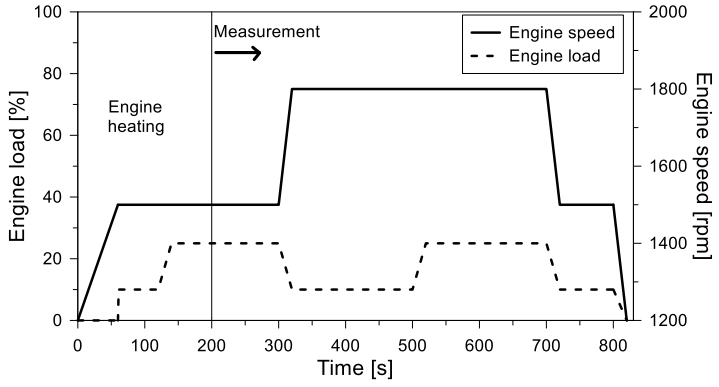

Figure 4.33. Step proposed to evaluate the validity of the map-based approach on predicting the main emissions on transient conditions.

Figure 4.34 depicts the comparison for the different emissions between the numerical and experimental results for the proposed step. It should be stated that transient soot emissions are not reported since they require specific measurement devices. Figure 4.34 (a) illustrates the nitrogen oxides

cumulative emissions. As it is shown, variations lower than 2 % can be evidenced. It should be remarked that the absolute values of this pollutant on this combustion regime are as low as 0.4 g/kWh. Similar agreements employing this approach were presented by Luján et al. [9] and Morra et al. [10]. By contrast, HC (Figure 4.34 (b)) and CO (Figure 4.34 (c)) seem to be more difficult to be predicted from steady-state interpolation. The analysis of the graphs suggests that larger warming times should be employed, as the differences starts to be constant from 300 s. This could be correlated with the wall temperatures that can take longer times to achieve steady-state than the one proposed as warming, enhancing wall quenching in the first period of the step.

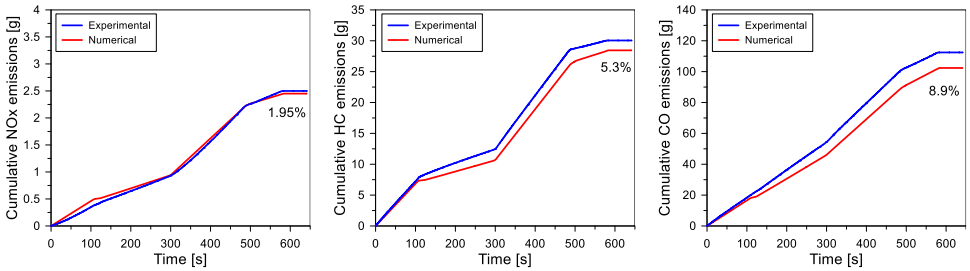

Figure 4.34. Experimental and simulated cumulative (a) nitrogen oxides, (b) unburned hydrocarbon and (c) carbon monoxide emissions.

4.3.3. DMDF performance and emission results in driving cycle evaluations

This section presents the results obtained through the simulations performed in GT DRIVE with both original CDC and DMDF calibration maps. First, the performance results are presented and discussed. Finally, the results obtained for the emissions are analyzed aiming to obtain insights about the benefits and disadvantages of using DMDF combustion. The normative states that in the absence of statistical evaluation of the representing payload for the truck, 50 % to 60 % of its maximum payload

should be used as reference [7]. Nonetheless, additional parametric payload studies are performed to demonstrate the impact on the operating zone and the consequences of this parameter on the results.

4.3.3.1. Effect of DMDF calibration and driving conditions on performance results

The simulations in GT Drive can deliver both instantaneous and cycle averaged results. The first is useful to understand the critical driving conditions where the combustion concept can be penalized, while the second provides a direct reference to compare different calibration maps. Therefore, the average results will be first analyzed and in sequence the instantaneous results will be discussed to assess the operating differences in both calibration maps.

For all the following bubble graphs, bluer bubbles stand for reductions compared to the CDC while red bubbles mean an increase of the parameter for the DMDF concept. This type of graph is useful to depict large amount of information for comparison purposes. Figure 4.35 presents a summary depicting the brake specific fuel consumption percentage differences between DMDF and CDC for the different truck payloads and driving cycles. As it can be seen, the DMDF always delivers a higher fuel consumption independently on the driving cycle and truck payload. Nonetheless, some remarks can be done by analyzing the figure data. First, the higher increases are found at low truck load conditions. This is mainly related to the fact that the engine operates at low load where the higher fuel consumption penalizations are located as consequence of the low combustion efficiency. Finally, it seems that full cycle evaluations, which present highway phases (i.e., high truck velocities), tend to deliver the best fuel consumption results for the DMDF concept, reaching differences lower than 1 %. Therefore, it can be considered that the application of the concept on combined driving conditions and with higher payloads provides the best benefits. This means

that this combustion mode is more suitable for long haul than for urban (deliver and service trucks) or rural (production flow) applications.

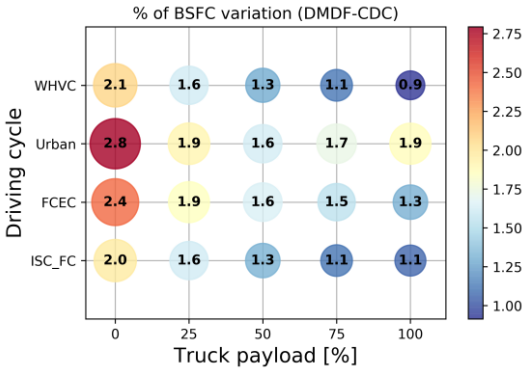

Figure 4.35. Percentage difference for the average brake specific fuel consumption at the end of the cycle for the different driving cycles and payloads evaluated.

Figure 4.36 gives further explanation on the decrease of the fuel consumption difference for medium to high payloads for the WHVC driving cycle. The depicted background map is a percentage BSFC difference map comprehending the original calibration and the proposed DMDF setup. As the driving cycles are based on the value interpolation of steady-state maps, these differences will be always constant independently of the payload and driving cycle. The driving cycle output differences will be given by the value that the operating condition takes for each time step during the simulation. From the previous results of Figure 4.35, it is expected that as the payload is increased, the operating conditions should be nearer to a lower loss or positive zone for the DMDF concept.

To assess the expected differences, an operating condition distribution map inside the BSFC differences plot was done. For this, the instantaneous engine speed and BMEP values were exported and separated in 400 bins. The number of operating conditions inside the bin was counted and divided by the total number of operating conditions. Higher values of this ratio (darker

shades) mean that the engine ran more time inside this region. Every value lower than an arbitrary threshold of 0.0001 was discarded to keep only the most representative conditions. The same procedure was employed for the three payloads and the results are depicted in Figure 4.36. As it can be seen, for 0 ton (no payload), the zone containing the maximum of operating condition falls on the range of -5 to 0 of BSFC difference. As the payload is increased, this zone is steeply shifted to a region where the BSFC difference is positive, which means a better fuel consumption for the DMDF. In this region, it is possible to attain a fully premixed combustion with short combustion durations, low pumping losses and proper phasing, overcoming the CDC performance.

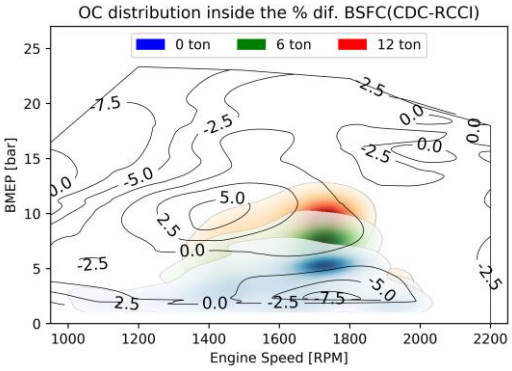

Figure 4.36. Operating condition distribution inside the brake specific fuel consumption percentage difference map according to different truck payloads (0 (0 %), 6 (50 %) and 12 (100 %) ton).

Another interesting remark is that the operating points distribution can follow different patterns according to the driving cycle in analysis. They can differ in both engine speed and BMEP distribution. Figure 4.37 exemplifies these differences for three driving cycle categories evaluated: urban, WHVC and ISC_FC for a payload of 6 ton (50 % of payload - representative of normative conditions). The differences for driving cycles that belongs to the same category should be minimal, since they must respect several constraints during their measurement. As it can be seen, the engine

speed distribution seems to be centered around 1600 to 1800 rpm, independently of the driving cycle. Nonetheless, the BMEP distribution differs significantly among them. The urban driving cycle presents higher frequency of vales in the low BMEP region (0-5 bar) while both WHVC and ISC are centered in medium load conditions. It is sometimes difficult to read the graph using the conventional histogram distribution. Moreover, the final shape of the histogram can be dependent on the dataset size.

A statistical metric called maximum likelihood estimation was employed to have the same basis of evaluation. The aim of this method is to find the best set of values μ and σ to match the original data with its most likely a Gaussian bell curve. Its mathematical description will not be addressed, and more details can be found in [11]. The results of this analysis are illustrated by the solid lines in the graph following the same color pattern than the histogram. As it can be seen, the engine speed distribution is even more similar allowing to conclude that it has low sensibility with respect to the driving cycle. Nonetheless, the BMEP distribution depicts a strong dependence with the driving cycle in analysis. The urban driving cycle is centered at $\approx$5 bar with maximum values up to 15 bar. This high amount of values at low load conditions justifies the higher fuel consumption with respect to full cycles. An interesting difference can also be visualized in the comparison of the WHVC and ISC driving cycle. While both PDFs have similar center, the ISC driving cycle has considerable higher number of operating conditions at high load. Despite of not having huge effect on BSFC, it can be determinant on achieving ultra-low soot emissions, since this pollutant is penalized at high load conditions.

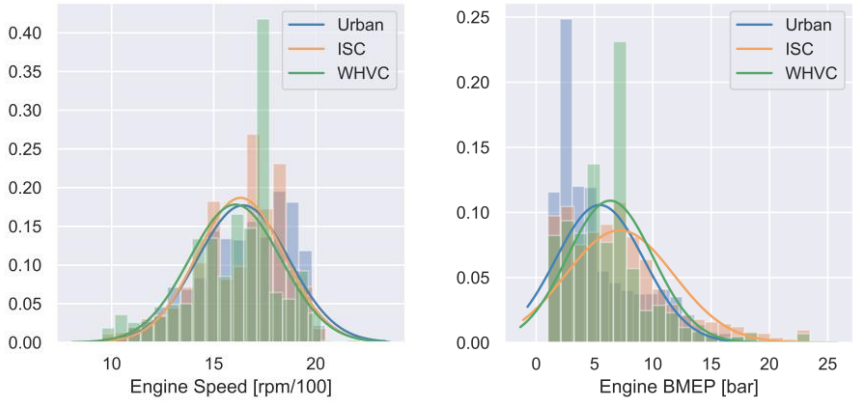

(a) (b)

Figure 4.37. Engine speed and brake mean effective pressure distributions and most likely Gaussian bell curve for three different driving cycle: WHVC, urban and ISC.

This brief analysis provided the necessary background in terms of the impact of the payload variation and the driving cycle characteristics on the operating condition distribution. Based on this, one can justify the final driving cycle results knowing the difference between maps (CDC-RCCI). This will serve as reference for the results presented in the following section.

4.3.3.2. Emissions

One of the claims of the low temperature combustion concepts are their ability of reducing the final emissions of soot and NOx at the same time, avoiding the NOx/Soot trade off. This should be an alternative to simplify the after-treatment system in which regards these pollutants. Therefore, both DPF and SCR can be reduced in size or, in the best scenario, removed. Since the DMDF proposed calibration concept does not fulfill normative in the whole steady-state engine map, the driving cycle evaluation should be carried to assess the impact of these zones on the final transient results. The results are compared to those of EUVI and the conditions that can fulfill its limits are depicted in green and with a black marker edge to differentiate them.

Figure 4.38 depicts the NOx results for the different truck loads and driving cycles evaluated. As it can be seen, promising results are obtained, with minimum reductions of 87 % compared to the CDC case at the same driving cycle. Moreover, an important trend is verified with respect to the truck payload. As this parameter is increased, lower are the benefits of the concept in terms of NOx emissions. This is strictly related with the higher NOx emissions found at high load conditions in the calibration map due to the dual fuel diffusive combustion. It should be also noted that most of the driving cycles were able to realize EUVI NOx emissions, independently on the payload evaluated. Nonetheless, payloads higher than 50 % exceed the normative targets for the WHVC. Therefore, it is clear that the high load region is a determinant in the successful application of the concept.

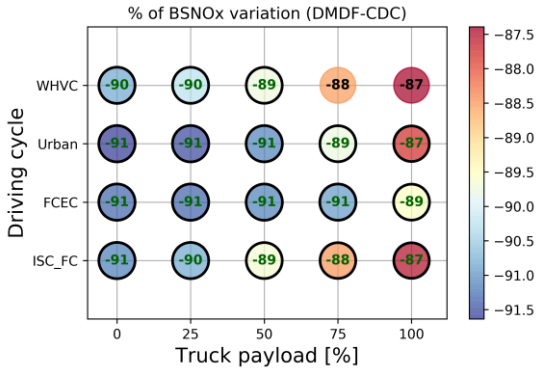

Figure 4.38. Percentage difference between DMDF and CDC combustion concepts for the average brake NOx emissions at the end of the cycle for the different driving cycles and payloads evaluated.

It can be stated that the concept is able to deal with the normative constraints without a dedicated after treatment system since the normative payload for driving cycles is 50 % (6 ton). This can be justified by analyzing Figure 4.39 where it is shown the total difference between the NOX emissions from the DMDF D-G minus the emissions from the CDC combustion. The graphs that follows presents the same color scheme: white stands for the zero difference while red stands for higher values of the DMDF and blue shades

stands for lower values for the DMDF. As it can be seen, the NOx differences graph presents only blue values allowing to infer that the DMDF concept provides always lower NOx values than the CDC concept. Moreover, it is possible to verify that the reduction of this emission ranges from 2 g/kWh to 8 g/kWh allowing to conclude that the DMDF concept will always benefit NOx emissions, even in the case of full load conditions.

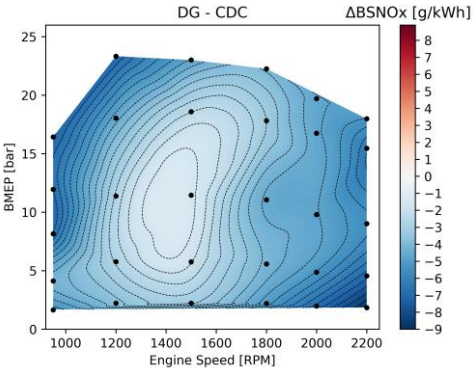

Figure 4.39. Total difference between the DMDF and CDC calibration maps for the NOx emissions.

Finally, Figure 4.40 presents the NOx cumulative results for the different truck payloads having the WHVC driving cycle as reference. As it can be seen, the highway phase is responsible to produce most of the NOx during the driving cycle, independently on the combustion mode. The higher truck velocities imply a higher power demand since there is a quadratic dependence with respect to velocity in its equation. This shifts the operating conditions to high engine loads where the NOx emissions are higher, penalizing the final cycle results.

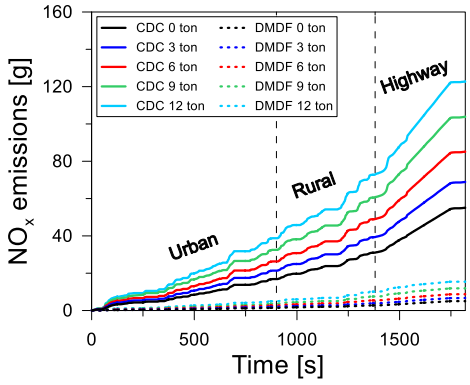

Figure 4.40. Cumulative NOx emissions comparison between CDC and DMDF calibration for the different payloads.

The same analysis employed for the NOx can be extended to the soot emissions. It should be remarked that the black borders of the graph correspond to soot values lower than 0.01 g/kWh (this does not means that soot is lower than EUVI targets since the optical measurement of the smoke meter may underestimate the condensable organic compounds that represent part of the particulate matter, which in the case of DMDF were demonstrated to stand to more than half of the particulate matter[12]). Unfortunately, in this case, the results are less favorable for the proposed calibration. As it can be seen in Figure 4.45, the effect of using DMDF changes according to the truck load. For low truck loads, the engine runs mainly in the conditions where a fully premixed combustion is employed inferring low to zero soot emissions. As the truck load is increased, so are the soot emissions. At 75 % of the nominal load, increases in the soot emissions lead to levels comparable to the original CDC. At nominal payload, the worst scenario was found for the urban driving condition which presented a percentage increase of 21 % compared to the original diesel calibration. This result can be directly correlated with the diffusive combustion employed at full load conditions.

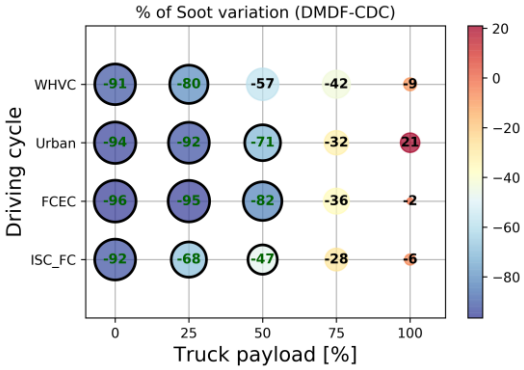

Figure 4.41. Percentage difference between DMDF and CDC combustion concepts for the soot emissions at the end of the cycle for the different driving cycles and payloads evaluated.

As demonstrated in Figure 4.42, these conditions are prone to produce soot, since high EGR levels are used with the turbocharging operating at limiting conditions, implying a lack of oxygen. The black solid line demarks the zone where the soot values starts to be higher for the DMDF concept. This means that the DMDF produces more soot in absolute terms. It is clear that the driving cycle results are not directly proportional to this, since the utilization time of each zone is distinct and depends on the truck payload as well as the driving cycle. For example, once the payload is increased, the engine should deliver higher power outputs to be able to follow the velocity profile. Consequently, higher BMEP values are achieved during the driving cycles. As they approach to this high sooty region, the driving cycle soot output starts to increase, surpassing the values from the CDC original calibration.

Figure 4.43 illustrates the operating condition distribution during the driving cycle according to the different payloads evaluated. This helps to visualize the effects previously discussed. Low truck payloads remain almost completely in low load conditions, in zones where the soot emissions are virtually zero. However, as the payload is increased, the operating conditions are steeply moved towards full load, falling in the zones where the soot

emissions are far superior to those of CDC. Consequently, the driving cycle result exceeds the ones from CDC and the normative constraints.

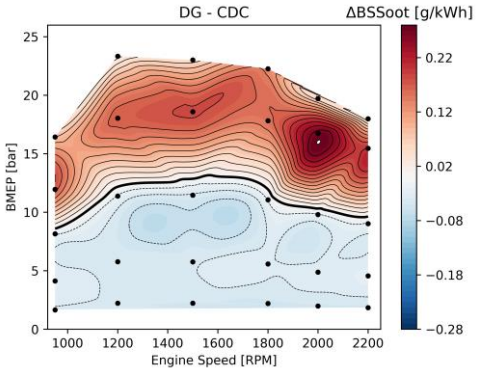

Figure 4.42. Total difference between the DMDF and CDC calibration maps for the soot emissions.

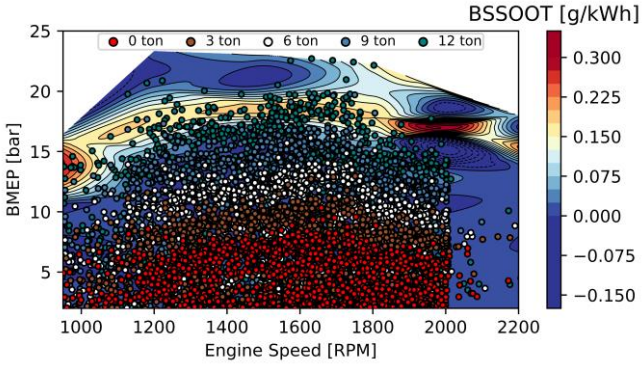

Figure 4.43. Operating points distribution inside the soot production map as a function of the different payloads evaluated for the WHVC driving cycle.

Each one of the circles from the graph above contributes with an instantaneous soot production. The sum of these values, considering the driving cycle duration, will result in the total mass. Therefore, one can follow the cumulative mass in each instant of time to analyze the critical driving

conditions in respect to this pollutant as previously done for the NOx emissions. Figure 4.44 presents the cumulative soot emissions for CDC and DMDF and the different payloads. It is interesting to note that, again, the highway phase is responsible for most of the soot production (almost the same that the urban and rural phase together). Nonetheless, the soot mass tends to also increase considerably at the end of the rural phase.

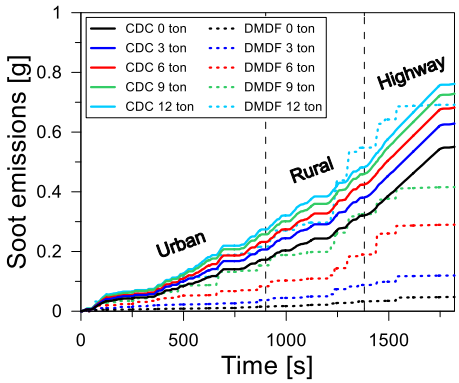

Figure 4.44. Cumulative soot emissions comparison between CDC and DMDF calibration for the different payloads in the WHVC driving cycle.

Premixed concepts are characterized by excessive quantities of unburned products as carbon monoxides and hydrocarbons. Because the fuel enters the cylinder as early as the intake valves are open, the air-fuel mixture can move towards the piston gaps where the heat losses are high (low temperature) inhibiting the oxidation reactions. In addition to this, phenomena as fuel pooling in the intake port and wall impingement are pronounced in these concepts. Therefore, one should expect higher emissions of these components, mainly for the cases of low load conditions. This can be visualized in the CO values depicted in Figure 4.45. Independently on the driving cycle, the CO increase is always higher for the low truck payload, exceeding the EUVI limits at normative conditions. As the cargo mass is increased, the operating conditions are shifted to higher engine load conditions, resulting in a decrease of the difference between the DMDF and

the CDC maps. Despite of this, the DMDF concept is not able to achieve the normative values of 4 g/kWh for most of driving cycles and payloads.

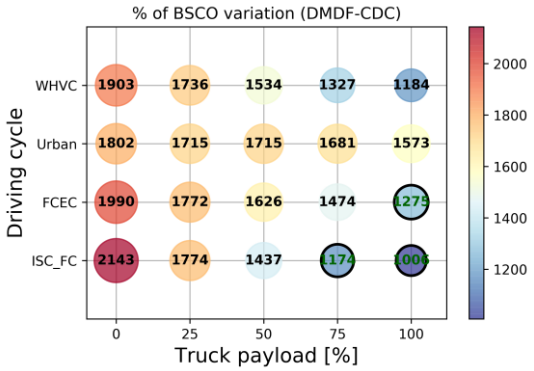

Figure 4.45. Percentage difference between DMDF and CDC combustion concepts for the average brake specific carbon monoxide engine-out emissions at the end of the cycle for the different driving cycles and payloads evaluated.

The difference map presented in Figure 4.46 also highlights the considerable increase in the CO emissions compared to the CDC combustion. As it can be seen, the CO increase ranges from values of 5 g/kWh (at medium to high loads) up to 25 g/kWh in low load conditions. This should present a challenge for the conventional ATS system since it must convert a high amount of this component while having low exhaust temperatures.

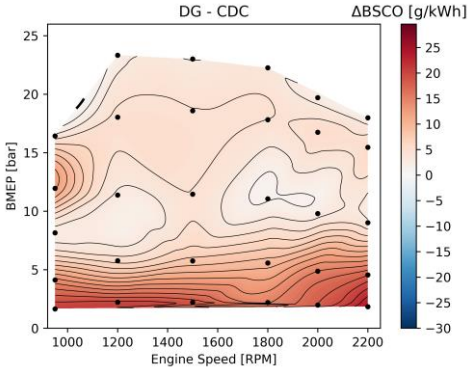

Figure 4.46. Total difference between the DMDF and CDC calibration maps for the carbon monoxide emissions.

The cumulative CO values along the reference WHVC driving cycle are also presented in Figure 4.47. The first DMDF 100 s can produce nearly the same amount of total CO mass than the whole driving cycle with the stock CDC calibration. In addition, it is interesting to note that both payload and high demanding driving conditions (highway) favors the reduction of CO production. It was previously demonstrated that at these conditions, the CO is reduced as a consequence of using a diffusive combustion.

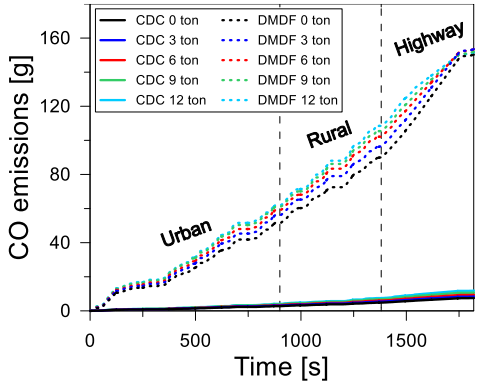

Figure 4.47. Cumulative CO emissions comparison between CDC and DMDF calibration for the different payloads in the WHVC driving cycle.

Figure 4.48 presents the HC variation for the DMDF concept compared to the CDC operation. A first interesting behavior can be noted as the truck load is increased. Different to the other emissions, the differences increase as the truck load is increased. This means that the emissions from the CDC decrease at a higher ratio than the DMDF. Consequently, the differences are higher. Moreover, the DMDF is not able to achieve EUVI limits independently of the case evaluated. This can be a challenge for the stock after treatment system, as it is not designed to deal with levels of HC an order of magnitude higher than those from the CDC. This subjected will be further discussed in chapter 5.

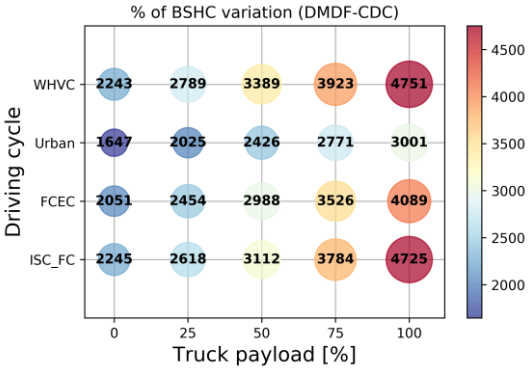

Figure 4.48. Percentage difference between DMDF and CDC combustion concepts for the average brake specific unburned hydrocarbon engine-out emissions at the end of the cycle for the different driving cycles and payloads evaluated.

The total differences of HC emissions are presented in Figure 4.49. Low to medium load conditions seems to be the most affected zones in terms of combustion inefficiency. The differences at this region can achieve values up to 6 g/kWh. Nonetheless, as the load is increased, the HC decreases since the GF values are lower and the combustion process is modified to a diffusive one.

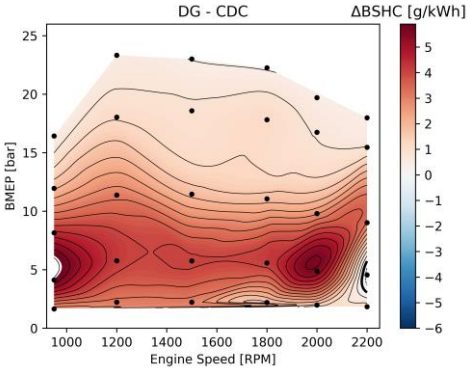

Figure 4.49. Total difference between the DMDF and CDC calibration maps for the unburned hydrocarbon emissions.

The cumulative results comparing the CDC and DMDF calibration on the WHVC driving cycle for the different payloads are depicted in Figure 4.50. As it can be seen, as the load as increased, lower are the differences among the payload lines for the DMDF concept. Moreover, the CDC provides final values lower than 5 g at the end of the cycle which means a high combustion efficiency. By contrast, considering an average value of 50 g of HC at the end of cycle, the DMDF tends to produce more than 10 times HC than the CDC calibration.

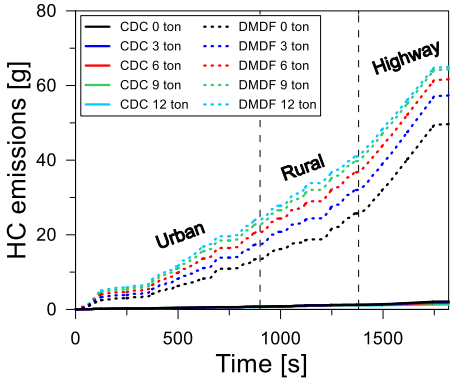

Figure 4.50. Cumulative HC emissions comparison between CDC and DMDF calibration for the different payloads in the WHVC driving cycle.

The effect of HC and CO is somewhat difficult to be visualized in an isolated manner. Therefore, the combustion efficiency previously calculated by equation 3.12 accounting the exhaust emissions of HC, CO and H_2 is presented in Figure 4.51. It is possible to verify that the truck load effect is predominant over the driving cycle type. There are slight differences for each driving cycle, but they are far inferior to the differences verified comparing the payload effect. As this parameter is increased, the losses by combustion efficiency for the DMDF concept tend to decrease. This is a direct consequence of using higher engine load conditions, reducing the time usage of the fully premixed conditions where the combustion efficiency present poor results.

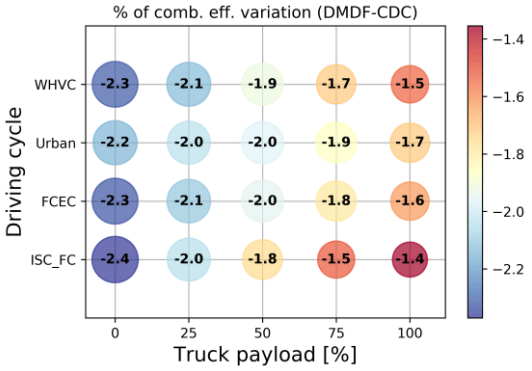

Figure 4.51. Percentage difference between DMDF and CDC combustion concepts for the combustion efficiency at the end of the cycle for the different driving cycles and payloads evaluated.

The total difference between the values of combustion efficiency from the DG calibration and the original CDC is presented in Figure 4.52. It is possible to verify that low load conditions present the higher differences compared to the CDC while medium to full load conditions seem to be less affected by the proposed calibration. Therefore, the improvement of these low load conditions can be a path to increase the overall efficiency of the concept and reduce the fuel consumption difference compared to the original

calibration. In addition, it should avoid secondary issues, as the ones that could be faced by the ATS system in achieving EUVI regulation.

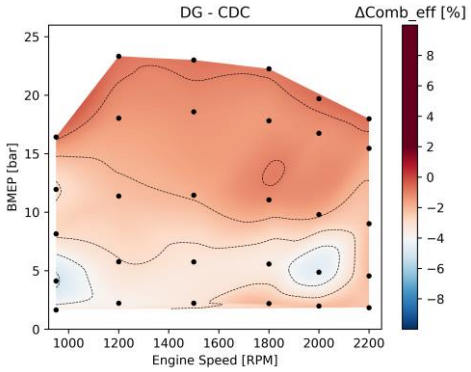

Figure 4.52. Total difference between the DMDF and CDC calibration maps for the combustion efficiency.

Finally, the engine-out CO_2 emissions are shown in Figure 4.53 for the set of driving cycles and truck loads evaluated. Despite of the increases in fuel consumption verified in Figure 4.53, the CO_2 values are similar or lower than those from conventional diesel combustion. It is true that the reduction is still far from the future scenario that aims at reductions of 15 % (H2025) and 30 % (H2030). Nonetheless, there are conditions that can provide benefits of 2.5 % even with fuel consumption 3 % higher than the CDC. This can be justified by analyzing the difference map presented in Figure 4.54. It depicts a contrasting behavior that is strongly related to the ISFC values. In addition, the conditions operating with fully premixed combustion tends to have lower exhaust mass flow. In this sense, it is possible to reduce the CO_2 emissions even in the case of having higher fuel consumption, as the CO_2 hydrocarbon molar mass of diesel and gasoline are similar (3.16 and 3.09, respectively). It should be noted that the data herein presented are engine-out values. Its final amounts will certainly be affected once the unburned products are converted which may result in similar values to those obtained by the CDC calibration.

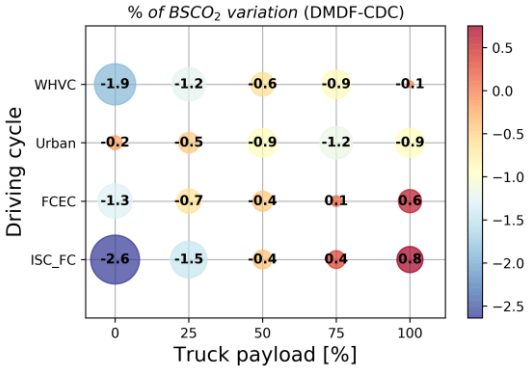

Figure 4.53. Percentage difference between DMDF and CDC combustion concepts for the average brake specific CO2 emissions at the end of the cycle for the different driving cycles and payloads evaluated.

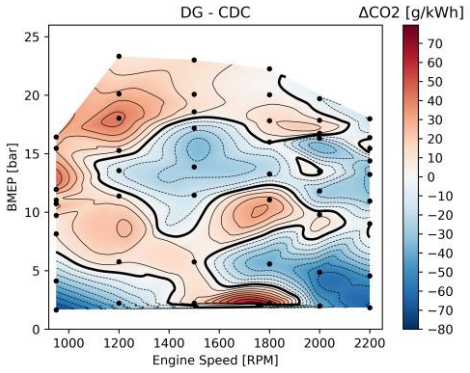

Figure 4.54. Total difference between the DMDF and CDC calibration maps for the CO2 emissions.

4.4 Drawbacks of the concept under real applications

Despite the favorable results in which regards soot and NOx emissions, with similar fuel consumption than that of the original calibration, the concept still offers challenges for real applications. The analysis of the

emission maps illustrated a high unburned hydrocarbon and carbon monoxide concentration at low load conditions. The coupling of this with the low temperatures at the turbine outlet can impair the DOC operation once that not enough energy is provided to achieve light off conditions. Besides, the use of the DMDF concept can also mean an operational issue for the DPF in terms of its regeneration capabilities, both passive and active forms. The low NOx levels at the engine-out can reduce the efficiency of the passive regeneration of the DPF while the low temperatures at the DPF inlet can also difficult the active regeneration.

In addition, the concept was not able to fulfill EUVI normative for soot emissions in the WHVC driving cycle considering truck payloads higher than 50 %. The air management requirements led the turbocharger system to achieve its limiting conditions in terms of pressure (turbine inlet) and temperature (compressor outlet). Moreover, the results from NOx emissions demonstrated that it can only fulfill EUVI normative up to 50 % of payload. This allows to conclude that the NOx/Soot trade-off could not be modified to achieve better results for soot. In other words, the engine calibration was the optimal one for the hardware and fuels employed. This means that further benefits can be only obtained by redesigning the air management system or modifying the characteristics of the LRF and the HRF. The first option cannot be accomplished since the OEM requires that the engine platform and its supplementary hardware should be maintained as similar as possible than those that equips the commercial truck. Finally, the CO_2 reductions are still far from those of the short-term scenarios as H2025, requiring additional modifications to realize fuel consumption improvements or the introduction of fuels that can attain decreases in the well to wheel CO_2 footprint.

In this sense, the next chapters will address each one of the challenges. First, a complete evaluation of both DOC and DPF critical conditions will be performed to determine the performance of these devices under DMDF conditions. Finally, the impact of the both fuel (LRF and HRF) characteristics will be evaluated trying to optimize the concept in terms of

soot and NOx emissions reduction as well as improvements in fuel consumption while aiming lower well-to-wheel CO_2 emissions.

4.5 Summary and conclusions

This chapter described the experimental implementation of the DMDF concept and the evaluation of its potential by means of a GT-Drive model on a multi-cylinder medium duty engine. The experimental maps provided an open loop calibration to be used as inputs in current ECUs. Despite of this, its main findings rely on the different strategies that were employed to overcome the challenges and achieve the same power output that was found during the calibration. The results of this strategy can be split according to the engine load range in which it was used:

- Low to medium loads (60 %): fully premixed combustion with the HRF injection moved towards the compression stroke as the load is increased. This can be realized due to the increase of in-cylinder pressure and temperature as the load is increased, allowing to obtain a stable fully premixed combustion. For this region, the benefits of the RCCI could be explored, allowing to achieve EUVI NOx emissions with virtually zero soot.
- Medium (60 %) to ≈ 80 % of engine load: the firsts drawbacks of the fully premixed combustion start to appear. The high amount of energy released in a short period of time results in an excessive pressure gradient, higher than the maximum allowable for this engine. The increase of the EGR at these conditions affected both combustion stability and soot production. Therefore, the GF values started to be decreased, coupled with higher compositional stratification to achieve higher loads without exceeding the mechanical constraints. Nonetheless, the soot emissions were relaxed as the lower GF increased the richer zones inside the cylinder.

- 80 % to full load: for these engine loads, the air requirements achieve limiting conditions in which regards the compressor outlet temperatures and turbine exhaust pressure. In this sense, neither the VGT can be closed nor the mass flow through the compressor can be increased. Consequently, the global equivalence ratio approaches to the stoichiometric, enhancing the soot production. Therefore, the EGR levels started to be decreased to avoid excessive soot values. As a side effect, the NOx must be relaxed up to 2g/kWh.

The second part assessed by means of numerical simulation the potential of the calibrated engine compared to the commercial diesel one for different driving cycles and payloads. In terms of performance, the DMDF concept demonstrated to be able to achieve similar levels of fuel consumption to those of CDC for most of the driving cycle, with maximum fuel consumption penalization of 2.8 %. Nonetheless, more power demanding cycles tended to decrease the BSFC penalization demonstrating that the combustion concept is well suited for long haul applications. In addition, a detailed analysis of the different engine out emissions were performed demonstrating that:

- The proposed concept can reduce the NOx emissions at least 87 % compared to the original calibration. In addition, it can achieve EUVI normative for the whole set of driving cycle considering the 50 % of payload as the representative of the truck.
- Soot emissions are strongly impacted by the increase of the truck payload since it shifts the operating conditions towards the high load zone, where the soot emissions are pronounced. Moreover, the proposed calibration is not able to achieve EUVI normative for this pollutant for the representative payload.
- HC, CO and combustion efficiency are always penalized by the DMDF concept as consequence of the premixed part of the combustion process. Besides, low to medium load conditions

presented excessive amounts of HC and CO together with low exhaust temperature. This can be a challenge for the DOC system since it can inhibit the oxidation reaction inside this device.

- CO_2 emissions present a reduction compared to the CDC case, independently of the payload and driving cycle evaluated. Nonetheless, this scenario can be changed once the unburned species are converted. Moreover, the reduction is still far from the short-term targets for heavy duty transportation.

In this sense, it can be concluded that the proposed DMDF calibration is able to deliver a similar fuel consumption in mass basis to the original CDC calibration while fulfilling EUVI NOx constraints without dedicated after treatment devices. This allows to reduce both production and operation costs of the truck, since the SCR is not required neither the urea consumption. Nonetheless, the same cannot be extended to the soot emissions as the cycle results are impacted by the soot production at high loads. Moreover, both HC and CO exceed by far the normative limits, presenting a challenge for conventional oxidation catalysts. The next chapter will assess the real impact of DMDF combustion on the stock DOC and DPF under representative operating condition

4.6 Bibliography

[1] DelVescovo D., Kokjohn S., Reitz R. "The Effects of Charge Preparation, Fuel Stratification, and Premixed Fuel Chemistry on Reactivity Controlled Compression Ignition (RCCI) Combustion". *SAE International Journal of Engines,* Vol. 10, 2017.

[2] Boronat Colomer V. *Dual-Fuel Dual-Mode combustion strategy to achieve high thermal efficiency, low NOx and smoke emissions in compression ignition engines*. Doctoral Thesis, Universitat Politécnica de València, Departamento de Máquinas y Motores Térmicos, 2018.

[3] Pedrozo V.B., May I., Lanzanova T.D.M., Zhao H. "Potential of internal EGR and throttled operation for low load extension of ethanol-diesel dual-fuel reactivity controlled compression ignition combustion on a heavy-duty engine". *Fuel*, Vol., 179 pp. 391–405, 2016.

[4] Olmeda P., García A., Monsalve-Serrano J., Lago Sari R. Experimental investigation on RCCI heat transfer in a light-duty diesel engine with different fuels: Comparison versus conventional diesel combustion". *Applied. Thermal. Engineering*, Vol., 144 pp. 424–436, 2018.

[5] Wahlström J., Eriksson L., Nielsen L. "EGR-VGT control and tuning for pumping work minimization and emission control". *IEEE Transactions in Control System Technologies*, Vol. 18, pp. 993–1003, 2010.

[6] Splitter D., Wissink M., Kokjohn S., Reitz R. "Effect of compression ratio and piston geometry on RCCI load limits and efficiency". *SAE Technical Papers*, n° 2012-01-0383, 2012.

[7] The European Comission. "Commission regulations (EU) 2019/318 of February 2019 amending Regulation (EU) 2017/2400 and Directive 2007/46/EC of the European Parliament and of the Council as regards the determination of the CO2 emission and fuel cunsumption of heavy-dut," *Official Journal of European Union*, Vol. 2001, pp. 20–30, 2019.

[8] The European Comission. "Commission Regulation (EU) No 582/2011," *Official Journal of European Union*, pp. 1–168, 2011.

[9] Morra E., Spessa E., Ciaravino C., Vassallo A., Analysis of various operating strategies for a parallel-hybrid diesel powertrain with a belt alternator starter, *SAE Technical Papers*, n° 2012-01-1008, 2012.

[10] Luján J.M., García A., Monsalve-Serrano J., Martínez-Boggio S., Effectiveness of hybrid powertrains to reduce the fuel consumption and NOx emissions of a Euro 6d-temp diesel engine under real-life driving conditions, *Energy Conversion and Management*, Vol. 199, 2019.

[11] Towards data science. Maximum Likelihood Estimation Explained - Normal Distribution. Available at https://towardsdatascience.com/maximum-likelihood-estimation-explained-normal-distribution-6207b322e47f, accessed in June 2020.

[12] Benajes J., García A., Monsalve-Serrano J., Boronat V. "An investigation on the particulate number and size distributions over the whole engine map from an optimized combustion strategy combining RCCI and dual-fuel diesel-gasoline". *Energy Conversion and Management*, Vol. 140 , pp. 98–108, 2017.

Chapter 5

After treatment system response to DMDF combustion

Content

5.1 Introduction

Chapter 4 has demonstrated that the DMDF combustion concept is a promising technology in which regards NOx and soot emissions. Moreover, the driving cycle results have shown similar values of fuel consumption and CO_2 emissions compared to the original calibration. Despite of this, an important drawback is perceived: the noticeable increase in the unburned hydrocarbons and carbon monoxide emissions. Besides, depending on the engine load, the operating condition distribution reaches, several times, high soot production zones in the engine map, surpassing the normative limits for this contaminant. In addition to this, the use of low pressure EGR in the calibration requires to clean the exhaust gases (remove water and particulates from the exhaust flow) prior to mixing with the intake air, avoiding possible damages of the EGR valves and moving parts of the compressor as the blades.

In this sense, it can be concluded that both the DOC and DPF will still be used in the DMDF concept. This requires the identification of what may be the impacts of the DMDF combustion on both devices. Therefore, this chapter addresses this subject by experimental and numerical analysis. First, experimental tests were performed to assess the DOC response to the DMDF boundary conditions at both steady and transient conditions. A detailed analysis was carried out to understand the impact of the GF values on the unburned hydrocarbon species at the exhaust. Second, the DPF passive and active regeneration were characterized to assess their effectiveness on cleaning the DPF. Finally, dedicated 0-D and 1-D models were characterized and calibrated in GT-Power (based on the experimental evaluations) and employed in driving cycle simulations to assess the engine compliance with current EUVI normative using its stock aftertreatment system.

5.2 Oxidation catalyst evaluation

Diesel oxidation catalyst efficiency on reducing unburned HC and CO is strongly dependent on the boundary conditions at its inlet. The residence time, inlet temperature and unburned species have dominant role on achieving a proper reduction of the contaminants [1]. An additional variable can be defined by introducing the heat capacity of the device, i.e., the capability to store energy and maintain the DOC wall temperatures during a certain period [2]. Therefore, this section intends to evaluate these set of variables by means of specific steady-state and transient tests that will be detailed in the following subsections.

5.2.1. Steady-state evaluation

Steady-state evaluations have as advantage the possibility to set fixed conditions at the DOC intake and assess the impact of these parameters on the DOC performance once pre-established steady-state criteria are achieved. The experimental setup and the methodology employed during this investigation will be present in the following subsection.

5.2.1.1. Methodology

The DOC evaluation at steady-state operation requires a definition of a parameter to guarantee that the dominant properties are stable through the time. Generally, the most critical property is the temperature at the DOC outlet. This is a measure of the conversion efficiency variation and its subsequent stabilization. Therefore, a reference value for the maximum outlet temperature variation allowed must be set. Values lower than this reference means that the device is under steady-state conditions and the tests can start.

To define the reference value, a set of temperature variations were evaluated and defined from the temporal evolution of the temperature profiles. The criteria should be accurate enough to avoid quasi-steady

conditions as the one presented in Figure 4.2. This plateau can be obtained in some short time intervals given the interaction of cycle to cycle variability of the engine, thermocouple response and test cell facility cooling.

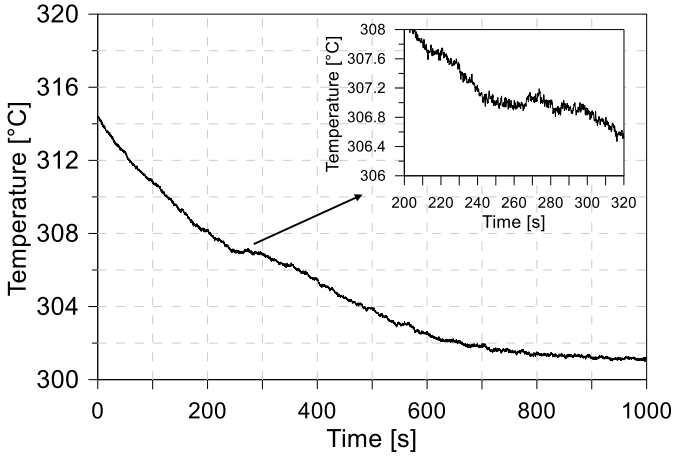

Figure 5.1. Oxidation catalyst outlet temperature as a function of time for a steady-state inlet boundary demonstrating the plateaus that can be obtained even in the case of an unsteady oxidation catalyst operation.

Therefore, three different periods (n) were chosen and evaluated aiming to avoid these quasi steady-states: 60 s, 120 s and 180 s. Figure 5.2 presents the different derivatives in respect with the selected time steps calculated from Equation 5.1.

$$\Delta_T\ [°C/s] = \frac{T_{i+1}[°C] - T_i[°C]}{n\ \ [s]} \qquad 5.1$$

As it can be seen, the first timestep reaches the criteria in the early seconds of the measurement time. This can lead to a "false" criteria fulfillment, that should be related to the quasi steady zones previously discussed. As the time step is increased, the fulfillment of the criterium is shifted towards the end of the measurement period. For the longer time step, the criteria cannot be reached, since the observation time always provide

differences higher than 1 °C. Nonetheless, its minimum value corresponds to the conservative time step of 120 s.

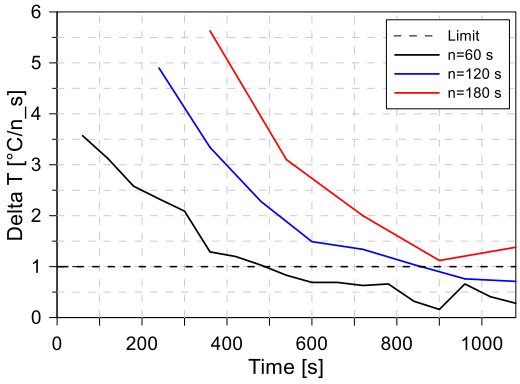

Figure 5.2. Different criteria assessed to guarantee the steady-state operation of the oxidation catalyst: 60 s, 120 s and 180 s.

Therefore, 120 s was chosen as time step to calculate the steady-state operation criterion. This means that the measurements should start once the temperature variation in a period of 120 s does not exceeds 1 °C. Figure 5.3 exemplifies the concept with a temperature evolution from the experiments.

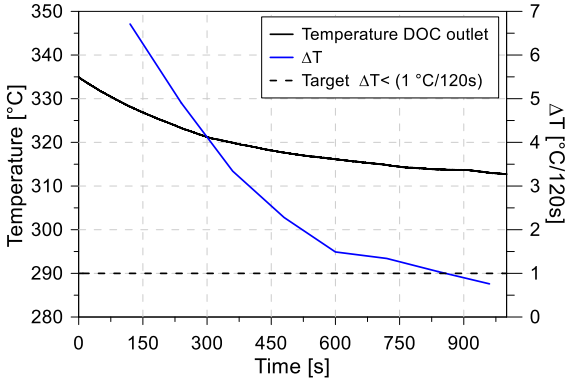

Figure 5.3. Evaluation of the proposed criteria (1°C/120s) for a random operating condition.

Once the steady-state criterion is defined, the measurement methodology should be developed. An important point to be remarked is that the same initial condition must be guaranteed for each operating point to be evaluated. In this sense, a cleaning phase, consisting of a high exhaust temperature and high combustion efficiency point was employed at the beginning of each measurement. This condition is maintained until the exhaust HC and CO concentrations are stabilized and with an absolute value as low as the measurement uncertainty of the gas analyzer (≈5 ppm). After that, the operating condition to be measured is adjusted and the temperature criterion is continuously evaluated at each 120 s. If the criterion is fulfilled, the measurement of the operating condition is performed. The procedure consists of three measurements of 45 s each at the inlet and outlet of the DOC with two different gas analyzers: a flame ionization detector (Horiba Mexa) and a Fourier transformed interferometry (Horiba FT). The first one was employed to obtain the measurements of total unburned hydrocarbons and carbon monoxide while the second was used to obtain the different unburned hydrocarbon species in the exhaust gas. Figure 5.4 depicts the measurement approach used in the steady-state evaluation.

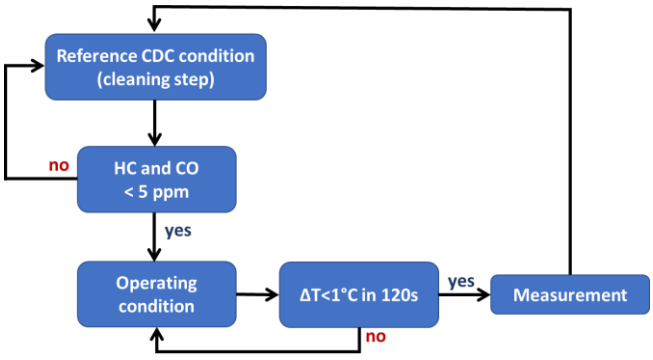

Figure 5.4. Steady-state methodology to assess the oxidation catalyst.

5.2.1.2. Oxidation catalyst results

Figure 5.5 presents the HC and CO results after and before the DOC for the different engine speeds evaluated at 10 % of engine load. The dashed line stands for the EUVI steady-state limits of both components. Each operating condition is reported as the mean value of three repetitions with the standard deviation depicted as a vertical bar. The same representation is maintained for the different operating conditions evaluated.

At low engine load conditions, the fully premixed combustion results in low temperature values at the exhaust and high engine out emissions of HC and CO. In this sense, the conversion efficiency of both emissions is impaired as depicted in Figure 5.5. The unburned hydrocarbon emissions are not able to fulfill de EUVI normative independently on the engine speed. Some improvements can be seen as the engine speed is increased. This is directly related to the higher exhaust mass flows and their consequent high energy resulting in lower temperature decrease up to the DOC inlet. In this case, the values of HC after the DOC are near to the EUVI limits. The CO emissions present similar behaviors than that from the HC emissions. As the activation energy of the CO oxidation is lower than the HC, this component can be better reduced at the DOC, achieving EUVI normative at high engine speed conditions [3]. This fact also contributes to the increase of the monolith temperature, improving the HC conversion efficiency.

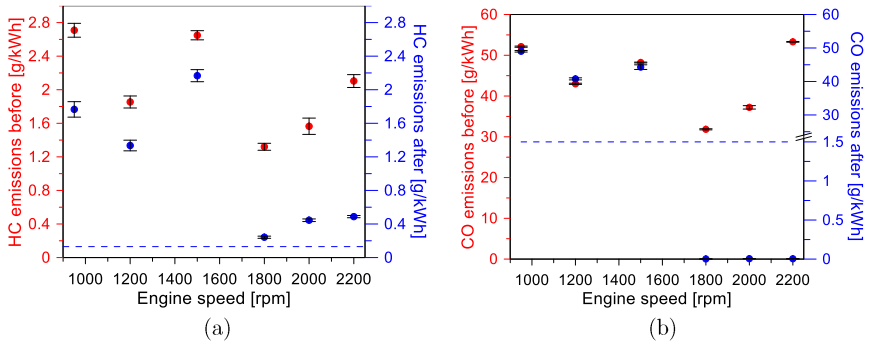

Figure 5.5. Results of (a) unburned hydrocarbon and (b) carbon monoxide emissions before and after the oxidation catalyst for different engine speeds ad 10 % of engine load.

As the engine load is increased, some improvements in the DOC conversion efficiency for both emissions can be observed (see Figure 5.6). The DOC achieves light-off conditions for all the engines speeds higher than 950 rpm. Only 950 rpm does not provide enough energy to convert the unburned hydrocarbons, presenting similar values of this emissions at both DOC inlet and outlet. For the remaining engine speeds, the conversion efficiencies are higher than 80 %, achieving values closer to the normative limits. This is also related to the carbon monoxide conversion at the DOC. As aforementioned, the proper CO oxidation increases the monolith temperature supporting the conversion of the hydrocarbons. An almost complete oxidation of the carbon monoxide emissions is achieved for engine speeds higher than 950 rpm. This is a consequence of the higher energy flow through the DOC as the mass flow increases with the engine speed as well as the inlet temperature. Therefore, EUVI CO tailpipe emissions could be achieved for almost all the 25 % of engine load, demonstrating that even high CO concentrations can be dealt with in the DOC without modifications.

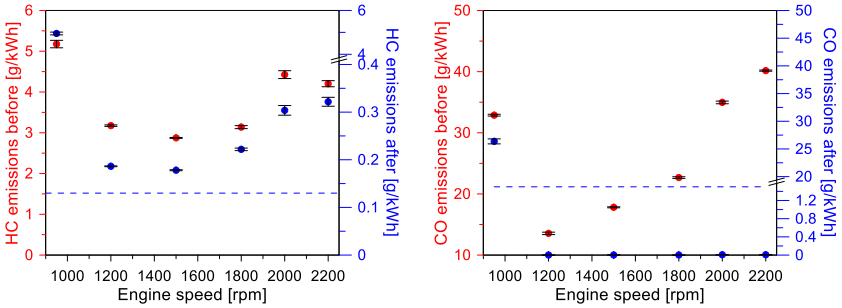

Figure 5.6. Results of (a) unburned hydrocarbon and (b) carbon monoxide emissions before and after the oxidation catalyst for different engine speeds ad 25 % of engine load.

Medium load conditions are characterized by fully premixed combustion achieved by means of early injections around 60 CAD bTDC. This results in high conversion efficiency with virtually zero NOx and Soot (see chapter 4, section 4.2.3). By contrast, the HC and CO emissions are considerably higher than the CDC combustion with low exhaust temperatures. This should be a critical operating condition for the DOC. Nonetheless, as depicted in Figure 5.7, the device is able to deal with the adverse boundary conditions, reducing both emissions to levels lower than the EUVI normative. It is interesting to note, that CO emissions present values closer to zero, demonstrating that this emission is easily reduced in the stock aftertreatment system. The analysis can be extended up to full load conditions. Nonetheless, as the engine load is increased, so is the exhaust temperature and the mass flow, enhancing the conditions in the DOC inlet to convert the unburned products.

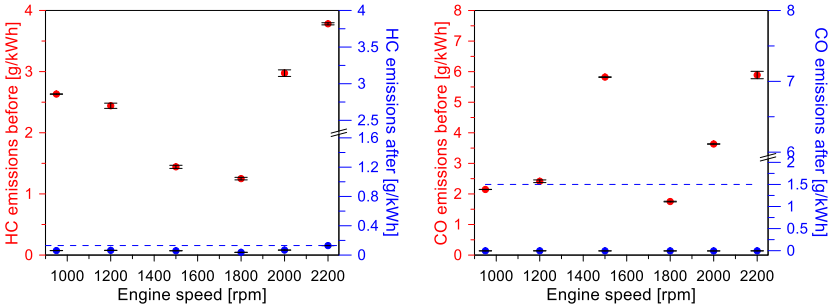

Figure 5.7. Results of (a) unburned hydrocarbon and (b) carbon monoxide emissions before and after the oxidation catalyst for different engine speeds ad 50 % of engine load.

Nonetheless, to be sure that the assumption is correct, an additional load step was evaluated. Four engine speeds (left and right boundaries of the operating map) were evaluated for 60 % of engine load (Figure 5.8). As it was expected, the conversion efficiency is maintained over 90 %, reducing the unburned species to values under the EUVI normative. Therefore, it can be stated that the stock DOC is able to deal with the DMDF engine out emissions for engine loads higher than 25 %. Low load conditions are an issue that should be addressed. It should be bore in mind that this study did not evaluate the impact of DOC heating or the use of the thermal capacity to guarantee proper efficiency under idle/low load conditions. The latter will be the subject of the transient evaluation that is presented in next sections.

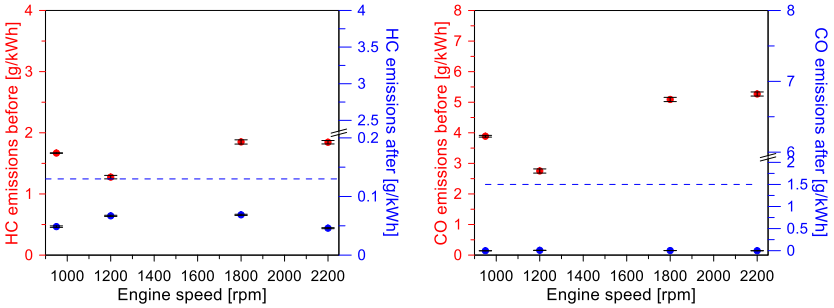

Figure 5.8. Results of (a) unburned hydrocarbon and (b) carbon monoxide emissions before and after the oxidation catalyst for different engine speeds ad 60 % of engine load.

5.2.1.3. Summary

The results obtained from the operating conditions evaluated can be combined and depicted in a contour map as presented in Figure 5.9. This can illustrate where the critical conversion efficiency zones are found inside the operating map. Moreover, two boundaries were inserted to be used as references in the analysis: the EUVI limits and a boundary corresponding to two times the EUVI values.

As it can be seen, more than half of the evaluated conditions are not able to fulfill the EUVI limits. If the limits are extended to be the double of EUVI constraints, the area is considerably increased. Nonetheless, the low load conditions are still a problem to be evaluated/solved in which regards the HC emissions. Regarding carbon monoxides, the problem is much more isolated in low engine speeds low engine load conditions. The constraint relaxation does not affect the area shrouded by the line. It is interesting to note that the maximum HC emissions after DOC are found in the zone where the CO conversion is low. The improvement of the conversion of one of the emissions could be decisive in achieving proper conversion efficiency at these conditions. This could be achieved by means of a proper DOC design, targeting the specific hydrocarbon species that are found in the products from

the DMDF combustion. Nonetheless, this requires detailed analysis by means of hydrocarbon speciation, to understand the impact of modifying the fuel composition as well as the combustion environment on the unburned combustion produces. Therefore, the next subsection details the speciation analysis for the same operating conditions discussed in this section aiming to identify what are the critical species that should be tackled during an oxidation catalyst design.

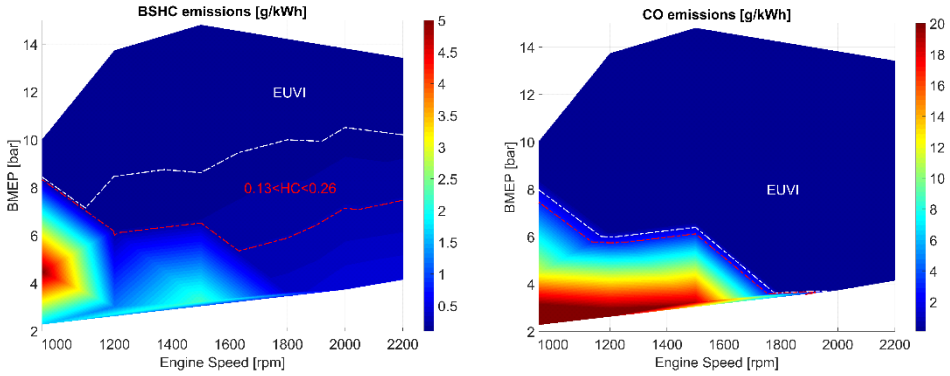

(a) (b)

Figure 5.9. Iso contour graphs representing the tailpipe emissions of (a) unburned hydrocarbons and (b) carbon monoxide from low to medium load operation. The white line demarks the zones that can fulfill EUVI limits, while the red line represents the zones that are lower than two times the EUVI constraints.

5.2.1.4. Exhaust hydrocarbon speciation

The effectiveness of the DOC in converting the partially oxidized compounds is affected by the chemical properties of the species that constitute them [4][5]. The knowledge of the species that will be dealt in the DOC allows to design the catalyst targeting specific coverage materials to convert them. Previous studies found in the literature address the quantification of the different hydrocarbon species that can be found in the engine exhaust for the most common operation of spark ignition and

compression engines [6][7]. The results suggested that the wide range of hydrocarbons present in the exhaust can be effectively divided in two major groups: low reactivity and high reactivity hydrocarbons. For both engines, propylene demonstrated to be a representative hydrocarbon for the high reactivity group while the low reactivity hydrocarbons are more dependent on the fuel employed [8]. Generally, diesel vapor can emulate the effects of the low reactivity compounds in the DOC for diesel engines. In spark ignited engines, propane or iso-octane are species that can be employed. General splits of low reactivity and high reactivity hydrocarbons are widely found in the literature. In the case of concept presented in this work, both diesel and gasoline are employed in different fractions during the calibration. This implies that the hydrocarbons that are found at the exhaust gases can be originated from both fuels. Therefore, the previously discussed split should account this by combining both low reactivity hydrocarbons.

In this sense, a speciation study was proposed to assess the impact of the GF variation on the hydrocarbon composition of the exhaust gases for the DMDF combustion. For this, 16 operating conditions from the calibration proposed in chapter 4 were chosen addressing GF values from minimum (0 %) up to the maximum (87 %) value obtained in the calibration. In addition, fully premixed conditions were prioritized as both HC and CO present their maximum values at these conditions and these are the most challenging conditions for the DOC, as previously presented. Table 5.1 depicts the test matrix employed during the speciation evaluation. The operating conditions come from the calibration map presented in chapter 4, maintaining similar settings regarding air management and injection parameters. For each measurement, the concentration of C_3H_6, C_2H_4, C_2H_6, 1,3-C_4H_6, C_6H_6 and C_7H_8 were recorded. Then, each specie was reduced to a C1 hydrocarbon basis and its respective contribution in the total hydrocarbon was determined.

Table 5.1. Operating conditions evaluated during the speciation tests.

Load [%]	Engine speed [rpm]	O_2 [%]	GF [%]	EGR [%]
10	950	13.45	0	50
10	1200	12.08	0	48
10	1800	12.87	0	52
10	2200	10.87	0	54
25	950	10.46	49	43
25	1200	8.61	49	36
25	1800	9.11	44	43
25	2200	10.08	43	48
50	950	3.91	68	41
50	1200	2.88	81	41
50	1800	2.83	80	45
50	2200	6.76	84	38
60	950	3.82	61	37
60	1200	3.88	70	32
60	1800	4.33	57	30
60	2200	4.78	56	35

The results of the different species at the exhaust are presented in Figure 5.10, being separated in sub graphs by engine speed. As it can be seen, there are two different peaks with respect to the hydrocarbon species. Both ethane and ethylene have the highest concentration in the left-hand side of the graph while toluene stands as the most common specie in the exhaust gases which concurs with the results from [7]. Species as benzene, butane, methane, etc., are present in lower concentration. It is also interesting to note that the quantity of high reactivity hydrocarbons is scaled with the gasoline fraction of the operating conditions. For conditions at 10 % engine load, were the GF is zero, high reactivity hydrocarbons (short chain hydrocarbons) are predominant. As the engine load is increased, and so are the GF values, high concentration of longer chain hydrocarbons starts to be found. This is evident

from the analysis of the results for both 50 % and 60 % of engine load, which are the conditions with higher GF levels.

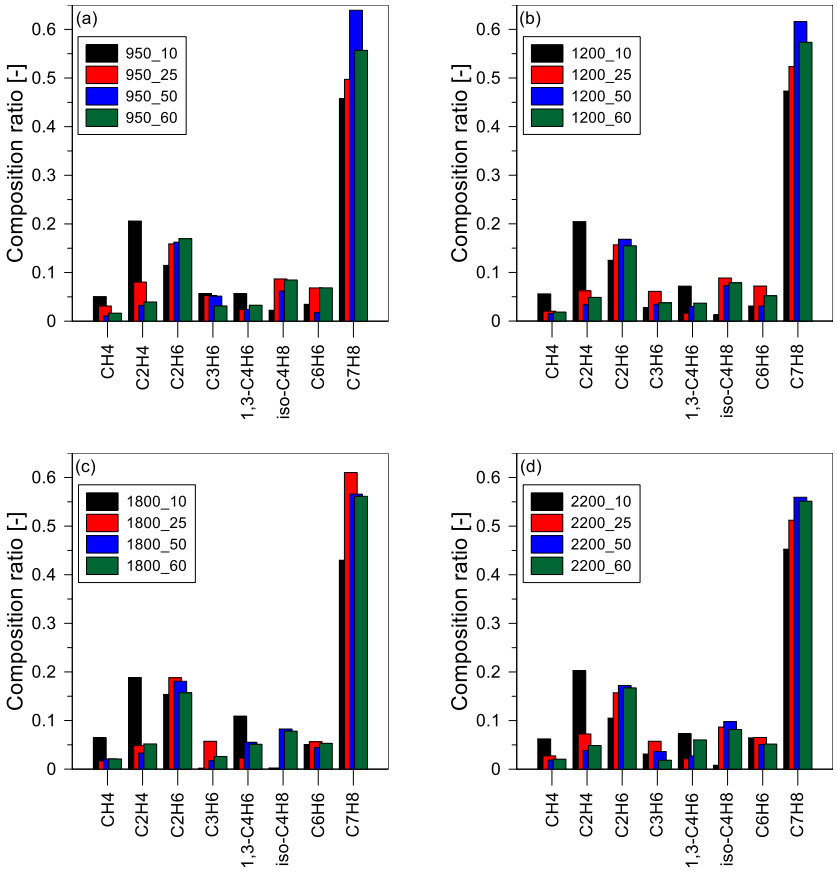

Figure 5.10. Hydrocarbon compounds at the exhaust gases for different engine loads and (a) 950 rpm, (b) 1200 rpm, (c) 1800 rpm and (d) 2200 rpm.

From this analysis, it can be inferred that the gasoline fraction plays an important role over the species found at the engine exhaust. As was mentioned, the different hydrocarbons were split in two groups: low reactivity and high reactivity. The first one comprehends the hydrocarbon chains ranging from C_4 to C_7 while the second addresses the chains from C_1 to C_3.

After grouping, the results were plotted against the GF being depicted in Figure 5.11. The analysis of the graph allows to visualize that there is a direct increase in the low reactivity hydrocarbons as the GF is increased. This means that more energy is required to obtain a proper oxidation of the partially unburned compounds at the DOC. Moreover, a regression fit was employed, obtaining two different equations. Each one of them allows the determination of either the low reactivity hydrocarbon or the high reactivity hydrocarbon concentration, enabling the proper quantification of the split that should be found at a specific operating condition based on its GF value. Finally, it can be concluded that the correct hydrocarbon split for dual mode dual fuel application should consider toluene as low reactivity specie and species with carbon chains ranging from C_2-C_3 (e.g., ethylene or propylene) as high reactivity hydrocarbon to properly describe the composition of the exhaust hydrocarbons.

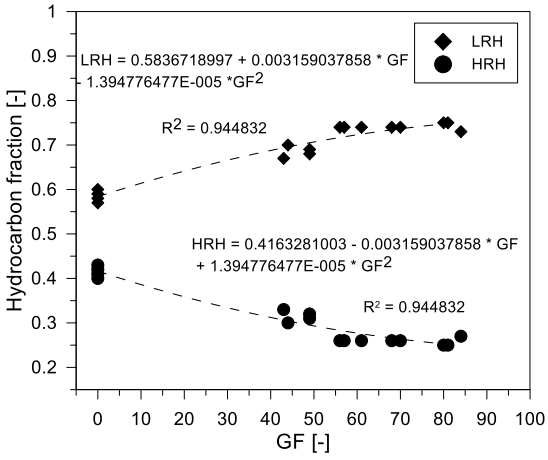

Figure 5.11. Exhaust low reactivity (LR) and high reactivity (HR) hydrocarbons dependence on gasoline fraction values.

5.2.2. DOC Transient evaluation

Steady-state conditions are useful to understand the ATS response to the imposed boundary conditions. Nonetheless, they are rarely found at real truck operation [9]. Moreover, the after-treatment system is often operated in closed loop, interacting with the engine ECU [10][11]. This allows to employ techniques to prevent the wall temperature of this device from falling to values lower than the light-off conditions. Some examples of this are the fast heating techniques used right after the engine starts to heat up the DOC or late post injections to regenerate the DPF. Recently, the powertrain electrification enabled the heating of the DOC without requiring energy from the fuel directly [12].

Once the monolith is heated, it can support the temperature levels for a determined period, due to both the thermal storage capacity of the device and the exothermal oxidation reactions of the unburned compounds. Therefore, these paths can be a route to improve the conversion efficiency at low load conditions pursuing to fulfill EUVI in the whole engine map for both HC and CO. In this sense, specific transient conditions were evaluated to assess the impact of different thermal loadings of the DOC on the conversion efficiency of HC and CO.

5.2.2.1. Methodology

The evaluation of the transient response of the DOC requires the use of simultaneous measurements at the inlet and outlet of it. In this sense, two different gas analyzers were employed: a Horiba FT (FTIR) at the DOC inlet and a Horiba Mexa (FID) at the DOC outlet. Therefore, time resolved signals of HC and CO could be obtained at the same time interval allowing to calculate the conversion efficiency of these components. In parallel, the values of temperature and pressure at the same locations (ATS inlet and outlet) and inlet mass flow were also acquired at an acquisition frequency of 10Hz by the AVL FEM-A acquisition boards. The characteristics of the measuring devices and sensors are those presented in the methodology section.

Different transient verifications were proposed, aiming to assess the impact of the boundary condition variation on the DOC performance efficiency. First, the ATS was heated employing an operating condition of 50 % of engine load and 1800 rpm at CDC operation, guaranteeing a high thermal flow through the device. After, the engine was directly moved to an operating condition of 950 rpm and 10 % of engine load, where the conversion efficiency of both HC and CO presents the lowest values, i.e., a critical condition. The instantaneous values of the different emissions, temperatures, mass flow and pressures were acquired allowing to evaluate the effect of the DOC thermal storage on its conversion efficiency.

Following the same idea of the previous evaluation, a second step was proposed. Nonetheless, at this time, an operating condition of 25 % of engine load and 1500 rpm was added between the previous operating conditions to account for more pessimist scenarios where critical operating conditions are preceded by similar low load conditions, which can represent deceleration to idle operation. Figure 5.12 illustrates both steps in terms of engine load, engine speed and time. Both cases are similar regarding the duration, the start and the final conditions and their results are useful to assess the characteristic times were the DOC can support the oxidation reactions through the energy storage.

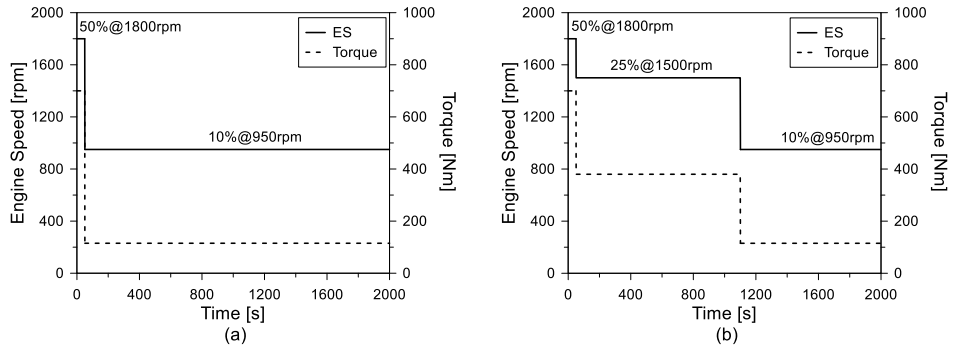

Figure 5.12. Graphical representation of the engine speed and load profiles considering (a) fast transitions to low load operation (50% to 10%) and (b) steeply reduction of engine load (50%-25%-10%).

Moreover, an additional step was proposed aiming to represent more realistic scenarios that can be found during the truck operation. To do this, the engine speed and IMEP profiles obtained for the WHVC in chapter 4 with 50 % of payload were analyzed searching for low engine power conditions. As it can be seen in Figure 5.13, these conditions are mostly verified at the first driving cycle phase that corresponds to the urban part. In this sense, a step was proposed as a simplification of the phase highlighted in yellow in Figure 5.13. In this period, the IMEP is reduced from 12 bar to ≈1 bar (idle operation). Then, the engine load is maintained during nearly 273 s, being increased again at the end of this period. During the 273 s, several engine speed variations are verified. This fast engine speed dynamic cannot be emulated by the engine once it is not equipped neither with closed loop control nor the engine maps are refined enough for this kind of application. In this sense, the process was simplified addressing only the engine load variations (a load step), neglecting the accelerations that exists during this period.

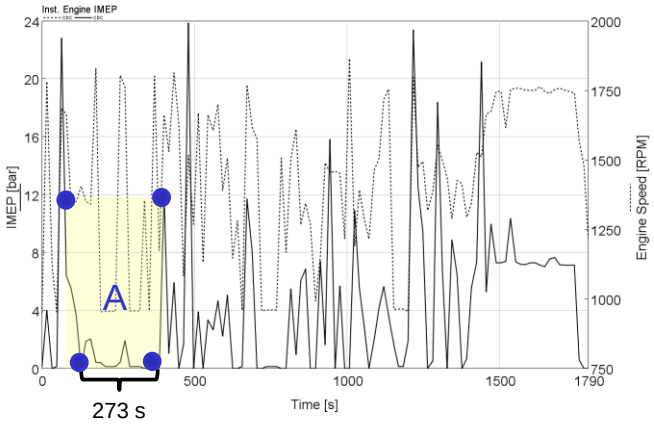

Figure 5.13. Indicated mean effective pressure and engine speed profiles for the truck on the WHVC driving with 50% of payload.

Finally, a supplementary engine test (SET) was proposed accounting for continuous changes in the boundary conditions regarding heat flow and emissions. Table 5.2 was obtained from the normative and presents the main

steps and guidelines to be followed during the test evaluation [13] (see Figure 5.14).

Table 5.2. Operating conditions and modes that should be considered during the supplementary engine test.

Ramped mode cycle	Time [s]	Speed [rpm]	Load [%]
1a	170	Warm idle	0
1b	20	Linear transition	Linear transition
2a	173	A	100
2b	20	Linear transition	Linear transition
3a	219	B	50
3b	20	B	Linear transition
4a	217	B	75
4b	20	Linear transition	Linear transition
5a	103	A	50
5b	20	A	Linear transition
6a	100	A	75
6b	20	A	Linear transition
7a	103	A	25
7b	2	Linear transition	Linear transition
8a	194	B	100
8b	20	B	Linear transition
9a	218	B	25
9b	20	Linear transition	Linear transition
10a	171	C	100
10b	20	C	Linear transition
11a	102	C	25
11b	20	C	Linear transition
12a	100	C	75
12b	20	C	Linear transition
13a	102	C	50
13b	20	Linear transition	Linear transition
14	168	Warm idle	0

Each one of the engine speed values are defined in the same manner than in the ESC (European Stationary Cycle) cycle following the rules from the equations 5.1 to 5.3.

$$A = n_{lo} + 0.25 \cdot (n_{hi} - n_{lo}) \quad 5.1$$

$$B = n_{lo} + 0.50 \cdot (n_{hi} - n_{lo}) \quad 5.2$$

$$C = n_{lo} + 0.75 \cdot (n_{hi} - n_{lo}) \quad 5.3$$

Where,

n_{lo}= the minimum engine speed where 50 % of rated power is achieved.
n_{hi}= the maximum engine speed where 70 % of rated power is achieved.

The load profile was scaled to account mainly conditions where fully premixed combustion is used, i.e., most challenging conditions. In this sense, the engine was submitted to the SET cycle obtaining information about the transient emission behavior considering operating conditions inside the D-G calibration that was presented previously in chapter 4. This scaling was proposed to avoid using high load conditions which could provide excessive heat flow, mitigating the effect of low engine load conditions. Figure 5.14 presents a simplified scheme of the cycle with the respective load percentage and engine speed ranges that should be employed during the testing.

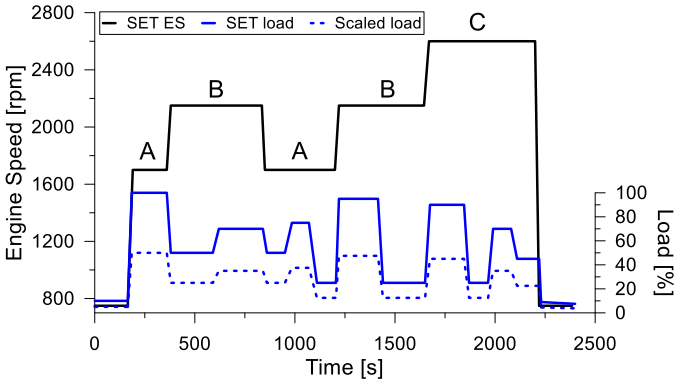

Figure 5.14. Graphical representation of the supplementary engine test illustrating the engine speed profiles as well as both original and rescaled engine load.

5.2.2.2. Oxidation catalyst transient results

The results for the different transient evaluations are presented in this section. The first two steps will be called step 1 and step 2, respectively. The third step will be referred as WHVC step as it was originated from this cycle while the last one will be named as SET.

Figure 5.15 illustrates the results for step 1, addressing the transition from an initial condition at 50 % load (12.4 bar IMEP) and 1800 rpm to a final condition at 10 % load (2.3 bar IMEP) and 950 rpm. As depicted in Figure 5.15 (b), the DOC starts with high conversion efficiency since the temperature at the outlet is considerably higher than that at the inlet. This means that the exothermic reactions in the DOC provide enough energy to heat the exhaust gases even in the case of losing part of the energy by heat transfer to the environment. These reactions are supported up to 800 s while operating at a 10 % engine load condition. From this time, the difference between both temperatures (inlet and outlet) starts to decrease, indicating lower conversion efficiencies. This can be better visualized in Figure 5.15 (c) and Figure 5.15 (d) where the DOC out emissions and the conversion efficiency of both HC and CO are presented. During the first 800 s, HC

conversion efficiency is maintained in values higher than 95 % resulting in DOC out HC emissions near EUVI limits. Once the inlet temperature decreases to levels below 180 °C, the unburned hydrocarbon oxidation reactions at the oxidation catalyst are drastically reduced. Consequently, the DOC out HC emissions increase near 15 times compared to the first period, surpassing by far the limits from EUVI. CO conversion reactions are supported for longer a time and do not demonstrated to be affected by the modification of the boundary conditions, allowing to maintain the tailpipe emissions under EUVI constraints even at the end of the step.

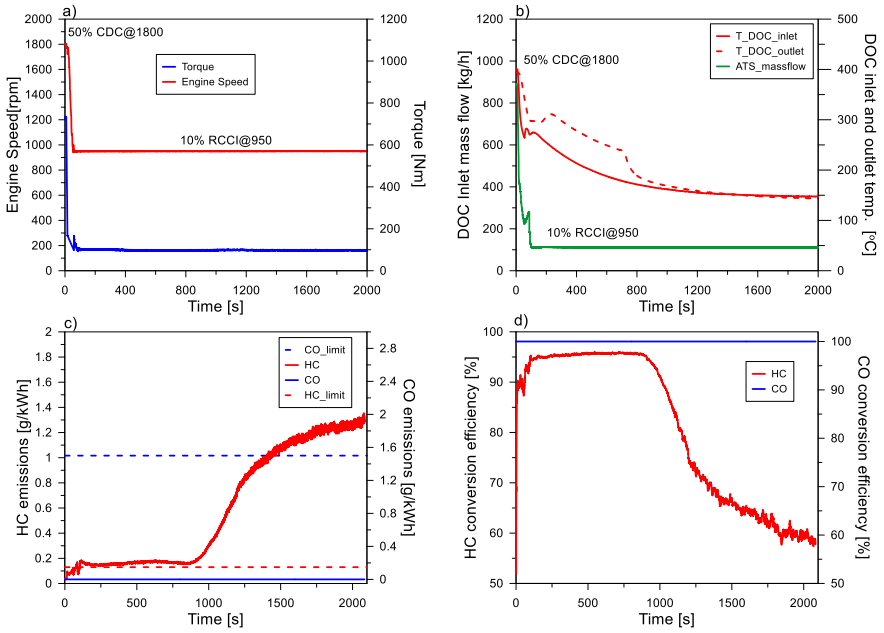

Figure 5.15. Instantaneous evolution of the (a) engine speed and torque profiles (b) mass flow and temperatures at the oxidation catalyst inlet and outlet, (c) tailpipe carbon monoxide and unburned hydrocarbon emissions, with its respective EUVI limits demarked in dashed lines and (d) carbon monoxide and unburned hydrocarbon conversion efficiencies for the step 1.

To obtain deeper insights about the DOC response to the modification of the boundary conditions an additional step was evaluated (step 2). The

main difference relies on the addition of an intermediate condition at 25 %@1500 rpm. This condition has lower temperature and probably will reduce the time where proper conversion efficiency is found at 10 %@950 rpm.

Figure 5.16 (b) confirms the reduction of the interval where high conversion efficiency for HC is achieved. As it can be seen, once the operating condition is modified from 25 % to 10 % of engine load, the difference between the DOC inlet and outlet temperature starts to decrease for an interval of up to 400 s. This is half the time found for the previous step (50 % → 10 %). It is interesting to note that despite of the differences in time, the temperature threshold from which the efficiency starts to decrease is nearly the same for both steps.

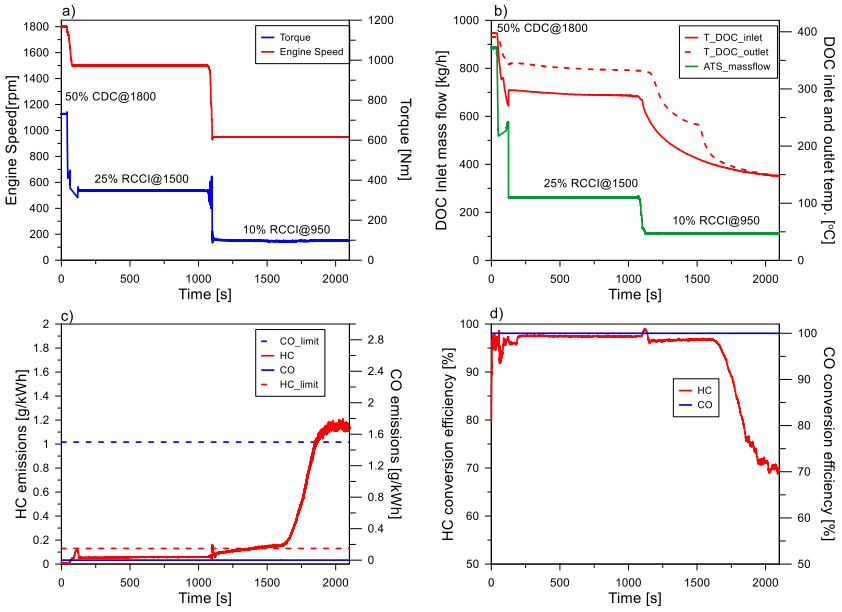

Figure 5.16. Instantaneous evolution of the (a) engine speed and torque profiles (b) mass flow and temperatures at the oxidation catalyst inlet and outlet, (c) tailpipe carbon monoxide and unburned hydrocarbon emissions, with its respective EUVI limits demarked in dashed lines and (d) carbon monoxide and unburned hydrocarbon conversion efficiencies for the step 2.

Once the temperature crosses the 180 ºC threshold, the HC conversion efficiency starts to decrease exponentially. This indicates that the DOC is close to its light-off condition. Even though, EUVI values for both HC and CO could be achieved up to 1500 s. In addition, the interval of 400 s at low load is difficult to be achieved in normative cycle. Nonetheless, its importance is justified by real driving conditions where the truck can be stopped for large periods in heavy traffic conditions.

The previous steps were intended to illustrate the light-off temperature of the oxidation catalyst and the critical times during which the conversion efficiency could be maintained ($> 95\%$) from using the thermal storage of the DOC. To obtain this, they were designed to have large duration (2200 s). Nonetheless, as demonstrated in Figure 5.13 (methodology section) they are not representative of normative driving conditions, where idle times are shorter. In this sense, the DOC was submitted to the previously described WHVC based step. Figure 5.17 depicts the results obtained in terms of temperature, emissions, and conversion efficiency. It is worth to mention that the transition between the operating points is done manually, which results in peaks during the transition due to instabilities in the engine speed. This should be neglected during the analysis.

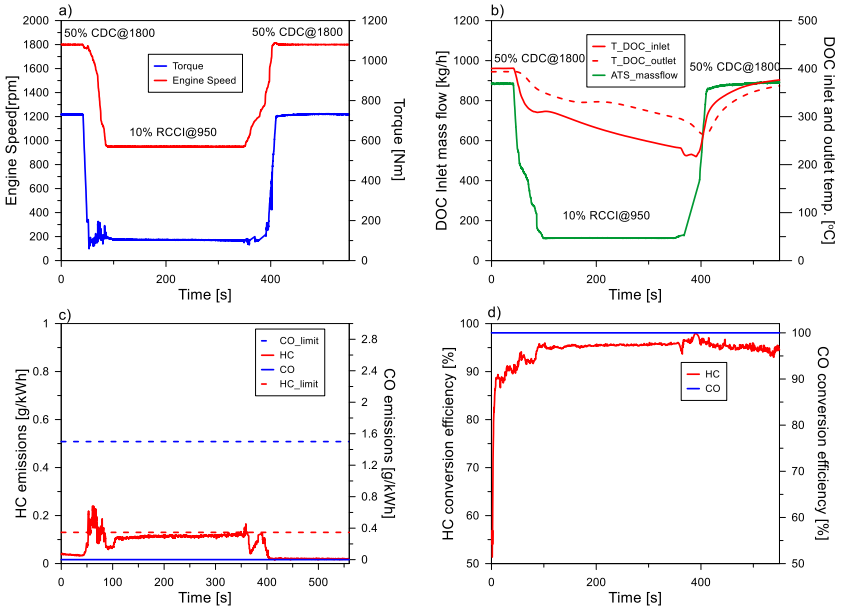

Figure 5.17. Instantaneous evolution of the (a) engine speed and torque profiles (b) mass flow and temperatures at the oxidation catalyst inlet and outlet, (c) tailpipe carbon monoxide and unburned hydrocarbon emissions, with its respective EUVI limits demarked in dashed lines and (d) carbon monoxide and unburned hydrocarbon conversion efficiencies for the WHVC based step.

The initial condition is a medium load condition that provides enough energy to convert the unburned hydrocarbons and carbon monoxides. Once the operating condition is modified to a low load condition (10 %@950 rpm), the conversion should be maintained by means of the stored energy from the previous condition. This is confirmed by Figure 5.17 (b), (c) and (d). Figure 5.17 (b) demonstrates that the outlet temperature is maintained above the inlet temperature values during the whole period in which the engine is at low load condition. This is caused by the conversion efficiencies up to 95 % during this period (Figure 5.17 (d)) which guarantees EUVI compliant HC and CO levels (Figure 5.17 (c)). Therefore, when the load is increased again, the DOC is still operating under light-off condition. The high load condition

that follows in the step is a high temperature condition that allows to heat up the DOC again and to assure stable and efficient conversion of both unburned hydrocarbons and CO as can be evidenced from the figure analysis.

Finally, the DOC was submitted to the supplementary engine tests to assess its performance on a wider range of operating conditions and in a representative cycle. The different results obtained during the evaluation are presented in Figure 5.18. Before starting the tests, the engine was heated up in motoring condition until achieving 80 °C of oil and water temperature. As seen in subfigure Figure 5.18 (b), the DOC temperature also increased as the hot air from the compression flowed through the DOC during the warming time. Once the temperature thresholds were achieved, the SET cycle was performed.

Figure 5.18 (a) depicts the absolute values of engine speed and engine torque during the SET. The variation of both implies different boundary conditions in which regards the temperature and air flow at the DOC inlet as illustrated in Figure 5.18 (b). The comparison of the inlet and outlet temperature indicates that it takes more than 400 s until they crossed each other. This suggests that during this time, the oxidation catalyst, still, did not reach its light-off temperature. In this sense, the low conversion provides energy values that are not able to overcome the DOC heat losses, resulting in lower temperatures at the outlet. This 400 s can be defined as the DOC warming period, which is known to be the most significant stage in terms of tailpipe unburned species production during normative evaluation [14].

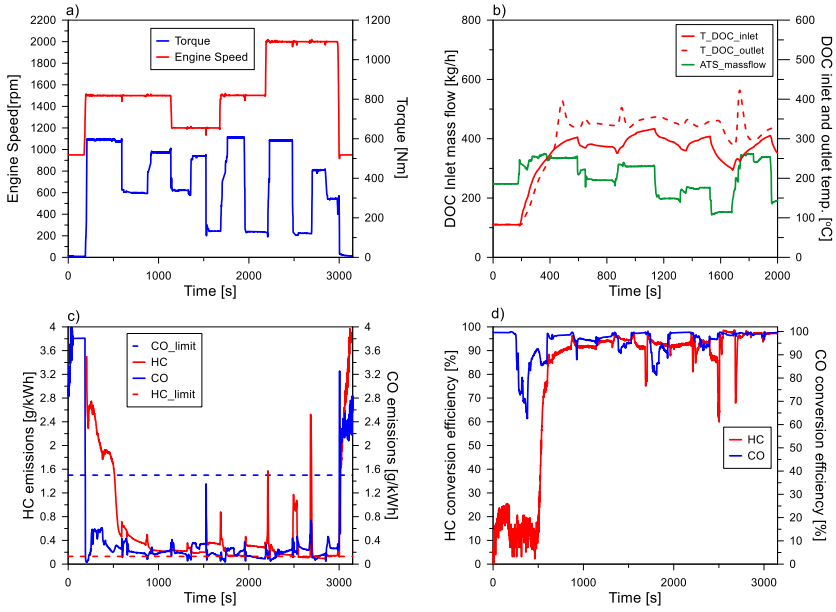

Figure 5.18. Instantaneous evolution of the (a) engine speed and torque profiles (b) mass flow and temperatures at the oxidation catalyst inlet and outlet, (c) tailpipe carbon monoxide and unburned hydrocarbon emissions, with its respective EUVI limits demarked in dashed lines and (d) carbon monoxide and unburned hydrocarbon conversion efficiencies for the scaled SET cycle.

As the cycle progresses, the light-off operation is achieved (≈190 °C) and the exothermic reactions can be supported, achieving conversion efficiencies higher than 90% for both HC and CO during the remaining part of the transient cycle (Figure 5.18 (d)). It should be remarked, again, that the conversion efficiency peaks that are found in the engine velocities modifications are mainly related to abrupt changes in the intake air mass flow, which impacts the determination of the pollutants mass fraction at the exhaust.

The analysis of the absolute values of CO and HC, presented in Figure 5.18 (c) suggests that once the light-off condition is surpassed, the carbon monoxide emissions can be reduced to levels far inferior from those of the

EUVI normative. By contrast, the unburned hydrocarbon conversion seems to be a hurdle. The combination of longer warming periods and the operation at engine loads lower than 50% during the cycle, are a challenging scenario once the low exhaust temperatures from the fully premixed combustion and the excessive concentration of the unburned products at the exhaust are combined. Therefore, the values of tailpipe HC are not able to fulfill the normative constraints, independently on the operating condition. Yet, the tailpipe HC are at levels where small enhancements that allow increasing the conversion efficiency could provide the required decrease to achieve the EUVI emissions. It should be remarked that these challenging scenarios are found only in the early phases of the normative driving cycles. As the cycle progress towards highway phases the conversion efficiency should be enhanced because of the high temperatures at the exhaust. The evaluation of the full driving cycle should improve the overview about the DMDF impact on the DOC once it allows to obtain a weighted value of the tailpipe emissions according to the whole operating points. Since the experimental facilities do not allow to perform this analysis, a numerical approach is proposed. This will be further discussed in the subsequent sections.

5.2.2.3. Summary

After the transient verifications, it can be concluded that the use of the thermal inertia to maintain the oxidation reactions during low load/low temperature conditions can provide significant improvements on the global perspective of the DOC compared to the steady-state results. Figure 5.19 summarizes and updates the previous DOC out HC and CO maps with the results obtained in this last section. The transient points are those addressed in the SET test, described above. As it can be seen, the maximum HC value was reduced from 5 g/kWh to 0.5 g/kWh, i.e., one order of magnitude. Moreover, the zone fulfilling $0.13<HC<0.26$ (higher than EUVI limits and lower than two times the limit) was also extended. Only small regions do not meet these first criteria and are in the two extremes of the map. This should

be related with the lower temperature (low engine speeds) and with short residence time (higher engine speed).

CO emissions were also considerably improved, reducing its maximum value by a factor of 60. This allowed to fulfill EUVI for the whole set of operating conditions evaluated. It should bore in mind that this corresponds to conditions where the DOC already achieved its light off operation. As it was demonstrated in the SET, there is a significant period to achieve this condition with the current configuration. Additional evaluations should be made to optimize the DOC architecture to deal with this issue. Moreover, the performance of the DOC must be evaluated in a driving cycle condition to allow the weighting of the critical conditions on the driving cycle results. This will also allow to identify what are the most challenging phases as well as to suggest possible solutions to tackle this issue. The application of heating by external methods (e.g. electric resistances) could be a potential solution. However, powertrain electrification and extra fuel consumption need to be analyzed. As this is out the scope of this work, it is proposed as future work.

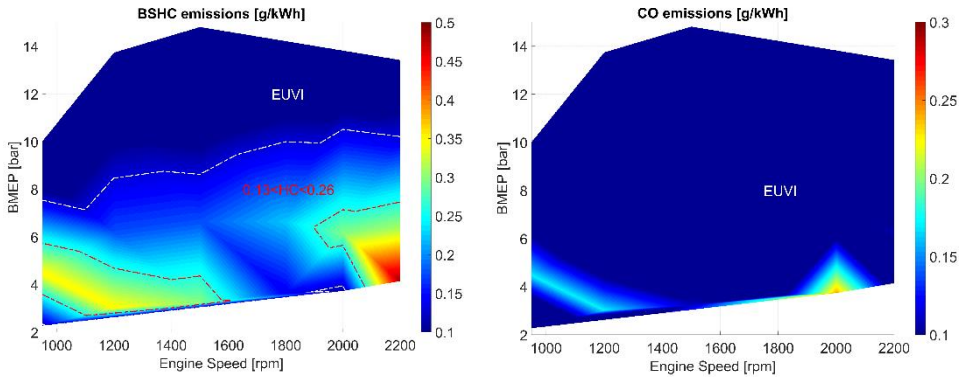

(a) (b)

Figure 5.19. Iso contour graphs representing the tailpipe emissions considering the DOC heat storage capacity for (a) unburned hydrocarbons and (b) carbon monoxide from low to medium load operation. The white line demarks the zones that can fulfill EUVI limits, while the red line represents the zones that are lower than two times the EUVI constraints.

5.3 DPF assessment

The results from Chapter 4 demonstrated that the proposed calibration operating on DMDF combustion was able to fulfill NOx EUVI limits under normative conditions. Nonetheless, the same cannot be extended for soot. This scenario is even more challenging as the payload is increased towards full truck load since the soot emissions drastically increased due to the amount of operating conditions at the diffusive combustion regime. In addition, the proposed calibration map is based on dual route EGR (HP and LP EGR). Therefore, the use of the DPF cannot be avoided as the exhaust gases should be cleaned before entering the air route to avoid damages on turbocharger, valves, and piston [15].

The working principle of the DPF requires periodical cleaning of the soot that is filtered in the channels. This can be achieved by means of both passive and active regeneration [16]. The first relies on the conversion of the solid carbon by the reaction with NO_2 from the exhaust [17]. The second requires higher temperature and oxygen excess atmosphere to oxidize the solid carbon [18]. Both methods can be impaired in the DMDF concept, since the NO_2 concentration in the exhaust gases is very low (total NOx < EURO VI in most of the calibration map) and the exhaust temperature is reduced because of the low temperature combustion regime. In this sense, this section proposes the evaluation of both DPF regeneration methods through dedicated experimental routines.

5.3.1. Passive Regeneration

The high reactivity of NO_2 and particulate matter at moderate temperatures (≈100 °C - 500 °C) has become an effective way off assisting the DPF cleaning during the engine operation. This cleaning mode does not require additional fuel consumption (fuel injection to increase the exhaust temperature) and occurs naturally in the presence of NO_2 and soot in a

passive manner by two main reaction pathways as described by reaction 5.1 and reaction 5.2 [19].

$$C+2NO_2 \rightarrow CO_2 + 2NO \qquad r.5.1$$

$$C+ NO_2 \rightarrow CO+NO \qquad r.5.2$$

The passive regeneration process can be evaluated by means of tracing the NO_2/NOx ratio along the DPF (inlet and outlet), as the reaction of the NO_2 with solid carbon will modify the proportion of NO_2 in the NOx emissions as it passes through the DPF. The DMDF combustion introduces some questions regarding the passive regeneration process. First, the low NOx concentration found at the exhaust gases can be a challenge in reducing the soot trapped in the DPF. Moreover, the NO_2 ratio in the NOx can be also different from those of conventional diesel combustion (which ranges from 5 % to 30 %) [20] once the environment in which the DMDF combustion take places changes significantly with respect to CDC in terms of temperature, composition, etc.

Therefore, a detailed analysis of the passive regeneration process is proposed by assessing the NO_2, NO and NOx concentrations at representative sites on the aftertreatment system. First, these species were measured just before the DOC inlet avoiding any reaction that could take place inside the DOC to account the real proportion of NO_2/NOx of the exhaust gases. Finally, measurements were also made at both DPF inlet and DPF outlet assessing the possible NO_2 variation in the DPF, which should be attributed to the passive regeneration process. The evaluation process consisted of a first cleaning step to assure a regenerated DPF prior to testing followed by increasing temperature points from 170 °C to 360 °C.

Figure 5.20 depicts the NO_2/NOx ratio at each after treatment location that was previously introduced. The analysis of the results just before the DOC allows to identify an interesting phenomenon. The NOx composition differs significantly from the values for diesel combustion found in the literature results. As it can be seen in Figure 5.20 (a), the NOx

produced during the DMDF combustion are composed in majority by NO_2 rather than NO, which could be beneficial for the passive regeneration. The next measurement point is placed between the DOC outlet and the DPF inlet, allowing to monitor the boundary conditions prior entering the DPF. But, before starting the DPF analysis, a modification of the NO_2/NOx ratio profile is worth of discussion, which is depicted in Figure 5.20 (b). It can be evidenced that the NO_2 concentration for temperatures below 200 °C is significantly reduced once the exhaust gas flows through the DOC. Literature investigations have reported that this phenomenon is not restricted only to the DMDF concept, being also visualized for CDC combustion for conditions with low temperature and high concentration of unburned products. At these environments, the unburned hydrocarbons can act as reductants, reacting with the NO_2 in the gases to form NO [21][22].

Lastly, Figure 5.20 (c) presents the NO_2/NOx results at the DPF outlet which enable the direct comparison with the NO_2/NOx ratios from the DPF inlet accounting the NO_2 consumption that could occur during the passive regeneration. As it can be seen, the DPF outlet profile does not show any appreciable change compared to the respective DPF inlet. Therefore, it can be concluded that both reaction 5.1 and reaction 5.2 are not occurring, since the NO_2 ratio remains unaltered. In other words, the soot mass trapped in the DPF is not reduced by the NO_2 concentration. It is suggested that this can be attributed to the low concentration of this specie coupled with the low soot mass that is produced during the DMDF operation, which reduces the area to surface reactions.

Therefore, the passive regeneration of the DPF was proven to not be an effective way of reducing the soot amount during the operation. In this sense, alternative methods must be employed to avoid the problems that can be associated with the DPF filling as the increase of backpressure and the consequent reduction of conversion efficiency. Such active methods are generally based on increasing the temperature at the DPF to levels where the soot can be oxidized. This can be accomplished by injecting an extra fuel quantity prior to the DOC. Once this fuel is converted, the exothermic

reactions will increase the flow temperature to levels where the active regeneration is possible [23]. Nonetheless, the DMDF concept already presents excessive amounts of HC and CO, that could be enough to increase the exhaust temperature to levels which enable an active regeneration process. Therefore, dedicated studies were performed to identify the potential of this approach on reducing the soot mass trapped on the DPF and will be discussed in the next subsection.

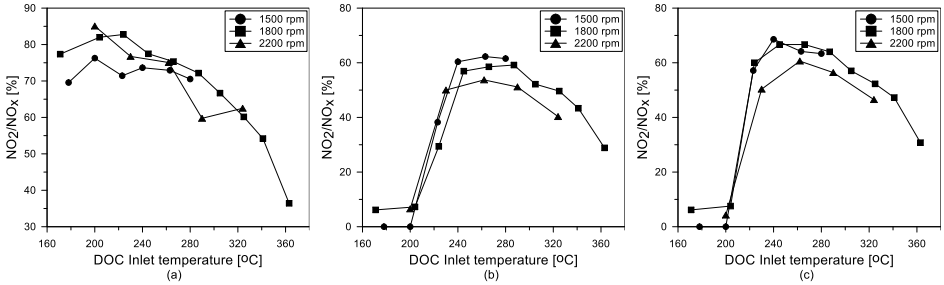

Figure 5.20. NO_2/NOx profiles at (a) oxidation catalyst inlet, (b) oxidation catalyst outlet/particulate filter inlet and (c) particulate filter outlet.

5.3.2. Active Regeneration

Active regeneration has demonstrated to be an effective way of reducing the soot emissions trapped in the DPF. Its working principle is based on the soot oxidation by means of the reaction with oxygen at high temperatures [24]. However, getting such high levels of temperature generally requires the implementation of strategies that penalize the fuel consumption. The most conventional methods that are found in conventional diesel engines are the use of post injections [25], which burn at late phases of the compression stroke and increase the exhaust temperature, or the introduction of an additional fuel injector at the exhaust to add fuel prior to the DOC [26]. Once this fuel passes through the DOC, it will be oxidized, significantly increasing the overall exhaust temperature.

Depending on the engine configuration and the operating condition, high exhaust temperatures can be obtained without the introduction of the techniques previously described. These conditions generally last for short periods during engine operation, mainly at high engine loads. Despite, this works as an auxiliar regeneration method, which can increase the interval between active regenerations and reduce the fuel consumption penalization. Although CDC combustion has room for this kind of regeneration, it is believed that the extension of these assertions to LTC combustion can be difficult to accomplish. This is justified by the overall lower exhaust temperature which is a consequence of the higher dilution levels within the cylinder. On the other hand, the DMDF combustion has demonstrated to provide excessive concentration of unburned products at the exhaust. This could be a way of counterbalancing the low temperature at the exhaust, since the unburned products should be converted in the DOC, providing heat to the flow. This may increase the exhaust temperature to similar levels than those found with and additional fuel injection.

Therefore, studies dedicated to evaluating the feasibility of these strategies on the DMDF were proposed. Initially, the soot mass trapped in the DPF was increased by means of running the engine in DMDF condition with high soot production. Next, a high temperature condition on CDC combustion was used to regenerate the DPF. Finally, the DPF was submitted again to a condition with high soot production. Nonetheless, the regeneration process was then attempted with a DMDF operating condition at medium load operation with high amounts of HC and CO aiming to assess the effect of the unburned products conversion on the temperature at the DPF inlet and its subsequent regeneration. Figure 5.21 depicts the results obtained for the first evaluation, considering a CDC operating condition to regenerate the DPF. As discussed, first, the DPF was loaded to assure significant soot mass prior to the start of the regeneration. This was accomplished by running the engine during 15 hours in a high soot operating condition from the calibration map. The soot mass evolution was obtained by removing the DPF in hot conditions and weighing it at intervals of five hours. The evolution of the soot mass trapped in the DPF can be evidenced in Figure 5.21 (a) allowing

to infer that the DPF weight variation obtained after 15 h was as small as 10 g as a consequence of the low soot production at the DMDF operation.

Then, the regeneration process was started by employing a CDC operating condition at 60 % of engine load and 1800 rpm with exhaust temperatures of 390 °C for one hour. Every 20 min, the DPF was removed at hot conditions and weighted, allowing to draw the soot reduction profile that is presented in Figure 5.21 (b). As it can be seen, the most significant reductions are verified in the first 20 min, where almost 70 % of the total soot mass was reduced (≈ from 10 g to 3 g). As the soot mass decreases, slow reduction rates are verified, with reductions of 2 g during the following 40 min. This can be attributed to the decrease of the soot surface area available to react with the oxygen in the exhaust environment [27][28]. Therefore, it can be concluded that the temperature levels found at a CDC operation are suitable to reduce the soot amounts in a faster rate than soot is produced, allowing to maintain the DPF under proper operating conditions.

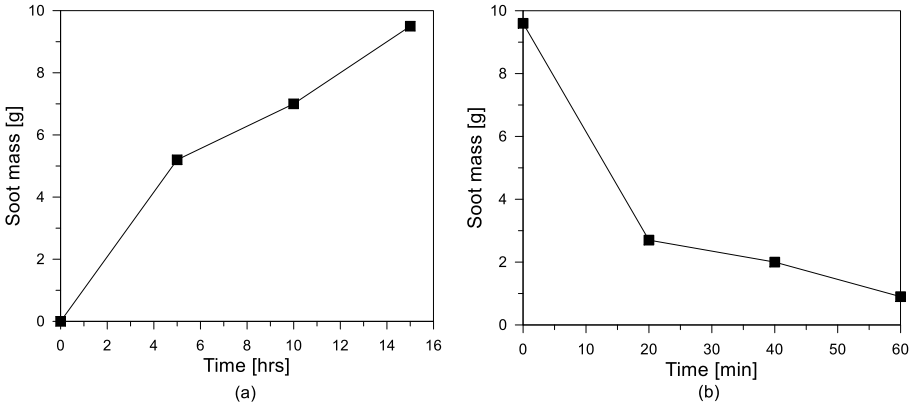

Figure 5.21. Variation of the soot mass in the DPF during the (a) loading (DMDF operating condition) and (b) regeneration phases (CDC operating condition).

In spite of the interesting results obtained with CDC regeneration, the replication of these conditions with DMDF combustion presents a challenge since exhaust temperatures of 390 °C are rarely found in the DMDF

calibration. As discussed, the high HC and CO concentration may provide an alternative to increase the pre-DPF temperatures by means of the oxidation of these species in the DOC. In this sense, the temperature increase at the DOC was assessed for an engine speed sweep at 50 % of engine load. This load was chosen due to the trade-off between exhaust temperature and HC and CO levels. Figure 5.22 illustrates the temperature before and after the DOC for the different engine speeds. In addition, the previous CDC temperature that was used for the first regeneration is also included for comparison purposes. As shown, there is a significant temperature increase as the gas flows through the DOC because of the unburned products conversion, being as high as 50 °C at 1800 rpm. This temperature increase allows to achieve similar temperature levels than that presented in the CDC operation. Therefore, it can be suggested that the operating condition of 1800 rpm at 50 % load should be capable of enabling the DPF regeneration by O_2 reaction. Reductions on the regeneration efficiency should be expected due to the lower exhaust mass flow of the DMDF compared to the CDC, resulting from the different EGR quantities.

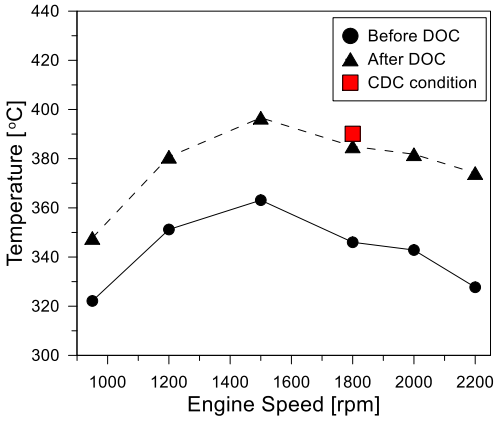

Figure 5.22. Temperature values before and after the oxidation catalyst at 50% of engine load and different engine speeds for DMDF operation. The red marker stands to the oxidation catalyst outlet temperature of a similar conventional diesel combustion condition.

Figure 5.23 illustrates the results of the DPF regeneration considering a DMDF operating condition at 50 % of engine load and 1800 rpm. First, the DPF was loaded with soot. It should be remarked that a different operating condition was selected to load the DPF, with modified settings to speed up the filling phase. As it can be seen in Figure 5.23 (a), the loading process was faster than the previous case, allowing to obtain 25 g of soot in only one hour. Next, the proposed operating condition for regeneration was set and the DPF weight evolution was assessed following the same strategy than before (measurements every 20 min).

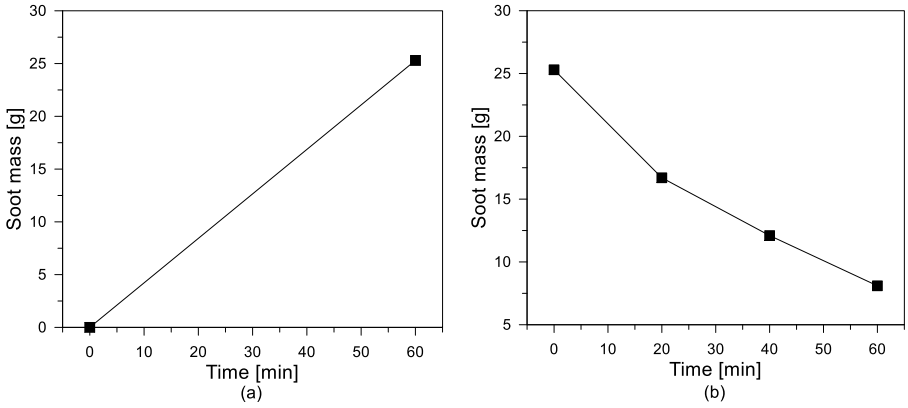

Figure 5.23. Variation of the soot mass in the DPF during the (a) loading (with DMDF high soot condition) and (b) regeneration phases (DMDF condition).

The analysis of the results presented on Figure 5.23 (b) allows to conclude that the DMDF operation enables to realize a significant soot reduction by means of oxygen regeneration. Nonetheless, it can be inferred that the regeneration rates are smaller than those from CDC. This can be evidenced when comparing the total reduction obtained considering that the regeneration process starts at the third measurement point on Figure 5.23 (b) which has a similar soot mass than the CDC regeneration. While the CDC operating condition was able to reduce the soot mass in seven grams in 20 min, the DMDF only achieved a reduction of two g for the same time. As discussed, this behavior may be a result of the low energy that flows through

the DPF due to the low exhaust mass flow from the DMDF combustion. Yet, it can be concluded that the DMDF operation was demonstrated to achieve the required temperatures by means of the unburned products conversion to realize soot oxidation by means of O_2 reaction.

5.4 DOC and DPF evaluation through driving cycle approach

From the previous discussions, it was concluded that the DOC is able to maintain a stable conversion of the unburned products as long as the light-off conditions are achieved. Nonetheless, it was also identified that the warming times of the DOC are generally higher due to the low exhaust temperatures, with excessive tailpipe HC emissions during this period. The contrasting behaviors raise the necessity of evaluating the DOC at normative conditions, where both warm-up phase and the following DOC operation can be assessed in a weighted manner. This allows to account the average emissions at the end of the cycle and compare them against the normative limits.

In this sense, this section intends to describe the calibration and posterior incorporation of both DPF and DOC models on the previous GT-Drive model described on Chapter 3. This model update will allow to assess the CO, HC and soot emissions after the ATS system (tailpipe emissions). In this sense, it will enable a better assessment of the DMDF effect on the performance of the ATS system. First, the DOC and DPF models will be calibrated using the available experimental measurements for both steady and transient conditions. Afterwards, the calibrated models will be used in the main truck model to assess the HC and CO conversion efficiency as well as the soot ATS-out emissions. This analysis will be extended to the same conditions presented in chapter 4 and the results will be compared to the normative constraints.

5.4.1. Methodology

The proseded evaluation follows the lines offered in chapter 4, with the addition of the ATS devices. In this sense, the methodology addressing the driving cycle will be not herein discussed. This subsection will be focused on the coupling of the DOC model to the main GT-drive model and the use of the outputs of the simulation as inputs in the DPF model.

First, a detailed DOC model was configured in GT-Power to allow the calibration of the important constants of the single step reactions from Sampara and Bisset's mechanism [29][30]. Then, the optimization of the calibration constant was performed by means of a genetic algorithm optimizer. The detailed procedure for this phase is described in the next subsections. Finally, the calibrated DOC model was included in the GT-Drive model as presented in Figure 5.24.

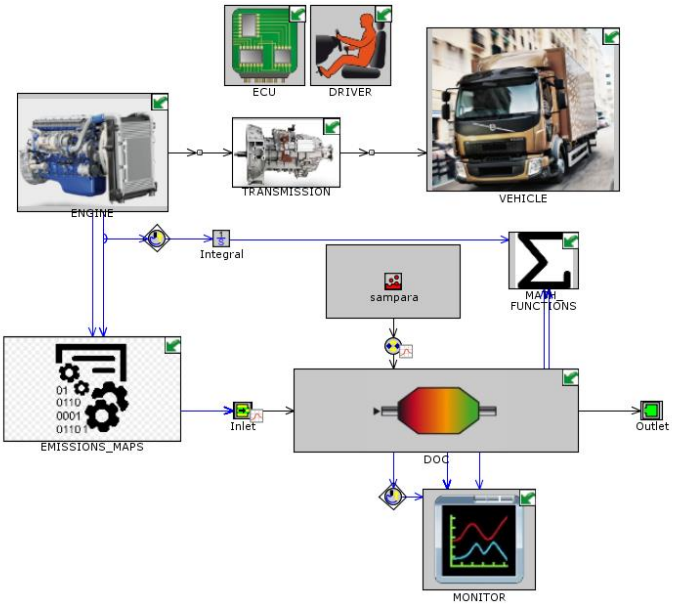

Figure 5.24. GT-Drive model consisting of the vehicle model at the upper part of the figure and the diesel oxidation catalyst model with its respective boundary conditions at the bottom part.

Additionally, experimental maps were included in the model to allow the determination of the experimental boundary conditions at the DOC inlet. First, the air mass flow as well as the inlet temperature were inserted by means of a three-dimensional array, resulting in the surface maps presented in Figure 5.25.

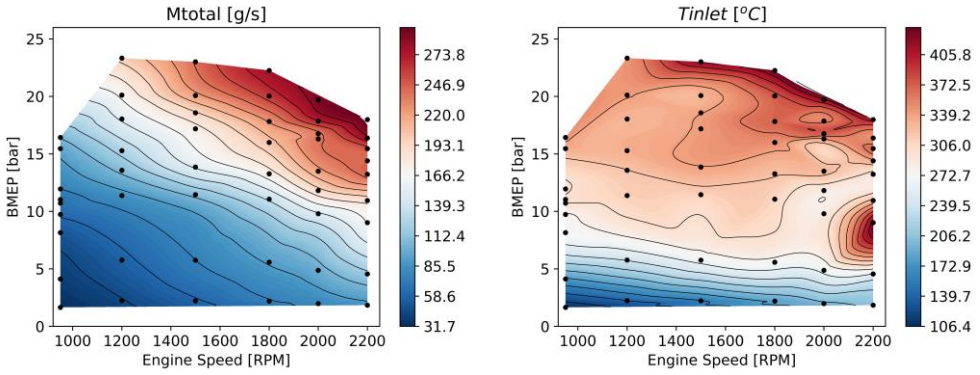

Figure 5.25. Iso-surface maps depicting the (a) total mass that flows through the oxidation catalyst and (b) the temperature just before entering the oxidation catalyst as function of the engine speed and brake mean effective pressure.

Finally, the composition of the exhaust gas was specified by means of the molar fraction of the most significant species at the exhaust. This was determined considering the experimental measurements from the gas analyzer and solving a set of equations for a 11 species global reaction as described in chapter 4. This allows to determine the concentrations of the remaining species to be considered in the DOC inlet (e.g., H_2O and H_2). Moreover, the different hydrocarbon composition in the exhaust gases was modelled following a dedicated methodology to account o account low reactivity hydrocarbons from diesel and gasoline. First, the total hydrocarbons were split with respect to the gasoline fraction as an indicative of the source (gasoline or diesel) employing equations 5.4 and 5.5.

$$X_{gasoline} = X_{total\ hydrocarbons} \cdot GF \quad 5.4$$

$$X_{diesel} = X_{total\ hydrocarbons} \cdot (1 - GF) \quad 5.5$$

From this moment, each fuel was treated separately and was split in low and high reactivity species following the literature recommendations [30]. For diesel, 40 % in molar basis of the total hydrocarbons were considered as high reactivity hydrocarbon (propylene – C_3H_6) and the remaining were considered low reactivity hydrocarbons (diesel vapor). Regarding gasoline, propylene was used as high reactivity hydrocarbon (80 % of total hydrocarbons) while propane was considered to emulate the low reactivity species (20 % of total hydrocarbons). The division was made following the steps presented from equation 5.6 to equation 5.9.

$$X_{C_3H_{6_g}} = X_{gasoline} \cdot 0.8 \quad 5.6$$

$$X_{C_3H_8} = X_{gasoline} \cdot 0.2 \quad 5.7$$

$$X_{C_3H_{6_d}} = X_{diesel} \cdot 0.4 \quad 5.8$$

$$Y_{dieselvap} = Y_{diesel} \cdot 0.6 \quad 5.9$$

Based on this, the final equation representing the exhaust hydrocarbon composition can be written as:

$$X_{totalhydrocarbons} = X_{C_3H_{6_d}} + X_{C_3H_{6_g}} + X_{C_3H_8} + X_{dieselvap} \quad 5.10$$

Figure 5.26 presents the resultant maps for each hydrocarbon specie that was used during the simulation. A look-up table-based approach was employed in the simulation, where for each time step, a molar fraction of each component was interpolated considering the BMEP and engine speed. This information was passed to the DOC inlet updating the boundary conditions at the same time step than the simulated quantities. Once the

model is set, the same driving cycles and payloads evaluated in chapter 4 were simulated again to obtain the DOC out emissions.

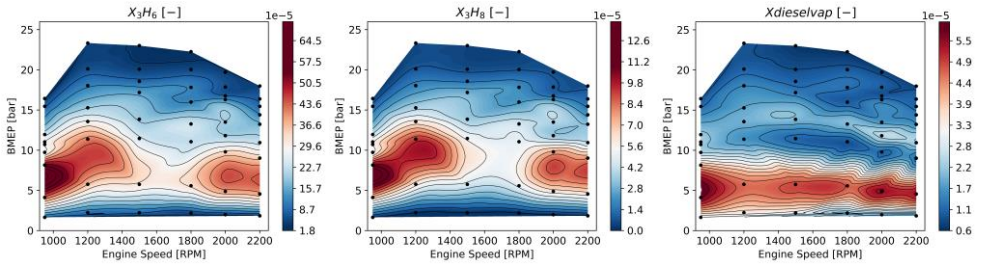

Figure 5.26. Iso-surface maps depicting the molar fractions of (a) propylene (b) propane and (c) diesel vapor as function of the engine speed and brake mean effective pressure.

5.4.2. DOC calibration

Prior to the cycle assessment, the DOC model should be calibrated. This includes the proper characterization of the energy of activation and pre-exponential factors of the simplified reaction mechanism that is employed. This also addresses the heat transfer characterization of the model to emulate the experimental conditions. Once this is achieved, the numerical model will be able to predict the conversion efficiency of both HC and CO, as well as to deliver the values of temperature at its outlet. The subsections that follow describe the detailed procedures that were followed during the calibration.

5.4.2.1. Methodology

The data set obtained in section 5.2.1 contains more than 20 operating conditions addressing different combinations of GF, EGR, load, ES, etc. This provides a range of temperature, species concentrations and mass flow conditions at the DOC inlet which govern the DOC conversion efficiency. In this sense, the data set was then divided in two groups: a calibration and a verification dataset. The first group was ordered according to the

temperature values at the inlet and the conversion efficiency of CO and HC, from the lower to the higher value. This allows to identify characteristic conditions as the light-off of the DOC (condition where the species starts to have conversion efficiency higher than 50 %). The different operating conditions used to calibrate the DOC are presented in Table 5.3.

Table 5.3. description of the operating conditions used as calibration dataset for the DOC model.

Op. Cond.	ES [rpm]	BMEP [bar]	$\dot{m}$ [g/s]	T_DOC$_{inlet}$ [°C]	HC [ppm]	CO [ppm]	O2 [%]	HC$_{conv}$ [%]	CO$_{conv}$ [%]
1	1200	2.15	43.46	176	432	2436	12.08	42.80	12.04
2	1800	2.10	75.72	208	742	1433	12.88	89.90	99.69
3	2000	1.91	81.00	214	720	1501	12.31	91.61	99.72
4	2200	1.78	85.25	227	329	2335	10.88	92.20	99.79
5	1200	5.66	57.48	256	3912	1420	8.62	96.47	99.88
6	1500	5.74	76.90	273	3432	1737	8.95	96.78	99.64

Once the operating conditions are defined, the calibration process can be started. For this, a DOC simulation model was built in GT-Power and it is presented in Figure 5.27. As depicted, the model is composed by two environment structures were the boundary conditions are defined. At the inlet, the temperature, gas composition and mass flow are set while at the outlet, the backpressure and environment temperature are defined. Both flow splits work as the DOC canning, modeling the flow expansion from the pipe to the higher diameter of the DOC.

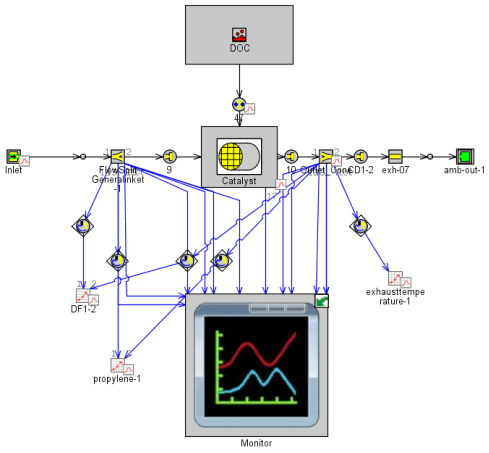

Figure 5.27. Oxidation catalyst model developed in GT-Power.

The catalyst brick allows the user to specify all the geometric characteristics as well as the materials of the substrates and walls. Moreover, this object contains the information used to calculate the heat transfer from the gases to the wall and from the wall to the environment through convection and radiation. These are some of the characteristics that should be adjusted with respect to the experimental observations in transient conditions to observe the thermal inertia of the device and the energy balance.

The object in the top of the figure comprehends the chemical reactions that govern the conversion of the unburned species to the burned ones. As previously stated, the mechanism from Sampara and Bisset was chosen to be used in this research, since it demonstrated to predict the conversion efficiency of both gasoline and diesel engines with reasonable accuracy [30]. The set of reactions of the mechanism are presented from reaction 5.3 to reaction 5.10.

$$CO + 0.5O_2 = CO_2 \qquad r.5.3$$

$$CO + 0.5O_2 = CO_2 \qquad r.5.4$$

$$C_3H_8 + 0.5O_2 = CO_2 + H_2O \qquad r.5.5$$

$$DF_1 + 19.4O_2 = 13.5CO_2 + 11.8H_2O \quad r.5.6$$

$$H_2 + 0.5O_2 = H_2O \quad r.5.7$$

$$NO + 0.5O_2 = NO_2 \quad r.5.8$$

$$Z + DF_1 = ZDF_1 \quad r.5.9$$

$$ZDF_1 = Z + DF_1 \quad r.5.10$$

Each one of the single step reactions above has a pre-exponential factor and an activation energy associated. As mentioned, both parameters should be optimized to represent the experimental results. Generally, most of methodologies are based on finding a representative function to be minimized accounting the different experimental cases that are being used during the calibration. Once the function is defined, a search algorithm can be employed to speed up the process, relying in automatic optimization to perform the task [31]. In this work, a genetic algorithm with a population size of 40 and a total number of 10 generations was used to find the 16 constants (eight Pre exponential factors and eight activation energies). As some of these constants can vary in a wide range ($1x10^8$ to $1x10^{20}$), a logarithm modification of the equations was employed providing an exponential dependency with the value to be optimized. Therefore, the searching range could be reduced from $1x10^{20}$ to $1x10^2$, speeding up the optimization process.

Figure 5.28 compares the results obtained from the calibration optimizer with those from the experimental conditions. As it can be seen, the optimization was able to find a set of values for both PEF and Ea which are able to capture the dependence of the composition variation as well as the temperature from the experimental results. It should be remarked that each reaction has a unique value of PEF and Ea. This means that this set of parameters is used for all the operating conditions. It is possible to evidence that the HC conversion profile has some differences with respect to the experimental profiles. This can be attributed to the difficulty in achieving completely steady-state operation in the engine as well as in capture the multitude of hydrocarbon species in the exhaust by means of the three species representation. By contrast, carbon monoxide conversion efficiency seems to

not present the same issues. Nonetheless, its profile provides 100 % of conversion efficiency most of the time.

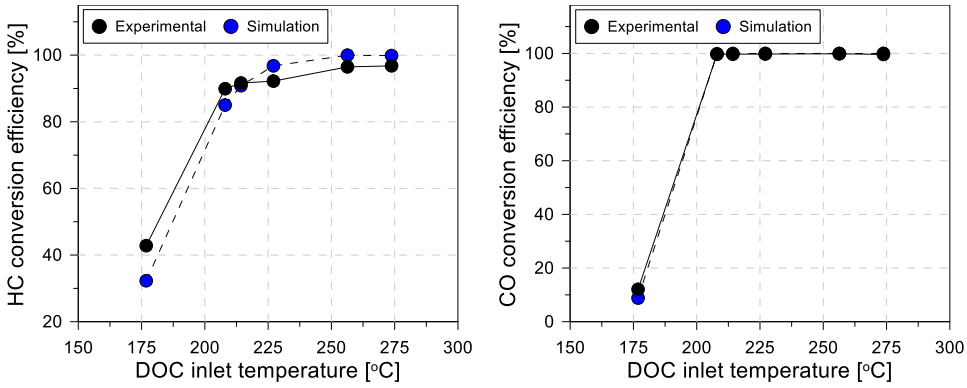

Figure 5.28. Calibrated and experimental comparison of conversion efficiency values for both (a) unburned hydrocarbons and (b) carbon monoxide emissions at steady-state conditions.

5.4.2.2. Steady-state results

Once the optimized constants were found, they were verified against a large dataset, containing both the calibration points and plus nine verification conditions. Figure 5.29 depicts the results for both HC and CO conversion efficiencies with respect to the experimental values. It is possible to verify that the numerical results follow the same pattern than the experimental ones. Moreover, the absolute values are similar, except for the conditions at low temperature where the differences are as high as 10 % in absolute basis. Low exhaust temperature conditions are generally found at low load operation which presents high cycle-to-cycle variability, impacting the composition of the exhaust gases. Therefore, the numerical representation of the hydrocarbon concentration may imply higher deviations from the real concentration, affecting the model capability to reproduce the conversion efficiency.

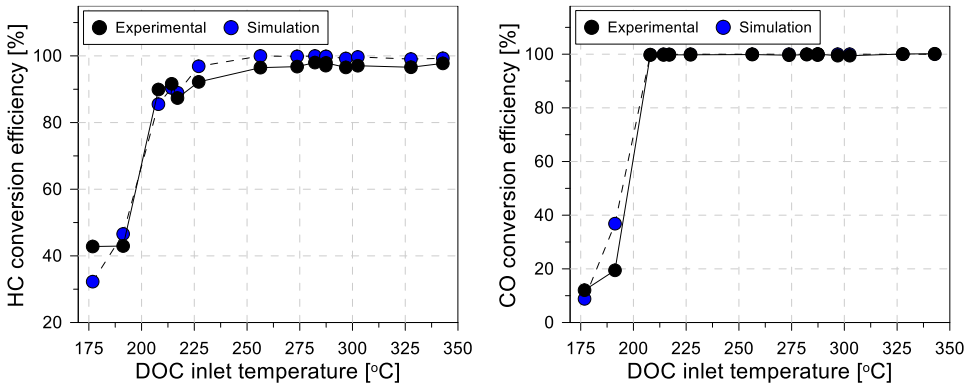

Figure 5.29. Simulated and experimental comparison of conversion efficiency values for both (a) unburned hydrocarbons and (b) carbon monoxide emissions at steady-state conditions.

5.4.2.3. Transient results

Finally, the simulation results were compared to those from transient conditions to assure both reliable description of the conversion efficiencies as well as proper energy balance between the exothermal reactions and heat transfer to the environment. To do this, the previous results obtained for the WHVC step were used as reference to calibrate the model. This step was chosen since it can convey the essence of the normative driving cycle, as idle time, engine load transitions, and absolute values. Figure 5.30 depicts the comparison between the experimental results and the numerical simulation outputs. It is possible to infer that the model is able to predict both HC and CO conversion efficiency. It is also interesting to note that a significant divergence between both results can be evidenced at 400 s which matches with the engine speed modification. Fast modifications of the boundary conditions may infer higher measurement uncertainties on fundamental magnitudes, as temperature measurement since the k-type thermocouples used in this investigation are not designed to capture high dynamic signals. Once this temperature value is a boundary condition to the oxidation catalyst

evaluation, some divergences can be expected in the transition between operating conditions. In spite of that, it can be concluded that the numerical model is able to reproduce the transient conversion efficiencies in most of the time.

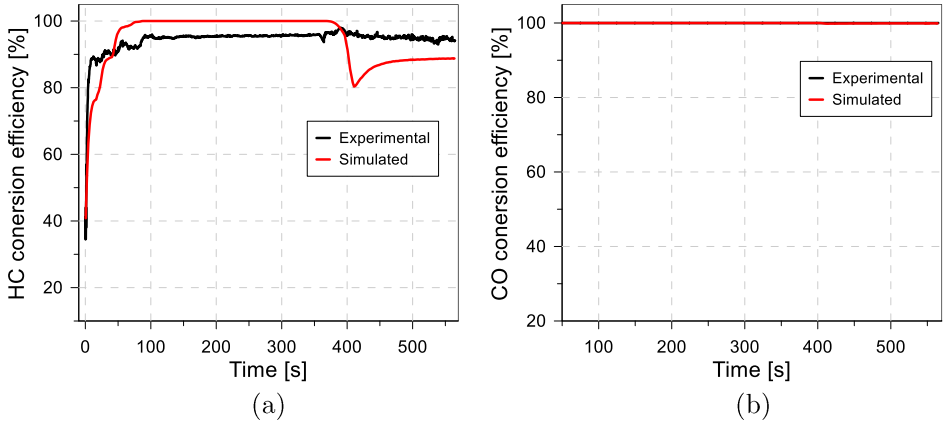

Figure 5.30. Simulated and experimental comparison of conversion efficiency values for both (a) unburned hydrocarbons and (b) carbon monoxide emissions at transient conditions derived from world harmonized vehicle cycle driving cycle.

A major concern lies on the capability of the model on reproducing the experimental measurements at the oxidation catalyst outlet. This is justified due to the need of using such predicted quantities as boundary conditions in the particulate filter external module. In this sense, the comparison of the results obtained for the numerical and experimental oxidation catalyst outlet temperature are presented in Figure 5.31. As it is shown, both temperatures are similar in absolute values and behavior. The absolute difference between them is depicted in the bottom part of the figure. Some slight differences can be remarked at both the first 150 s and at 400 s. These time intervals are closely related to the moment at which the boundary conditions are modified, reinforcing that the differences may be related to the low response time of the thermocouples, yielding a bias on the boundary conditions of the simulation. Despite this, the differences never surpass the 10 % threshold,

suggesting a good agreement between the numerical and experimental results which validates the use of the oxidation catalyst model for transient simulations.

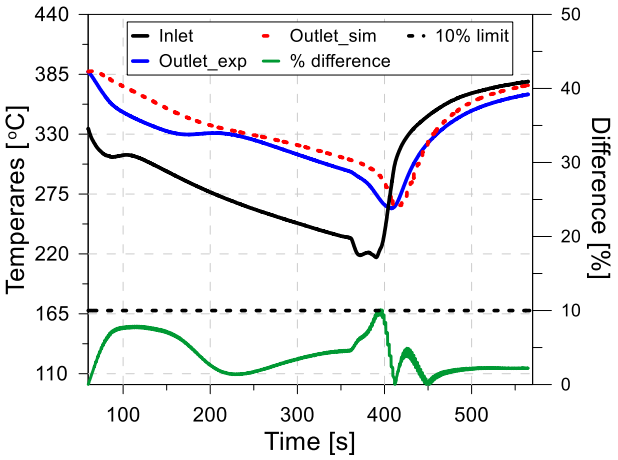

Figure 5.31. Temperature evolution at oxidation catalyst inlet, comparison between simulated and experimental oxidation catalyst outlet temperature and absolute difference between them.

5.4.3. DPF Calibration

As previously discussed, the proposed DMDF calibration is prone to yield high soot amounts at high load conditions. Moreover, the importance of using a particulate filter in the low pressure EGR line was also highlighted. Both statements allowed to conclude that the DPF system will still be present in the DMDF powertrain system. Nonetheless, it can be suggested that the significant reduction of soot production at low and medium load conditions may enable the resizing of the DPF system. This should be further assessed in normative and real driving conditions to identify the impact of the operating points distribution on the soot production and consequent DPF loading which may increase the back-pressure losses, reducing the engine efficiency. Therefore, the stock DPF was modelled in an in-house DPF model developed by Piqueras et al. [32]. The respective formulation, solution scheme and detailed description of

the modelling process can be verified at [33]. Since the programming language and solver scheme are not the same as that of GT-Power, a decoupled routine was proposed. First, both vehicle and oxidation catalyst are simulated. During the simulations, the instantaneous profiles of state variables as well as composition are written in a file. Finally, this file is loaded in the DPF sub model as inlet boundary condition.

The previous results presented in section 5.3.2 were used as inputs in the calibration process to tune the model values to represent the different phenomena (soot loading, passive and active regeneration) that are aimed to be modeled at the DPF. The results of the calibration process can be evidenced in Figure 5.32 where the first graph illustrates the DPF loading results obtained while the second graph depicts the active regeneration results. As it is shown, both processes are well reproduced by the model, allowing to follow the experimental transient evolution of both DPF loading and regeneration. In this sense, it is suggested that the numerical model can be used to assess the impact of the soot production on the DPF loading during driving cycle operations with different payloads. Moreover, the capability of predicting the DPF regeneration allows to obtain a realistic soot mass balance trapped in the DPF at the end of the cycle.

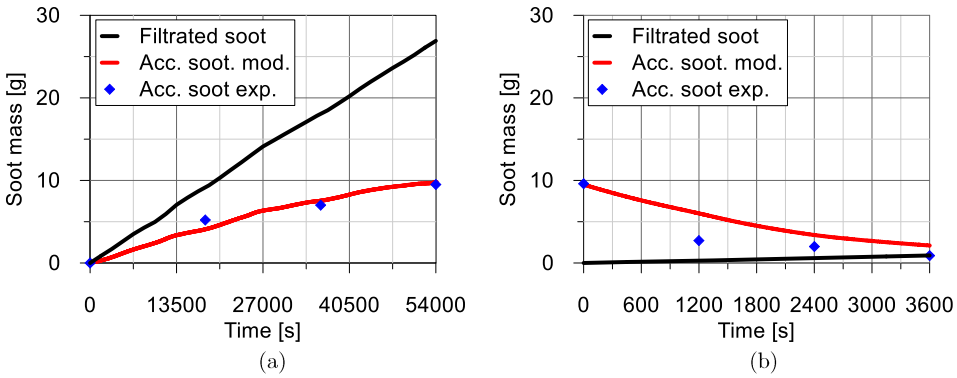

Figure 5.32. Comparison between experimental and predicted values of (a) accumulated soot evolution and (b) accumulated soot mass reduction during regeneration.

5.4.4. Results

The result section is divided in two subsections according to the device in discussion: DOC or DPF. First, the impact of the DMDF combustion concept on the DOC performance for different payloads and driving cycles is discussed. Finally, the DOC out results, as temperature and species concentrations, are used as boundary conditions for the DPF evaluation allowing to assess the impact of the soot produced during the driving cycles on different DPF phenomena as filtration, accumulation and regeneration.

5.4.4.1. DOC response to DMDF under driving cycle conditions

Figure 5.33 depicts the DOC performance in terms of CO and HC conversion efficiency for the WHVC, considering normative conditions (50 % of payload). As it is shown, there is a strong correlation between the conversion efficiency and the truck velocity. At the early stages (urban phase), the velocity profile presents several conditions with 0 km/h value, i.e., conditions were the truck is stopped. In this sense, it is not possible to achieve temperature levels to properly oxidize the unburned products in the exhaust gases. Moreover, the larger stopped periods enhance the DOC cooling, requiring a warming period whenever the vehicle exits the idle condition. This can be verified by analyzing the DOC outlet temperature profiles of Figure 5.33. As it is shown, the outlet temperature presents a high inertia which is a consequence of the size of the DOC and its associated thermal capacity. In this sense, the temperature peaks are always shifted from the higher velocity values, indicating a high DOC heating period. All these phenomena contribute to achieve low conversion efficiency during almost the complete urban phase of the WHVC. Nonetheless, as the cycle progresses, the vehicle velocity is increased, requiring higher energy from the engine to overcome the external forces acting on the vehicle. Therefore, the operating conditions are shifted to higher engine loads which provides higher exhaust temperatures at the DOC inlet, enhancing the catalysis inside the DOC and consequently the conversion efficiency. This statement can be

extended to the highway phase, where the high velocities allow to obtain conversion efficiencies near 100 % for both HC and CO. It is interesting to remark that the carbon monoxide conversion efficiency achieves full conversion levels at earlier times than the unburned hydrocarbons, reinforcing its higher reactivity. In addition, as previously described, the high levels of gasoline contribute to low reactivity hydrocarbons in the exhaust gases which require high temperatures to be oxidized.

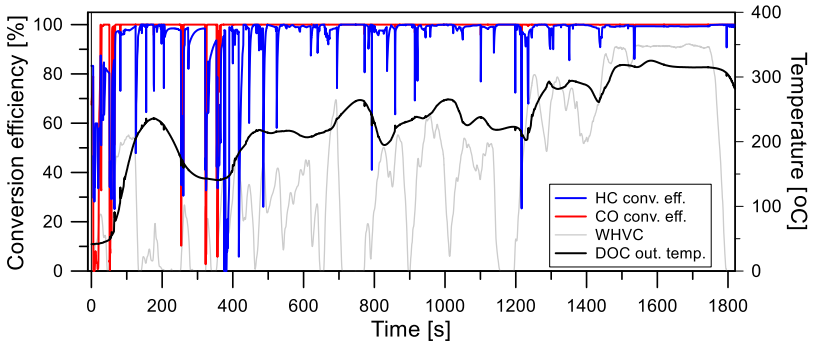

Figure 5.33. Oxidation catalyst unburned hydrocarbon and carbon monoxide conversion efficiency at normative conditions, i.e. world harmonized vehicle cycle (background line) with 50 % of payload. Moreover, the values of oxidation catalyst outlet temperatures are also represented.

Once it is demonstrated that the velocity impacts the performance of the DOC, it should be expected that similar correlations would be achieved with respect to the payload. To assess this, three different payloads were assessed (0 %, 50 % and 100 %) for the WHVC driving cycle. The results considering the conversion efficiency of the unburned hydrocarbons are presented in Figure 5.34 (a). The information was summarized by means of kernel density estimation techniques which allow to visualize the range of representative values as well as the concentration of points in a specific range.

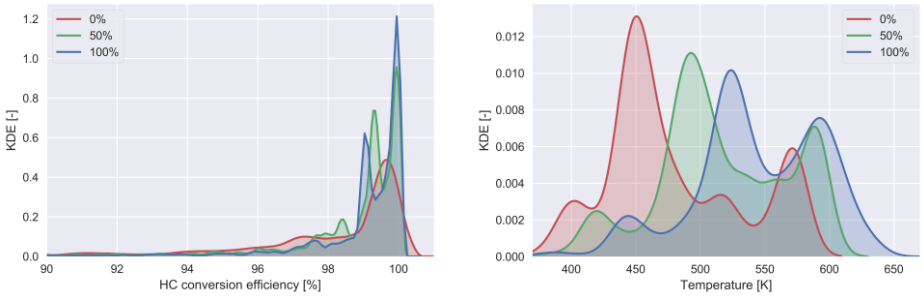

(a) (b)

Figure 5.34. Kernel density estimation plots of (a) unburned hydrocarbon conversion efficiency and (b) exhaust temperature for 0 %, 50 % and 100 % of payload at the word harmonized vehicle cycle.

It can be suggested that the increase of the payload has benefits on the HC conversion efficiency. As it is shown, the increase from 0 % to 50 % provides a narrower and peaky kernel density estimation (kde) profile, i.e., higher concentration of conversion efficiency near to the 100 %. An additional payload step from 50 % to 100 % allows to enhance the conversion efficiency. Nonetheless, the differences are much less significant than those of the previous step. To understand this, the kde temperature profiles for the different payloads at the DOC inlet are presented in Figure 5.34 (b). As it can be seen, the temperature kde presents a similar behavior, independently on the payload: a small peak at the beginning, the kernel of the distribution at the center and a last peak at the end. Two interesting trends can be evidenced according to the payload. First, the position of the kernel is consistently shifted towards high temperature values as the payload is increased. This is a consequence of using more operating conditions at high load. Second, the distance between the kernel and the last peak as well as the differences on their absolute values are reduced.

The analysis of the distribution for 0 % of payload allows to identify that in most cases, the DOC operates with inlet temperatures around to 450 K, which represents conditions near the light-off condition, as it is depicted in Figure 5.28 and Figure 5.29, which could provide the partial oxidation of

the hydrocarbons at the exhaust. As the payload is increased to 50 % and 100 %, the kernel of the distribution is moved to temperatures of 490 K and 525 K. This significant temperature increase provides the required energy of activation to sustain the oxidation reactions, enhancing the conversion efficiency of the unburned species. Therefore, it can be concluded that the truck operation with higher payloads is beneficial to the DOC operation for the WHVC driving cycle.

Once the effect of the velocity profile and the payload variation on the DOC performance are assessed, an overall analysis is performed to address the different driving cycles, payload sweeps, and their potential of achieving the normative limits with the current aftertreatment system. To do this, the four different driving cycles (WHVC, Urban, FCEC and ISC_FC) were assessed at five distinct payloads (0 %, 25 %, 50 %, 75 % and 100 %). For each combination, the tailpipe emissions were compared to those from CDC engine-out. The same color scheme than that presented in chapter 4 was employed to differentiate the operating conditions that are able to achieve EUVI normative (black border and green text label).

Figure 5.35 summarizes the results for both HC (a) and CO (b) emissions for the complete test matrix. As it is shown, the use of the stock DOC can deliver EUVI compliant HC and CO emissions considering normative conditions. While the CO can be converted independently on the condition evaluated, the HC presents critical conditions that are not able to achieve the limits imposed by the normative. They are found in both the WHVC and FCEC driving cycles for low payloads values. As aforementioned, these conditions are prone to having low DOC inlet temperature which impairs the oxidation of the unburned hydrocarbons.

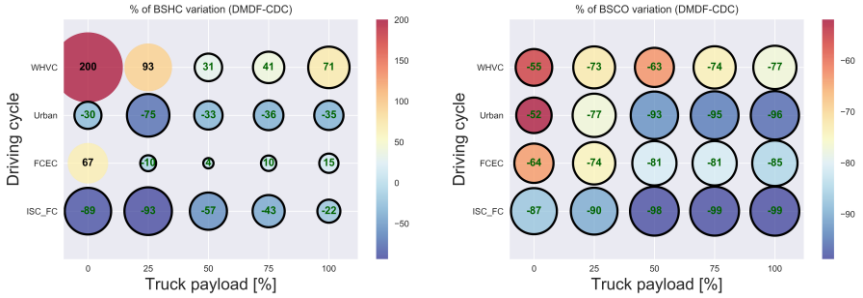

(a) (b)

Figure 5.35. Overview of the driving cycle results depicting the percentage variation with respected to the stock calibration for (a) unburned hydrocarbons and (b) carbon monoxide emissions for different driving cycles and payloads.

Figure 5.36 presents an overview of the CO and HC absolute values before and after the DOC for the complete test matrix, referenced to the EUVI normative limits. It should be noted that the limits for the ISC driving cycles have relaxation factors of 1.5. Nonetheless, it was chosen to specify the EUVI normative as the standard reference for all the driving cycles. The close analysis of the HC engine-out emissions allows to identify a linear trend with respect to the payload increase. Moreover, the dispersion among the cycles for the same payload are low, suggesting that the velocity profile has low impact on the engine-out HC emissions for the DMDF combustion. This can be related to the experimental steady-state map for HC which has a wide zone of high HC production in the center of the map, consequence of the high premixing levels. As the payload is increased, lower are the average engine-out emissions due to the more frequent use of the high load portion of the map, where the unburned products decrease due to the diffusive combustion. A similar analysis can be performed for the tailpipe emissions. First, it is interesting to note that driving cycles with higher duration seem to be more effective in achieving normative limits. Both urban and ISC_FC present durations higher than 2.5 hours (see Table 4.1). This driving cycle extension decreases the importance of the first DOC warm up phase, which is responsible of producing most of the tailpipe products. In this sense, the low

pollutant mass produced in this phase is divided by a higher denominator, i.e., the total power (kW), allowing to achieve EUVI normative limits, independently on the payload. By contrast, shorter cycles, like the FCEC and WHVC, that lasts up to 30 min presents a more significant warm up phases, increasing the weight of this part on the total tailpipe emissions. In this sense, they require higher truck payloads, (i.e., temperatures) to fulfill the legislation requirements. The effect of the payload can be visualized in the WHVC driving cycle where an exponential increase of the tailpipe emissions is found as the payload is decreased.

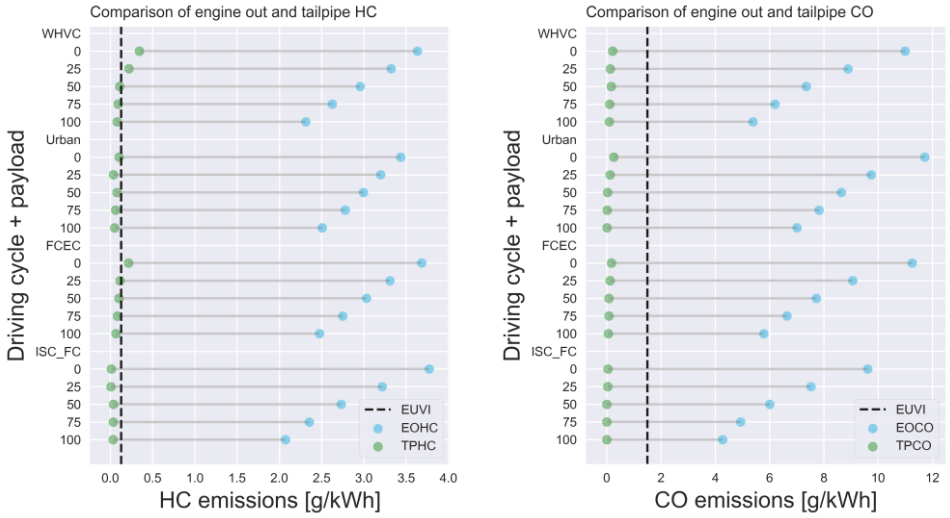

Figure 5.36. Summary of engine-out and tailpipe (a) unburned hydrocarbon and (b) carbon monoxide emissions with respect to different payloads and driving cycles.

As it was previously discussed, the carbon monoxide emissions are more reactive than the large hydrocarbons present in the exhaust gases. This allows to achieve the normative targets independently on the payload and driving cycle evaluated. In spite of this, some conclusions can be drawn regarding the CO behavior at engine-out for the different cycles and payloads. As it can be seen in Figure 5.36 (b), this pollutant seems to be highly affected by the

velocity distribution as well as the driving cycle. The comparison among the different driving cycles suggests that short and low velocity driving cycles (FCEC, WHVC and urban) provide higher values of carbon monoxide, which is the opposite of the trend verified for the HC emissions. It is suggested that this driving cycle typology is prone to have a higher distribution of operating conditions at low load, where the CO emissions are maximized. By contrast, the ISC_FC is a more demanding driving cycles, which tends to use portions of the map with high engine loads, decreasing the penalization on CO emissions from the low load portion.

It is also interesting to remark that the CO emissions tend to decrease in a more abrupt manner as the payload is increased due, also, to the shifting of the operating conditions to medium and high engine loads. This opposite trend between the HC and CO emissions is a direct consequence of the DMDF combustion concept, which decouples the formation mechanism of these species. While HC emissions are dominated by the amount of LRF that enters and remains in the piston gaps and crevices, the CO production is a consequence of the partial oxidation of minor hydrocarbon compounds by the absence of the temperature to sustain the reactions process. This last condition is verified mainly at low load operation while the higher premixing levels (↑LRF) which enhances the formation are generally used at medium load conditions.

From this analysis, it can be concluded that the stock oxidation catalyst can deal with the high levels of unburned products from the DMDF combustion, providing tailpipe emissions compliant with those from EUVI for normative conditions. In this sense, the proposed calibration concept is able to fulfill engine out NOx emissions normative limits, as stressed in chapter 4, while providing boundary conditions to the DOC, which allows to reach tailpipe EUVI CO and HC without requiring significant modifications of the oxidation catalyst.

5.4.4.2. DPF

As discussed in Chapter 4, the proposed calibration using the DMDF combustion has as drawback the significant penalization in terms of soot emissions from high to full load. Moreover, the use of a low pressure EGR system would require a pre-filtration of the exhaust gases prior entering the compressor to avoid the early damage of the compressor parts. In this sense, it can be concluded that the DPF will still have an important role in the DMDF concept. By these reasons, a dedicated evaluation was proposed to assess the impact of the DMDF combustion on the DPF process, such as filtration and regeneration, as well as the pressure drop associated to the different filtrated mass. This analysis is limited to the WHVC driving cycle, since it was the only driving cycle that did not achieved the EUVI target, considering the total mass produced (accounting the measurements that could be done with the AVL 415S).

Figure 5.37 depicts the cumulative soot production along the driving cycle for the different payloads. It should be remarked that these values refer to the engine-out emissions and not the accumulate soot in the DPF, which is a balance between the filtrated and regenerated mass. As previously discussed in chapter 4, the increase of the payload leads to higher soot mass at the end of the driving cycle because of the usage of high load operating conditions. Moreover, the highway phase provides almost half of the total soot produced independently on the truck payload. These soot quantities must be addressed by the DPF to avoid the releasing of this particulate matter to the atmosphere.

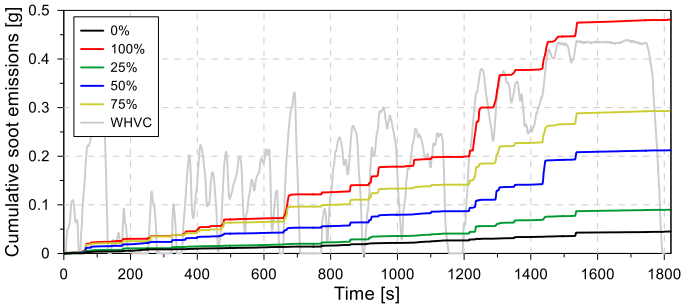

Figure 5.37. Cumulative engine-out soot emissions for the world harmonized vehicle cycle for 0 %, 25 %, 50 %, 75 % and 100 % of payload.

Diesel particulate filters or simply particulate filters works in a different manner than the remaining aftertreatment devices. While the DOC and SCR present chemical reactions that reduce the pollutants, particulate filters rely on trapping the particulate material, requiring additional processes to reduce this pollutant [35]. In this sense, the performance of a DPF is directly related to the capacity to filtrate the exhaust gases and remove the particulate from them. Generally, conventional DPFs presents filtration efficiencies higher than 99 % at clean conditions [36]. Moreover, as the DPF load is increase, higher are the filtration efficiencies. In this sense, the filtrated soot mass was assessed and presented in Figure 5.38. As it is shown, the filtrated mass values are similar to those produced, indicating that the DPF is able to filtrate all the soot mass produced by the DMDF combustion concept in the WHVC driving cycle, independently on the truck payload.

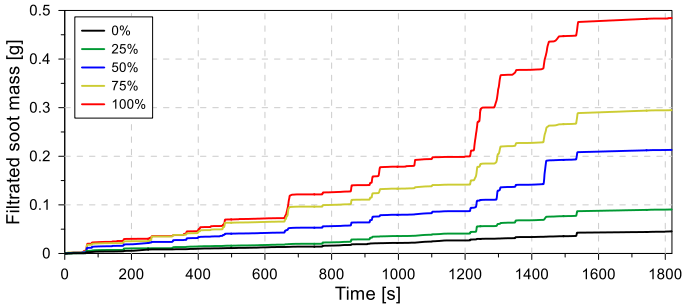

Figure 5.38. Filtrated soot mass for the world harmonized vehicle cycle for 0 %, 25 %, 50 %, 75 % and 100 % of payload.

It must be highlighted that the trapped mass in the DPF results in a decrease of the flow area, i.e., the equivalent diameter of the porous media is decreased. Therefore, it is expected that a higher pressure drop should be experienced for higher soot mass. Figure 5.39 presents the pressure drops in the monolith for the different operating conditions evaluated. The pressure drop is a consequence of both fluid inertia and viscous losses [37]. As it is shown, the higher truck payloads result in an increase of almost twice the pressure drops in the monolith. Nonetheless, it should be remarked that this represents a maximum value of 30 mbar, which may have a low impact on the engine performance [38]. These low values can be attributed to the size of the DPF as well as the low soot trapped. In this sense, it can be suggested that the stock particulate filter could be resized aiming to decrease its associated cost by reducing it, as it seems oversized for the current application.

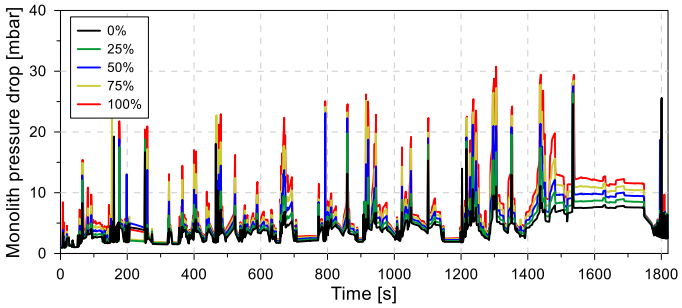

Figure 5.39. Regenerated soot mass for the world harmonized vehicle cycle for 0 %, 25 %, 50 %, 75 % and 100 % of payload.

Finally, the DPF regeneration is assessed considering the same, previously proposed, test matrix. It should be clarified that no active regeneration process is here evaluated as, generally, active regeneration stands for the regeneration process that is achieved by means of additional fuel injection. Nonetheless, as stated in section 5.3.2, the HC and CO conversion at the DOC increases the temperature at the DPF inlet, which can provide enough energy to realize soot oxidation by means of O_2 reaction. Moreover, the low temperature soot oxidation route by NO_2 is also included in the evaluations.

Therefore, the total regenerated soot mass is a consequence of both processes. Figure 5.40 illustrates the results of regenerated soot mass as function of the truck payload. The analysis of the results suggests that both urban and rural phases do not provide the required conditions to oxidize the soot trapped in the DPF either by the absence of NO_2 or by the low temperature of the exhaust gases. As previously demonstrated, these conditions operate in low to medium engine loads, where the total NOx concentration do not exceed 50 ppm and the exhaust temperatures are low as consequence of the fully premixed combustion. As the driving cycle progresses to the highway phase, the regeneration process starts to be apparent because of both higher NOx concentrations and higher temperatures at high loads. Despite this, the total soot mass regenerated during the driving

cycle can be considered negligible which means that active regeneration techniques should be employed to guarantee a proper cleaning of the DPF.

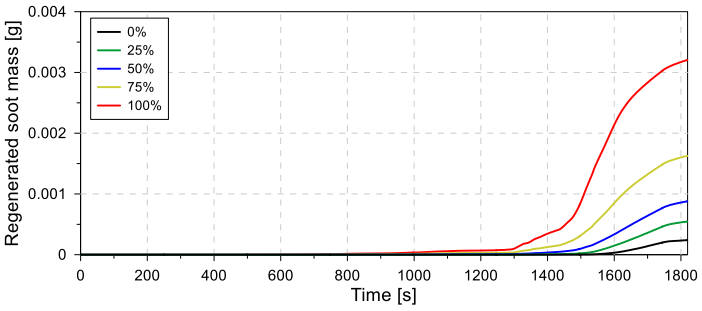

Figure 5.40. Start of injection (a) and injection duration (b) of the pilot injection for the complete engine map.

5.5 Summary and conclusions

This chapter has evaluated the response of the aftertreatment system to the DMDF combustion concept at steady-state and transient conditions. The research efforts have been dedicated to both oxidation catalyst as well as the particulate filter. Selective catalytic reduction and ammonia slip catalyst were not addressed since the proposed calibration is able to fulfill de EUVI NOx constraints without requiring these devices.

The steady-state analysis of the oxidation catalyst has promoted the understanding of the critical conditions at which the stock DOC was not able to operate under light off condition, exceeding the normative emissions concentration. It was evidenced that the combination of low exhaust temperatures and high unburned products concentration were a hurdle from 10 % to 25 % of engine load, independently on the engine speed evaluated. A deeper look on the hydrocarbon composition by means of speciation evaluation has allowed to identify the significant concentration of low reactivity hydrocarbons as toluene, which is increased at conditions where high gasoline fractions were used. The introduction of thermal inertia as a

variable in the DOC evaluation through different transient steps and simplified cycles demonstrated to be a pathway to improve the conversion efficiency whenever a high load condition precedes the low temperature condition.

Moreover, the particulate filter regeneration paths were also assessed to verify the efficacy of passive and high temperature oxygen regeneration by means of steady-state evaluation. The passive regeneration results allowed to conclude that the low NO_2 concentration combined with the low soot production does not seems to activate the passive regeneration path during the engine operation. By contrast, high temperature oxygen regeneration seems to be much more effective to clean the DPF. The use of a high flow, high temperature conventional diesel combustion operating condition was able to reduce in $\approx$ 70 % de total soot trapped in 20 min. It was also demonstrated that, although DMDF exhaust temperatures are far inferior to those from CDC, the conversion of the unburned products at the DOC allows to increase the exhaust temperature in more than 50 °C. This temperature increment has allowed to obtain an effective soot oxidation, but at lower rates than the CDC conditions due to the low exhaust flow.

Finally, both DOC and DPF were modeled and included at the driving cycle evaluation approach, allowing to account the cycle averaged tailpipe emissions and compare them to the normative limits. As expected, the early phases of the driving cycle evaluation were challenging in obtain light-off conditions due to the low engine speed velocity. As the cycle progressed, the high temperature from the demanding velocity allowed to increase the conversion efficiency of the DOC. Moreover, the truck payload was found to be a determinant parameter in achieving normative values. The increases of payload were responsible to shift the operating conditions to higher exhaust temperature, enhancing the warm-up times. In this sense, the use of the stock DOC was able to deliver EUVI HC and CO tailpipe emissions at its normative setup (50 % of payload).

The particulate filter assessment has allowed to perceive underlaying benefits of the DMDF concept. In spite of not being able to achieve the EUVI soot emissions without a dedicated aftertreatment system, the ultra-low values of soot found in most of the engine map result in small soot mass trapped at the DPF at the end of the cycle. This significantly low quantity associated with the low mass flow compared to the original CDC calibration introduces negligible pressure drops. Therefore, it can be inferred that the DPF can be resized aiming at low DPF volumes, reducing the cost and focusing on an optimized packing setup to the powertrain.

Summarizing, it was demonstrated that despite the adverse boundary conditions in terms of exhaust temperature and unburned products, which can significantly influence steady-state evaluations, the extension of the analysis to normative driving cycles has allowed to conclude that the concept was able to deliver tailpipe HC and CO as well as soot emissions with the stock aftertreatment system. This should be added to the previous conclusions that remarked the concept's capability on fulfilling NOx emissions without dedicated aftertreatment with small penalties on fuel consumption. However, it should be recalled that a last issue remains: the necessity of reducing the CO_2 emissions targeting short term horizons (H2025). In this sense, the next chapter will be focused on assessing different low reactivity and high reactivity fuels aiming to optimize the combustion process as well as introduce CO_2 benefits from a lifecycle perspective.

5.6 Bibliography

[1] Russell A., Epling W.S. "Diesel oxidation catalysts". *Catalysis Reveview: Science and Engineering,* Vol. 53, pp. 337–423, 2011.

[2] Hamedi M.R., Tsolakis A., Herreros J.M. "Thermal Performance of Diesel Aftertreatment: Material and Insulation CFD Analysis". *SAE Technical Papers*, n° 2014-01-2818, 2014.

[3] Song X., Surenahalli H., Naber J., Parker G., Johnson J. "Experimental and modeling study of a diesel oxidation catalyst (DOC) under transient and CPF active regeneration conditions". *SAE Technical Papers,* n° 2013-01-1046, 2013.

[4] Johnson J.E., Kittelson D.B. "Physical factors affecting hydrocarbon oxidation in a diesel oxidation catalyst". *SAE Technical Papers* , n° 941771, 1994.

[5] Prikhodko V.Y., Curran S.J., Parks J.E., Wagner R.M. "Effectiveness of diesel oxidation catalyst in reducing HC and CO emissions from reactivity controlled compression ignition". *SAE Technical Papers* , n° 2013-01-0515, 2013.

[6] Kaiser E.W., Matti Maricq M., Xu N., Yang J. "Detailed hydrocarbon species and particulate emissions from a HCCI engine as a function of air-fuel ratio". *SAE Technical Papers* , n° 2005-01-3749, 2005.

[7] Kaiser E.W., Siegl W.O., Henig Y.I., Anderson R.W., Trinker F.H. "Effect of Fuel Structure on Emissions from a Spark-Ignited Engine". *Environmental Science and Technology,* Vol. 25, pp. 2005–2012. 1991.

[8] Ramanathan K., Sharma C.S. "Kinetic parameters estimation for three way catalyst modeling". *Industrial and Engineering Chemistry Research,* Vol. 50, pp. 9960–9979, 2011.

[9] Luján J.M., Climent H., García-Cuevas L.M., Moratal A. "Pollutant emissions and diesel oxidation catalyst performance at low ambient

temperatures in transient load conditions". *Applied Thermal Engineering,* Vol. 129, pp. 1527–1537, 2018.

[10] Guan B., Zhan R., Lin H., Huang Z. "Review of the state-of-the-art of exhaust particulate filter technology in internal combustion engines". *Journal of Environmental Management,* Vol. 154, pp. 225–258, 2015.

[11] Song Q., Zhu G. "Model-based closed-loop control of urea scr exhaust aftertreatment system for diesel engine". *SAE Technical Papers* , n° 2002-01-0287, 2002.

[12] Ferreri P., Cerrelli G., Miao Y., Pellegrino S., Bianchi L. "Conventional and Electrically Heated Diesel Oxidation Catalyst Physical Based Modeling." *SAE Technical Papers* , n° 2018-37-0010, 2018.

[13] Heavy-Duty Supplemental Emissions Test (SET). Available at https://dieselnet.com/standards/cycles/set.php, acessed in June 2020.

[14] Gao J., G. Tian, Sorniotti A., Karci A.E., Di Palo R. "Review of thermal management of catalytic converters to decrease engine emissions during cold start and warm up". *Applied Thermal Engineering,* Vol. 147, pp. 177–187, 2019.

[15] Serrano J.R., Piqueras P., Angiolini E., Meano C., De La Morena J. "On Cooler and Mixing Condensation Phenomena in the Long-Route Exhaust Gas Recirculation Line". *SAE Technical Papers* , n° 2015-24-2521, 2015.

[16] Bai S., Tang J., Wang G., Li G. "Soot loading estimation model and passive regeneration characteristics of DPF system for heavy-duty engine". *Applied Thermal Engineering,* Vol. 100, pp. 1292–1298, 2016.

[17] Kim J.H., Kim M.Y., Kim H.G. "NO_2-assisted sort regeneration behavior in a diesel particulate filter with heavy-duty diesel exhaust gases". *Numerical Heat Transfer, Part A: Applications*, Vol. 58, pp. 725–739, 2010.

[18] Rothe D., Knauer M., Emmerling G., Deyerling D., Niessner R. "Emissions during active regeneration of a diesel particulate filter on a

heavy duty diesel engine: Stationary tests". *Journal of Aerosol Sciences*, Vol. 90, pp. 14–25, 2015.

[19] Jacquot F., Logie V., Brilhac J.F., Gilot P. "Kinetics of the oxidation of carbon black by NO_2 influence of the presence of water and oxygen". *Carbon*, Vol. 40, pp. 335–343, 2002.

[20] Rößler M., Velji A., Janzer C., Koch T., Olzmann M. "Formation of Engine Internal NO_2: Measures to Control the NO_2/NO_X Ratio for Enhanced Exhaust After Treatment". *SAE Internatiolnal Journal of Engines*, Vol. 10, n° 2017-01-1017, 2017.

[21] Katare S.R., Patterson J.E., Laing P.M. "Aged DOC is a Net Consumer of NO_2: Analyses of Vehicle, Engine-dynamometer and Reactor Data". *SAE Technical Papers* , n° 2007-01-3984, 2007.

[22] Henry C., Currier N., Ottinger N., Yezerets A. "Decoupling the Interactions of Hydrocarbons and Oxides of Nitrogen Over Diesel Oxidation Catalysts". *SAE Technical Papers* , n° 2011-01-1137, 2011.

[23] Singh P., Thalagavara A.M., Naber J.D., Johnson J.H., Bagley S.T. "An experimental study of active regeneration of an advanced catalyzed particulate filter by diesel fuel injection upstream of an oxidation catalyst". *SAE Technical Papers* , n° 2006-01-0879, 2006.

[24] Haralampous O.A., Koltsakis G.C. "Oxygen diffusion modeling in diesel particulate filter regeneration". *AIChE Journal,* Vol. 50, pp. 2008–2019, 2014.

[25] Ito T., Kitamura T., Kojima H., Kawanabe H. "Prediction of Oil Dilution by Post-injection in DPF Regeneration Mode". *SAE Technical Papers* , n° 2019-01-2354, 2019.

[26] Singh N., Rutland C.J., Foster D.E., Narayanaswamy K., He Y. "Investigation into different DPF regeneration strategies based on fuel economy using integrated system simulation". *SAE Technical Papers* , n° 2009-01-1275, 2009.

[27] Neoh K.GHoward., J.B., Sarofim A.F. "Soot Oxidation in Flames". *Particulate Carbon*, pp. 261–282, 1981.

[28] Lee K.B., Thring M.W., Beér J.M. "On the rate of combustion of soot in a laminar soot flame." *Combustion and Flame,* Vol. 6, pp. 137–145, 1962.

[29] Sampara C.S., Bissett E.J., Chmielewski M., Assanis D. "Global kinetics for platinum diesel oxidation catalysts". *Industrial and Engineering Chemistry Research,* Vol. 46, pp. 7993–8003, 2007.

[30] Sampara C.S., Bissett E.J., Chmielewski M. "Global kinetics for a commercial diesel oxidation catalyst with two exhaust hydrocarbons". *Industrial and Engineering Chemistry Research,* Vol 47, pp. 311–322, 2008.

[31] Polifke W., Geng W., Döbbeling K. "Optimization of rate coefficients for simplified reaction mechanisms with genetic algorithms". *Combustion and Flame*, Vol. 113, pp. 119–134, 1998.

[32] Macián V., Serrano J.R., Piqueras P., Sanchis E.J. "Internal pore diffusion and adsorption impact on the soot oxidation in wall-flow particulate filters". *Energy*, Vol. 179, pp. 407–42, 2019.

[33] Payri F., Arnau F.J., Piqueras P., Ruiz M.J. "Lumped Approach for Flow-Through and Wall-Flow Monolithic Reactors Modelling for Real-Time Automotive Applications". *SAE Technical Papers* , n° 2018-01-0954, 2018.

[34] Pedrozo V.B., May I., Lanzanova T.D.M., Zhao H. "Potential of internal EGR and throttled operation for low load extension of ethanol-diesel dual-fuel reactivity controlled compression ignition combustion on a heavy-duty engine". *Fuel,* Vol. 179, pp. 391–405, 2016.

[35] Yang S., Deng C., Gao Y., He Y. "Diesel particulate filter design simulation: A review". *Advances in Mechanical Engineering,* Vol. 8, pp. 1–14, 2016.

[36] Serrano J.R., Climent H., Piqueras P., Angiolini E. "Filtration modelling in wall-flow particulate filters of low soot penetration thickness". *Energy,* Vol. 112, pp. 883–898, 2016.

[37] Payri F., Broatch A., Serrano J.R., Piqueras P. "Experimental-theoretical methodology for determination of inertial pressure drop distribution and pore structure properties in wall-flow diesel particulate filters (DPFs)". *Energy*, Vol. 36, pp. 6731–6744, 2011.

[38] Bermúdez V., Serrano J.R., Piqueras P., Sanchis E.J. "On the impact of particulate matter distribution on pressure drop of wall-flow particulate filters". *Applied Sciences,* Vol. 7, 2017.

Chapter 6

DMDF: Towards H2025 scenario

Content

6.1 Introduction

From the previous discussions presented in both chapter 4 and chapter 5, it was evidenced that the DMDF concept enables the achievement of EUVI NOx emissions without ATS, with small penalizations in terms of fuel consumption. Moreover, it was also demonstrated that the stock oxidation catalyst and particulate filter can deal with the exhaust emissions of the concept. By contrast, no appreciable benefit in terms of CO_2 emission was experienced along these two chapters, which should be addressed in the scope of the concept.

While the combustion process itself with commercial diesel and gasoline cannot deliver the required improvements on efficiency and CO_2 emissions, it is believed that the concept still has room for improvements whether the fuel characteristics are modified. The introduction of new fuels opens two main paths. First, the modification of the reactivity characteristics should enable the extension of fully premixed combustion to wider zones of the operating map, which would enhance the overall efficiency of the concept, while modifying the emissions formation to some extent (e.g. soot production). Second, if renewable fuels or e-fuels are considered, the CO_2 balance can be improved by accounting the use of this pollutant in the fuel lifecycle.

In this sense, this chapter aims to present a comprehensive investigation aiming to determine the impact of the low reactivity and high reactivity fuel characteristics on the performance and emissions of the DMDF concept targeting at improvements on emissions and CO_2 by means of both fuel consumption and lifecycle reduction. To accomplish this, the research was divided in two main parts. First, the impact of the low reactivity fuel characteristics on the DMDF combustion was assessed by evaluating different research octane numbers and sensitivities in conditions representative of the WHVC driving cycle while maintaining diesel as high reactivity fuel. Next, a merit function was developed as an attempt of balancing the weights of each

parameter (fuel consumption and emissions) enabling to realize the best low reactivity fuel for the concept.

Later, different high reactivity fuels with potential to reduce both soot emissions and wheel-to-wheel CO_2 emissions were identified in the literature and evaluated at four conditions (25 %, 50 %, 80 % and 100 % of engine load) and 1800 rpm. This allowed to assess the impact of the high reactivity fuels on both performance and emission parameters in different combustion regimes of the DMDF concept, identifying the best candidate for the DMDF combustion and allowing to place the proposed concept as an alternative to face the restrictive H2025 scenario. Finally, the best set of fuels were used to perform an engine recalibration and a posterior numerical driving cycle analysis for a complete overview of the potential in real applications.

6.2 Potential of octane modification on DMDF combustion

The research octane number (RON) determination was introduced to determine the knock resistance of a specific fuel. To do this, a standard engine was developed named cooperative fuel research (CFR) engine, enabling the tight control of the state parameters that dominate the auto ignition process. This allowed to tailor the octane demand and realize knocking conditions, i.e., conditions where the octane requirements exceed the octane quality of the fuel. This knock trend was then compared to that of a blend of neat paraffins, iso-octane (RON=100) and n-heptane (RON=0) [1].

During the 80's, reports suggested that commercial fuels were behaving differently than expected from the CFR tests, causing knocking problems and early deterioration of the engine [2]. In this respect, several researchers investigated what could be the possible origins of this phenomenon. Leppard [3] suggested that the chemical origin relied on the negative temperature coefficient from the paraffinic compounds (n-heptane and iso-octane) referring to it as a consequence of the low temperature reactions from the

alkyl hydro peroxides (ROOH) decomposition that could occur in specific state conditions. The heat released from these initiation reactions creates a mixture pre-conditioning by increasing the temperature, pressure and providing active radicals that enhances the posterior high temperature reactions. It was verified that both aromatics and olefins (which represent a high fraction of the commercial fuels composition) did not present low temperature chemistry [4]. Since the pressure-temperature (PT) trajectory from RON tests generally avoided the Negative Temperature Coefficient (NTC) region (i.e., zone where the reactivity decreases with increasing the temperature), this difference in reactivity could not be captured. Therefore, an additional test was introduced to represent PT trajectories like those found during real engine operation allowing to capture the NTC behavior from the paraffins. This new test was named Motor Octane rating originating a second metric: Motor Octane Number (MON). The difference between RON and MON was then defined as the fuel sensitivity (S). Non-sensitive fuels (as paraffins) do not present differences between RON and MON, while sensitive fuels as those with aromatics and olefins will behave as RON de-rated fuels at motor conditions [5]. The differences for each one of the tests are presented in Table 6.1.

Table 6.1. Some of the engine boundary conditions for both research octane number and motor octane number evaluation.

Engine Parameter	RON method	MON method
Engine speed [rpm]	600	900
Intake Temperature [°C]	52	149
Spark advance [CAD bTDC]	13	19-26

Reactivity controlled combustion concepts rely on the reactivity stratification inside the cylinder, which is a consequence of both low reactivity fuel and high reactivity fuel properties. Therefore, both RON and sensitivity should play a fundamental role on the combustion development. In spite of the apparent importance of these properties, the literature review indicated that this subject is not deeply addressed in combustion concepts as reactivity-

controlled compression ignition and DMDF. Most of the investigations are focused on earlier combustion concepts like homogeneous charge compression ignition and gasoline spark ignition engines [2][6][7]. In this sense, this section intends to evaluate the impact of these fuel characteristics on the performance and emissions results for representative operating conditions aiming at improving the CO_2 balance though fuel consumption reduction. Moreover, the use of low RON fuels may be a path to reduce the production cost, the consequent well to tank CO_2 emissions and the fuel price.

6.2.1. Research Octane Number effect

The research octane number stands as the most common measure of ignition resistance of a fuel. As previously discussed, this characteristic is of great importance on reactivity-controlled combustion modes. Therefore, the determination of the optimum RON values provides a way to extract the potential of the combustion mode and to get insights to promote a dedicated fuel design for the DMDF concept.

6.2.1.1. Methodology

The evaluation methodology of the optimum octane number for the DMDF combustion concept was composed by two different steps. First, a RON sweep was performed, addressing RON values of 100, 95 (same RON as the gasoline that was used in chapter 4), 92.5, 90, 87.5, 85 and 80. Each one of the fuel mixtures was evaluated at 8 different operating conditions (engine speeds and loads). The impact of the RON modification in the combustion, performance and emission was investigated for each one of the operating conditions depicted in Figure 1.3. These conditions were found to be representative of driving cycle conditions from the results presented in chapter 4. Each one of these conditions was optimized following the methodology proposed in section 3.5.1 to obtain the best fuel consumption values fulfilling the emissions constraints of each zone at which the operating condition belongs.

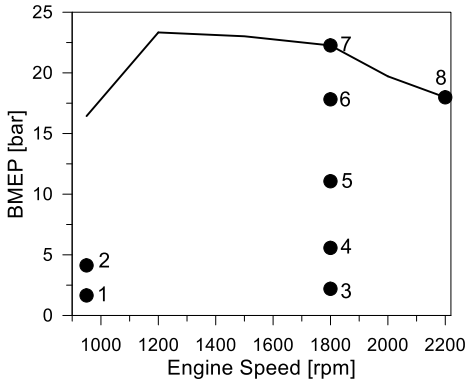

Figure 6.1. Operating conditions investigated during the octane number evaluations.

Despite of the efforts to realize the best octane number from steady-state conditions, the extension of these conclusions to transient conditions is not straightforward since the importance of each operating condition is not the same throughout a driving cycle. Nonetheless, the calibration of a whole engine map for each one of the RONs is time expensive and costly. Therefore, to tackle this point, an equivalent driving cycle methodology was proposed having as reference a full map driving cycle obtained in the evaluations of chapter 4. By doing this, the results of the eight steady-state calibration process can be extrapolated as an estimation of what could be found over the worldwide harmonized vehicle cycle (WHVC). This methodology will be defined as eight-mode as an analogy with the past 13-modes cycle employed to assess the new European driving cycle in the past (NEDC) used for light duty vehicles.

A validation step was considered to guarantee the reliability of the results obtained by this approach. To do this, the results of the complete truck model presented in chapter 4, accounting the complete calibration maps were compared to those obtained with the eight-mode method. The weight of each steady-state operating point in the final eight-mode method calculation was defined by means of an adaptive approach. It considers an equivalent area in which the surrounding map values are similar to that

experimentally measured. The embedded area was steeply increased from an initial small area, while the results have a deviation lower than 2%. Since the performance and emissions parameters can have different trends according to the engine speed and load, the area was incremented following three different strategies that seek to maximize the embedded driving cycle operating conditions and minimize the error. First, a rectangular area was proposed which was defined by a fixed load height and an incrementing rectangle width aiming to capture trends that are invariant in engine speed. Second, the width was fixed while the height was steeply increased to capture trends that are invariant in engine load. Finally, a mixed mode with an expansion factor was applied to expand the area in both directions. This strategy allowed to capture trends that are invariant in both engine speed and load. Figure 6.2 presents a schematic representation of each strategy employed for the area definition.

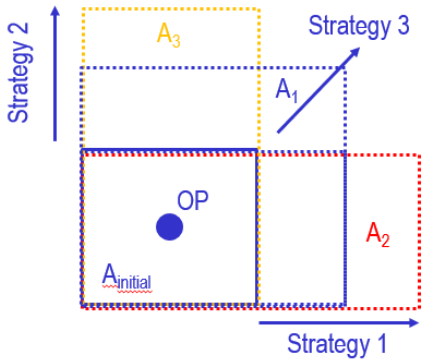

Figure 6.2. Strategies to increment the embedded area for the adaptative approach.

Independently on the method, the area was incremented according to fixed steps, having as a stopping criterion a maximum deviation of 2% compared to that from the experimental operating condition. Once this condition was achieved, the resultant areas were superposed over the operating condition distribution from the complete driving cycle simulations. Then, the total number of the driving cycle operating conditions covered by

each one of the areas was counted (N_{Ai}). A points usage metric was calculated by dividing the number of points covered by the area by the total number of points from the complete driving cycle. In this sense, the results of the driving cycle could be approximated by the equation 6.1. It should be noted that BSFC can be replaced by any of the emission parameters evaluated.

$$BSFC_{final} = \sum_{i=1}^{8} x_i \cdot BSFC_i \qquad 6.1$$

Where the ponderation factor x_i is obtained by:

$$x_i = \frac{N_{Ai}}{\sum_{i=1}^{8} N_{Ai}} \qquad 6.2$$

Table 6.2 summarizes the results obtained with the equation above compared to those from GT Drive for different engine maps. As it is shown, strategy one gives the best results in terms of BSFC and soot. By contrast, strategy three is more suitable to describe the NOx, HC and CO emissions which can be attributed to the dependency of these variables with respect to the engine load and speed. In this sense, strategy one and strategy three were used to describe the significant properties along the equivalent driving cycle. Table 6.3 compares the GT-Drive results with those from the selected strategy for each parameter. As it can be seen, most of the parameters have differences under 5 % comparing the 8 modes and the driving cycle approach. Nonetheless, it should be remarked that soot emissions present significant differences (25 %) because of their ultra-low values.

Table 6.2. Summary of the results obtained from each of the area increase strategies compared to the GT-Power full cycle evaluation.

	BSFC [g/kWh]	NOx [g/kWh]	CO [g/kWh]	HC [g/kWh]	Soot [g/kWh]	Points usage [%]
GT- Power	261.00	0.36	12.63	3.33	0.003	100.0
Strg.1	253.51	0.35	13.90	4.09	0.004	38.1
Strg.2	287.85	0.35	13.45	4.27	0.006	60.4
Strg.3	269.03	0.36	12.59	3.53	0.006	41.8

Table 6.3. Comparison between the full cycle GT Power simulation and the values from the selected strategies.

	BSFC [g/kWh]	NOx [g/kWh]	CO [g/kWh]	HC [g/kWh]	Soot [g/kWh]
GT power	261.00	0.36	12.63	3.33	0.003
Eight-mode	253.51	0.36	12.59	3.53	0.004
Error [%]	2.9	0	0.32	5.6	25

Once a robust method is available to determine the driving cycle results from the eight operating conditions, a merit function approach was proposed to select the best RON for the combustion mode. The importance of each parameter (fuel consumption and emissions) was pondered by a weighting factor and a limit imposed for each parameter. The EUVI targets were used as limits for emissions (NOx_{limit}=0.46 g/kWh, CO_{limit}=4 g/kWh, HC_{limit}=0.16 g/kWh and $Soot_{limit}$=0.01 g/kWh) while the BSFC reference limit was that obtained from the vehicle running under CDC operation along the WHVC ($BSFC_{limit}$=252 g/kWh). Equation 6.2 presents the merit function equation employed to determine the best RON. The calculation in the brackets can result in a negative or positive value. In case of having negative results, the operation is forced to be zero. The weighting factors were selected aiming to minimize BSFC, NOx and soot, as the previous results from chapter 4 and chapter 5 demonstrated that the HC and CO emissions will exceed the EUVI

target independently on the case, but can be reduced by the stock DOC system. The proposed weighting factors for each one of the parameters are: F1=200, F2=0.2, F3=0.02, F4=1 and F5=0.1. These factors were selected with the same order of magnitude of the parameters, otherwise, the merit function would be unbalanced. In this sense, the most important parameters to be minimized are soot, NOx and BSFC as their weighing factor is twice the others.

$$MF_{PRFi} = F1 \cdot \left(\frac{BSFC_{final}}{BSFC_{limit}} - 1\right) + F2 \cdot \left(\frac{NOx_{final}}{NOx_{limit}} - 1\right) + F3 \cdot \left(\frac{Soot_{final}}{Soot_{limit}} - 1\right) + F4 \cdot \left(\frac{CO_{final}}{CO_{limit}} - 1\right) + F5 \cdot \left(\frac{HC_{final}}{HC_{limit}} - 1\right) \quad 6.2$$

6.2.1.2. Results

The results subsection is divided according to each engine load evaluated illustrating the impact of having different RONs at each condition. The RON sweep is demonstrated in some key operating conditions for brevity sakes. They comprehend 25 %@950 rpm, 50 %@ 1800 rpm and 100 %@2200 rpm. Finally, the results from performance and emissions from the complete set of operating conditions (eitght operating conditions) are merged into the merit function equation to find the RON range that provides the most benefits for the DMDF combustion. It is worth to remark that the methodology employed to prepare the fuels is that presented in chapter 3.

6.1.1.1 Low load, low speed operating condition

Table 6.4 presents the main settings employed for each one of the fuel blends evaluated. As it can be seen, both intake and exhaust pressure are maintained constant for all mixtures. At this operating condition, the compressor cannot increase the intake pressure to values higher than 1.1 since the turbine is exposed to low temperature and mass flow. The increase of the

pressure ratio in the compressor also means an operation outside its operating map, resulting in compressor stall. The use of such low intake pressures should impact the conversion efficiency, since the mechanical compression ratio is low to provide a proper combustion process and the dynamic compression ratio cannot be increased. In this sense, the combustion process takes place in a low pressure and low temperature environment. This means that the amount of energy required for the oxidation reactions is limited, probably impairing the use of higher-octane fuels. The analysis of Table 6.4 allows to identify that RON 100 required modifications of the injection setup to achieve the same constraints the remaining fuels had. Since this fuel presents lower reactivity, the use of early injections extends the ignition delay, moving the combustion process to the expansion stroke and provides a low global efficiency. To overcome this, the injection was moved to zones with higher pressure and temperature, shortening the ignition delay and bringing the combustion process closer to the TDC. In addition, the gasoline fraction was reduced to enable a shorter combustion process, compared to the original settings. The remaining fuels were able to use similar air management and injection settings because of their higher reactivity.

Table 6.4. Engine settings for each research octane number evaluated at 25 % of engine and 950 rpm.

RON	P_{intake}	$P_{exhaust}$	Air mass	EGR	SoI	GF
[-]	[bar]	[bar]	[g/s]	[%]	[CAD bTDC]	[%]
100	1.08	1.16	37.23	44.15	15	38.83
92.5	1.08	1.16	35.19	44.45	19	47.31
87.5	1.07	1.15	35.94	44.08	19	46.70
85	1.08	1.16	36.33	43.23	19	47.49
80	1.08	1.16	35.25	44.50	19	46.09

The impact of the different octane numbers on the combustion process can be also visualized from the HRR profiles. As depicted in Figure 6.3, PRF 100 presents the most delayed combustion process. This means that despite the modifications to improve the combustion and advance it, the lower

reactivity of this fuel blend makes impossible to replicate similar combustions to those of high reactivity mixtures just by modifying injection settings. By contrast, as the RON is decreased, the HRR profiles start to demonstrate similarities. For example, all mixtures have similar LTHR profile, indicating that the preconditioning of temperature, pressure and radicals should be similar for all mixtures. The HTHR presents some differences regarding the maximum value and the slope of the early phases. Nonetheless, the bulk part of the combustion process seems to be maintained, indicating that the decrease of the octane number has low influence on the combustion process in this operating condition.

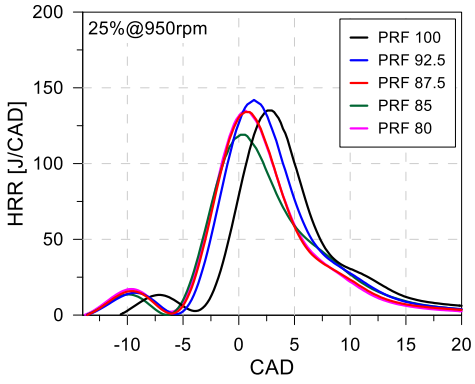

Figure 6.3. Heat release profiles for the different octane numbers evaluated at 25 % of engine load and 950 rpm.

It is also interesting to analyze the effect of the octane modification on the main performance and emission parameters as well as the characteristics combustion metrics. These results are presented in Figure 6.4 (a) (performance and combustion) and Figure 6.4(b) (emissions). The evaluation of the efficiency results presented in Figure 6.4 (a) allows to conclude that, despite the differences on the heat release profiles, the brake efficiency could be maintained at similar levels independently on the RON evaluated. The remaining combustion results (combustion phasing, duration, and pressure gradient) follow the expected trend. As the RON is decreased, faster and earlier is the combustion process. As a side effect, the pressure gradients are

also increased. Nonetheless, for this operating condition, this is not a significant problem since they are far from the limiting conditions.

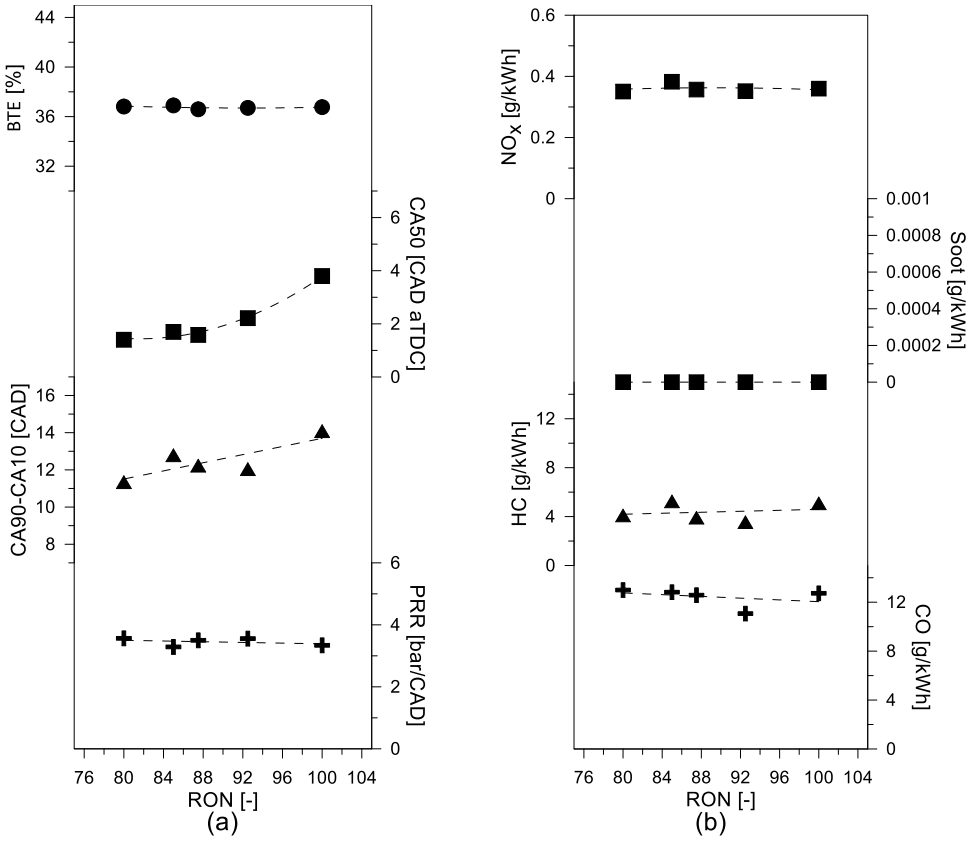

Figure 6.4. Effect of octane number variation on the (a) performance and combustion metrics and (b) main emissions at 25 % of engine load and 950 rpm.

Regarding the emission results, it is suggested that the octane number modification did not present a challenge to obtain the proposed EUVI constraints during the evaluation. The whole set of fuels was able to achieve NOx and soot in EUVI, with similar values of HC and CO. In this context, it can be concluded that at low engine loads, the engine settings can be

tailored as required to obtain the desired emissions while maintaining similar efficiency.

6.1.1.2 Medium load, medium speed operating condition

The octane manifestation presents a high sensibility to the pressure-temperature trajectory that anticipates the combustion. These state parameters dictate what should be the required octane value to guarantee a normal combustion process (i.e., without knock occurrence). At medium load, medium speed conditions, the inlet pressure and temperature are significantly increased compared to 25 % load, increasing the octane demand. Therefore, it can be expected that the combustion process will be significantly affected by the octane modification.

Indeed, this can be confirmed by analyzing the required settings for each fuel blend in Table 6.5. As it can be seen, the settings of each fuel were tailored to account for the differences in the fuel reactivity and achieve the desired constraints in terms of emissions and mechanical limits. The PRF 100 allowed to achieve the highest GF values with early injections. In addition, low EGR levels were required to control the pressure gradients. This is an important point since it was found in previous results that the excess of EGR flow can overload the air management system, presenting excessive compressor outlet temperatures. Once the RON is reduced to 92.5, both the EGR and GF were modified. The first was increased to allow the control of the reaction rates of the oxidation reactions. By contrast, the GF values were decreased to guarantee a better combustion stability in this extremely diluted environment. The reduction of the octane number to 87.5 required modifications in the injection timing because the direct replication of the settings of the previous condition produce pressure gradients higher than the mechanical limits, i.e., the octane demand surpassed the fuel octane quality. By contrast, some of the settings could not be modified, like the EGR levels. The increase of the EGR would mean higher pumping losses and a reduction of the oxygen content, impairing the conversion efficiency and enhancing the

soot formation. Therefore, the most effective modification found was delaying of the SoI. Once the SoI is delayed, the mixing time is reduced, and the fuel reactivity stratification is increased allowing to decrease the pressure gradients due to both compositional and RON stratifications. Nonetheless, the ignition delay is reduced due to the richer zones near the HRF injector, advancing the combustion process.

As expected from the previous discussion, the most critical conditions were verified for both low RON fuels evaluated. At these conditions, both SoI and GF were modified to compensate the reactivity increase from the LRF. The SoI modification strategy was herein used following the same, previously discussed, justification. By contrast, the introduction of the GF decrease was employed to control the combustion process, decreasing the importance of the premixed combustion, and enlarging the combustion by means of heavy fuel stratification on the combustion chamber. The higher local reactivity from the HRF injection promotes short ignition delays, which shift the combustion process to the compression stroke. Therefore, the combustion cannot be tailored to operate in the maximum efficiency condition because of the restrictions from the fuel octane quality and the emissions targets imposed during the calibration process.

Table 6.5. Engine settings for each research octane number evaluated at 50 % of engine and 1800 rpm.

RON	P_{intake}	$P_{exhaust}$	Air mass	EGR	SoI	GF
[-]	[bar]	[bar]	[g/s]	[%]	[CAD bTDC]	[%]
100	2.11	2.44	145.08	38.98	50	88.97
92.5	2.10	2.73	114.30	46.31	50	78.81
87.5	1.99	2.44	112.71	43.00	40	79.34
85	2.16	2.61	120.58	44.57	30	77.05
80	2.21	2.66	129.20	43.12	24	69.81

Figure 6.5 depicts the heat release rates obtained for the different RONs evaluated allowing to visualize the previous comments in the evolution of

each HRR profile. As it can be seen, the use of PRF 100 provides a delayed combustion process allowing to use higher gasoline fractions. This means that the use of high RON fuels is better suited for these conditions, allowing to properly phase the combustion process while fulfilling both mechanical and emissions constraints.

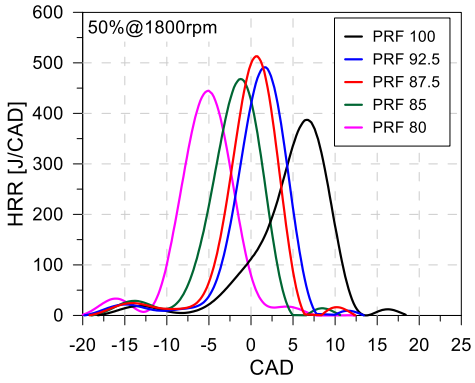

Figure 6.5. Heat release profiles for the different octane numbers evaluated at 50 % of engine load and 1800 rpm.

The RON decrease implies a short combustion duration with higher peaks, which translates to an increase of the pressure gradients, thus requiring the modifications previously described. From RON 87.5, the delayed SoI coupled with the GF modifications results in higher combustion durations decreasing the HRR profile peak. It should be noted that the early combustion process means a high amount of energy released during the compression stroke which may reduce the cycle efficiency.

The different settings requirements for each PRF should impact the performance and emissions results. This can be confirmed from the results presented in Figure 6.6, where the emission, performance and combustion results for the different PRF are summarized. As it can be observed, the use of PRF100 allows to obtain a higher brake efficiency than the remaining PRFs, surpassing the 40 % level. This high level can be related to the better combustion phasing (after the TDC), coupled with an appropriated

combustion duration, improving the work output. The remaining fuels presented similar brake efficiency results and combustion duration. The main difference is noticed for the combustion phasing. As previously discussed, lower GF coupled with delayed SoIs were the fundamental strategy employed to overcome the issues entailed by the RON decrease. The approach provided richer zones from the HRF injection that decreased the mixture ignition delay, as presented in the HRR profiles depicted in Figure 6.5 and the combustion phasing results presented in Figure 6.6. It is also possible to see that all the mixtures where maintained at a similar pressure gradient level, the maximum allowable as mechanical constraint.

Figure 6.6 (b) depicts the engine-out emissions for NOx, soot, HC and CO. The nitrogen oxides emissions demonstrate that EUVI results can be achieved independently of the RON employed. Nonetheless, there is a notable reduction for both PRF 92.5 and PRF 87.5 because of the fast combustion process realized by them. This reduces the residence time (proportional to the combustion duration) of the nitrogen molecules on high temperature conditions compared to the other cases inhibiting the formation mechanism.

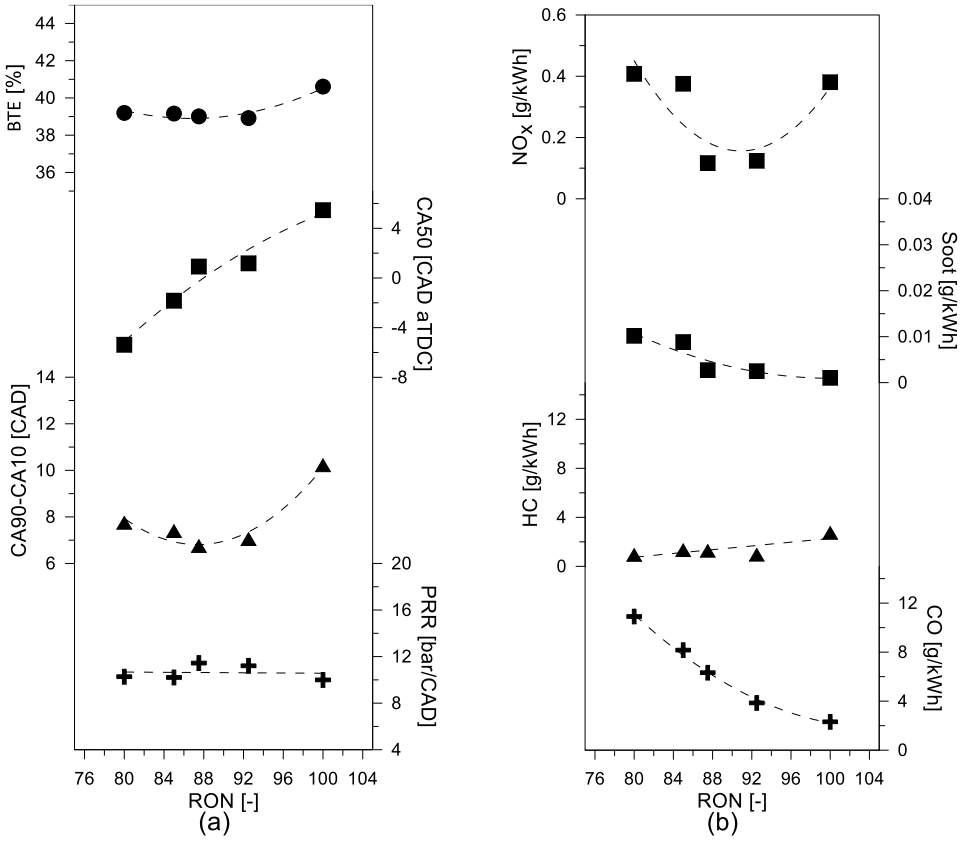

Figure 6.6. Effect of octane number variation on the (a) performance and combustion metrics and (b) main emissions at 50 % of engine load and 1800 rpm.

Unlike the 25 % load, this operating condition works in equivalence ratios closer to the stoichiometric, where there is low oxygen availability to mitigate the soot formation, requiring high mixing times to allow a proper fuel - oxidizer mixing. Nonetheless, as the RON was decreased, the mechanical constraints required the use of delayed injections as well as low GF. Both strategies enhance the soot formation mechanism due to the high amount of HRF injected and lower mixing times. Therefore, as the RON is decreased, the engine-out soot values increase towards the EUVI limits. It should be noted that PRF 85 and PRF 80 presented both soot and NOx at

EUVI limits. The use of strategies to reduce one of them will impair the other. Therefore, it can be concluded that it is not possible to achieve simultaneous EUVI limits for both NOx and soot for RON values lower than 80.

By contrast, the use of lower GF decreases the amount of LRF meaning less fuel available to enter the piston gaps during the compression stroke. Consequently, the engine out HC emissions can be reduced for low RON fuels. A significant increase is experienced for the CO emissions as the RON is decreased. This can be attributed to the higher mixture stratification resulted from the delayed injections. In this regard, the conditions with low air fuel equivalence ratio enhances the CO formation as well as soot.

6.1.1.3 High load, high speed operating condition

The last operating condition addresses a full load operating point at the maximum engine speed (2200 rpm) aiming to identify the impact of the RON modification at high temperatures and pressures. As described in chapter 4, full load operating conditions are based on a dual fuel diffusive combustion with low premixing levels and a single HRF injection close to the TDC. This provides a first phase based on premixed burning, which comprises the LRF mass, followed by a diffusive sustained combustion, which provides the required energy to fulfil the target load. Table 6.6 presents some of the most important air management and injection settings found for each PRF with the calibration routine optimization previously described. It is possible to note that minor modifications were done as the RON was decreased. Despite the apparent variations, intake and exhaust pressure, EGR and air mass presented modifications lower than 5 % with respect to the average of each parameter. The most significant modifications address the start of injection and the gasoline fraction values. The last was one decreased as the RON was reduced aiming at lower premixing, enhancing the compositional stratification to improve the control over the combustion development. By contrast, the use of high diesel quantities is prone to the

formation of rich zones where the hydrocarbon cannot be properly oxidized, originating soot.

Table 6.6. Engine settings for each research octane number evaluated at 100 % of engine and 2200 rpm.

RON	P_{intake}	$P_{exhaust}$	Air mass	EGR	SoI	GF
[-]	[bar]	[bar]	[g/s]	[%]	[CAD bTDC]	[%]
100	2.79	3.33	276.35	19.90	10	41.15
92.5	2.61	3.10	263.34	19.15	11	38.82
87.5	2.59	3.05	260.34	20.72	12	38.95
85	2.83	3.38	273.17	21.56	13	38.65
80	2.72	3.19	265.66	20.18	12	36.71

As it can be seen in Figure 6.7, the whole set of blends presents similar end of combustion. This allows to conclude that the RON modification does not affect the last phase of the combustion process. The previous statement concurs with the operating principle at these full load conditions, which relies on the use of diffusive combustion to burn the HRF fuel. As the SoI and HRF characteristics are maintained, the end of the combustion process is also not significantly modified.

Regarding the combustion start, a similar trend to the previously verified for 50% of engine load is found. Nonetheless, it is important to remark that the dominant mechanism for these early combustion processes is not the same. While at 50 %, the injection timing was considerably modified, at the current operating condition, the maximum shift in the SoI was 3 CAD. Moreover, the SoI modification does not follow a direct relation with respect to the RON decrease. Therefore, the early combustion start can be related mainly to the mixture reactivity increase for the lower RONs and not to the SoI modification.

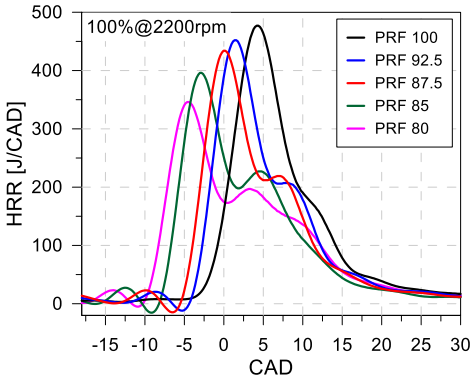

Figure 6.7. Heat release profiles for the different octane numbers evaluated at 100 % of engine load and 2200 rpm.

The average results for performance, combustion, and emissions for the different PRFs are presented in Figure 6.8. As it is shown, the brake thermal efficiency is not significantly affected by the RON modification at this operating condition (Figure 6.8 (a)). Slight changes can be perceived for PRF 80, mainly attributed to the larger combustion durations, as presented in the previous graph. The simultaneous analysis of the CA 50 and combustion duration results allows to identify that the high reactivity of the mixtures provides early ignition and larger combustion process. The pressure rise rate is maintained at the limit condition independently on the RON, aiming to extract the maximum benefits from the premixed combustion.

Figure 6.8 (b) depicts the impact of the RON variation on the different emissions. It should be recalled that this operating condition is not able to fulfill EUVI normative for neither soot or for NOx due to the requirements on the turbocharger and the mechanical constraints. Therefore, the NOx emissions were relaxed to 2 g/kWh while the soot emissions constraint was increased to two FSN (≈0.2 g/kWh at this operating condition). However, the reduction of the gasoline fraction and increase of the dilution levels as the RON was increased have demonstrated to be prejudicial in terms of soot production. Unburned hydrocarbon emissions seem to be highly affected by the RON variation, presenting a reduction of up to 50 % considering the

lowest RON compared to PRF 100. By contrast, CO emissions are invariable with respect to the different RONs.

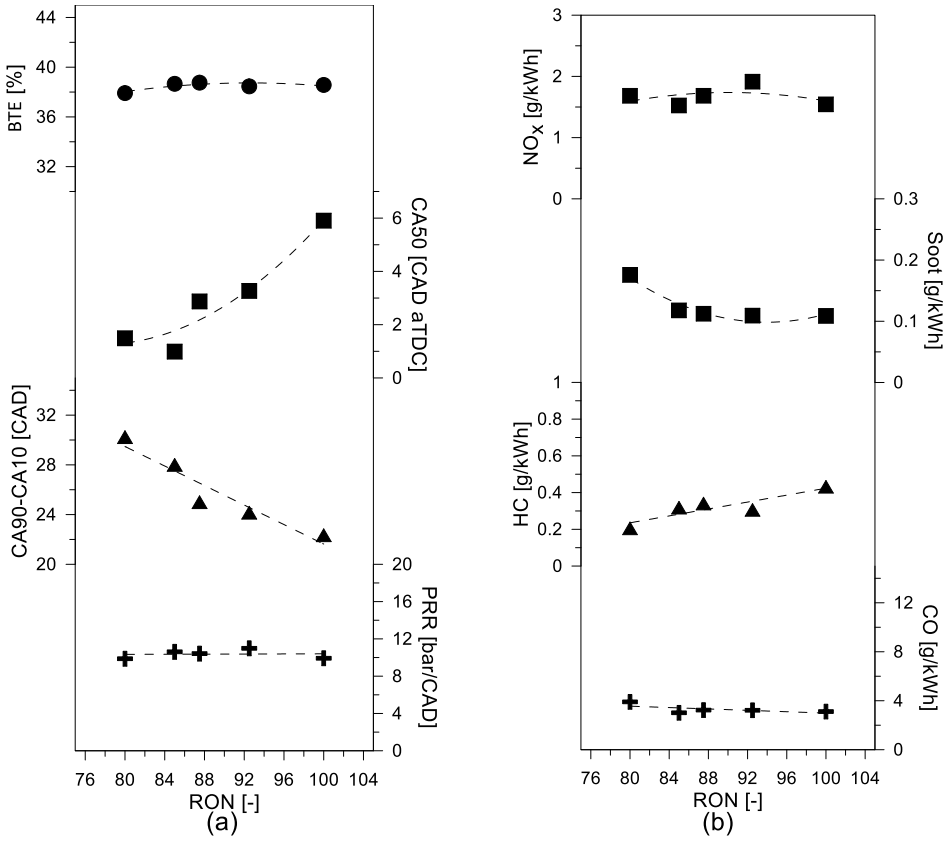

Figure 6.8. Effect of octane number variation on the (a) performance and combustion metrics and (b) main emissions at 100 % of engine load and 2200 rpm.

6.2.1.3. Merit function evaluation

The previous analysis allowed to understand the octane manifestation with respect to different operating conditions, representative of the DMDF calibration. Nonetheless, it was evidenced that the trends do not favor always the same RON depending on the parameter and operating condition in

analysis, which is a hurdle for direct selection of the optimum RON. Moreover, transient evaluation operation should be considered to weight the importance of each operating condition on the analysis. Therefore, the 8-point cycle methodology previously described was employed followed by a merit function evaluation. Figure 6.9 presents the merit function results with respect to the different RONs evaluated.

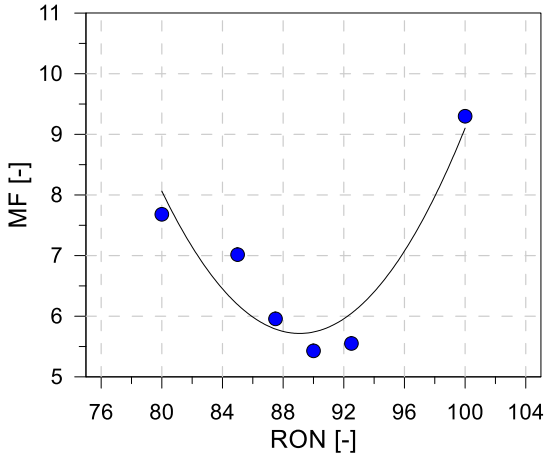

Figure 6.9. Merit function results for the different research octane number evaluated.

As it can be seen, RON values from 94 to 88 tend to deliver the minimum MF results, indicating that they are the optimum choices for the DMDF combustion. This comes from the combination of low soot and NOx emissions that can be realized with these fuels, together with a proper conversion efficiency. It should be remarked that this solution is dependent on both hardware and HRF employed. The use of strategies that can deliver lower soot levels might shift this balance towards low RON fuels, while the opposite should favor high RONs.

6.2.2. Sensitivity effect on representative DMDF conditions

The previous section focused on the assessment of the research octane number on the performance and emissions results for the proposed concept. Despite of the importance of the RON in the combustion process, additional fuel characteristics also play a fundamental role in the combustion development. Historically, the introduction of a single octane quality metric based on single paraffins was proven to not capture the complex chemistry of multicomponent commercial fuels. This fact propitiated the introduction of a new octane quality metric, the motor octane number and with it, the concept of sensitivity, which reflects the importance of the low temperature reactions on the fuel reactivity for specific RONs at specific P-T trajectory. Therefore, this subsection addresses the effect of the fuel sensitivity variation on representative operating conditions of the DMDF combustion. For this purpose, an experimental evaluation was employed, aided by 0-D simulations, to understand the impact of each combustion mode and the implications of the low temperature chemistry on the combustion development.

6.2.2.1. Methodology

The sensitivity variation can be attained by blending aromatic compounds with paraffinic components. Among the different aromatics, toluene is one of the most used ones due to its properties, like solubility in a wide range of components. In this sense, different binary and ternary blends were made targeting specific sensitivities considering toluene, n-heptane, and iso-octane as single components. Table 6.7 presents some of the important characteristics of each one of these components. Diesel is also presented because it is the HRF used during the investigations.

Table 6.7. Chemical and physical properties of the different fuels used in the sensitivity effect evaluation.

	Diesel	n-heptane	iso-octane	Toluene
Density [kg/m^3] (T=15 °C)	842	645	658	866
Viscosity[mm^2/s] (T=40 °C)	2.929	-	-	-
RON [-]	-	0	100	121
MON [-]	-	0	100	107
Cetane number [-]	51	-	-	-
Lower heating value [MJ/kg]	42.50	44.57	44.43	40.59

Two RONs where chosen as basis for the evaluation. RON 92.5 was selected from the previous RON evaluation, representing the best research octane number for the DMDF concept. In addition, RON 80 was also chosen addressing potential low octane fuels that could be used in the short-term future. From the selection, an overview of the sensitivity impact on contrasting RONs could be achieved. Three different sensitivity values were used for each one of the fuels: 0, 5 and the maximum achievable. This last value was defined as the maximum toluene content that can be mixed while maintaining the desired RON. The methodology described in chapter 3 for TRF definition was followed to determine the ternary composition for each sensitivity and RON. Table 6.7 summarizes the mass fraction of each component as function of the sensitivity and research octane number.

Table 6.8. Mass fraction of each component for both research octane number of 92.5 and 80 and different sensitivities (0, 5 and max.).

	RON 92.5			RON 80		
	S=0	S=5	S=9	S=0	S=5	S=8
Y Toluene	0.000	0.293	0.577	0.000	0.326	0.604
Y Iso-octane	0.925	0.575	0.247	0.800	0.412	0.087
YN-heptane	0.075	0.132	0.176	0.200	0.263	0.309

Each one of the mixtures was evaluated at the same operating conditions presented in section 6.2.1, covering different engine load and speed, i.e., different combustion regimes of the DMDF combustion. The engine settings of each PRF fuel were determined by means of the same calibration methodology described in chapter 4. Afterwards, the TRFs were evaluated, maintaining the same injection and air management settings to isolate the effect of the fuel composition variation. In this sense, the combustion metrics as well as performance and emission results should evidence the impact of the sensitivity variation of the fuel.

Complementing the experimental evaluation, a numerical approach was developed in Cantera® to evaluate the effect of the fuel modification on the mixture reactivity at controlled conditions, like those found in perfectly stirred reactors. This allows to isolate the chemical Kinects in contrast to the multi variable problem found at an internal combustion engine. To do this, a homogeneous adiabatic constant volume reactor was configured in Cantera addressing different boundary conditions. At first, both RON 92.5 and RON 80 and their respective sensitivities were assessed for a given range of temperatures and equivalence ratios, while maintaining the initial pressure to emphasize the differences among the fuels. Subsequently, the experimental conditions in terms of state properties as well as composition (EGR + Φ) were used as boundary conditions for different simulations. Pressure and temperature were those obtained using the in-house combustion analysis routine CALMEC. Different reactors were solved, representing different instants of the compression stroke up to the first noticeable heat release. For each reactor, the ignition delay was assessed considering the considering the maximum value of the OH radical. Andrae's [28] mechanism was chosen among the most recent mechanisms for toluene reference fuels since it was demonstrated by the literature to deliver the most accurate results at engine conditions [36]. It involves 137 species and 633 reactions with sub mechanisms for toluene oxidation description.

Different from the homogenous combustion concepts, like spark ignition and HCCI engines, the assumption of perfectly mixed in-cylinder charge is

difficult to be defended in RCCI combustion, since it, by definition, relies on the chemical stratification inside the cylinder. Therefore, different assumptions should be made prior to the simulations stressing the limitations of the numerical analysis:

- The in-cylinder stratification tends to decrease for early injection processes in the compression stroke compared to those near to the TDC.
- The LRF is assumed to be fully vaporized and perfectly mixed inside the combustion chamber.
- The EGR composition was approximated by H_2O, CO_2 and N_2 considering an 11 products reaction that uses measured species to determine the unknowns as H_2O. The detailed procedure can be found in [44].
- There is no temperature gradient inside the combustion chamber.
- N-Heptane is used as the surrogate for the HRF (diesel). As demonstrated in previous studies, this surrogate fuel is able to emulate the ignition qualities of diesel. As n-Heptane is presented also in the blend in the LRF, its mass fraction is determined considering the GF values.

Considering the assumptions above, it is evident that they intend to obtain a 0-D simplification of the problem. Independently on the case, this will never be completely correct. Nonetheless, the approximation of the analysis can be improved if the importance of the high reactivity fuel is decreased. Moreover, this should be also enhanced in the case of having earlier injections in the compression stroke, providing a significant mixing time and, consequently, a more homogeneous mixture. From the extensive discussion about the combustion modes used in the calibration and their particularities, one can easily identify that these conditions are generally found at medium engine load condition, where a fully premixed combustion is applied. In this sense, the operating condition of 50 % of engine load at 1800 rpm was selected

to perform the Kinects evaluation as an attempt to identify underlying chemistry phenomena that could influence the combustion development.

6.2.2.2. Kinects results

As previously discussed, two fuels with different RONs and sensitivities were evaluated following specific methodologies. Figure 6.10 presents an example of the sensitivity impact on induction time (i.e. reactor ignition delay) results obtained for each one of the fuel blends with respect to the different temperatures at a fixed equivalence ratio (0.6) and pressure (44 bar). It is worth to mention that this equivalence ratio represents the global equivalence ratio that is obtained considering air and the low reactivity fuel. The NTC affected zone is evident from the graph analysis, which can be seen as a discontinuity on the induction time monotonically increase with respect to the temperature decrease. Higher sensitivity values tend to minimize this effect, independently on the RON evaluated.

It can also be implied that the use of lower RON does not affect the position of the NTC zone, which can be explained by the fact that this phenomenon is dominated by the low temperature kinetics of the paraffins, which are presented in both cases. The inhibition of these reactions by the aromatic content should be similar for both cases, since the toluene mass fraction on the blends does not present significant variations. Finally, lower RONs provide lower induction times because of their higher reactivity. Nonetheless, it should be stated that depending on the in-cylinder pressure temperature trajectory, the NTC affected zones that are presented at the left-hand side of the graph can be achieved, meaning that sensitive fuels would provide larger induction times than non-sensitive ones even on the case of having 12.5 points of difference in RON values.

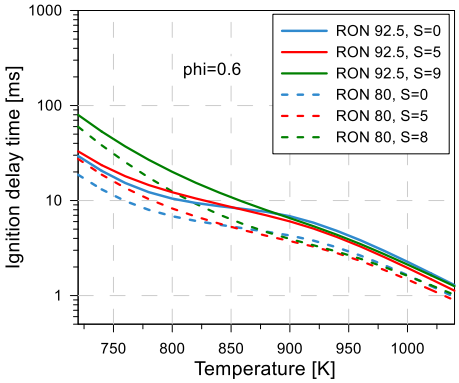

Figure 6.10. Ignition delay times for both research octane number of 92.5 and 80 and different sensitivities (0, 5 and max.) addressing temperatures from 700 K to 1050 K, Φ=0.6 and 44 bar of pressure.

In spite of the results presented in Figure 6.10, several additional properties can still influence the mixture reactivity, modifying the overall effect of the RON variation in different zones. One of the most fundamental characteristics of fuel blends is its equivalence ratio, which can shift the dominant reaction paths for radical formation and the amount of energy released in each reaction. Therefore, its impact on the mixture reactivity was assessed by considering two sets of equivalence ratios: 0.5 and 1. The first considers the equivalence ratio that could be obtained assuming that the LRF is fully premixed prior to the injection of the HRF, and the equivalence ratio does not present stratification. The second is the minimum overall equivalence ratio that is obtained in the exhaust gases considering both HRF and LRF. It is clear that the local equivalence ratio should be higher than 1, but the proper determination of this value includes the assessment of spray penetration, fuel mixing, turbulence description, etc., that generally requires the use of 3-D finite volume approaches.

Figure 6.11 depicts the results of this analysis for each one of the equivalence ratios, RONs and sensitivities evaluated. Solid lines stand for the higher equivalence ratios while the dashed ones refer to the leaner condition of each case. As it can be seen, the equivalence ratio manifests its effects in

different ways depending on the sensitivity evaluated. At sensitivity zero, both equivalence ratios present similar behaviors. As the fuel sensitivity is increased, it is interesting to note that the $\Phi = 1$ case has a more noticeable NTC zone for both cases (S=5 and S=max), while the lean conditions are less impacted by this phenomenon. This statement can be extended to the complete set of mixtures evaluated as it can be seen in Figure 6.11 (a) and Figure 6.11 (b). These results concur with those observed by Curran [8], Herzler [9] and Vandersickel [10]. In this sense, it can be concluded that the increase of the fuel stratification at reactive conditions should impact the engine ignition delay in such a manner that the 0-D approach is not able to capture.

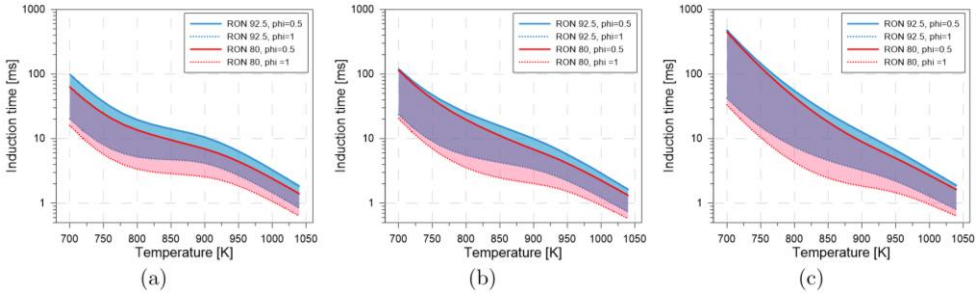

Figure 6.11. Ignition delay times for both research octane number of 92.5 and 80 addressing temperatures from 700 K to 1050 K, Φ=0.5 to 1 and 44 bar of pressure for sensitivities of (a) zero, (b) five and (c) the maximum allowable by the ternary blend.

From the previous fundamental analysis, it is suggested that any Kinects evaluation should stick to conditions where the compositional stratification is minimized. As discussed, the 50 % of engine load is the condition that is better suited for these constraints. Therefore, a detailed analysis was performed as an attempt to correlate the numerical and experimental results for this condition. Figure 6.12 depicts the HRR obtained for both PRFs at 50% of engine load and the different sensitivities evaluated in the multi-cylinder engine. As it is shown, there is an interesting difference between both RONs. While RON 92.5 seems to be heavily impacted by the

sensitivity modification, RON 80 heat release could be maintained, even at highly sensitive blends. The differences are also noted on the low temperature heat release zone, which happens early and is consistently independent on the sensitivity for PRF 80 compared to PRF 92.5.

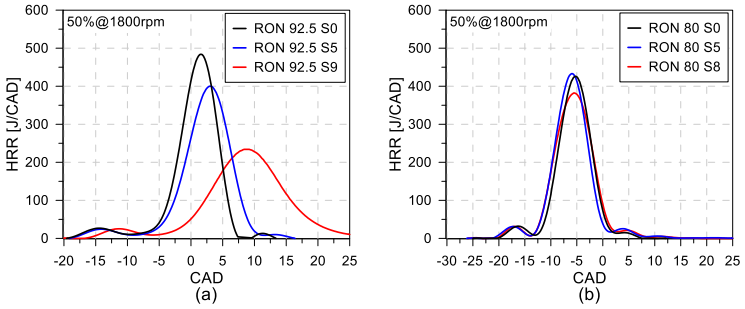

Figure 6.12. Experimental heat release profiles for the different RONs and sensitivities evaluated for the operating condition of 50 %@1800 rpm: (a) RON 92.5 and (b) RON 80.

Taking a deeper look on the engine settings (see Table 6.9), it is possible to identify some key parameters that should be influencing the combustion development. First, it can be evidenced that the settings for sensitivity 0 are similar to those from the RON evaluation presented in section 6.2.1.2.2, with different injection strategies to decrease the pressure gradients inside the cylinder for the low RON fuel. Moreover, the higher intake pressure represents an increase of the mass through the compressor, while having similar levels of EGR. This results in higher temperatures at the manifold for PRF 80 due to the higher compression at the compressor as well the increase of the thermal load to be dissipated at the intercoolers. Higher air mass was required to increase the oxygen availability and improve the soot oxidation because this condition has lower gasoline fractions, i.e., high amount of diesel, modifying the stoichiometry.

Table 6.9. Operating condition settings for PRF92.5 and PRF 80 with the different sensitivities (0, 5 and max.) at 50 % of engine load and 1800 rpm.

RON	S	Speed	Load	P_{intake}	T_{intake}	EGR	Soi_{Main}	GF
[-]	[-]	[rpm]	[%]	bar	[°C]	[%]	[CAD_{bTDC}]	[%]
92.5	0	1800	50	2.11	65.19	47.62	50	78.81
92.5	5	1800	50	2.11	64.37	48.13	50	78.93
92.5	9	1800	50	2.10	63.20	47.85	50	79.05
80	0	1800	50	2.21	78.11	46.56	24	70.19
80	5	1800	50	2.22	77.06	47.09	24	70.92
80	8	1800	50	2.22	76.01	46.47	24	71.10

The impact of these modifications can be visualized on Figure 6.13 which depicts the pressure (Figure 6.13 (a)) and temperature (Figure 6.13 (b)) profiles for each one of the sensitivities for both RONs evaluated. It should be remarked that these profiles are an average of the 200 cycles and the six cylinders. As it can be seen, no noticeable changes are found at the pressure temperature profiles during the early phases of the compression stroke. The differences start to appear as the process approaches to the TDC firing, where the state conditions are high enough to enable the first low temperature heat releases. It can be also inferred that even the small quantities of heat released verified in Figure 6.12 are enough to decuple the pressure and temperature trajectories of each PRF. But one important question is: should these differences only be attributed to the reactivity modification of the fuel, or may the compositional, reactivity and temperature stratification also influence the combustion development?

As an attempt to decouple the multiphysics problem from the Kinects one, the pressure-temperature profiles were used as boundary conditions for the Cantera® simulations, emulating the different states that are achieved from the compression up to the combustion start. For each state, the OH concentration was monitored, and the ignition delay was calculated considering its maximum value as reference. The experimental values of EGR and GF were also considered in the boundary conditions.

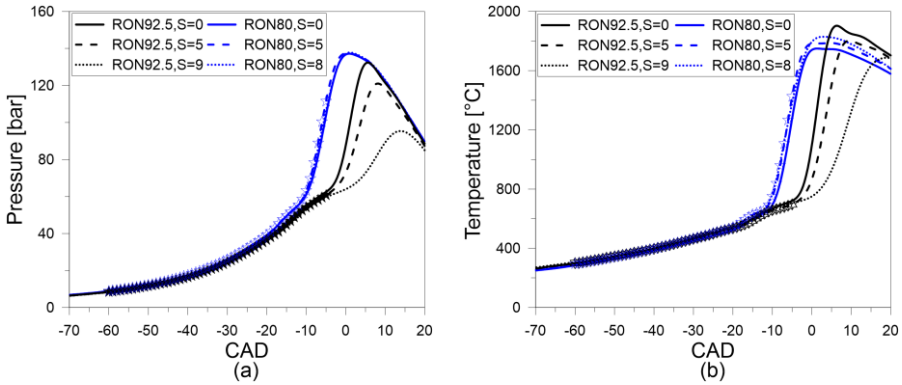

Figure 6.13. Pressure and temperature profiles for the different research octane numbers and sensitivities evaluated at 1800 rpm and 50 % of engine load.

Nonetheless, it should be remarked that, given the level of stratification that could exists and the delayed injection of PRF 80 (-22 CAD aTDC), the determination of a representative equivalence ratio is somewhat difficult. Therefore, it was chosen to consider 0.6, i.e., the equivalence ratio that is obtained if only LRF is considered to perform the investigations, avoiding assumptions about the injection process that are beyond the capability of the current setup. The results of this analysis are presented in Figure 6.14, depicting the ignition delay time that would be found at the represented state condition of a given crank angle. As it is shown, PRF 92.5 presents a significant higher ignition delay than that of PRF 80, given the experimental boundary conditions. It is possible to infer that it takes almost 10 CAD of temperature and pressure evolution for PRF 92.5 to achieve the same reactivity of PRF80. Moreover, it is also possible to conclude that the pressure-temperature trajectory passes though different zones during the compression stroke. From -50 up to -20 CAD aTDC, the sensitivity affects the reactivity of the blend in a negative manner, leading to longer ignition delays independently on the case evaluated. Nonetheless, as the mixture starts to react, this trend is inverted, which may indicate that the mixture is inside NTC affected zones.

Finally, the fact that the mixtures cross each other at the same crank angle interval suggests that their low temperature heat release should start at the same time. While this seems to align with that verified on the HRR for PRF 80, the same cannot be extended to PRF 92.5. This may indicate that additional phenomena are affecting the combustion process such as mixture inhomogeneities, boundary condition variations, compositional and reactivity stratification. This allows to conclude that alternative methods that can capture these phenomena as the non-dimensional zone temperature (NZT) method for temperature description should be included to achieve a better representation in 0-D calculations [11][12]. Nonetheless, it is suggested that a much more representative description could be attained if a 3-D CFD approach is considered.

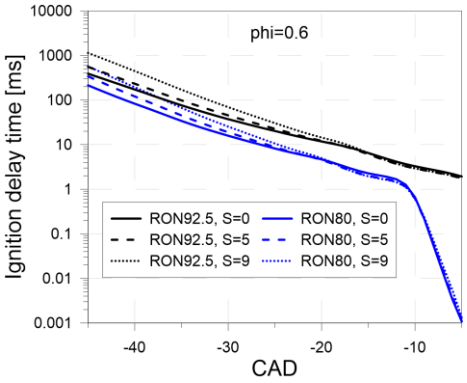

Figure 6.14. Ignition delay evolution according to the different states along the compression stroke for the set of PRFs (92.5 and 80) and sensitivities evaluated (0, 5 and max.) for the operating condition of 50 %1800 rpm.

6.2.2.3. Combustion results

The Kinects simulations were not able to capture the stratification effects that could exists in the combustion chamber and therefore will not be extended to the remaining operating conditions, since even worst results are expected due to the stratified nature of them. Nonetheless, the impact of the sensitivity on the combustion process of these conditions is still worthy to be

evaluated. To do this, an experimental campaign aided by heat release analysis was performed on the experimental pressure traces using the in-house combustion routine CALMEC. The methodology was then applied to the remaining operating conditions which could not be addressed in the Kinects evaluation: 25 %@950 rpm, 25 %@1800 rpm, 100 %@1800 rpm and 100 %@2200 rpm for both PRFs evaluated. Table 6.10 presents the boundary conditions in terms of fuel injection and air management for each one of the sensitivities and operating conditions evaluated for RON 92.5. As it can be seen, the boundary conditions were maintained as similar as possible among the sensitivities aiming to isolate their effect on the combustion development, and, consequently, on the performance and emissions results.

Table 6.10. Injection and air management settings for the different sensitivities and operating conditions evaluated with RON 92.5.

S	Speed	Load	P_{intake}	T_{intake}	EGR	Soi_{Pilot}	Soi_{Main}	GF
[-]	[rpm]	[%]	bar	[°C]	[%]	[CAD_{bTDC}]	[CAD_{bTDC}]	[%]
0	950	25	1.08	41.37	44.91	29	19	46.56
5	950	25	1.09	42.39	45.02	29	19	46.95
9	950	25	1.09	43.61	44.95	29	19	47.37
0	1800	50	2.11	65.19	47.62	60	50	78.81
5	1800	50	2.11	64.37	48.13	60	50	78.93
9	1800	50	2.10	63.20	47.85	60	50	79.05
0	2200	100	2.53	58.50	20.26	-	11	38.93
5	2200	100	2.54	58.38	20.16	-	11	38.89
9	2200	100	2.54	57.26	20.05	-	11	39.30

As it is shown in Figure 6.15 (a), low load and low engine speed operating conditions experiences a significant contribution of the LTHR on the combustion process. Even highly sensitive fuels as S=9 still present a considerable part of its energy on the LTHR zone. Nonetheless, the phasing of each case is different, suggesting that the sensitivity may influences the early stages of the heat release. Considering the previous discussion presented in section 6.2.2.2, Figure 6.10, it was concluded that there is a narrow zone

in the temperature dependency where the sensitivity improves the mixture reactivity up to a determined level (≈S=5). By contrast, a sucessive increase of the sensitivity impairs the mixture reactivity, providing larger induction times. This similar behavior can be evidenced on both Figure 6.15 (a) and Figure 6.15 (b) where the combustion phasing is advanced for S=5 and delayed with S=9 compared to the reference PRF 92.5. It is also interesting to note that the HTHR is correlated with the phasing of the LTHR. Higher engine speeds tend to present a lower discrepancy among the different sensitivities, but, undoubtedly, the same phenomenon is present.

From an application perspective, low load conditions are challenging to be implemented, since the engine geometric modifications, e.g., the reduction of the compression ratio, results in worsened state conditions to obtain a proper fuel oxidation (low combustion efficiency, combustion instabilities, etc.). Therefore, the improvement of the fuel reactivity in these specific conditions should be perceived as an enhancement towards the solution of low load issues. This was accomplished with the introduction of five points of sensitivity on the blend, being the best compromise at this engine load.

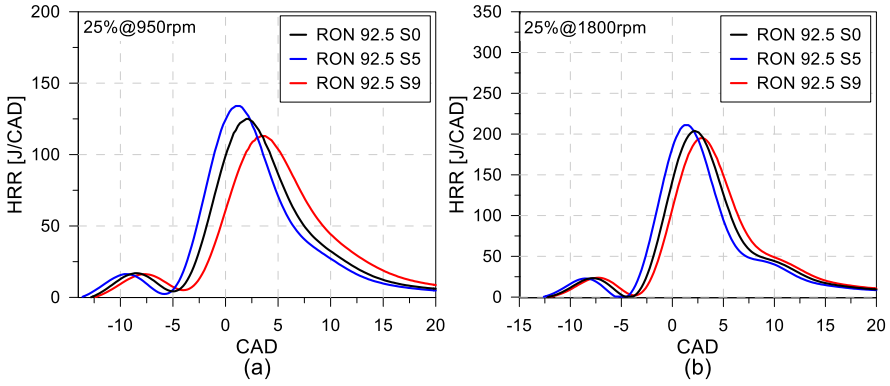

Figure 6.15. Heat release rates for (a) 25 %@950 rpm and (b) 25 %@ 1800 rpm for RON 92.5 and different sensitivities.

By contrast, this should be avoided at high load conditions, where lower fuel reactivity is desired to slow down the reaction progress and decrease the

mechanical requirements. It is expected that the high temperature and pressures at the IVC should provide beyond-RON conditions, where the sensitivity variation would reduce the mixture reactivity, providing delayed combustion even in the case of low sensitivity increase. The analysis of Figure 6.16 allows to confirm this assumption since it reports delayed combustion for both engine speeds evaluated. As discussed, this behavior is interesting for these engine loads because they present excessive pressure gradients that limits the maximum premixing degree that could be used. Therefore, it can be concluded that RON 92.5, S=5 seems to present the best trade-off considering the combustion development for both low and high load conditions. This sensitivity is similar to that found in commercial gasolines, indicating that the DMDF concept is suited to use drop-in fuels, without additional modifications, exploring the already existing fuel distribution system.

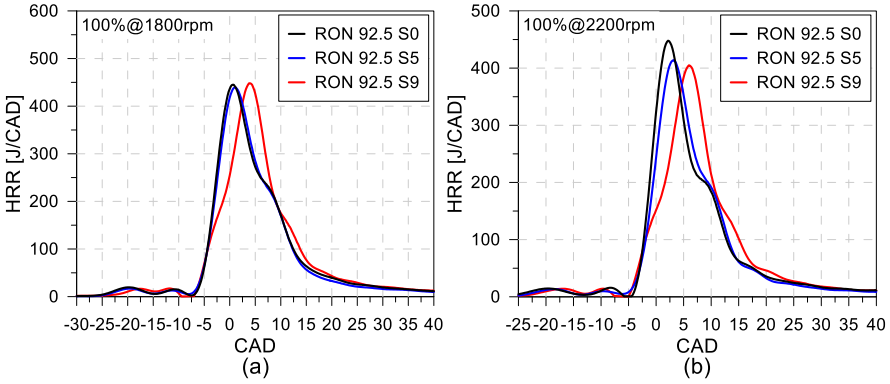

Figure 6.16. Experimental heat release rates for (a) 100 %@1800 rpm and (b) 100 %@ 2200 rpm for RON 92.5 and different sensitivities.

As an additional investigation, the effect of the sensitivity variation was also evaluated for low RON fuels, which can be an alternative to cost reduction in the fuel production process [13][14]. To do this, the same methodology was employed, considering similar boundary conditions to those employed for RON 92.5 when possible. Table 6.11 provides the air management settings as well as the injection parameters for each condition.

As it can be seen, there is low dispersion among each sensitivity for a same operating condition allowing to affirm that the variations observed for each case will be a consequence of the sensitivity variation itself.

Table 6.11. Injection and air management settings for the different sensitivities and operating conditions evaluated with RON 80.

S	Speed	Load	P_{intake}	T_{intake}	EGR	Soi_{Pilot}	Soi_{Main}	GF
[-]	[rpm]	[%]	bar	[°C]	[%]	[CADbTDC]	[CADbTDC]	[%]
0	950	25	1.08	45.19	47.61	29	19	47.02
5	950	25	1.08	45.17	48.39	29	19	47.26
8	950	25	1.07	45.47	47.39	29	19	47.64
0	1800	50	2.21	78.11	46.56	34	24	70.19
5	1800	50	2.22	77.06	47.09	34	24	70.92
8	1800	50	2.22	76.01	46.47	34	24	71.10
0	2200	100	2.72	73.86	20.18	-	13	36.58
5	2200	100	2.74	73.18	20.67	-	13	36.86
8	2200	100	2.71	73.97	20.52	-	13	37.04

Figure 6.17 depicts the heat release profiles for 25 % of engine load at 950 and 1800 rpm for the different sensitivities, considering the RON 80 fuel. As it can be seen, the RON modification influences the sensitivity manifestation at low engine load compared to RON 92.5. The first noticeable change experienced is the lower discrepancies among the sensitivities evaluated. This implies that, in some manner, the increase of fuel reactivity allows to avoid conditions affected by the NTC. Higher engine speeds provide slight differences in the HRR profiles which could be attributed to differences at the IVC conditions. In spite of the last statement, it can be concluded that the decrease of the RON tends to reduce the differences for the different sensitivities, considering the pressure-temperature trajectories obtained for low load conditions.

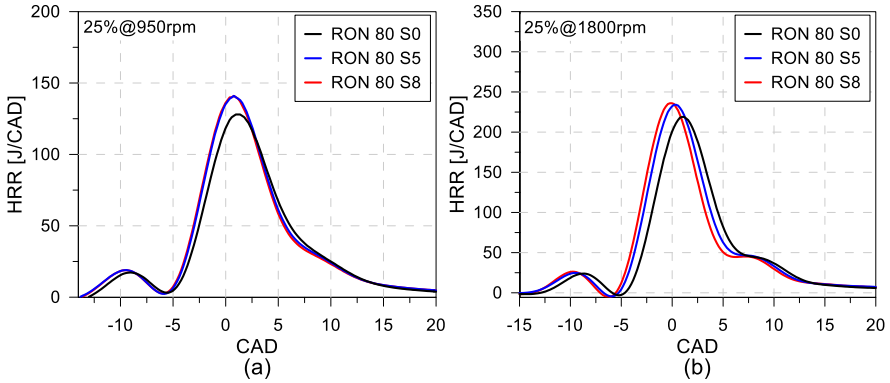

Figure 6.17. Experimental heat release rates for (a) 25 %@950 rpm and (b) 25 %@1800 rpm for RON 80 and different sensitivities.

By contrast, full load conditions seem to be highly affected by the sensitivity in low RON conditions, indicating a reactivity decreases for higher sensitivities. This behavior is pursued at high low conditions, where the combustion improvement is limited due to the mechanical constraints. It should be recalled that compositional, temperature and RON stratification play a fundamental role on the combustion development at these conditions. Therefore, deeper investigations should be pursued to identify what should be the most significant differences that are found for each one of the RONs evaluated. To do this, a 3-D description should be employed to capture the important phenomena that occurs simultaneously, like flow movement, spray vaporization, mixture preparation, etc. This analysis is out of the scope of the present work, but its importance is remarked being a suggestion for future investigations.

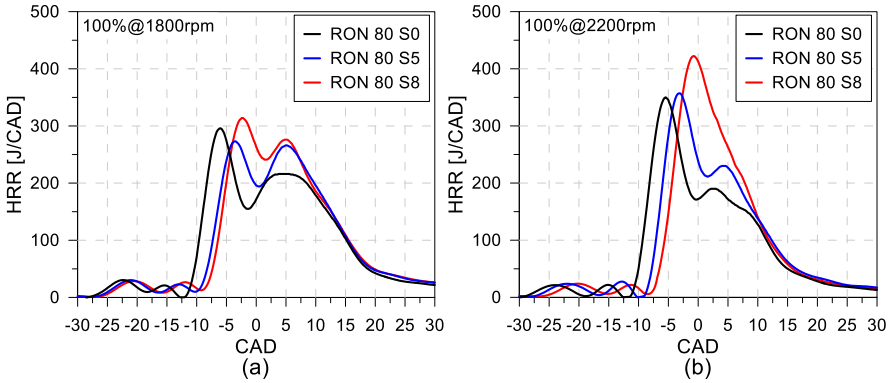

Figure 6.18. Experimental heat release rates for (a) 100 %@1800 rpm and (b) 100 %@2200 rpm for RON 80 and different sensitivities.

6.2.2.4. Performance and emissions results

Finally, the impact of the sensitivity variation on the performance and emissions values is evaluated for three different operating conditions, representing different combustion modes that are found in the DMDF concept. The results for RON 92.5 are presented first, followed by the RON 80 ones. Figure 6.19 depicts the equivalent fuel consumption results for the set of operating conditions (25 %@950 rpm, 50 %@1800 rpm and 100 %@2200 rpm) and sensitivities evaluated (S=0, S=5 and S=9). It should be remarked that the equivalent basis is herein used for the fuel consumption since fuels with different sensitivities differ in terms of lower heating value, e.g., toluene has a lower LHV than n-heptane and iso-octane. It can be evidenced that low load operating conditions present low variation in terms of fuel consumption for sensitivities up to five, which is in accordance with the combustion results presented in the HRR analysis.

Nonetheless, the increase of the sensitivity to nine delays the combustion process, enlarging its duration, which increases the fuel consumption due to heat losses and work transfer. As the engine load is increased to 50 %, even small variations on sensitivity are negative for the fuel conversion efficiency. At these conditions, the sensitivity effect should be

evidenced, since the LRF fuel stands for more than 85 % of the total energy released during the combustion. The previous discussions suggested that this operating condition provides state and chemical conditions which result in a degraded combustion process as the sensitivity is increased. Therefore, the fuel consumption values are consistently increased as the sensitivity increases. Lastly, full load operation is much less impacted by the fuel sensitivity variation for PRF 92.5. From the HRR analysis it was observed that neither the combustion starts, nor its end were affected by the sensitivity variation. Some differences were noticed in the HRR distribution, i.e., the burning process, which modifies the CA50 position. Nonetheless, as depicted in Figure 6.19 (c), the impact on the fuel consumption values is minimal.

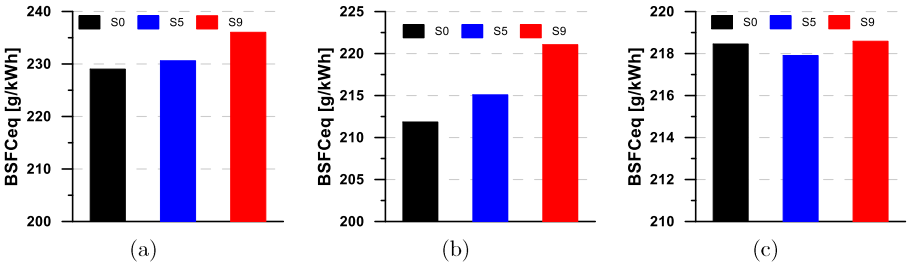

Figure 6.19. Equivalent brake specific fuel consumption for the different sensitivities evaluated at (a) 25 %@950 rpm, (b)50 %@1800 rpm and (c) 100 %@2200 rpm operating with RON 92.5

Following the results discussion, Figure 6.20 illustrates the impact of the sensitivity variation on the NOx and soot emissions for the different operating conditions evaluated. It is easy to evidence that the soot emissions for both 25 % and 50 % of engine load are not affected by the sensitivity modification. These operating conditions are based on fully premixed strategies, which inhibit the soot formation. In this sense, modifications of temperature and combustion duration, which are the main effects of the sensitivity will not impact the engine-out soot values at these conditions. Only the full load operation delivers significant soot emissions. S=0 provides the highest soot levels among the sensitivities evaluated. Nonetheless, considering that the injection characteristics and air management system are

similar, the soot production itself should not be highly impacted by the sensitivity modification. The dispersion evidenced in the figure may be related to the differences in the combustion development, which can modify the maximum temperatures inside the cylinder, impairing the soot oxidation process. Regarding the NOx results presented at the same graph, it can be implied that higher temperatures should be achieved for both S=5 and S=9. Sticking to this assumption should mean that the observed soot reduction in these sensitivities is a direct consequence of the better oxidation in the last part of the combustion process.

In addition, both operating conditions of 25 % (Figure 6.20 (a)) and 50 % load (Figure 6.20 (b)) fulfill EUVI NOx constraints. It is interesting to note that the variation of this emission follows closely that observed at the HRR results. At 25 %, S=5 demonstrated to be the more advanced combustion process, which should deliver the highest in-cylinder temperature and consequently, highest NOx emissions as evidenced Figure 6.20 (a). By contrast, 50 %@1800 rpm depicted a delayed combustion as the sensitivity was increased, which should also decrease the in-cylinder temperature profiles. This inhibits the Zeldovich's mechanism, reducing the engine-out emissions.

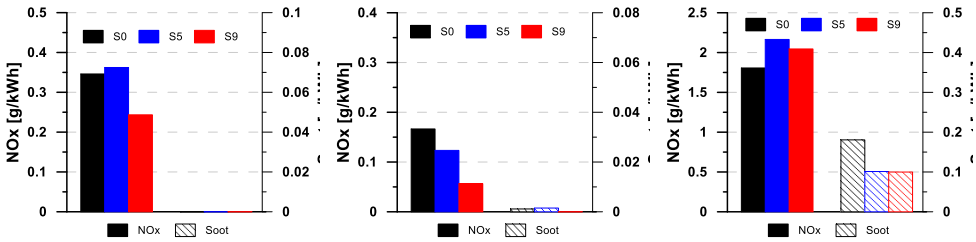

Figure 6.20. Brake specific nitrogen oxides and soot emissions for the different sensitivities evaluated at (a) 25 %@950 rpm, (b)50 %@1800 rpm and (c) 100 %@2200 rpm operating with RON 92.5

Figure 6.21 presents the influence of the sensitivity variation for RON 92.5 on the unburned products: HC and CO. As it was stated in previous

discussions, the high values of these components are a significant drawback of low temperature combustion processes, being a challenge for the aftertreatment system once they are combined with the low exhaust temperatures of the DMDF concept. The analysis of Figure 6.21 (a) allows to conclude that the use of S=5 at low load conditions provides the lowest unburned hydrocarbon emissions. Despite, the values are still high since the formation mechanism of this contaminant is more dependent on geometrical effects and quenching phenomena that cannot be significantly improved by the reactivity variation, as demonstrated in subsection 6.1.1.1. By contrast, the combustion deterioration impairs the fuel oxidation, providing a significant increase in both HC and CO for S=9 compared to S=5. The same conclusion can be extended to Figure 6.21 (b) which present the results for 50 % of engine load. As it is shown, the only difference with 25 % of engine load is that none of the sensitivities are beneficial to the combustion process. In this regard, both HC and CO are significantly increased, independently on the sensitivity evaluated. This can be an additional justification for the higher fuel consumption values presented in Figure 6.19, as a significant part of the fuels remains unburned. Lastly, Figure 6.21 (c) depicts the results for full load operation. HC emissions are minimized at this operating condition because it relies on a diffusive combustion process with low gasoline fractions, implying less fuel to be forwarded to piston gaps and crevices during the compression stroke. In general, both CO and HC are not affected by the sensitivity variation. Specifically, only HC emission for S=9 is impaired because of delayed combustion process compared to the remaining conditions.

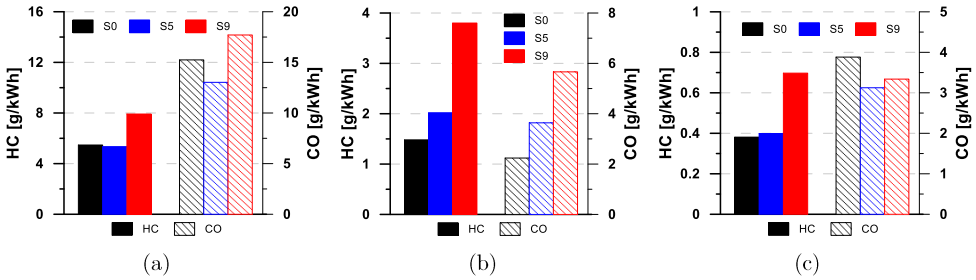

Figure 6.21. Brake specific unburned hydrocarbon and carbon monoxide emissions for the different sensitivities evaluated at (a) 25 %@950 rpm, (b) 50 %@1800 rpm and (c) 100 %@2200 rpm operating with RON 92.5.

From this thorough analysis, it can be concluded that the use of sensitivities up to 5 points seems to be beneficial in most of the operating conditions, allowing to improve fuel consumption while maintaining or even reducing the most critical pollutants. This conclusion reinforces those obtained during the combustion analysis, suggesting that the best fuel to be used in the DMDF combustion concept, considering the current engine hardware should be very similar to commercial gasoline.

The modification of the engine hardware or the inclusion of electric-based devices as an EGR-Pump and e-turbo can enable different scenarios in terms of fuel usage. A possible alternative would be the introduction of low RON fuels, aiming to use cheaper fuels which could benefit the consumer. In this sense, the sensitivity impact was also evaluated at RON 80 to understand the manifestation of the chemical effects on the DMDF combustion at the same operating conditions that were discussed for PRF 92.5.

The effect of the fuel sensitivity variation on the fuel consumption for the different operating conditions can be observed in Figure 6.22. As it is shown, there is no specific trend with respect to the sensitivity for both 25 % and 50 % of engine load. While the increase of the sensitivity from 0 to 5 slightly impairs the fuel consumption, the further sensitivity increase provides lower fuel consumption than those from S=5. Despite the variation, the previous analysis of the HRR profiles demonstrated that the combustion

process for each sensitivity is not strongly affected by the fuel sensitivity modification which is contradictory to the $BSFC_{eq}$ results. However, it should be remarked that the $BSFC_{eq}$ variations are as high as 2.2 % for these two operating conditions which can be attributed to uncertainties during the measurement process. Additional effects, like combustion efficiency variation could be also a source of brake fuel consumption variation and it will be discussed in the HC and CO results that follow. Differently from the low and medium load operating conditions, full load operation demonstrated to be improved in terms of fuel consumption as the sensitivity is increased. As it is presented in Figure 6.22 (c), the increase from S=0 to S=5 and the subsequent sensitivity step allows to decrease the fuel consumption values which is in consonance with the observations made in the HRR analysis for these conditions. Once the sensitivity was increased, the reactivity modification allowed to obtain more volumetric combustion processes, i.e., with shorter combustion duration, reducing the losses by heat transfer.

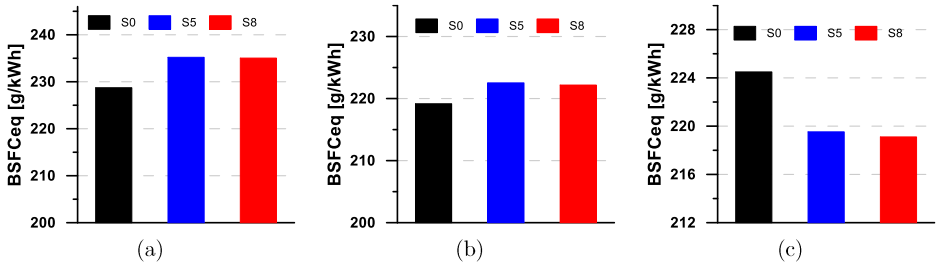

Figure 6.22. Equivalent brake specific fuel consumption for the different sensitivities evaluated at (a) 25 %@950 rpm, (b) 50 %@1800 rpm and (c) 100 %@2200 rpm operating with RON 80.

Figure 6.23 depicts the sensitivity effect in terms of NOx and soot emissions for the different operating conditions evaluated. It can be noted that soot values are not highly impacted considering the low RON fuel. Low and medium load conditions can mitigate or produce ultra-low soot levels due to the high premixing degree. Even full load operating conditions proved to not be highly affected by the sensitivity, presenting small decreases on the total engine-out soot for S=5 and S=8 which can be attributed to the higher

ignition delay and consequent higher mixing time of these mixtures. By contrast, NOx emissions can be divided in two groups: low and full load operating conditions and medium load. The first group has as similarity the low influence of the sensitivity on the NOx emissions, even with modification on the combustion process as in the case of full load operation. In this specific case, it can be suggested that a trade-off between maximum temperature and residence time coexist: the higher temperatures obtained due to the more volumetric heat release are balanced by the lower combustion duration, providing similar engine-out NOx, independently of the fuel evaluated. However, medium load operating conditions present an opposite behavior, having twice more NOx emissions when S=8 and S=0 are compared. Despite not having neither significant boundary condition modifications nor huge differences in the combustion process, it sems that the mixture reactivity and the small steeply increase on the combustion duration are critical for the NOx production at this specific operating condition.

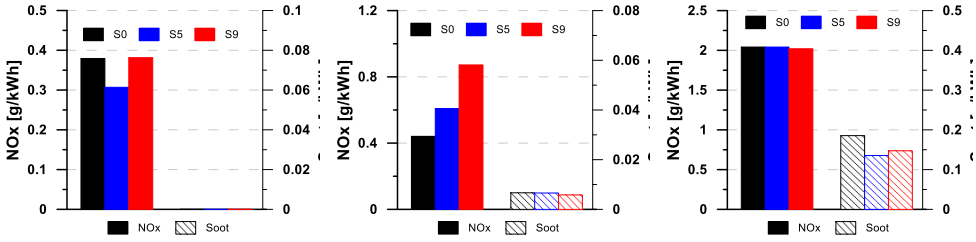

Figure 6.23. Brake specific nitrogen oxides and soot emissions for the different sensitivities evaluated at (a) 25 %@950 rpm (b) 50 %@1800 rpm and (c) 100 %@2200 rpm operating with RON 80.

Finally, the unburned productions (HC and CO) are presented in Figure 6.24 with respect to the set of operating conditions evaluated (sensitivity and engine points). While CO emissions present similar values, independently on the operating condition and sensitivity, unburned hydrocarbons are more affected, mainly at 50 % and 100 % of engine load. The mechanisms behind the variations at 50 % of engine load are not fully understood yet, since there is no evidence on the heat release rates or from

the boundary conditions that could justify this. On the other hand, the increase of HC emissions at 100% of engine load seems to be a direct consequence of the delayed combustion process that is rendered as the sensitivity increases.

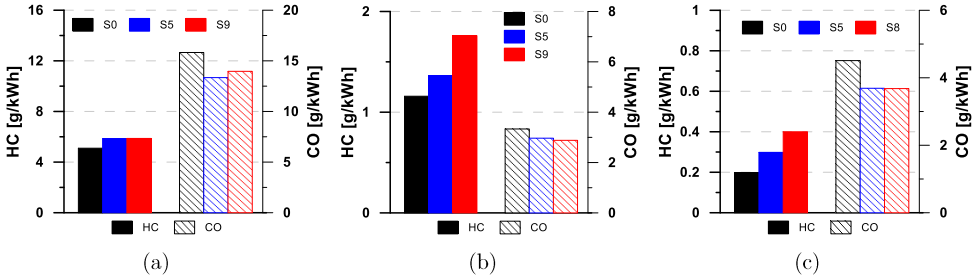

Figure 6.24. Brake specific unburned hydrocarbon and carbon monoxide emissions for the different sensitivities evaluated at (a) 25 %@950 rpm (b)50 %@1800 rpm and (c) 100%@2200 rpm operating with RON 80.

6.2.3. Summary

This subsection has aimed to identify the best low reactivity fuel characteristics in terms of research and motor octane number to be used in the DMDF combustion concept. First, octane numbers ranging from 100 to 80 were evaluated by means of steady-state conditions, followed by an equivalent driving cycle and a merit function approach. These evaluations allowed to conclude that RONs from 87.5 to 93 presents the best trade-off of performance and emissions, being the optimum range for the concept. The use of low RON fuels was restricted by increased pressure gradients, requiring significant modifications of the injection and air management settings, generally impairing the conversion efficiency. By contrast, high RON fuels do not perform well at low load conditions due to the lack of energy to achieve a proper oxidation. In this sense, the intermediate RON range was the one which presented the best trade-off between the drawbacks and benefits achieved by their modification.

Finally, the effect of the sensitivity variation was evaluated for both PRF 92.5 (in the optimum range) and PRF 80 (short-term future fuel) by means of experimental evaluation aided by numerical Kinects calculations. The results analysis has demonstrated that the introduction of moderate levels of sensitivity can be beneficial depending on the engine load in discussion. While low load conditions are slightly impaired by the sensitivity introduction, high load operation can be optimized, achieving better fuel consumption while maintaining similar emission levels.

It should be remarked that the suggested optimum fuel for the concept delivers characteristics like those from commercial gasoline (RON 95 and S≈7). The introduction of a new drop-in fuel with a RON standard three points lower than the commercial gasoline is difficult to defend given the small benefits. Even with an extensive RON variation, fuel consumption was just slightly improved with non-significant variation on the relevant emissions. In this sense, alternatives should be pursued to accomplish the required reductions of CO_2 and engine-out emissions. Although the LRF options were not effective, HRF modifications may provide better results. The reduction of the soot formation by the high reactivity fuel should provide an additional degree of freedom to optimize the air management system, reducing the pumping losses and increasing the efficiency. This could also enhance the combustion process as the use of highly advanced combustion to suppress the soot formation could be avoided. Once the direct combustion improvement has shown to not deliver significant CO_2 reductions, a well to wheel approach is proposed. In this context, the pursue of e-fuels or renewable fuels could be a path to achieve a lower CO_2 footprint. In this sense, the next section describes an extensive evaluation of potential high reactivity fuels by means of steady-state evaluation, well to wheel analysis and driving cycle approach.

6.3 Advanced high reactivity fuels: path to reduce emissions and CO_2 footprint

The introduction of a high reactivity fuel by means of direct injection in a pre-conditioned mixture field originates rich mixture zones. One of the main side effects of these regions is the soot production by the agglomeration of not fully oxidized carbon. From the previous chapters, it was clear that this was a critical point found during the implementation of the DMDF concept using diesel and gasoline. As the load is increased towards full load, both soot and NOx emissions must be relaxed to achieve the same power output than the original CDC calibration.

On the other hand, the outlook regarding CO_2 reductions seems to be challenging. The targets of 15 % (2025) and 30 % (2030) represents a disruptive point in terms of CO_2 improvements, which were not obtained with the DMDF calibration. As it is well known, this parameter has a direct link with the fuel consumption. Therefore, to reduce the fuel consumption to fulfil with the EU legislation is a hard task. Despite of not being currently considered in the normative, the introduction of the well-to-wheel CO_2 analysis offers a feasible solution to achieve the future targets and obtain cleaner vehicles. Both the usage of biofuels and e-fuels on wide scale application are possible means to achieve this. The biofuels claim relies on the assumption that most of the CO_2 released during the combustion process can be absorbed by the raw material during its photosynthesis process releasing glycoses, water, and oxygen [15]. Some examples of widely used biofuels are hydrogenated vegetable oils, biodiesel, and ethanol. E-fuels can also deliver CO_2 savings during its lifecycle because they use this pollutant as raw material during the methanol synthesis step and consumes energy from renewable sources during their production process [16][17]. Nonetheless, the CO_2 saving potential is highly dependent on the energy source that is used during the process, as it demands energy intensive steps as water electrolysis, etc.[18].

The use of fuels that can deliver low soot tendency and CO_2 savings at the same time should be a pathway to realize improvements on the DMDF concept. Among the different fuels that fulfill these characteristics, e-Fischer Tropsch (e-FT) and OMEx are two promising options which have been demonstrating the capability to reduce the soot emissions in conventional diesel combustion [19][20][21]. E-Fischer Tropsch also known as e-diesel has similar combustion characteristics to conventional diesel in which regards lower heating value, cetane number and the remaining transport properties. The main difference relies on the absence of aromatic compounds in its structure which is pointed in literature as the main reason for the decrease of soot emissions [22]. E-FT is already produced in large scale for diesel engines. Its production process relies on the use of CO and H_2 to produce polymeric hydrocarbons trough sequential hydrogenation of CO [23]. Hydrogen can be obtained from both renewable feedstocks or from water electrolysis while CO may be produced from the reverse water-gas shift (RWGS) of CO_2 [24]. Any of these paths can deliver substantial CO_2 savings.

OMEx presents considerable differences with respect to diesel in which regards combustion and transport properties. Moreover, its molecular structure does not contain carbon-carbon bonds and it presents an oxygen concentration that surpasses 40 % in mass basis [25]. This reduces by almost half the stoichiometric air-fuel ratio, meaning that less air is required to oxidize completely the fuel. Nonetheless, this lower carbon content reduces the lower heating value, requiring more fuel to maintain the same energy output. OMEx has been recently introduced as an alternative fuel. Therefore, its benefits and challenges are still unclear, even for conventional applications. Its production process relies on the reduction of CO_2 by using H_2 originated compounds as methanol [26]. The following reaction of methanol produces a wide range of carbon chain compounds called OMEx. Since the production process consumes CO_2, it can also contribute to the CO_2 balance [27].

In this sense, this subsection intends to evaluate the potential of both e-FT and OMEx as alternative fuels for the DMDF combustion concept by

means of experimental and numerical evaluation. First, a comprehensive investigation is performed in representative operating conditions of the DMDF concept aiming to understand the impact of the fuel characteristics on the combustion, performance, and emission parameters. Next, well-to-wheel analysis tools are employed to determine the potential CO_2 savings of e-FT and OMEx considering different sources and energy matrix compared to conventional diesel and gasoline. From these results, the most promising fuel considering the trade-off between soot and CO_2 reduction is selected and used to recalibrate the whole engine map having commercial gasoline as LRF. The final maps are then introduced as boundary conditions to perform a driving cycle evaluation similar to the one from chapter 4, allowing to compare the benefits and drawbacks of the new calibration compared to the D-G one.

6.3.1. Potential of e-FT and Oxymethil ester (OMEx) as high reactivity fuels for DMDF combustion

This section intends to assess the impact of using both OMEx and e-FT as high reactivity fuels in the DMDF concept through different perspectives. First, the combustion and performance results are evaluated in an equivalent basis. Thereafter, the emissions results are compared aiming at improvements in soot emissions. Finally, a well-to-wheel analysis is performed to quantify the benefits of using e-fuels in terms of CO_2 reduction.

6.3.1.1. Methodology

The engine speed range from 1800 to 2000 rpm has demonstrated to be a challenging condition during the analysis of the diesel gasoline calibration maps. The high load conditions presented excessive values of both soot and NOx. Moreover, the distribution graphs from the driving cycle analysis pointed out that the maximum values of these emissions are found near to the 1800 rpm, confirming that these conditions are frequently used during the driving cycle. Therefore, this part of the study was focused on engine

speeds from 1800 and 2000 rpm. The aim was to evaluate the potential benefits of using fuels with low soot formation potential in the DMDF concept. Diesel, e-FT and OMEx were evaluated at four different engine loads: 25 %, 50 %, 80 % and 100 %. In all cases, gasoline was chosen as LRF.

Each operating condition was optimized following the methodology proposed for the calibration process. They can be directly compared because both have as basis their optimized values of BSFC under the same constraints. It is worth to state that the BSFC comparison was done on an equivalent basis, i.e., the fuel mass was corrected according the LHV difference of each fuel as previously discussed. Equation 6.4 is herein presented to recall the definition of the equivalent brake specific fuel consumption.

$$BSFC_{eq}[g/kWh] = \frac{\dot{m}_{HRF} \cdot \left(\frac{LHV_{HRF}}{LHV_{diesel}}\right) + \dot{m}_{LRF} \cdot \left(\frac{LHV_{LRF}}{LHV_{gasoline}}\right)}{P_b} \qquad 6.4$$

Table 6.12 provides some of the chemical and physical characteristics of the different fuels that were used during this part of the investigation. As it can be seen, both e-FT and diesel have similar characteristics except for the cetane number that is more than 35 % higher for e-FT. By contrast, OMEx differs from diesel in every single property. The most challenging differences are the low LHV which implies excessive energizing times of the injection and the low viscosity which can be a hurdle to the high-pressure fuel injection system (FIS).

Table 6.12 Properties of the different fuels used in the evaluation of the best high reactivity fuel for the DMDF concept.

	Gasoline	Diesel	e-FT	OMEx
Density [kg/m^3] (T=15 °C)	720	842	832	1067
Viscosity [mm^2/s] (T=40°C)	0.545	2.929	3.25	1.18
Cetane number [-]	-	55.7	75.5	72.9
Carbon content [% m/m]	-	86.2	85.7	43.6
Hydrogen content [% m/m]	-	13.8	14.3	8.82
Oxygen content [% m/m]	-	0	0	47.1
RON [-]	95.6	-	-	-
MON [-]	85.7	-	-	-
Lower heating value [MJ/kg]	42.4	42.44	44.2	19.04

6.3.1.2. Effect of the high reactivity fuels on combustion parameters

The effect of the high reactivity fuel properties on the combustion process is presented in this subsection. The heat release profiles are presented together with some of the relevant metrics of the combustion process: CA50 (50 % of mass fraction burned) and CA90-CA10 (combustion duration). This allows to depict the differences for each fuel for the set of operating conditions evaluated.

Figure 6.25 presents the results obtained for the operating condition of 25 %@1800 rpm. The injection strategy employed for each one of the fuels is presented at the top of the Figure 6.25 (a). As it can be seen, the injections were not maintained at the same location for all the mixtures, since this would result in an early combustion process and high BSFC values. Yet, OMEx and diesel allowed to use similar injection timings. The main difference was the increase of the injection dwell between the pilot and main injection for the case of the OMEx, since the lower LHV results in higher injection durations. The comparison between them allows to visualize the effect of the

OMEx high cetane number which results in early ignition start and more abrupt heat release rate. This is also noted in the low temperature heat release. The lower reactivity of the diesel increases the ignition delay compared to the remaining blends, shifting the combustion process towards the expansion stroke, taking place in a low pressure and temperature environment. This results in a delayed combustion with slightly increase in its duration.

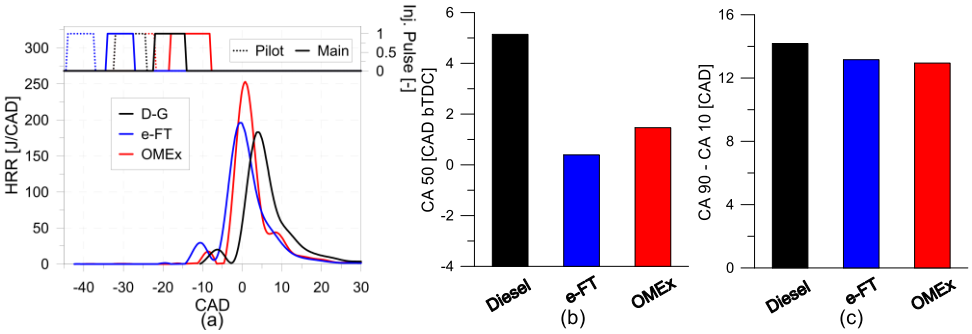

Figure 6.25. Representation of (a) rate of heat release profiles as well as energizing times (b) center of combustion (c) combustion duration for the three high reactivity fuels evaluated at 25 % of engine load and 1800 rpm.

The use of e-FT as high reactivity fuel requires some modifications in the injection strategy since it has the highest cetane number among the fuels evaluated. Consequently, the use of a similar injection strategy would result in an early mixture ignition. In this sense, the injections were advanced to introduce the high reactivity fuel in the compression stroke (low temperatures and pressures), enhancing the premixing of the fuel and increasing its ignition delay due to the inhibition of local high reactivity zones (low RON). This allowed to move the combustion process closer to the previous fuels, achieving improvements in fuel consumption. The EGR levels were maintained at 38 %, 42 % and 42.5 % for diesel, e-FT and OME, respectively. Further increase of these values impairs the soot oxidation, since it means a direct replacement of the fresh air by exhaust gases. It is also possible to evidence that there is a high dependence of the CA50 values with respect to the mixture cetane

number, demonstrating that an advanced combustion process is achieved as the cetane number is increased. By contrast, the combustion duration values are not significantly affected by the fuel composition as the three high reactivity fuels provided similar results, with slightly increases for diesel.

As the engine load is increased to 50 %, the differences among the combustion processes become smaller. This is a direct consequence of the high GF levels used at this operating condition, exceeding 70 % independently on the fuel evaluated. Despite this, a remarking difference can be perceived in the OMEx rate of heat release. The higher OMEx mass decreases the GF, increasing the global reactivity of the mixture. This provides a fast heat release rate as it can be seen in Figure 6.26. It is also interesting to note that the injection strategy could be maintained almost equal for the different fuels. The main modification regards the OMEx where the injection start was advanced to accommodates the higher amount of fuel injected. Nonetheless, the injection end is like those from the e-FT and diesel providing similar combustion start. Both combustion phase and duration are similar among the fuels with maximum deviations with respect to the average of 1.3 CAD for the CA50 and 1.5 CAD in the combustion duration.

The next operating condition evaluated addresses the engine load of 80 %. This condition is characterized by lower GF values than the previous operating condition (50 % of engine load) with one HRF injection close to the TDC firing. Therefore, the energy delivered by the HRF becomes more relevant. As it can be seen in Figure 6.27, the low temperature heat release start before the diesel injection, demonstrating that most of the diesel is injected in a zone in which oxidation reactions are already occurring .

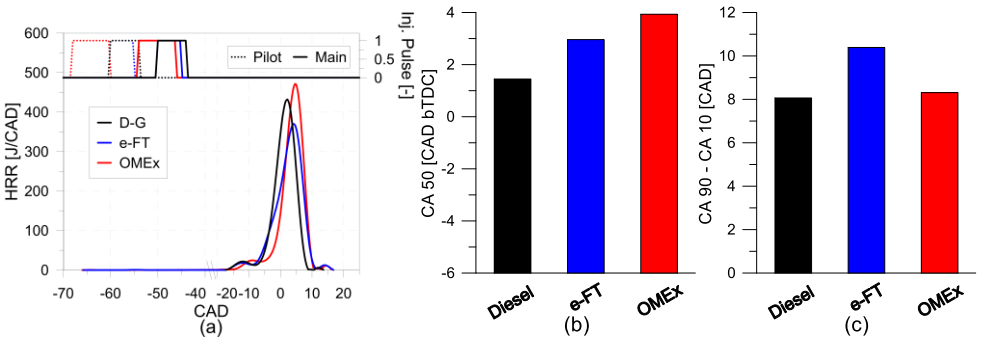

Figure 6.26. Representation of (a) rate of heat release profiles as well as energizing times (b) center of combustion (c) combustion duration for the three high reactivity fuels evaluated at 50 % of engine load and 1800 rpm.

Once the diesel is injected, the high temperature heat releases appears in a short CAD interval (≈4 CAD for all mixtures). This ignition delay is slightly impacted by the cetane number (≈1.5 CAD), where e-FT presents the shorter ignition delay while diesel presents the larger one (see Figure 6.27 (a)). This shorter ignition delay impacts the total combustion duration for e-FT, being higher than the others. It is also possible to conclude that e-FT and diesel have a similar combustion development. Nonetheless, the same cannot be extended to OMEx as its use results in a significant energy release after the top dead center due to the lower LHV of this fuel.

Finally, the results of full load operation are depicted in Figure 6.28. The conclusions drawn regarding the early phases of the combustion process for the previous condition can also be stated here. The main difference involves the high temperature heat releases. While diesel and e-FT present a similar combustion development, OMEx combustion is decoupled from the others from the TDC. This is justified by the amount of energy that can be delivered by the mass fuel injected/CAD. Once the injection system and configurations (injection pressure) is the same for all fuels, the injector delivery rate for OMEx should not present significant variations.

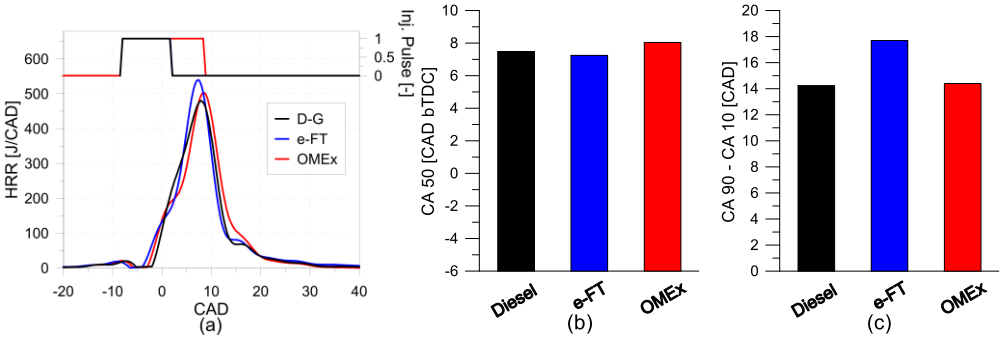

Figure 6.27. Representation of (a) rate of heat release profiles as well as energizing times (b) center of combustion (c) combustion duration for the three high reactivity fuels evaluated at 80 % of engine load and 1800 rpm.

The energy delivered for each crank angle is lower, reaching lower HRR peaks. In addition, the time to deliver the same amount of energy considerably increases, i.e., almost 20 CAD more than diesel and e-FT. It is also possible to see that the energizing time is maintained during 10 CAD more compared to the other fuels with a total time almost twice greater than diesel. This combustion enlargement can be also verified in Figure 6.28 (b) also impacting the center of the combustion process that is shifted towards the expansion stroke.

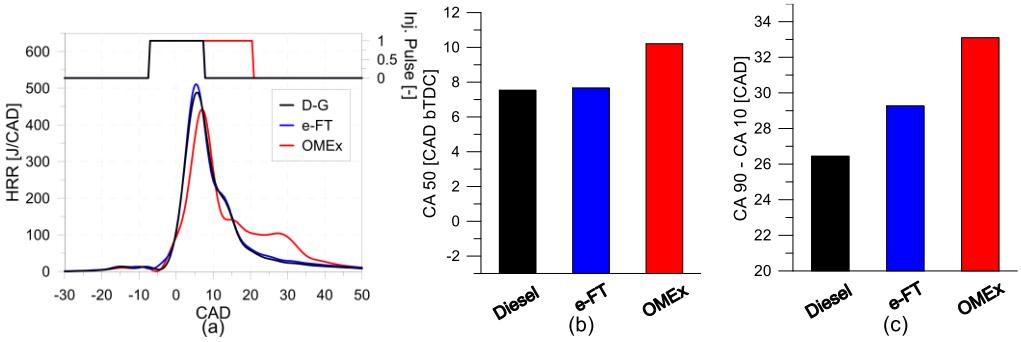

Figure 6.28. Representation of (a) rate of heat release profiles as well as energizing times (b) center of combustion (c) combustion duration for the three high reactivity fuels evaluated at 100 % of engine load and 1800 rpm.

6.3.1.3. OMEx and e-FT effect on performance and emission results: comparison with diesel

The combustion process variation with respect to the different HRFs should impacts the fuel consumption as well as the emission parameters of the engine. In addition, each fuel has peculiar characteristics that should provide unique results in terms of soot emissions, allowing to obtain different outputs than those from the diesel-gasoline combustion for the remaining emissions. In this sense, this subsection presents the impact of the fuel modification on the performance and emission results.

Figure 4.2 presents the values of equivalent fuel consumption for the different loads and fuels evaluated. This is a mean to evaluate the engine performance on a similar energy basis. As it can be seen, the fuels present different behaviors depending on the engine load. At low load conditions, e-FT provides the better equivalent fuel consumption. This can be attributed to the fast combustion process and slightly early combustion phasing due to its higher cetane number. OMEx demonstrates to have the higher fuel consumption. Despite of having similar combustion duration, a considerable amount of energy is released before the TDC, in higher volumes, resulting in a decrease of work delivery. As the engine load is increased to 50 %, the trend is inverted. OMEx provides the lower fuel consumption since it has the advantage of low soot combustion. Therefore, the combustion can be phased in its optimum point, without exceeding the limits imposed for the calibration (soot<0.01 g/kWh). At this condition, both e-FT and diesel are limited by the soot production, requiring early combustion to enhance the soot oxidation.

As the engine load is increased towards full load operation (80 % and 100% of engine load), the OMEx usage starts to present drawbacks in terms of equivalent fuel consumption. As it was previously discussed, the larger energizing times increase the combustion duration, resulting in higher heat transfer intervals and lower work conversion. It could be argued that the use of injectors with higher hydraulic diameter could be an alternative to tackle

this issue. Nonetheless, literature results indicate that several phenomena as the mixing capability, could compensate the higher flow rates, yielding no direct benefit in terms of fuel consumption [28]. Both e-FT and diesel present similar results as a consequence of their similar combustion properties. The cetane difference seems to not affect the efficiency results at this condition. It is suggested that the high load operation with a single injection near to the top dead center reduces the ignition delay to scales lower than 2 CAD for both fuels, which decreases the significance of the cetane number on the early phases of the combustion process.

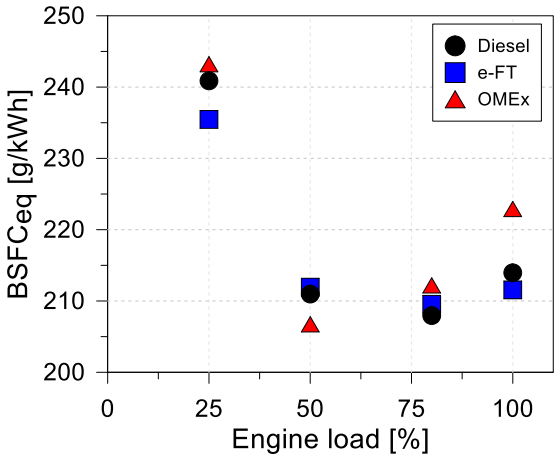

Figure 6.29. Equivalent brake specific fuel consumption with respect to the different engine loads evaluated considering diesel, OMEx and e-FT as high reactivity fuels.

The most significant differences for the engine-out emissions are verified for NOx and soot results. As it can be seen in Figure 6.30 (a) and Figure 6.30 (b), low and medium loads do not present significant variations in terms of both pollutants. Nonetheless, this scenario is not maintained for engine loads from 80 %. As it can be seen, even in the case of having relaxed soot constraints, it is difficult to obtain EUVI compliant NOx emissions for diesel and e-FT. By contrast, OMEx can delivers both NOx and soot under

normative constraints, even in the case of having a more diffusive combustion. It is suggested that this can be related to the high oxygen content in its molecule and the lack of direct carbon-carbon bond inhibiting the soot formation process. In this context, the EGR levels can be increased, reducing the available oxygen concentration while a proper soot oxidation can be still guaranteed. A similar behavior is verified at 100 % of engine load. The only difference regards the e-FT which provides lower values of NOx and soot compared to the diesel. This can be attributed to the absence of paraffinic compounds in this fuel, decreasing the soot formation potential as stressed in the introduction.

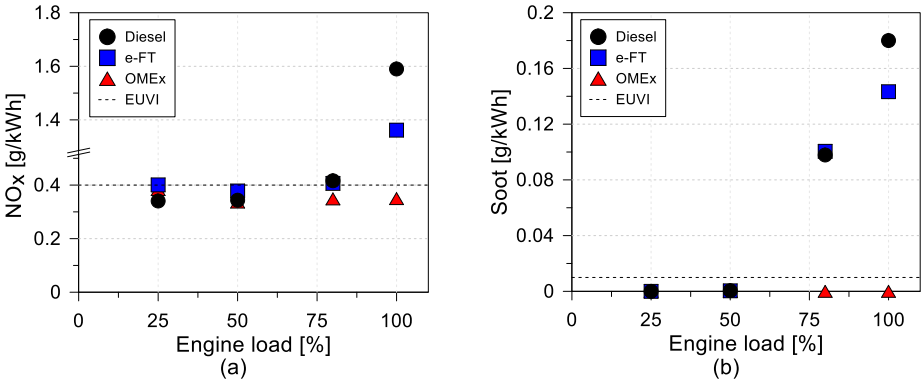

Figure 6.30. Dependence of (a) nitrogen oxides and (b) soot emissions with respect to the different engine loads evaluated considering diesel, OMEx and e-FT as high reactivity fuels.

Finally, the results of HC and CO emissions are presented in Figure 6.31. As it can be seen, both emissions are scaled according its cetane number at low load conditions, indicating that the HRF reactivity is a dominant factor on the combustion efficiency. The remaining loads presents similar values, independently on the high reactivity fuel evaluated. This means that the diesel substitution by e-FT or OMEx will not provide considerable differences on the DOC, compared with the original D-G calibration. Indeed, improvements in the conversion efficiency are expected for these

contaminants, because these fuels present lower engine-out values at critical conditions (low load) and have higher reactivity compared to diesel.

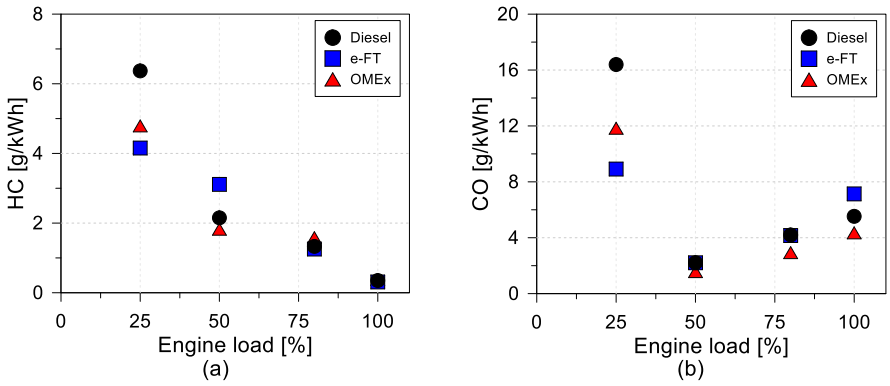

Figure 6.31. Dependence of (a) unburned hydrocarbons (b) carbon monoxide emissions with respect to the different engine loads evaluated considering diesel, OMEx and e-FT as high reactivity fuels.

This subsection allowed to conclude that the use of an alternative fuel can be a path to obtain a calibration map that delivers virtually zero soot while fulfilling the EUVI constraints for NOx. While e-FT was not able to drastically reduce the soot emissions at high load operation, OMEx enabled virtually zero soot emissions along the whole set of operating conditions evaluated. In this sense, it can be suggested that the aftertreatment system can be simplified, accounting only for a DOC and smaller DPF to clean the exhaust recirculated gases. The SCR subsystem can be removed, decreasing the vehicle cost and the subsequent operational costs from the urea consumption.

In spite of the promising emissions results, the efficiency results do not demonstrate any significant improvement compared to the diesel reference. Therefore, it is expected that the total CO_2 production in a tank to wheel basis should be similar to that of the diesel. It is suggested that including a well-to-wheel (WTW) basis should be the ultimate path to realize CO_2 benefits, which is a significant factor to be considered in choosing the high

reactivity fuel that suits best the concept. In this respect, the next subsection presents a detailed WTW analysis to account the benefits that can be obtained by using the advanced fuels herein proposed.

6.3.1.4. Well-to-wheel assessment for the different HRF

This subsection addresses the well-to-wheel analysis of the different fuels, considering some of the current renewable production paths. It provides an overview about the potential of using synthetic or renewable fuels in reducing the CO_2 impact on the environment, placing them as possible solutions to deal with the future normative constraints. This is a key factor on deciding the future fuels to be introduced in the market.

6.1.1.4 Well-to-tank analysis

The well-to-tank analysis requires a wide dataset addressing the different processes that are employed during the fuel manufacturing. The analysis relies on quantifying the representative emissions in the production, manufacture and distribution of a given fuel. Moreover, this analysis also considers the CO_2 emissions produced by the fuel production infrastructure. This is done by stablishing an expected lifetime for each production unit and distributing the associated costs along it. The values of well-to-tank CO_2 for the different fuels were obtained from previous publications using an LCA model developed on the software application GaBi®, licensed by thinkstep®. It comprehends several parameters associated to the fuel production chain as the type of water electrolysis, the electricity matrix, etc. Some of these parameters are presented in Table 5. More details about the calculation process can be found in García et al.[29].

The results of the well-to-tank analysis are depicted in Figure 6.32, which addresses the set of fuels used in the investigation as well as the energy sources used in the production process. As it is shown, the CO_2 values for OMEx, considering the photovoltaic power, are substantially higher

compared to the remaining evaluated cases. The solar panel manufacturing process still presents a high CO_2 footprint, which combined with the low OMEx LHV, becomes the most CO_2 expensive process. By contrast, the use of wind power can reach negative values for both OMEx and e-FT. This significant improvement is a consequence of considering that CO_2 is provided by means of direct air capture summed to the use of an ultra-low carbon intensity energy source. Moreover, e-FT seems to provide the best results in terms of CO_2 savings because its production process is simpler than the OMEx one, with less energy intensive process.

Table 6.13 description of the relevant production process accounted during the wheel to tank analysis.

Parameter	Value
CO_2 source for FT and methanol production	Direct air capture
H_2 source for FT and methanol production	Alkaline water electrolysis
Thermal energy source for all processes	Electricity
Electricity source for all processes	100 % Wind power or 100 % PV power
Methanol production process (for OMEx)	Direct production
Allocation basis for FT process products	Mass-based attributional allocation

It is interesting to note that both gasoline and diesel presents CO_2 values lower than those from OMEx produced from photovoltaic power. This can be attributed to the optimized production processes of these fuels. Moreover, low variations on the absolute values between them are verified being mainly a difference on the energy requirement during the pyrolysis and hydrotreating processes.

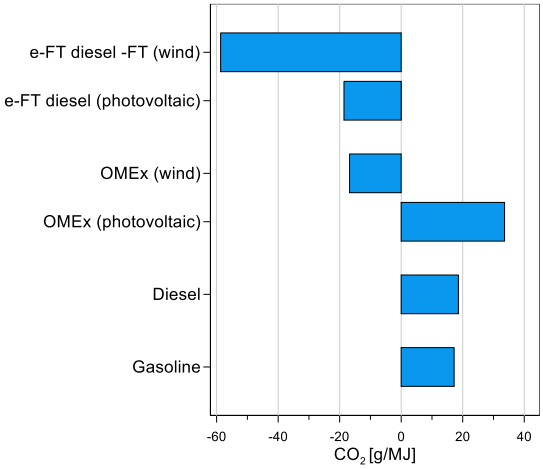

Figure 6.32. Well-to-tank analysis for diesel, gasoline, OMEx and e-FT considering different energy sources in the production process.

6.1.1.5 Tank-to-wheel

The second step addresses the quantification of the CO_2 produced during the conversion of the chemical energy of the fuel to work in the internal combustion engine. For this, each operating condition was evaluated in an isolated manner, to assess the impact of having different combustion process in the total CO_2 emitted. As both LRF and HRF are present in the DMDF concept, the total TTW CO_2 must be weighted by the mass of each fuel. This is accomplished by specifying the total CO_2 mass divided by the energy delivered by each fuel as presented in equation 6.4.

$$TTW\ CO_2 = \frac{BSCO_{2\_engine\ out} \cdot Pb}{\dot{m}_{HRF} \cdot LHV_{HRF} + \dot{m}_{LRF} \cdot LHV_{LRF}} \qquad 6.4$$

Figure 6.33 presents the values obtained for each one of the operating conditions. The higher difference is perceived at full load conditions, where OMEx has an increase of ≈20 % compared to the original D-G calibration. This is a direct consequence of the higher combustion durations with lower efficiency, that requires more fuel to achieve the same engine load. It can also

be inferred that the differences of the OMEx CO_2 are correlated with the GF. The values of GF for each operating condition are presented in Table 6.14. The differences for low and medium load conditions are under 22 % compared to the mean of the GF values. Nonetheless, as the load is increased towards full loads, this difference increases, reaching values higher than 40 % for full load operation. Despite having a negative impact on the TTW analysis, this can be beneficial when the WTT is considered.

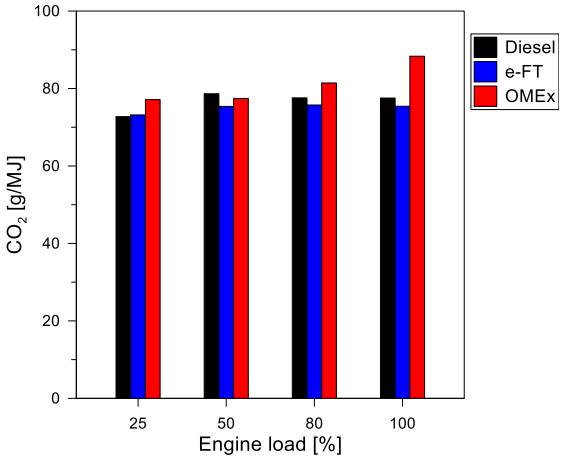

Figure 6.33. Tank to wheel analysis for diesel, gasoline, OMEx and e-FT considering the different operating conditions evaluated.

Table 6.14 Gasoline fraction values for the different fuels an operating conditions evaluated.

	25% load	50% load	80% load	100% load
Diesel	44.08	79.93	54.71	34.22
e-FT	55.70	89.02	53.87	36.91
OMEx	34.53	72.07	34.26	17.25

6.1.1.6 Well-to-wheel

Once both WTT and TTW values were determined, one can add them up and determine the global CO_2 impact on its lifecycle, i.e., the WTW results. Therefore, the results from TTW were combined with those from WTT considering the different sources to obtain both e-FT and OMEx. These results are illustrated in Figure 6.34. As it can be seen, the use of OMEx obtained from photovoltaic energy renders the worst scenario, presenting higher CO_2 values independently on the load evaluated. By contrast, the wind power source can provide benefits to both OMEx and e-FT. OMEx from wind power can provide a reduction of almost 20% in the total CO_2 emitted considering its production and usage paths while e-FT can deliver benefits higher than 50 % at full load conditions.

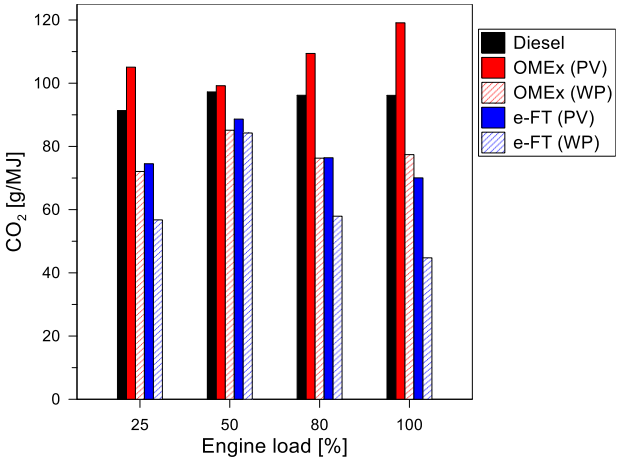

Figure 6.34. Well to wheel analysis considering the different energy sources for the fuel production and the set of operating conditions evaluated for diesel, gasoline, OMEx and e-FT.

6.3.1.5. Summary

From this previous analysis it is possible to conclude that both fuels tested (e-FT and OMEx) can improve the concept operation in terms of

emissions. While e-FT can slightly improve NOx and soot emissions at high load and maintain similar efficiency than diesel, OMEx fulfills normative restriction for these contaminants for the entire set of engine loads evaluated. By contrast, OMEx impairs the engine efficiency at high load conditions. The WTW analysis demonstrated that this efficiency increase can also impact the TTW results, considering the lower GF values employed for OMEx. Nonetheless in a WTW basis and considering wind power as the power source, both OMEx and e-FT can provide savings in the CO_2 production and consequent decrease of the CO_2 footprint in the fuel lifecycle. While OMEx can reach almost an average of 20 % reduction, e-FT is able to achieve an average reduction value of 35 %.

Nonetheless, it should bore in mind that the normative addresses the set of emissions (NOx, soot, HC, CO and CO_2) and therefore, the decision of the fuel should account all of them. In this sense, OMEx demonstrated the higher potential, since it can realize CO_2 savings while achieving virtually zero soot emissions fulfilling EUVI NOx constraints. It is clear that this analysis was based on four operating conditions and it cannot be assured that this potential can be extended to the whole engine operation. Therefore, the next section addresses this point by providing a new engine calibration considering the replacement of diesel by OMEx as high reactivity fuel. This will allow to compare both fuels at a global perspective by means of driving cycle results from the different performance and emissions parameters.

6.3.2. Full map calibration with OMEx

OMEx has demonstrated to be able to realize virtually zero soot emissions and EUVI NOx while maintaining similar efficiencies to those from diesel-gasoline calibration. In addition, it provided a significant reduction on the well to wheel CO_2 balance. However, these results were obtained for a fixed engine speed and four engine loads which can mask the overall performance of the fuel. Therefore, the investigation was extended to the whole engine operation map, aiming to obtain a calibration map following

the same procedure employed in chapter 4. This section presents the methodology employed during the calibration and the respective results of these evaluations in terms of performance, combustion, and emission parameters at different driving cycles. Finally, a driving cycle analysis is introduced allowing to compare the results of the new proposed calibration with those from chapter 4. It should be stated that the settings results are omitted as they are not the focus of this investigation.

6.3.2.1. Methodology

A similar methodology to the proposed for the calibration in chapter 4 was used to obtain the optimized calibration maps for OMEx-G combustion. However, there is a particularization that should be highlighted. As OMEx always yields zero soot emissions (from the AVL smoke meter response), the second part of the methodology section only addresses the cases where the operating condition fulfills NOx and soot or exceeds the first one. In this sense, the second stage of the calibration process can be simplified as presented in Figure 6.35. The other calibration stages remain the same in this chapter, being the first step an iterative routine to achieve the desired engine load, and the third step an optimization process to realize the best fuel consumption under the calibration constraints (see chapter 3).

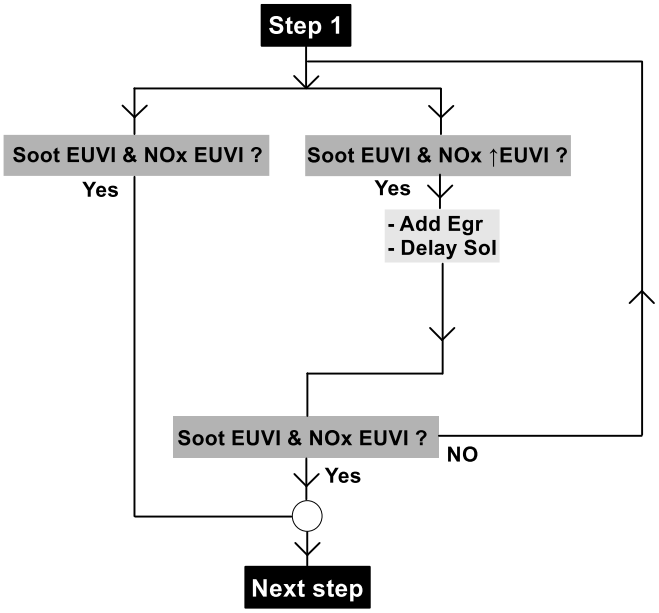

Figure 6.35. Step 2 of the calibration process for OMEx as high reactivity fuel.

6.3.2.2. Combustion results

The performance results of the calibration map in terms of brake efficiency are presented in Figure 6.36. As it is shown, the use of OMEx has allowed to increase the maximum brake efficiency up to 44 %. Its direct comparison with the previous D-G results allows to evidence important features from the OMEx calibration. The first noticeable change is the increase of the brake efficiency for most of the operating map. A few operating conditions were impaired by using OMEx and are located mainly at low engine speeds and full load operation. The latter was extensively discussed in the previous section, demonstrating that the significant increase on the injection durations and the extension of the combustion process towards the expansion stroke justify the brake efficiency decrease. Yet, the penalizations rarely surpass the 1 % level. On the other hand, the efficiency increase is far more significative, depicting a 2 % absolute improvement in a wider range of

the map. It is also interesting to remark that the conditions where the benefits are perceived may favor the concept concerning to its application on high payloads and velocities.

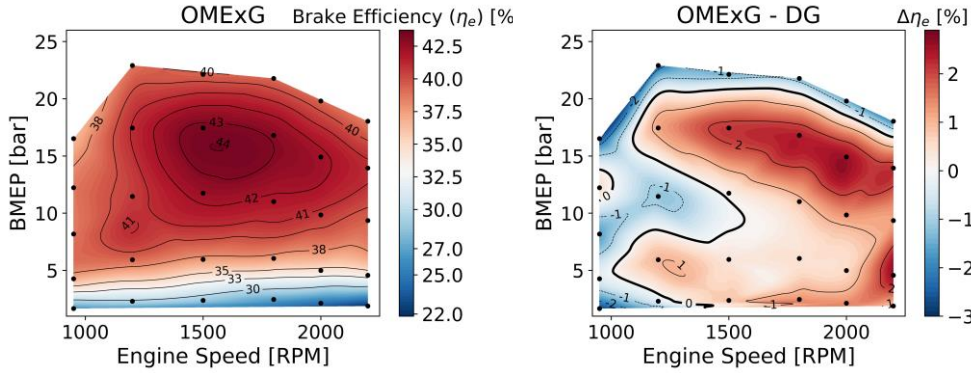

(a) (b)

Figure 6.36. Iso contour maps for (a) brake efficiency for OMEx-gasoline calibration and (b) its absolute difference with respect to the diesel gasoline calibration.

The question is how is it possible to have these improvements by employing an alternative low LHV fuel. To answer this, one should recall the most significant losses mechanism that coexists during the engine operation: combustion efficiency, pumping, heat transfer, friction, and combustion losses. From this set of mechanisms, it can be suggested that only friction losses should remain unaltered for both fuels since its governing parameters are maintained. Heat transfer losses are also omitted in the analysis. Thereafter, the remaining losses are directly compared with the previous calibration to identify the sources of improvements and penalizations.

Firstly, the combustion efficiency results are analyzed as an attempt to identify improvements that could deliver the enhancements of brake efficiency previously discussed. As it is shown in Figure 6.37, the proposed OMEx-G calibration delivers combustion efficiencies higher than 97 % for most of the operating map, indicating low amount of unburned products at the exhaust gases. The lowest values are found at those conditions where a

fully premixed combustion is used due to the amount of LRF that goes to the crevices during the compression stroke. Moreover, its comparison with the previous D-G calibration allows to conclude that, generally, both calibrations are able to deliver similar combustion efficiency results with differences lower than 1 % in most of the map except for high engine speeds at 25 % of engine load where the differences can be as high as 2 %. These variations go to the opposite direction of the brake efficiency results, suggesting that there should be an additional parameter that is able to compensate these losses of combustion efficiency and provide improvements on the conversion efficiency.

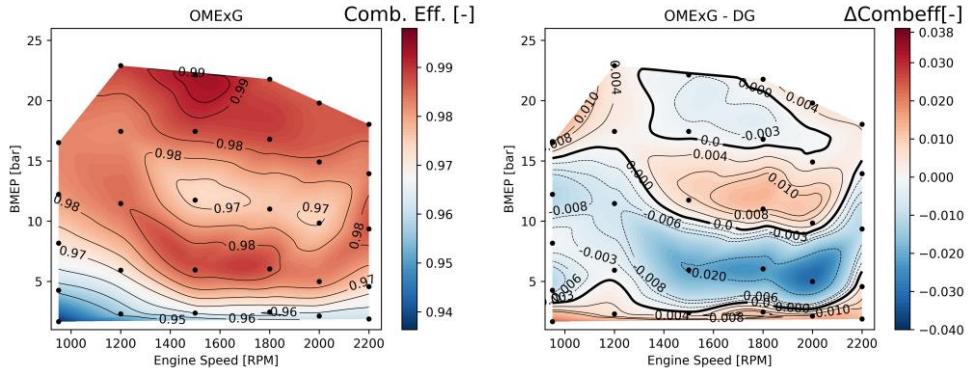

(a) (b)

Figure 6.37. Iso contour maps for (a) combustion efficiency for OMEx-gasoline calibration and (b) its absolute difference with respect to the diesel gasoline calibration.

The combustion process characterization is presented in both Figure 6.38 and Figure 6.39. The first figure presents the results for the combustion phasing, demonstrating that in general the CA50 values range from 2 to 8 CAD aTDC, which have been demonstrated in the literature to be good values for this combustion metric, depending on the combustion mode employed. Although this is an interesting result, the comparison with the reference D-G calibration allows to draw a more comprehensive scenario. As it is shown in Figure 6.38, two different behaviors can be evidenced. From

low to medium load conditions, the use of OMEx generally results on delayed combustion processes compared to the original calibration. This relies on the fact that the use of diesel as HRF required early combustion processes at low and medium load to mitigate the soot formation. In addition, the longer injection durations may increase the combustion duration, displacing the CA50 to different values than those of the original D-G calibration. Despite this, the differences at this load range are generally low, being as small as 2 CAD, except for isolated conditions.

From medium to high load operation, the high cetane number from OMEx becomes more relevant since the gasoline fractions are drastically reduced to accommodate the higher reactivity of the blend. Despite of an intuitive strategy, it should be remembered that this cannot be extended to both diesel and e-FT because the high soot tendency of this operating conditions would result in higher soot levels than the imposed constraints. Due to the lower gasoline fraction levels, the first part of the combustion process is faster than the D-G combustion, providing earlier phasing. This is steeply reduced as full load operation is approached, where the combustion is mainly diffusive and the injection durations are extended to several degrees as a way of deliver the same energy amount, which provides similar or delayed phasing to the D-G calibration.

It is also interesting to note that despite the advanced CA50 found at medium to high load, the combustion durations are still longer than those from the original D-G calibration as it is demonstrated in Figure 6.39. It can be suggested that this is a consequence of the two-phase combustion: the premixed part and the diffusive one. At the first part, the higher cetane number enhances the reactivity of the blend, providing a fast combustion process. By contrast, the diffusive part is directly correlated with the HRF characteristics and its injection process. As aforementioned, the lower OMEx LHV requires a significant extension of the injection durations, which supports the combustion process during the expansion stroke.

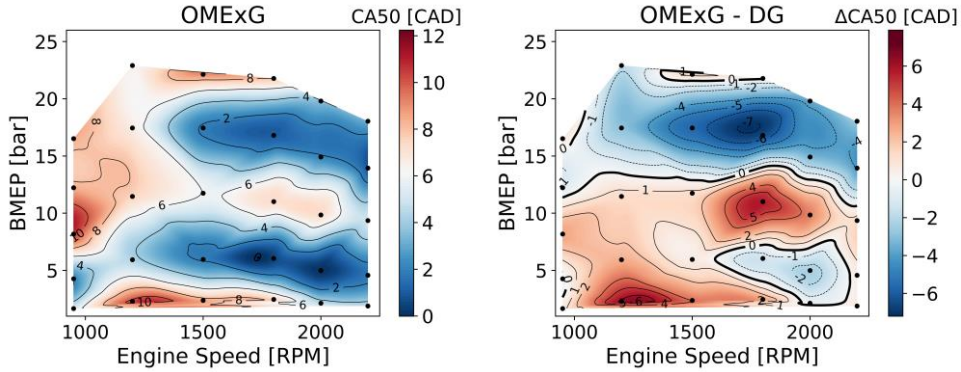

(a) (b)

Figure 6.38. Iso contour maps for (a) combustion phasing (CA50) for OMEx-gasoline calibration and (b) its absolute difference with respect to the diesel gasoline calibration.

This second part is much less energy intensive than the diesel gasoline case, since the injection rate is not significantly modified while the LHV is reduced by more than half. The increase of the injector orifices and consequently higher delivery rates could be an alternative to overcome this issue. Nonetheless, as demonstrated by Garcia et. al [28], there are competing effects that impair the combustion development and reduce the conversion efficiency if higher injection diameters are employed. Both analysis of CA50 and combustion duration demonstrated that despite the modifications of the combustion process, there is no evident benefit that could justify the significant increase on the brake efficiency values observed for the OMEx calibration. In this sense, further analysis is performed to identify the possible sources of these improvements.

As previously said, pumping losses are an additional source of energy loss that may significantly impact the brake efficiency results. Figure 6.40 (a) depicts the pumping mean effective pressure values as well as its comparison with the original diesel-gasoline calibration. As it can be seen, the values of PMEP differs from those achieved in D-G calibration in both behavior and absolute values. The smooth variation of the PMEP values with respect to

the engine speed demonstrates that this property is not affected by secondary issues as extremely closed VGT. The dominance of fluid flow velocity at the exhaust gases on the PMEP values suggests that the OMEx can help in solving the prior issues in terms of air management capacity, which were one of the main drawbacks of the concept.

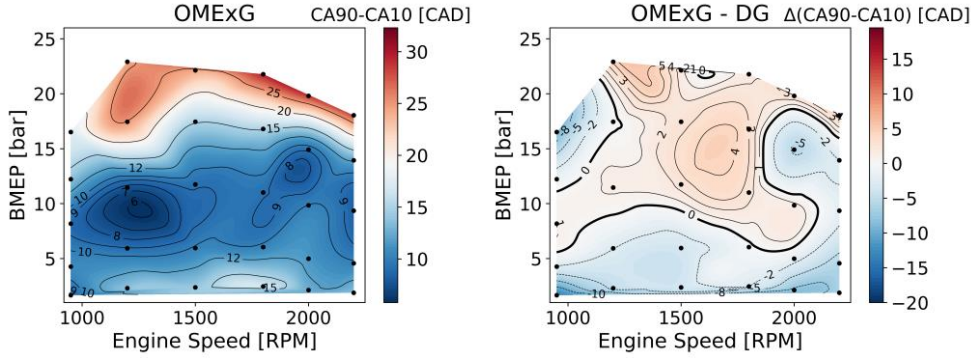

(a) (b)

Figure 6.39. Iso contour maps for (a) combustion duration (CA90 - CA10) for OMEx-gasoline calibration and (b) its absolute difference with respect to the diesel gasoline calibration.

The previous discussion is evidenced on Figure 6.40 (b) where the differences between both calibrations (with diesel and OMEx) are illustrated. As it is shown, the introduction of OMEx as HRF enables a reduction of the PMEP values in more than 0.7 bar at specific conditions. Moreover, the complete map presents benefits in terms of PMEP. This can be attributed to the fact that OMEx can provide virtually zero soot even in conditions with low oxygen concentration. In this sense, there is no need to push the turbine to its limits to provide extra air flow as in the diesel case. In a similar manner, the VGT position can be tailored together with the combustion to obtain the minimum pumping losses. Moreover, it is possible to tackle some of the drawbacks verified in the previous D-G calibration in terms of maximum pressure at the turbine inlet and compressor temperature.

These PMEP improvements can be directly translated to increases of the total work output since it reduces the cycle losses. A decrease of one bar in PMEP would result in a 5 % increase of the total BMEP and a consequent improvement of 5 % in the efficiency values. If one considers the results presented in Figure 6.36, it is possible to infer that the variation of efficiency from 42 % (diesel) to 44 % (OMEx) means an improvement of almost 5 %, being at the same order of the magnitude than the benefits of the PMEP reduction. In this sense, it can be concluded that the use of OMEx and its consequent benefits for the air management system plays a major role on obtaining a more efficient combustion process.

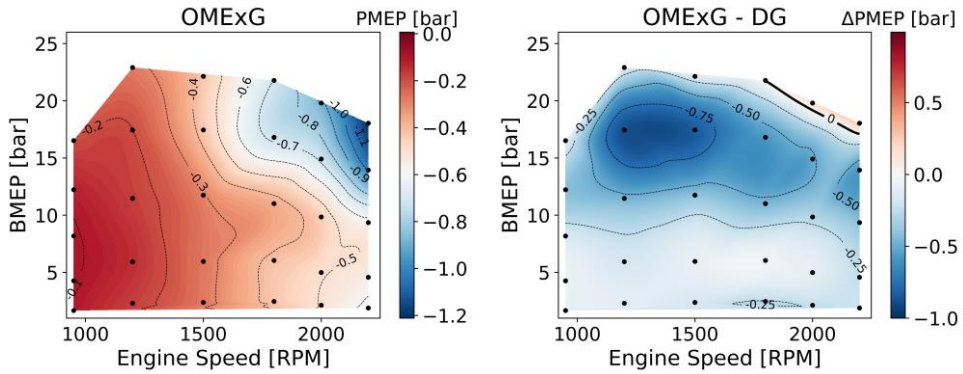

(a) (b)

Figure 6.40. Iso contour maps for (a) pumping mean effective pressure for OMEx-gasoline calibration and (b) its absolute difference with respect to the diesel gasoline calibration.

6.3.2.3. Emission results

One of the most significant achievements from using OMEx as HRF is depicted in Figure 6.41. These graphs illustrate the final soot and NOx emissions for the whole calibration map. As it can be seen, both are able to fulfill EUVI emissions, independently on the operating conditions. NOx emissions are significantly reduced at high load compared to the previous D-G calibration. This could be achieved by increasing the dilution levels by

EGR with no impact on the soot emission. Indeed, the soot emissions are always zero, independently on the operating condition evaluated. The limitations of the AVL 415 S smoke meter should be remarked again, not being able to provide a quantification of neither the condensable hydrocarbon compounds nor the particle number, which are intended to be investigated in future works. Yet, it is interesting to note that the accomplishment of zero soot in the whole engine map suggests that the molecular structure plays an important role on the formation mechanism of the soot emissions.

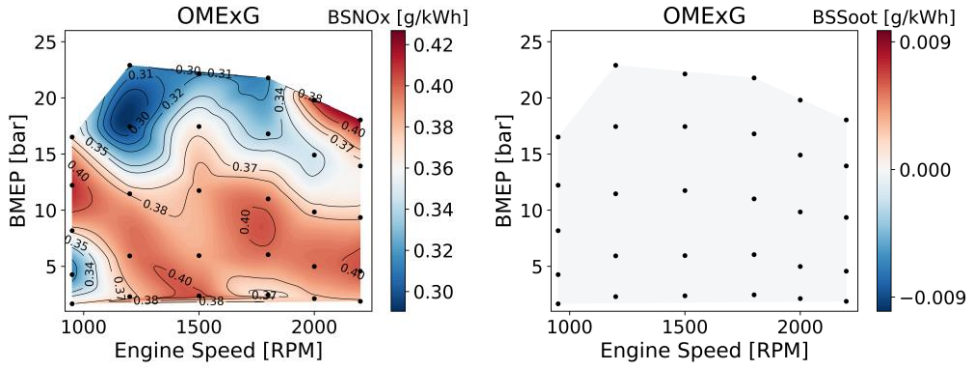

(a) (b)

Figure 6.41. Start of injection (a) and injection duration (b) of the pilot injection for the complete engine map.

Unburned hydrocarbons and carbon monoxide emissions are closely correlated with those from the original calibration, suggesting that the gasoline fraction profile and the type of combustion dominates the formation of these pollutants. This conclusion is drawn based on the fact that the higher HC emissions are verified from low to medium load, where a premixed combustion can be achieved and the higher GF values are employed. As the engine load is increased, both HC and CO are steeply reduced due to the dominance of the HRF and the use of diffusive combustion.

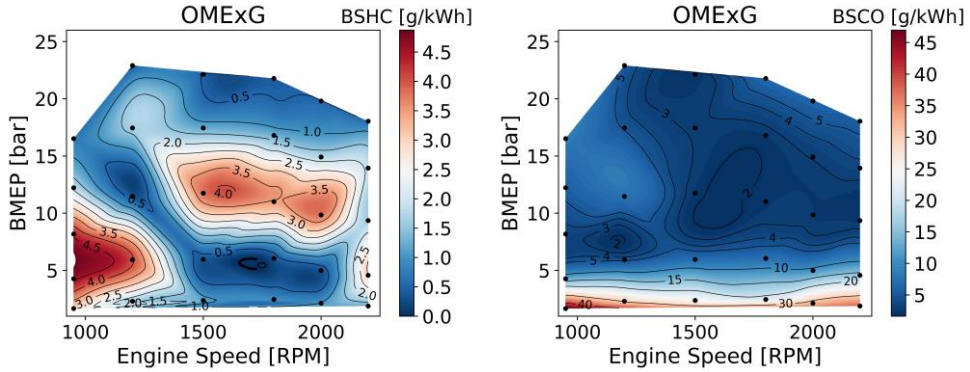

(a) (b)

Figure 6.42. Start of injection (a) and injection duration (b) of the pilot injection for the complete engine map

6.3.2.4. Driving cycle evaluation

Finally, a driving cycle assessment was performed aiming to obtain an overview of the OMEx-G calibration. The calibration maps obtained for performance and emissions were used as inputs to the model and were compared to the previous results from CDC and D-G. The same setup that employed in the chapter 4 was maintained in which regards the truck characteristics and driving cycle settings (payload sweep, gear shift strategy, etc.). In this sense, the benefits and drawbacks can be evidenced at the same basis. The only modifications rely on a coarser discretization of payloads. Small variations on the absolute values compared to those from chapter 4 can be a consequence of model optimization along the work.

Figure 6.43 present the percentage of brake efficiency variation for both D-G and OMEx-G in comparison to the CDC calibration. The results of D-G are herein presented as a reference value because they were deeply discussed in chapter 4. Yet, it can be remarked that the conclusions remain the same, where the D-G calibration is not able to provide benefits in terms of fuel consumption compared to the original CDC calibration with the differences being smaller as the payload is increased. By contrast, it can be

concluded that the replacement of diesel by OMEx as high reactivity fuel is an alternative to realize fuel consumption benefits in equivalent basis. It is demonstrated that OMEx provides reductions for the complete set of cases evaluated. The most prominent differences are found at 50 % of payload. It seems that this payload provides the balance between the operating condition distribution being neither located only at low loads nor at near full load where the efficiency is impaired by the longer combustion process.

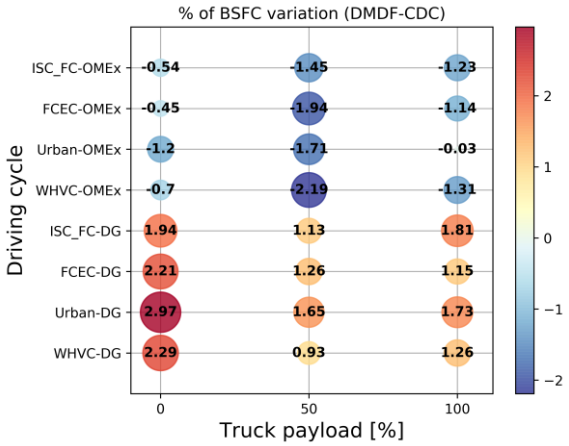

Figure 6.43. Equivalent brake specific fuel consumption percentage difference with respect to the different truck payloads and driving cycles evaluated considering diesel and OMEx as high reactivity fuels.

The previous results from chapter 4 have demonstrated that the D-G calibration was able to fulfill the EUV transient NOx limits at normative conditions, i.e., 50 % of payload. Nonetheless, as the payload was increased, the engine-out NOx emissions were penalized due to the high NOx production at high to full load operating conditions. Consequently, the use of the proposed diesel gasoline calibration rendered excessive NOx emissions at full payload, exceeding the EUVI constraints. Meanwhile, the use of OMEx has enabled the possibility of tuning the EGR levels as required to reduce the NOx emissions. Therefore, as shown in Figure 6.44, even full payload

conditions were able to fulfill the stringent limits of EUVI without any aftertreatment system.

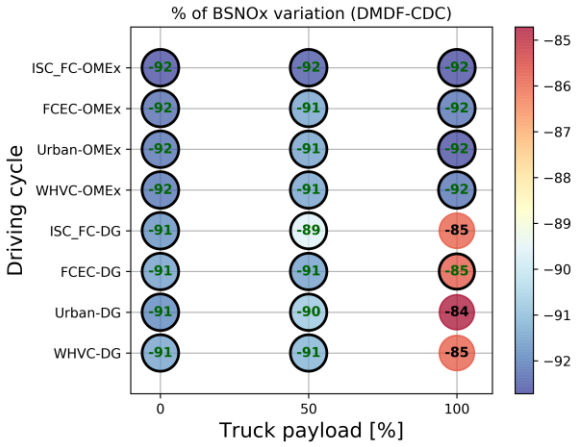

Figure 6.44. Brake specific nitrogen oxides emissions percentage difference with respect to the different truck payloads and driving cycles evaluated considering diesel and OMEx as high reactivity fuels.

This becomes even more interesting when the data from the soot emissions presented in Figure 6.45 are analyzed simultaneously. While D-G calibration was not able to fulfill EUVI soot limits at normative condition, OMEx has allowed to obtain a 100 % reduction considering the total soot emissions, independently on the driving cycle. This effect is more pronounced at full payload where the D-G calibration has provided almost twice of the soot emissions of CDC while OMEx-G was still able to maintain the soot levels at virtually zero engine-out emissions.

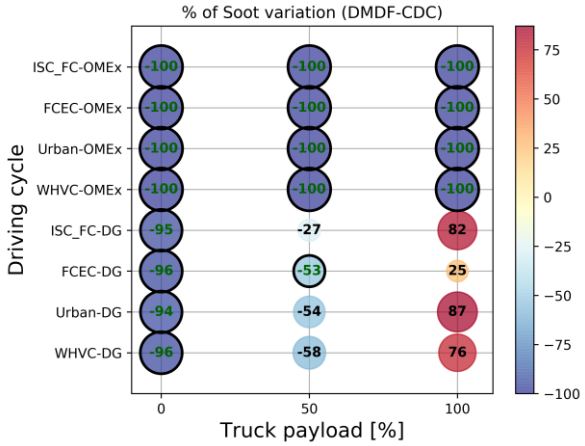

Figure 6.45. Brake specific soot emissions percentage difference with respect to the different truck payloads and driving cycles evaluated considering diesel and OMEx as high reactivity fuels.

Both CO and HC emissions follow similar trends tho those presented in chapter 4 either for OMEx-G and Diesel-G. The former presents differences in which regards to absolute values (as it is demonstrated in Figure 6.46), generally producing more CO than the latter. Once the payload is increased, there is an inversion in the trend, which benefits the OMEx calibration. Even though, the variations are not as significant as to impact the engine hardware. The unburned hydrocarbon emissions results, shown in Figure 6.47 allow to conclude that OMEx provides lower unburned emissions at low payload, which may enhance the DOC performance if temperature and oxygen concentration are maintained. Nonetheless, there is a significant increase of the hydrocarbon emissions as the payload is increased because of the low combustion efficiency caused by the extension of the diffusive flame towards the expansion stroke.

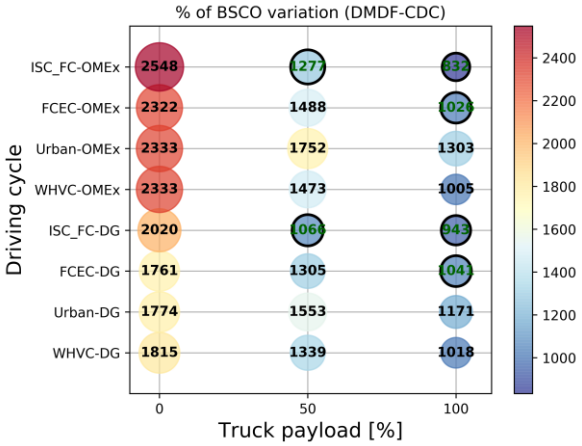

Figure 6.46. Brake specific carbon monoxide emissions percentage difference with respect to the different truck payloads and driving cycles evaluated considering diesel and OMEx as high reactivity fuels.

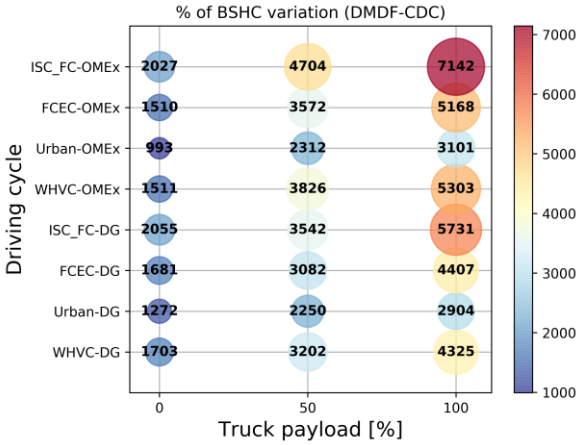

Figure 6.47. Brake specific unburned hydrocarbon emissions percentage difference with respect to the different truck payloads and driving cycles evaluated considering diesel and OMEx as high reactivity fuels.

Finally, a comprehensive well-to-wheel analysis is presented to enlighten the benefits that can be obtained if the CO_2 savings during the OMEx production process are considered. To do this, the results from TTW,

which address the amount of CO_2 produced in the tailpipe, are summed with those from the production process and transportation. As it was previously introduced, any result is weighted by the mass of each fuel (gasoline and OMEx) by means of the gasoline fraction. Differently from the analysis presented in section 6.1.3.4, where the comparison basis was gCO_2/MJ_{fuel}, the results herein presented are already in the normative basis, gCO_2/tkm, which represents the amount of CO_2 that is emitted by vehicle weight and kilometer.

Figure 6.48 depicts the comparison of the CO_2 production for each calibration with those from the original CDC calibration. As it can be seen, for 0 % of payload, both calibrations are able to deliver savings in CO_2. It can be suggested that D-G savings are intrinsically related with the combustion mode and consequently to the GF values. While both gasoline and diesel have similar LHV values, gasoline has the advantage of having lower CO_2 formation potential (3.09 compared to 3.17 from diesel)[30]. In this sense, if the efficiency is maintained, D-G can be more attractive than CDC in term of CO_2 production at a TTW basis. No benefits should be attained from a WTT basis for these fuels. As the payload is increased and the operating conditions are shifted towards high load, the efficiency is reduced as well as the GF values, vanishing any benefits in WTW for the D-G calibration.

By contrast, despite the worst performance in terms of CO_2 in a TTW basis for OMEx, the inclusion of the WTW analysis enables significant CO_2 savings. As it is shown, reductions up to 17 % can be realized compared to the original CDC calibration. This is attributed to the negative CO_2 footprint that can be accomplished if wind power is used as energy source during its production process. It is also possible to state that as the payload is increased, lower are the benefits of using OMEx, which is a consequence of the lower brake efficiencies at high to full load operation. Yet, the benefits are higher than 13 %, which almost fulfills with the H2025 targets. Therefore, it can be concluded that, in spite of not being considered in the normative, the use of e-fuels combined with a WTW analysis can provide a direct path to realize CO_2 savings able to fit in the short-term future normative. Moreover, the

introduction of these fuels in advanced combustion concepts as DMDF allows to realize additional benefits in terms of NOx and soot emissions, reducing the vehicle fixed and operational costs.

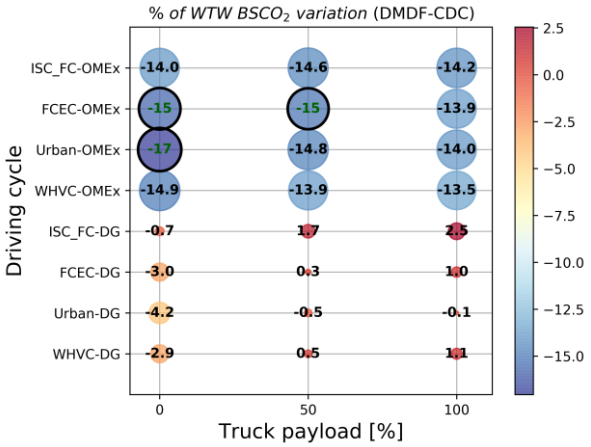

Figure 6.48. Well to Wheel CO_2 percentage difference with respect to the different truck payloads and driving cycles evaluated considering diesel and OMEx as high reactivity fuels.

6.4 Summary and conclusions

This last chapter has presented a comprehensive evaluation of the fuel effects on the DMDF combustion as an attempt to reduce the CO_2 emissions while maintaining the emission benefits from the conventional D-G calibration. The investigation was divided in two separate parts. First, both octane number and sensitivity effects were assessed to identify the best RON and MON that could deliver improvements for the concept. The RON evaluation was based on both steady-state and transient evaluation. The former was performed at representative operating conditions, addressing RONs from 100 to 80, while the latter included an 8-modes equivalent driving cycle with a posterior merit function evaluation. The main findings can be summarized as follows:

- Octane number plays a fundamental role on the definition of the limits for fully premixed combustion.
- High RONs enhances the operation at high to full loads while low RONs present benefits in low load operation, decreasing the concentration of unburned products.
- The contrasting behavior according to the operating condition evaluated requires the assessment on representative usage conditions which was accomplished by an 8-mode driving cycle followed by a merit function evaluation. This approach enabled the determination of the RON range from 87.5 to 92 as the optimum octane number range to obtain the benefits in performance and emissions.
- The sensitivity variation provides an alternative to tailor the fuel reactivity under specific operating conditions. While low engine loads are not significantly affected by the sensitivity variation, high engine loads deliver higher ignition delays once these conditions are found at beyond-RON operation.

Despite the comprehensive evaluation, the benefits in terms of fuel consumption improvement and consequent CO_2 reduction with the LRF characteristics modification where still far from those required at the short-term future (H2025). In this respect, different high reactivity fuels with potential for CO_2 well-to-tank and soot reduction were investigated in representative operating conditions. Both e-FT and OMEx were investigating focusing on their effects on the combustion, emissions and potential well-to-wheel CO_2 reduction allowing to conclude that:

- The modification of the high reactivity fuel had low effect upon low to medium load operation. The most noticeable changes were related with the ignition delay.
- e-FT has a limited capacity on reducing the soot emissions which does not allow to obtain EUVI compliant NOx and soot at high to full load. By contrast, OMEx enables virtually zero soot with NOx lower than the EUVI constraints. Nonetheless, its low LHV

impairs the conversion efficiency due to the extended injection durations that last several degrees during the expansion stroke.

- From a global perspective, OMEx demonstrated to be the best alternative for HRF in the DMDF concept since it can provide EUVI NOx emissions with ultra-low soot emissions while enabling WTW CO_2 reductions. In this sense, a recalibration was proposed with OMEx as HRF. The most significant conclusions were the efficiency improvement in almost the complete map while fulfilling NOx. Soot was virtually zero, independently on the operating condition evaluated.
- Finally, a well-to-wheel CO_2 analysis was performed reporting benefits of more than 13 % which approaches those from the H2025 horizon.

Therefore, it can be concluded that the fuel modification can be an alternative in achieving a cleaner transportation in a well-to-wheel basis. The fuel flexibility of the DMDF concept that was demonstrated throughout this chapter maximizes its potential on reducing the CO_2 footprint while providing ultra-low emissions of NOx and soot.

6.5 Bibliography

[1] American Standards. Standard Test Method for Motor Octane Number of Spark-Ignition Engine. *Fuel*, pp. 1–68, 2003.

[2] Szybist J.P., Splitter D.A. "Pressure and temperature effects on fuels with varying octane sensitivity at high load in SI engines". *Combustion and Flame*, Vol. 177, pp. 49–66, 2017.

[3] Leppard W.R. "The Chemical Origin of Fuel Octane Sensitivity". *SAE Technical Papers*, n° 902137, 1990.

[4] Leppard W.R. "The Autoignition Chemistries of Primary Reference Fuels, Olefin/Paraffin Binary Mixtures, and Non-Linear Octane Blending". *SAE Technical Papers*, n° 922325, 1992.

[5] Mittal V., Heywoodv, Green W.H. "The underlying physics and chemistry behind fuel sensitivity". *SAE Technical Papers*, n° 2010-01-0617, 2010.

[6] Javed T., Lee C., AlAbbad M., Djebbi K., Beshir M., Badra J., H. Curran, A. Farooq. "Ignition studies of n-heptane/iso-octane/toluene blends". *Combustion and Flame*, Vol. 171, pp. 223–233, 2016.

[7] Prakash A., Wang C., Janssen A., Aradi A., Cracknell R., Impact of Fuel Sensitivity (RON-MON) on Engine Efficiency". *SAE International Journal of Fuels and Lubricants*, Vol. 10, 2017.

[8] Curran H.J., Gaffuri P., Pitz W.J., Westbrook C.K. "A comprehensive modeling study of n-heptane oxidation". *Combustion and Flame*, Vol. 114, pp. 149–177, 1988.

[9] Herzler J., Jerig L., Roth P. "Shock tube study of the ignition of lean n-heptane/air mixtures at intermediate temperatures and high pressures". *Proceedings of Combustion Institute*, Vol. 30, pp. 1147–1153, 2005.

[10] Vandersickel A., Hartmann M., Vogel K., Wright Y.M., Fikri M., Starke R., Schulz C., Boulouchos K. "The autoignition of practical fuels at HCCI

conditions: High-pressure shock tube experiments and phenomenological modeling". *Fuel*, Vol. 93, pp. 492–501, 2012.

[11] Lawler B., Lacey J., Dronniou N., Dernotte J., Dec J., Guralp O., Najt P., Filipi Z. "Refinement and validation of the thermal stratification analysis: A post-processing methodology for determining temperature distributions in an experimental HCCI engine". *SAE Technical Papers*, n° 2014-01-1276, 2014.

[12] Zhou Y., Gainey B., Hariharan D., Lawler B., Mamalis S. "Understanding HCCI combustion in a free piston engine with a multi-zone, control-mass model with thermal stratification and chemical kinetics". *SAE Technical Papers*, n° 2019-01-0958, 2019.

[13] Hao H., Liu F., Liu Z., Zhao F. "Compression ignition of low-octane gasoline: Life cycle energy consumption and greenhouse gas emissions, Applied Energy, Vol. 181, pp. 391–398, 2016.

[14] Badra J., Viollet Y., Elwardany A., Im H.G., Chang J. "Physical and chemical effects of low octane gasoline fuels on compression ignition combustion". *Applied Energy*, Vol. 183, pp. 1197–1208, 2016.

[15] García A., Monsalve-Serrano J., Martínez-Boggio S., Rückert Roso V., Duarte N. "Potential of bio-ethanol in different advanced combustion modes for hybrid passenger vehicles". *Renewable Energy*, Vol. 150, pp. 58–77, 2020.

[16] Hank C., Lazar L., Mantei F., Ouda M., White R.J., Smolinka T., Schaadt A., Hebling C., Henning H.M. "Comparative well-to-wheel life cycle assessment of OME3-5 synfuel production via the power-to-liquid pathway". *Sustainable Energy Fuels*, Vol. 3, pp. 3219–3233, 2019.

[17] Liu C.M., Sandhu N.K., McCoy S.T., Bergerson J.A. "A life cycle assessment of greenhouse gas emissions from direct air capture and Fischer-Tropsch fuel production". *Sustainable Energy Fuels*, Vol. 4, pp. 3129–3142, 2020.

[18] Toyir J., Miloua R., Elkadri N.E., Nawdali M., Toufik H., Miloua F., Saito M. "Sustainable process for the production of methanol from CO2 and H2 using Cu/ZnO-based multicomponent catalyst". *Physics Procedia*, Vol. 2, pp. 1075–1079, 2009

[19] Pastor J. V., García A., Micó C., Lewiski F., An optical investigation of Fischer-Tropsch diesel and Oxymethylene dimethyl ether impact on combustion process for CI engines. *Applied Energy*, Vol. 260, 2020.

[20] Alleman T.L., McCormick R.L., Fischer-tropsch diesel fuels - Properties and exhaust emissions: A literature review. *SAE Technical Papers*, n° 2003-01-0763, 2003.

[21] Dworschak P., Berger V., Härtl M., Wachtmeister G., Neat Oxymethylene Ethers: Combustion Performance and Emissions of OME2, OME3, OME4 and OME5 in a Single-Cylinder Diesel Engine. *SAE Technical Papers*, n° 2020-01-0805, 2020.

[22] DeWitt M.J., Corporan E., Graham J., Minus D. "Effects of aromatic type and concentration in Fischer-Tropsch fuel on emissions production and material compatibility". *Energy and Fuels*. Vol. 22, pp. 2411–2418, 2008.

[23] Kim Y.D., Yang C.W., Kim B.J., Moon J.H., Jeong J.Y., Jeong S.H., Lee S.H., Kim J.H., Seo M.W., Lee S.B., Kim J.K., Do Lee U. "Fischer–tropsch diesel production and evaluation as alternative automotive fuel in pilot-scale integrated biomass-to-liquid process". *Applied Energy*, Vol.180, pp. 301–312, 2016.

[24] Van Vliet O.P.R., Faaij A.P.C., Turkenburg W.C. "Fischer-Tropsch diesel production in a well-to-wheel perspective: A carbon, energy flow and cost analysis". *Energy Conversion and Management*, Vol. 50, pp. 855–876, 2009.

[25] Deutz S., Bongartz D., Heuser B., Kätelhön A., Schulze L., Omari A., Walters M., Klankermayer J., Leitner W., Mitsos A., Pischinger S., Bardow A. "Cleaner production of cleaner fuels: Wind-to-wheel-

environmental assessment of CO2-based oxymethylene ether as a drop-in fuel". *Energy and Environmental Sciences*, Vol. 11, pp. 331–343, 2018.

[26] Bongartz D., Burre J., Mitsos A. "Production of Oxymethylene Dimethyl Ethers from Hydrogen and Carbon Dioxide - Part I: Modeling and Analysis for OME1". *Ind. Engineering and Chemical Research*, Vol. 58, pp. 4881–4889, 2019.

[27] Oestreich D., Lautenschütz L., Arnold U., Sauer J. "Production of oxymethylene dimethyl ether (OME)-hydrocarbon fuel blends in a one-step synthesis/extraction procedure". *Fuel*, Vol. 214, 2018.

[28] García A., Monsalve-Serrano J., José Sanchís E., Fogué-Robles Á. "Exploration of suitable injector configuration for dual-mode dual-fuel engine with diesel and OMEx as high reactivity fuels". *Fuel*, Vol. 280, 2020.

[29] García A., Monsalve-Serrano J., Villalta D., Lago Sari R., Gordillo V., Gaillard P. "Potential of e-Fischer Tropsch diesel and oxymethyl-ether (OMEx) as fuels for the dual-mode dual-fuel concept". *Applied Energy*, Vol. 253, 2019.

[30] Benajes J., García A., Monsalve-Serrano J., Martínez-Boggio S. "Potential of using OMEx as substitute of diesel in the dual-fuel combustion mode to reduce the global CO2 emissions". *Transportation in Engineering*, Vol. 1, 2020.

Chapter 7

Conclusions and suggestions for future work

Content

7.1 Introduction

This last chapter aims to provide a global summary of the main conclusions obtained throughout this investigation. It will also enable the verification of whether the objectives initially proposed where fulfilled or not. Finally, suggestions for future works are presented and discussed based on the different observations that were evidenced during the work.

7.2 Summary and conclusions

This thesis was developed as an attempt to reproduce a novel and cleaner combustion mode in a stock engine hardware to solve relevant issues of current diesel engines, as NOx and soot emissions, without penalizing conversion efficiency. The combustion concept herein employed is a practical evolution of the most known low temperature combustion concepts which were introduced in chapter 2.

During the literature review, it was evidenced that LTC concepts are a potential path to improve the conversion efficiency while solving the NOx soot dilemma from the conventional diesel combustion. Despite this, the former LTCs generally have a limited operating range inside the engine map, being constrained at high load due to excessive pressure gradients and at low load by significant combustion instabilities. Moreover, the kinetically controlled nature of these concepts presents a hurdle in controlling the combustion development since low dynamic variables like temperature are dominant factors in the combustion development.

Load extension was pursued by different techniques, like fuel modification and introduction of some level of stratification. The former demonstrated to be an alternative to achieve high loads by introducing high RON fuels at the cost of impairing low load operation. By contrast, the stratification was proven to be a more effective way, allowing to enlarge the combustion process while reducing the pressure gradients. Both

compositional and temperature stratification demonstrated to be effective in providing some level of benefit and control over the combustion development. Nonetheless, the most significant advancement was obtained by introducing an octane number stratification. This was accomplished by injecting two fuels with different reactivities, originating the concept known as Reactivity Controlled Compression Ignition (RCCI). Investigations on the subject have reported noticeable increase of conversion efficiency with simultaneous reduction of NOx and soot with wider operating limits than the conventional single fuel LTCs. In spite of this, RCCI was still not able to cover the full operating map due to similar issues to those of previous LTC.

Recently, the Dual-Mode Dual-Fuel (DMDF) combustion concept was introduced as an alternative to tackle the issues from RCCI combustion. This concept combines the use of a fully premixed combustion from low to medium load with a dual fuel diffusive concept at high to full load operation. In this sense, the benefits of RCCI can be explored whenever possible while maintaining the same power output of the stock engine. Although the results obtained in a single cylinder platform are promising, several challenges were identified like the excessive charge dilution requirements in most of the map and poor combustion efficiency at low load, which delivers high concentrations of unburned HC and CO. Moreover, the decrease of the geometric compression ratio to realize full load operation reduces the benefits that can be attained in terms of conversion efficiency. Finally, high intake pressures should be used to increase the dynamic compression ratio to balance the low geometrical CR to accomplish efficiency benefits.

The previous points have demonstrated to be challenges in which comprises the extension of the concept in a real application. The limited operating range of conventional turbochargers, the mechanical limitations and the aftertreatment capacity to reduce the unburned products are key factors that can dictate the successful application of the concept on higher TRL levels. Moreover, alternatives to reduce the CO_2 footprint of the concept must be pursued.

In this sense the present thesis has investigated the extension of the DMDF concept to a multi-cylinder engine platform. This allowed to shed light on the challenges and benefits of introducing a novel combustion concept in a commercial engine with a few hardware modifications by means of steady and transient evaluations. Moreover, the impact of the combustion concept on the aftertreatment performance was carried out to identify possible hurdles of the concept on the DOC and DPF performance. Finally, CO_2 reduction was targeted by modifying the characteristics of both low reactivity and high reactivity fuels. The most significant findings of each study are summarized in the next subsections.

7.2.1 Steady-state calibration and driving cycle assessment with diesel-gasoline

The implementation of the DMDF concept in a multi-cylinder engine, considering the guidelines identified in the literature, was presented in the first chapter of the results section. It was demonstrated that most of the results identified in a single cylinder engine could not be extended to the MCE platform. The main hurdles were faced on the air management system. At low engine load, the low exhaust flow energy could not provide enough energy to the turbocharger to achieve the desired boost pressure. This affected the dynamic compression ratio, delivering efficiencies far inferior to those reported in the literature. As the engine load was increased to medium loads, it was possible to increase the boost pressure enabling high gasoline fractions and then a fully premixed combustion without NOx and soot emissions. The further increase of the engine load and the attempt at extending the boundary conditions to those of SCE evaluations have promoted a mass flow issue on the turbocharger. This happened due to the simultaneous requirement of high fresh air mass and EGR levels at these operating conditions.

The use of only HP EGR to achieve the desired dilution levels promoted a lack of energy in the turbine, requiring and excessively closed VGT, which impaired the pumping losses. In that respect, the EGR was split in both LP

and HP EGR routes. Nonetheless, the use of LP EGR has increased the amount of mass flowing through the compressor, increasing its temperatures up to limiting levels. In this sense, the system was not possible to deliver both oxygen and EGR required to achieve the desired combustion process. Consequently, issues with pressure gradients and partial soot oxidation appeared, requiring the relaxation of the emission constraints. This situation was worsened as the engine load approached full load operation. At these conditions, it was sought to have a settings combination that could provide the same power output, while minimizing fuel consumption with emission levels far superior to those from the EUVI mandates.

The consequences of attaining to these strategies to achieve a full map calibration were then investigated in representative driving conditions of medium duty trucks. To do this, a VOLVO FE 350 (which uses the engine herein investigated) was described in a longitudinal vehicle model, considering the most significative characteristics. Thereafter, the truck was subjected to different driving cycles like the normative WHVC, the in-service conformity cycle, the urban driving cycle and a fuel consumption evaluation cycle under different payloads. This provided a perspective of the main benefits and drawbacks of the proposed calibration. The former was identified to have the capacity of providing ultra-low NOx emissions which allowed to fulfill the EUVI constraints under normative conditions. In addition, significant reductions of soot emissions were achieved for payloads lower than 50 %.

Finally, fuel consumption was penalized in a small extend compared to the original conventional diesel combustion calibration, being this difference minimal in loaded conditions at highway. By contrast, unburned products were found orders of magnitude higher than those of conventional diesel combustion, which could be a challenge for the stock aftertreatment system once combined with the low exhaust temperatures form the premixed combustion. Moreover, soot emissions were increased at full payload being at the similar level or even higher than those of CDC, depending on the driving cycle setup. Lastly, no benefit in terms of CO_2 abatement were identified once

the concept was not possible to improve it neither by efficiency improvement nor by fuel usage.

7.2.2 DOC and DPF evaluation under steady and transient conditions

This chapter was aimed at identifying the impact of the excessive amounts of unburned hydrocarbons and carbon monoxide emission on the stock oxidation catalyst performance as well as the filtration and regeneration mechanism of the original particulate filter. The former was deeply investigated by means of steady and transient evaluations with different aims. Steady-state evaluations were used to assess the impact of the boundary conditions from different operating points of the DMDF concept on the conversion efficiency if both CO and HC. From this analysis, it was possible to identify that low load and low engine speed conditions are the most challenging points in attaining light-off operation as consequence of the low exhaust temperature and significant concentration of unburned products.

As the engine load was increased towards medium load, the higher exhaust temperatures have enabled a proper conversion efficiency, allowing to obtain tailpipe emissions for both HC and CO lower than the normative limits. Thereafter, transient evaluation based on representative steps were proposed as an attempt of identifying the benefits of the DOC thermal capacity on supporting the oxidation reaction, even in conditions that were identifying as challenging in the steady-state evaluation. The results have demonstrated that the oxidation catalyst is able to provide a proper operation, i.e., over light-off conditions, for long periods when the load is reduced from a medium load to a low load operation. This behavior is beneficial whether real operation is considered, indicating that once the DOC heats up, the conversion efficiency can be maintained in proper levels even during idle operation.

A detailed investigation was also performed with the aim of understanding the impact of the DMDF boundary conditions on the

particulate filter process, more specifically passive and active regeneration. Passive regeneration was assessed by means of monitoring the ration of NO_2/NOx before and after the PF to identify any consumption of this specie by the reaction with the soot in the particulate filter. The results demonstrated that the NO_2 values suggested that no passive regeneration takes place at the operating conditions evaluated. By contrast, the active regeneration evaluation has demonstrated that the DMDF is able to provide conditions at the PF inlet suitable to enable the active regeneration process. It was identified that the conversion of the unburned products on the oxidation catalyst was a fundamental process to realize a proper soot oxidation in PF.

Finally, both DOC and PF were modelled by means of 0-D (PF) and 1-D (DOC) approaches to investigate their performance on the same driving cycles than those proposed in chapter 4. This comprehensive analysis has allowed to conclude that the oxidation catalyst is able to deliver normative HC and CO emissions from 50 % of payload. The most critical conditions were verified at the early driving cycle phases, i.e., the DOC warming phase. Moreover, the results from the PF have shown that the accumulated soot during the driving cycle is minimal, having negligible backpressure increase, allowing to even reduce its size to decrease the production costs.

In this sense, it was possible to conclude that the use of the stock DOC and PF are an alternative to assure EUVI compliant HC, CO and soot emissions for the proposed calibration, does not requiring any special coating or size increase. This means that the DMDF concept can avoids the use of an SCR, reducing the operational costs with urea while solving the issues of HC, CO and DPF with well stablished aftertreatment devices.

7.2.3 Fuel modifications to realize near future normative

In spite of the benefits and solutions proposed along the thesis, a question was still not answered: how to reduce the CO_2 footprint in a manner that could account for the targets that will be imposed in a near future

(H2025)? The last chapter was focused on identifying possible solutions for this issue, relying on the fuel modification to attain this. First, an extensive analysis was performed aiming at identifying the most suitable low reactivity fuel characteristics to accomplish efficiency improvements while maintaining the benefits in terms of soot and NOx emissions. To do this, different RON were assessed by means of steady-state evaluation. The results have suggested a strong relation between the RON manifestation and the engine load evaluation. Low load conditions benefit from low RON fuels, reducing unburned products and improving the conversion efficiency to some extent. By contrast, the RON appetite increases as the load is increased, requiring higher RONs to attain a proper combustion process. This trend has required to use a weighting factor for each point that was included b means of an 8 points equivalent driving cycle. Moreover, a merit function approach was considered to select the optimum RON range for the concept. The application of this methodology has evidenced that medium RON ranges from 87.5 to 92.5 are the optimum range for the concept.

Specific investigations have also evaluated the effect of the sensitivity of the fuel for selected RON fuels. It was possible to infer that small amount of sensitivity could benefit the fuel, attributing desired characteristics at high load as higher ignition delays without impairing low load conditions. Despite the wide test matrix, the optimum fuel was found to be similar to the commercial RON 95 gasoline. The small improvements suggest that the introduction of a new low reactivity fuel, at least in a tank to wheel basis, will not allow to fulfill the proposed short-term CO_2 targets.

Next, the modification of the high reactivity fuel characteristics was proposed as an attempt to achieve the benefits that were not possible to realize in the previous study. To do this, promising high reactivity fuels with proved benefits on both well-to-tank CO_2 and soot reduction were chosen and investigated on representative operating conditions, aiming to assess their potential on a performance, emission and WTW CO_2 basis. Among the most relevant fuels that fulfilled the pre-requisites, OMEx and e-FT were chosen and compared at different operating conditions at a critical engine speed of 1800 rpm. The results have suggested e-FT behaves very similar to

conventional diesel in terms of combustion and emissions. Benefits were only evidenced at high and full load conditions, were the absence of aromatic compounds have reduced the soot production. By contrast, OMEx have enabled virtually zero soot independently on the operating condition due to the high oxygen concentration in the molecule and non-direct carbon-carbon bonds. Moreover, the absence of soot emissions has allowed to tailor the EGR concentration to obtain EUVI NOx for the complete set of operating conditions evaluated. However, the low lower heating value have impacted the efficiency at full load operation due to the larger combustion process in the diffusive phase.

The WTW CO_2 results have shown a significant margin of reduction of this pollutant for both e-FT and OMEx if renewable energy from wind is considered in the production process. E-FT exceled OMEx independently of the energy path considered. Nonetheless, the combined analysis of soot, NOx, performance, and CO_2 suggests that OMEx was the most promising fuel for the concept. In this sense, an engine recalibration was performed considering OMEx as HRF and tested at the same driving conditions than those proposed in chapter 4. The use of OMEx allowed to obtain a fully EUVI compliant calibration in terms of soot and NOx. Moreover, the efficiency could be improved at conditions with high gasoline fraction, allowing to extend the benefits of the fully premixed combustion as soot was not a constraint anymore and the turbocharger could be used without implying unnecessary pumping losses. Finally, the WTW CO_2 emissions could be reduced at least to 13 %, close to the H2025 target (15 %). In this sense, the combination of a novel combustion concept with advanced high reactivity fuels have demonstrated to be a path to reduce the complexity of the aftertreatment system while attaining benefits in a WTW CO_2 basis.

7.3 Suggestions for future work

Throughout the investigation presented in this thesis, a number of works were identified as additional investigations to be performed. Unfortunately, they could not be done during this thesis either due time

restrictions or because the work required additional devices that were not available at the time. Therefore, they are here included as future work suggestions to further develop the concept as well as to address drawbacks that may enhance the applicability of the concept on real applications.

7.3.1 Assessment of the particulate composition and particulate number with OMEx

The particulate emission composition evaluation was identified as a work of paramount importance. Despite the excellent results obtained with the AVL 415 S smoke meter, it was not possible to assure that the concept was able or not to fulfill the EUVI legislation. As stressed, previous investigations found on the literature have identified that the D-G DMDF particulate is composed mainly by condensable hydrocarbons which cannot be measured by the smoke meter measurement principle. Therefore, even in the case of having zero soot measurement with OMEx, a significant amount of condensable can exists in the exhaust gases. In this sense, specific investigations should be done to understand and quantify the particulate composition with OMEx as HRF.

Moreover, literature suggests that oxygenated fuels are prone to produce more small size particulates. Once the current EUVI normative also limits the particulate number for each power unit produced, the quantification of the particulate number shall be done to homologates the engine prototype against the EUVI standards.

7.3.2 Implementation on a real demonstrator

The development and implementation of a new concept on the marked requires the fulfillment of different stages. According to its maturity level, it is classified in different TRSs (time readiness levels), which ranges from 1 to 9. The work presented in this thesis have pushed the concept to TRLs up to 5, which consists on the evaluation and validation of the concept on relevant

environments. Nonetheless, higher TRLs requires a real demonstrator of the concept, with the assemble of all subsystem in a representative truck to be tested in different scenarios. Therefore, the assemble of the engine in a real vehicle is mandatory to continue the development process. Some steps should be considered during this implementation:

- First, the calibration maps obtained in this thesis should be loaded in an ECU to provide information about the different settings that are required. Transients representative of those found in real driving conditions should be emulated in a test bench to assure the absence of gaps in the calibration maps as well as to guarantee the loop interaction among the injection, air management and control systems.
- Once the engine is full operative under the combustion concept and the calibration maps are refined, a packing study should be made to account the modifications in the air management path and after treatment system.
- Finally, an extensive work should be done on how to accommodate the different sensors and actuators from the vehicle with the new calibration setup of the DMDF combustion. At this phase, it is recommended to use the initial Labview based ECU to control the indispensable systems.

7.3.3 Electrification of turbocharger, DOC and DPF

Powertrain electrification offers operation flexibility and the possibility of recovering energy in specific cases. The former can be used for enhancing the operation of devices that usually relies only on the engine energy during its operation. An example of this was deeply discussed in chapter 5. In this specific case, it was demonstrated that the DOC heating period was dependent on the exhaust energy, being critical at driving conditions where the velocity was low as that verified in the urban phase. Based on this, several investigations have reported that the use of an electrical heater prior to the after treatment system can be an alternative to reduce the DOC light-off

period as well as to enhance the operation of other ATS systems as the SCR and DPF without significant penalizations on the energy consumption. In this sense, it is suggested that this technique may improve the ATS performance for the DMDF also and its utilization should be deeply investigated.

Additionally, the electrification of external devices can enable paths of energy recuperation at conditions where the exhaust flow provides more energy than that required to achieve the desired boost pressure. Despite of the intrinsically low exhaust energy of the premixed combustion, it is believed that there is margin to energy recuperation. Moreover, the electrification of turbocharger can also enhance the system response to transients and reduce the pressure lag, improving the combustion controllability.

7.3.4 Additional long-term suggestions: hybridization of the concept

In spite of the WTW CO_2 benefits that were realized by means of combining the DMDF concept with e-Fuels, the legislation requires the reduction of the CO_2 only in a tank to wheel basis. Nonetheless, it was demonstrated that the efficiency of the concept is already at a maximum value of 45 % in a brake basis, which makes its extension very challenging. In this sense, it is suggested that the hybridization of the powertrain can enables higher energy savings due to the capacity of recovering energy during the operation as well as the management of the engine to run only at its maximum efficiency line. Both can improve the TTW CO_2 balance to levels that may fulfill the restrictive future targets. Moreover, the combination of the combustion concept with a hybrid powertrain allow to combine the efficiency increase with a clean combustion concept that is able to full NOx EUVI limits without a dedicated ATS with ultra-low soot.

Therefore, a comprehensive evaluation of the DMDF powertrain hybridization is suggested as future work. It may consider different hybridization architectures as series, parallel and power split to evaluate

which provides the greater benefits. Moreover, the use of hybridization allows to use a de-rated engine, which could avoid the high to full load conditions where the concept is penalized which may add an extra margin of improvement to the concept.

Bibliography

[1] Statistical Office of the European Union (Eurostat). "Energy statistics-Energy balances." Available in https://www.iea.org/subscribe-to-data-services/world-energy-balances-and-statistics

[2] Kalghatgi, G. "Is it really the end of internal combustion engines and petroleum in transport?" *Applied Energy*, Vol. 225, pp. 965-974, 2018.

[3] Heywood J B. *"Internal Combustion Engine Fundamentals"*. McGraw-Hill, 2018, Second edition.

[4] Arrhenius, S. "On the influence of carbonic acid in the air upon the temperature of the ground". *Philosophical magazine and journal of science*, Vol. 41, pp. 237–276, 1896.

[5] Environmental Protection Agency. "Nitrogen Oxides (NOx), Why and How They Are Controlled". *Technical report*, 1999.

[6] World health organization. "Health-effects-of-particulate-matter". Available in http://www.euro.who.int/___data/assets/pdf_file/0006/189051/Health-effects-of-particulate-matter-final-Eng.pdf.

[7] Ioannis M., Elisavet S., Agathangelos S., Eugenia B. "Environmental and Health Impacts of Air Pollution: A Review". *Frontiers in Public Health*, Vol. 8, 2020.

[8] Yamaki Y., Mori K, Kamikubo H, Kohketsu S, Mori K, Kato T. "Application of Common Rail Fuel Injection System to a Heavy Duty Diesel Engine". *SAE Technical Paper,* n° 942294, 1996.

[9] Verlag Des Verein Deutscher Ingenieure GmbH. "Common-Rail Injection System for Di-Diesel Engines". *SAE Technical Paper,* n° 967009, 1996.

[10] Russell A, Epling W S. "Diesel Oxidation Catalysts". *Catalysis Reviews: Science and Engineering*. Vol. 53, pp. 337-423, 2011.

[11] Hori M., Oguchi M. "Feasibility Study of Urea SCR Systems on Heavy Duty Commercial Vehicles". *SAE Technical paper*, n° 2004-01-1944, 2004.

[12] Posada F., Chambliss S. and Blumberg K. "Costs of emission reduction technologies for heavy-duty diesel vehicles". *ICCT White paper*, 2016.

[13] European Environment Agency. "Global average near surface temperatures relative to the pre-industrial period". June, 2019. Available at https://www.eea.europa.eu/data-and-maps/daviz/global-average-air-temperature-anomalies-5#tab-dashboard-02, accessed in June, 2020.

[14] European Environment Agency. "EEA greenhouse gas-data viewer". Available at https://www.eea.europa.eu/data-and-maps/data/data-viewers/greenhouse-gases-viewer , accessed in June, 2020.

[15] Sadorsky P. "Energy Related CO2 Emissions before and after the Financial Crisis". *Sustainability*, Vol. 12, 2020.

[16] European union. Reducing CO2 emissions from heavy-duty vehicles Available at https://ec.europa.eu/clima/policies/transport/vehicles/heavy_en, accessed in June 2020.

[17] Luján J.M., García A., Monsalve-Serrano J., Martínez-Boggio S. "Effectiveness of hybrid powertrains to reduce the fuel consumption and NOx emissions of a Euro 6d-temp diesel engine under real-life driving conditions". *Energy Conversion and Management*, Vol. 199, 2019.

[18] U.S department of energy. "Medium- and Heavy-Duty Vehicle Electrification: An Assessment of Technology and Knowledge Gaps". December, 2019, available at https://info.ornl.gov/sites/publications/Files/Pub136575.pdf

[19] Pachiannan T., Zhong W, Rajkumar S, He Z, Leng X, Wang Q. "A literature review of fuel effects on performance and emission characteristics of low-temperature combustion strategies". *Applied Energy*, Vol. 251, 2019.

[20] Kokjohn S L, Hanson R M, Splitter D A, Reitz R D. "Fuel reactivity-controlled compression ignition (RCCI): a pathway to controlled high-efficiency clean combustion". *International Journal of Engine Research*, Vol. 12, pp. 209-226, 2011.

[21] Benajes J, Molina S, García A, Monsalve-Serrano J. "Effects of direct injection timing and blending ratio on RCCI combustion with different low reactivity fuels". *Energy Conversion and Management*, Vol. 99, pp 193-209, 2015.

[22] Reitz, R.D., Duraisamy, F. Review of high efficiency and clean reactivity-controlled compression ignition (RCCI) combustion in internal combustion engines. *Progress in Energy and Combustion Science*. Vol. 46, pp. 12-71, 2014.

[23] Benajes J, García A, Monsalve-Serrano J, Villalta D. Exploring the limits of the RCCI combustion concept in a light-duty diesel engine and the influence of the direct-injected fuel properties. *Energy Conversion and Management*, Vol. 157, pp. 277-287, 2018.

[24] Benajes, J., García, A., Monsalve-Serrano, J., Boronat, V. "Dual-Fuel Combustion for Future Clean and Efficient Compression Ignition Engines". *Applied Sciences*, Vol. 7, 2017.

[25] Benajes J, García A, Monsalve-Serrano J, Boronat V. "Achieving clean and efficient engine operation up to full load by combining optimized RCCI and dual-fuel diesel-gasoline combustion strategies". *Energy Conversion and Management*, Vol. 136, pp 142-151, 2017.

[26] Benajes J., Novella R., García A., Arthozoul S. "The role of in-cylinder gas density and oxygen concentration on late spray mixing and soot oxidation processes". *Energy*, Vol. 36, pp. 1599–1611, 2011.

[27] Desantes J.M., Payri R., Salvador F.J., Gil A. "Development and validation of a theoretical model for diesel spray penetration". *Fuel*, Vol. 85, pp. 910–917, 2005.

[28]Siebers D.L. "Liquid-phase fuel penetration in diesel sprays". *SAE Technical Papers,* n° 980809, 1998.

[29]Xin J., Ricart L., Reitz R.D. "Computer Modeling of Diesel Spray Atomization and Combustion". *Combustion Science and Technology*, Vol. 137, pp. 171–194, 1998.

[30]Bertoli C., Migliaccio M.N. "A finite conductivity model for diesel spray evaporation computations". I*nternational Journal of Heat Fluid Flow.* Vol. 20, pp. 552–561, 1999.

[31]Pastor J. V., Javier López J., García J.M., Pastor J.M. "A 1D model for the description of mixing-controlled inert diesel sprays". *Fuel*, Vol. 87, pp. 2871–2885, 2008.

[32]Andreassi L., Ubertini S., Allocca L. "Experimental and numerical analysis of high pressure diesel spray-wall interaction". *International Journal of Multiphase Flow.* Vol. 33, pp. 742–765, 2007.

[33]Higgins B., Siebers D., Aradi A., *SAE Technical Papers,* Diesel-Spray Ignition and Premixed-Burn Behavior, (2014).

[34]Chmela F.G., Orthaber G.C., Rate of heat release prediction for direct injection diesel engines based on purely mixing controlled combustion, *SAE Technical Papers,* (1999). doi:10.4271/1999-01-0186.

[35] Dec J.E., A conceptual model of di diesel combustion based on laser-sheet imaging, *SAE Technical Papers,* n° 970873, 1997.

[36] Arrègle J., Pastor J. V., López J.J., García A. "Insights on postinjection-associated soot emissions in direct injection diesel engines". *Combustion and Flame*, Vol. 154, pp. 448–461, 2008.

[37] Turns S.R. "Understanding NOx formation in nonpremixed flames: Experiments and modeling". *Progress in Energy and Combustion Sciences*, Vol. 21, pp. 361–385, 1995

[38] Desantes J.M., Arrègle J., López J.J., García A. "A comprehensive study of diesel combustion and emissions with post-injection". *SAE Technical Papers* , n° 2007-01-0915, 2007.

[39] Li T., Ogawa H. "Analysis of the trade-off between soot and nitrogen oxides in diesel-Like combustion by chemical kinetic calculation". *SAE International Journal of Engines*. Vol. 5, pp. 94–101, 2012.

[40] Neely G.D., Sasaki S., Huang Y., Leet J.A., Stewart D.W. "New diesel emission control strategy to meet US tier 2 emissions regulations", *SAE Technical Papers*, n°2005-01-1091, 2005.

[41] Pickett L.M., Siebers D.L. "Non-sooting, low flame temperature mixing-controlled di diesel combustion". *SAE Technical Papers,* n° 2004-01-1399, 2004.

[42] Kimura S., Aoki O., Kitahara Y., Aiyoshizawa E. "Ultra-clean combustion technology combining a low-temperature and premixed combustion concept for meeting future emission standards". *SAE Technical Papers,* n° 2001-01-0200, 2001.

[43] Benajes J., Molina S., Novella R., Belarte E. "Evaluation of massive exhaust gas recirculation and Miller cycle strategies for mixing-controlled low temperature combustion in a heavy duty diesel engine". *Energy,* Vol. 71, pp. 355–366, 2014.

[44] Kook S., Bae C., Miles P.C., Choi D., Pickett L.M. "The influence of charge dilution and injection timing on low-temperature diesel combustion and emissions". *SAE Technical Papers,* n° 2005-01-3837, 2005.

[45] Agarwal A.K., Singh A.P., Maurya R.K. "Evolution, challenges and path forward for low temperature combustion engines". *Progress in Energy and Combustion Sciences*, Vol. 61, pp. 1–56, 2017.

[46] Stanglmaier R.H., Roberts C.E. "Homogeneous Charge Compression Ignition (HCCI): Benefits, Compromises, and Future Engine Applications". *SAE Technical Papers,* n° 1999-01-3682, 1999

[47] Jin C., Zheng Z. "A Review on Homogeneous Charge Compression Ignition and Low Temperature Combustion by Optical Diagnostics". *Journal of Chemistry*, Vol. 2015, 2015

[48] Gray A.W., Ryan T.W. "Homogeneous charge compression ignition (HCCI) of diesel fuel". *SAE Technical Papers,* n° 971676, 1997.

[49] Christensen M., Hultqvist A., Johansson B. "Demonstrating the multi fuel capability of a homogeneous charge compression ignition engine with variable compression ratio". *SAE Technical Papers,* n° 1999-01-3679, 1999.

[50] Martins M., Fischer I., Gusberti F., Sari R., Nora M.D. "HCCI of Wet Ethanol on a Dedicated Cylinder of a Diesel Engine". *SAE Technical Papers,* n° 2017-01-0733, 2017.

[51] Yao M., Zheng Z., Liu H. "Progress and recent trends in homogeneous charge compression ignition (HCCI) engines". *Progress in Energy and Combustion Sciences*, Vol 35 pp. 398–437, 2009.

[52] Hyvönen J., Haraldsson G., Johansson B. "Supercharging HCCI to extend the operating range in a multi-cylinder VCR-HCCI engine". *SAE Technical Papers,* n° 2003-01-3214, 2003.

[53] Song H.H., Edwards C.F. "Understanding chemical effects in low-load-limit extension of homogeneous charge compression ignition engines via recompression reaction". *International Journal of Engine Research*, Vol. 10, pp. 231–250, 2009.

[54] Tanaka S., Ayala F., Keck J.C., Heywood J.B. "Two-stage ignition in HCCI combustion and HCCI control by fuels and additives". *Combustion and Flame. Vol.* 132, pp. 219–239, 2003.

[55] Chang K., Babajimopoulos A., Lavoie G.A., Filipi Z.S. "Assanis D.N., Analysis of load and speed transitions in an HCCI engine using 1-D cycle simulation and thermal networks". *SAE Technical Papers,* n° 2006-01-1087, 2006.

[56] Ganesh D., Nagarajan G., Mohamed Ibrahim M. "Study of performance, combustion and emission characteristics of diesel homogeneous charge compression ignition (HCCI) combustion with external mixture formation". *Fuel* Vol. 87 pp. 3497–3503, 2008.

[57] Christensen M., Johansson B. "Homogeneous Charge Compression Ignition with Water Injection". *SAE Technical Papers,* n° 1999-01-0182, 1999.

[58] Mack J.H., Aceves S.M., Dibble R.W. "Demonstrating direct use of wet ethanol in a homogeneous charge compression ignition (HCCI) engine". *Energy.* Vol. 34, pp. 782–787, 2009.

[59] Saxena S., Schneider S., Aceves S., Dibble R. "Wet ethanol in HCCI engines with exhaust heat recovery to improve the energy balance of ethanol fuels". *Applied Energy*, Vol. 98 pp. 448–457, 2012.

[60] Kalghatgi G.T. "Auto-ignition quality of practical fuels and implications for fuel requirements of future SI and HCCI engines". *SAE Technical Papers,* n° 2005-01-0239, 2005.

[61] Kalghatgi G.T., Risberg P., Ångström H. "Advantages of Fuels with High Resistance Auto-ignition in Late-injection, Low-temperature, Compression Ignition Combustion". *SAE Technical Papers,* n° 2006-01-3385, 2006

[62] Bessonette P.W., Schleyer C.H., Duffy K.P., Hardy W.L., Liechty M.P. "Effects of fuel property changes on heavy-duty HCCI combustion". *SAE Technical Papers,* n° 2007-01-0191, 2007.

[63] Shibata G., Urushihara T. "Realization of dual phase high temperature heat release combustion of base gasoline blends from oil refineries and a study of HCCI combustion processes". *SAE Technical Papers,* n° 2009-01-0298, 2009.

[64] Sjöberg M., Dec J.E., Cernansky N.P. "Potential of thermal stratification and combustion retard for reducing pressure-rise rates in HCCI engines, based on multi-zone modeling and experiments". *SAE Technical Papers* n°, 2005-01-0113, 2005.

[65] Krasselt J., Foster D., Ghandhi J., Herold R., Reuss D., Najt P. "Investigations into the effects of thermal and compositional stratification

on HCCI combustion - Part I: Metal engine results". *SAE Technical Papers,* n° 2009-01-1105, 2009.

[66] Inagaki K., Fuyuto T., Nishikawa K., Nakakita K., Sakata I. "Dual-fuel PCI combustion controlled by in-cylinder stratification of ignitabilit". *SAE Technical Papers,* n° 2006-01-0028, 2006.

[67] Kokjohn S.L., Hanson R.M., Splitter D.A., Reitz R.D. "Experiments and modeling of dual-fuel HCCI and PCCI combustion using in-cylinder fuel blending". *SAE International Journal of Engines,* Vol. 2, pp. 24–39, 2009.

[68] Kokjohn S., Reitz R.D., Splitter D., Musculus M. "Investigation of Fuel Reactivity Stratification for Controlling PCI Heat-Release Rates Using High-Speed Chemiluminescence Imaging and Fuel Tracer Fluorescence". *SAE International Journal of Engines,* Vol. 5, 2012.

[69] Splitter D., Kokjohn S., Rein K., Hanson R., Sanders S., Reitz R. "An optical investigation of ignition processes in fuel reactivity controlled PCCI combustion". *SAE Technical Papers,* n° 2010-01-0345, 2010.

[70] Kokjohn S.L., Hanson R.M., Splitter D.A., Reitz R.D. "Fuel reactivity controlled compression ignition (RCCI): a pathway to controlled high-efficiency clean combustion". *International Journal of Engine Research.* Vol. 12 pp. 209–226, 2011.

[71] Benajes J., Molina S., García A., Monsalve-Serrano J. "Effects of low reactivity fuel characteristics and blending ratio on low load RCCI (reactivity controlled compression ignition) performance and emissions in a heavy-duty diesel engine". *Energy,* Vol. 90 pp. 1261–1271, 2015.

[72] Benajes J., Molina S., García A., Monsalve-Serrano J. "Effects of direct injection timing and blending ratio on RCCI combustion with different low reactivity fuels". *Energy Conversion and Management,* Vol. 99, pp. 193–209, 2015.

[73] Benajes J., García A., Pastor J.M., Monsalve-Serrano J. "Effects of piston bowl geometry on reactivity controlled compression ignition heat

transfer and combustion losses at different engine loads". *Energy*, Vol. 98, pp. 64–77, 2016

[74] Benajes J., García A., Monsalve-Serrano J., Villalta D. "Exploring the limits of the reactivity controlled compression ignition combustion concept in a light-duty diesel engine and the influence of the direct-injected fuel properties". *Energy Conversion and Management,* Vol. 157 pp. 277–287, 2017.

[75] Benajes J., Molina S., García A., Belarte E., Vanvolsem M., An investigation on RCCI combustion in a heavy duty diesel engine using in-cylinder blending of diesel and gasoline fuels, *Applied. Thermal. Engineering,* Vol. 63 pp. 66–76, 2014.

[76] Olmeda P., García A., Monsalve-Serrano J., Lago Sari R. Experimental investigation on RCCI heat transfer in a light-duty diesel engine with different fuels: Comparison versus conventional diesel combustion". *Applied Thermal Engineering,* Vol. 144 pp. 424–436, 2018.

[77] Benajes J., A. García, J. Monsalve-Serrano, I. Balloul, G. Pradel. "An assessment of the dual-mode reactivity controlled compression ignition/conventional diesel combustion capabilities in a EURO VI medium-duty diesel engine fueled with an intermediate ethanol-gasoline blend and biodiesel". *Energy Conversion and Management,* Vol. 123, pp. 381–391, 2016.

[78] Reitz R.D., Duraisamy G. "Review of high efficiency and clean reactivity controlled compression ignition (RCCI) combustion in internal combustion engines". *Progress in Energy and Combustion Sciences*, Vol. 46, pp. 12–71, 2014.

[79] Li J., Yang W., Zhou D. "Review on the management of RCCI engines". *Renewable and Sustainable Energy Reviews*,Vol. 69 pp. 65–79, 2017.

[80] Splitter D., Hanson R., Kokjohn S., Reitz R. "Reactivity controlled compression ignition (RCCI) heavy-duty engine operation at mid-and high-loads with conventional and alternative fuels." *SAE Technical Papers,* n° 2011-01-0363, 2011.

[81] Benajes J., V J.. Pastor, García A., Monsalve-Serrano J. "The potential of RCCI concept to meet EURO VI NOx limitation and ultra-low soot emissions in a heavy-duty engine over the whole engine map". *Fuel,* Vol. 159, pp. 952–961, 2015.

[82] Monsalve J., *Dual-fuel compression ignition: towards clean, highly efficient combustion.* Doctoral Thesis, Universitat Politécnica de València, Departamento de Máquinas y Motores Térmicos, 2016.

[83] Boronat Colomer V. *Dual-Fuel Dual-Mode combustion strategy to achieve high thermal efficiency, low NOx and smoke emissions in compression ignition engines.* Doctoral Thesis, Universitat Politécnica de València, Departamento de Máquinas y Motores Térmicos, 2018.

[84] Benajes J., Pastor J. V., García A., Monsalve-Serrano J. "An experimental investigation on the influence of piston bowl geometry on RCCI performance and emissions in a heavy-duty engine". *Energy Conversion and Management,* Vol. 103, pp. 1019–1030, 2015.

[85] Katare S.R., Patterson J.E., Laing P.M. "Aged DOC is a Net Consumer of NO_2: Analyses of Vehicle, Engine-dynamometer and Reactor Data". *SAE Technical Papers,* n° 2007-01-3984, 2007.

[86] Alshammari M., Alshammari F., Pesyridis A. "Electric boosting and energy recovery systems for engine downsizing". *Energies,* Vol. 12, 2019.

[87] VOLVO trucks. Powertrain specification of VOLVO FE truck. Available in https://www.volvotrucks.es/es-es/trucks/trucks/volvo-fe/specifications/powertrain.html.

[88] Serrano J.R., Piqueras P., Angiolini E., Meano C., De La Morena J.. "On Cooler and Mixing Condensation Phenomena in the Long-Route Exhaust Gas Recirculation Line". *SAE Technical Papers,* n° 2015-24-2521, 2015.

[89] VOLVO trucks. VOLVO D8K Engine. https://www.volvo trucks.com.au/en-au/trucks/volvo-fe/features/d8k- engine. html#

[90] Payri F. and Desantes J.M. Motores de combustion interna alternativos. *Editorial Reverté*, 2011.

[91] KISTLER, PiezoStar ® Pressure Sensor kistler 6125C, Datasheet. (2013) 1–4.

[92] AVL 733S fuel balance. Technical information available at http://www.avl.com.

[93] Landau H.J. "Sampling, Data Transmission, and the Nyquist Rate". *Proceedings of IEEE*. Vol. 55, pp. 1701–1706, 1967.

[94] Dinh T.V., Choi I.Y., Son Y.S., Kim J.C. "A review on non-dispersive infrared gas sensors: Improvement of sensor detection limit and interference correction". *Sensors and Actuators B: Chemical,* Vol. 231 pp- 529–538, 2016.

[95] Tsai C.L., Fann C.S., Wang S.H., Fung R.F. "Paramagnetic oxygen measurement using an optical-fiber microphone". *Sensors and Actuators B: Chemical,* Vol. 73 pp. 211–215, 2001.

[96] Collier T., Gregory D., Rushton M., Hands T. "Investigation into the performance of an ultra-fast response NO analyser equipped with a NO2 to NO converter for gasoline and diesel exhaust NOx measurements". *SAE Technical Papers,* n° 2000-01-2954, 2000.

[97] Holm T. "Aspects of the mechanism of the flame ionization detector". *Journal of Chromatography A*, Vol. 842, pp. 221–227, 1999.

[98] U. Nations, UNECE Regulation 49, 2013.

[99] Silvis W.M. "An algorithm for calculating the air/fuel ratio from exhaust emissions". *SAE Technical Papers,* n° 970514, 1997.

[100] Smith B.C., Fundamentals of Fourier Transform Infrared Spectroscopy, 2011.

[101] AVL. Smoke Value Measurements with the Filter-Paper-Method, 2005.

[102] Northrop W.F., Bohac S. V., Chin J.Y., Assanis D.N. "Comparison of filter smoke number and elemental carbon mass from partially

premixed low temperature combustion in a direct-injection diesel engine". *Journal of Engineering for Gas Turbines Power,* Vol. 133, 2011.

[103] Benajes J., García A., Monsalve-Serrano J., Boronat V. "Gaseous emissions and particle size distribution of dual-mode dual-fuel diesel-gasoline concept from low to full load". *Applied. Thermal. Engineering,* Vol. 120, pp. 138–149, 2016.

[104] Morgan N., Smallbone A., Bhave A., Kraft M., Cracknell R., Kalghatgi G. "Mapping surrogate gasoline compositions into RON/MON space". *Combustion and Flame,* Vol. 157, pp. 1122–1131, 2010.

[105] Liu C.M., Sandhu N.K., McCoy S.T., Bergerson J.A. "A life cycle assessment of greenhouse gas emissions from direct air capture and Fischer-Tropsch fuel production". *Sustainable Energy and Fuels*, Vol. 4, pp. 3129–3142, 2020.

[106] Burre J., Bongartz D., Mitsos A. "Production of Oxymethylene Dimethyl Ethers from Hydrogen and Carbon Dioxide - Part II: Modeling and Analysis for OME3-5". *Industrial and Engineering Chemistry Research,* Vol. 58, pp. 5567–5578, 2019.

[107] Payri F., Olmeda P., Martín J., García., A. "A complete 0D thermodynamic predictive model for direct injection diesel engines". *Applied Energy,* Vol. 88 pp. 4632–4641, 2011.

[108] Lapuerta M., Ballesteros R., Agudelo J.R. "Effect of the gas state equation on the thermodynamic diagnostic of diesel combustion". *Applied Thermal Engineering,* Vol. 26, pp. 1492–1499, 2006.

[109] Martín J. *Aportación al diagnóstico de la combustión en motores Diesel de inyección directa.* Docctoral Thesis, Universitat Politécnica de València, Departamento de Máquinas y Motores Térmicos, 2007.

[110] Cantera userguide. Available at https://cantera.org/ science/reactors. html

[111] Payri F., Arnau F.J., Piqueras P., Ruiz M.J., Lumped Approach for Flow-Through and Wall-Flow Monolithic Reactors Modelling for Real-

Time Automotive Applications, *SAE Technical Papers,* n° 2018-01-0954, 2018.

[112] Macián V., Serrano J.R., Piqueras P., Sanchis E.J. "Internal pore diffusion and adsorption impact on the soot oxidation in wall-flow particulate filters". *Energy.* Vol. 179, pp. 407–421, 2019

[113] Gamma Technologies. Engine Performance Application Manual, 2016.

[114] Gamma Technologies. *Flow Theory Manual*, 2016.

[115] Gamma Technologies. *Aftertreatment manual*, 2016.

[116] Gamma Technologies, Vehicle Driveline and HEV application manual, 2016.

[117] DelVescovo D., Kokjohn S., Reitz R. "The Effects of Charge Preparation, Fuel Stratification, and Premixed Fuel Chemistry on Reactivity Controlled Compression Ignition (RCCI) Combustion". *SAE International Journal of Engines,* Vol. 10, 2017.

[118] Pedrozo V.B., May I., Lanzanova T.D.M., Zhao H. "Potential of internal EGR and throttled operation for low load extension of ethanol-diesel dual-fuel reactivity controlled compression ignition combustion on a heavy-duty engine". Fuel, Vol. 179 pp. 391–405, 2016.

[119] Wahlström J., Eriksson L., Nielsen L. "EGR-VGT control and tuning for pumping work minimization and emission control". IEEE Transactions in Control System Technologies, Vol. 18, pp. 993–1003, 2010.

[120] Splitter D., Wissink M., Kokjohn S., Reitz R. "Effect of compression ratio and piston geometry on RCCI load limits and efficiency". SAE Technical Papers, n° 2012-01-0383, 2012.

[121] The European Comission. "Commission regulations (EU) 2019/318 of February 2019 amending Regulation (EU) 2017/2400 and Directive 2007/46/EC of the European Parliament and of the Council as regards

the determination of the CO2 emission and fuel cunsumption of heavy-dut," Official Journal of European Union, Vol. 2001, pp. 20–30, 2019.

[122] The European Comission. "Commission Regulation (EU) No 582/2011," Official Journal of European Union, pp. 1–168, 2011.

[123] Morra E., Spessa E., Ciaravino C., Vassallo A., Analysis of various operating strategies for a parallel-hybrid diesel powertrain with a belt alternator starter, SAE Technical Papers, n° 2012-01-1008, 2012.

[124] https://towardsdatascience.com/maximum-likelihood-estimation-explained-normal-distribution-6207b322e47f

[125] Benajes J., García A., Monsalve-Serrano J., Boronat V. "An investigation on the particulate number and size distributions over the whole engine map from an optimized combustion strategy combining RCCI and dual-fuel diesel-gasoline". Energy Conversion and Management, Vol. 140 , pp. 98–108, 2017.

[126] Russell A., Epling W.S. "Diesel oxidation catalysts". *Catalysis Reveview: Science and Engineering,* Vol. 53,, pp. 337–423, 2011

[127] Hamedi M.R., Tsolakis A., Herreros J.M. "Thermal Performance of Diesel Aftertreatment: Material and Insulation CFD Analysis". *SAE Technical Papers*, n° 2014-01-2818, 2014.

[128] Song X., Surenahalli H., Naber J., Parker G., Johnson J. "Experimental and modeling study of a diesel oxidation catalyst (DOC) under transient and CPF active regeneration conditions". *SAE Technical Papers,* n° 2013-01-1046, 2013.

[129] Johnson J.E., Kittelson D.B. "Physical factors affecting hydrocarbon oxidation in a diesel oxidation catalyst". *SAE Technical Papers* , n° 941771, 1994.

[130] Prikhodko V.Y., Curran S.J., Parks J.E., Wagner R.M. "Effectiveness of diesel oxidation catalyst in reducing HC and CO emissions from reactivity controlled compression ignition". *SAE Technical Papers* , n° 2013-01-0515, 2013.

[131] Kaiser E.W., Matti Maricq M., Xu N., Yang J. "Detailed hydrocarbon species and particulate emissions from a HCCI engine as a function of air-fuel ratio". *SAE Technical Papers* , n° 2005-01-3749, 2005.

[132] Kaiser E.W., Siegl W.O., Henig Y.I., Anderson R.W., Trinker F.H. "Effect of Fuel Structure on Emissions from a Spark-Ignited Engine". *Environmental Science and Technology,* Vol. 25 pp. 2005–2012. 1991.

[133] Ramanathan K., Sharma C.S. "Kinetic parameters estimation for three way catalyst modeling". *Industrial and Engineering Chemistry Research,* Vol. 50, pp. 9960–9979, 2011.

[134] Luján J.M., Climent H., García-Cuevas L.M., Moratal A. "Pollutant emissions and diesel oxidation catalyst performance at low ambient temperatures in transient load conditions". *Applied Thermal Engineering,* Vol. 129, pp. 1527–1537, 2018.

[135] Guan B., Zhan R., Lin H., Huang Z. "Review of the state-of-the-art of exhaust particulate filter technology in internal combustion engines". *Journal of Environmental Management,* Vol. 154, pp. 225–258, 2015.

[136] Song Q., Zhu G. "Model-based closed-loop control of urea scr exhaust aftertreatment system for diesel engine". *SAE Technical Papers* , n° 2002-01-0287, 2002.

[137] Ferreri P., Cerrelli G., Miao Y., Pellegrino S., Bianchi L. "Conventional and Electrically Heated Diesel Oxidation Catalyst Physical Based Modeling." *SAE Technical Papers* , n° 2018-37-0010, 2018.

[138] Heavy-Duty Supplemental Emissions Test (SET). Available at https://dieselnet.com/standards/cycles/set.php

[139] Gao J., G. Tian, Sorniotti A., Karci A.E., Di Palo R. "Review of thermal management of catalytic converters to decrease engine emissions during cold start and warm up". *Applied Thermal Engineering,* Vol. 147, pp. 177–187, 2019

[140] Bai S., Tang J., Wang G., Li G. "Soot loading estimation model and passive regeneration characteristics of DPF system for heavy-duty engine". *Applied Thermal Engineering,* Vol. 100, pp. 1292–1298, 2016.

[141] Kim J.H., Kim M.Y., Kim H.G. "NO_2-assisted sort regeneration behavior in a diesel particulate filter with heavy-duty diesel exhaust gases". *Numerical Heat Transfer, Part A: Applications*, Vol. 58, pp. 725–739, 2010.

[142] Rothe D., Knauer M., Emmerling G., Deyerling D., Niessner R. "Emissions during active regeneration of a diesel particulate filter on a heavy duty diesel engine: Stationary tests". *Journal of Aerosol Sciences*, Vol. 90, pp. 14–25, 2015.

[143] Jacquot F., Logie V., Brilhac J.F., Gilot P. "Kinetics of the oxidation of carbon black by NO_2 influence of the presence of water and oxygen". *Carbon*, Vol. 40, pp. 335–343, 2002.

[144] Rößler M., Velji A., Janzer C., Koch T., Olzmann M. "Formation of Engine Internal NO_2: Measures to Control the NO_2/NO_X Ratio for Enhanced Exhaust After Treatment". *SAE Internatiolnal Journal of Engines*, Vol. 10, n° 2017-01-1017, 2017.

[145] Henry C., Currier N., Ottinger N., Yezerets A. "Decoupling the Interactions of Hydrocarbons and Oxides of Nitrogen Over Diesel Oxidation Catalysts". *SAE Technical Papers* , n° 2011-01-1137, 2011.

[146] Singh P., Thalagavara A.M., Naber J.D., Johnson J.H., Bagley S.T. "An experimental study of active regeneration of an advanced catalyzed particulate filter by diesel fuel injection upstream of an oxidation catalyst". *SAE Technical Papers* , n° 2006-01-0879, 2006.

[147] Haralampous O.A., Koltsakis G.C. "Oxygen diffusion modeling in diesel particulate filter regeneration". *AIChE Journal,* Vol. 50, pp. 2008–2019, 2014.

[148] Ito T., Kitamura T., Kojima H., Kawanabe H. "Prediction of Oil Dilution by Post-injection in DPF Regeneration Mode". *SAE Technical Papers* , n° 2019-01-2354, 2019.

[149] Singh N., Rutland C.J., Foster D.E., Narayanaswamy K., He Y. "Investigation into different DPF regeneration strategies based on fuel economy using integrated system simulation". *SAE Technical Papers* , n° 2009-01-1275, 2009.

[150] Neoh K.GHoward., J.B., Sarofim A.F. "Soot Oxidation in Flames". *Particulate Carbon*, pp. 261–282, 1981.

[151] Lee K.B., Thring M.W., Beér J.M. "On the rate of combustion of soot in a laminar soot flame." *Combustion and Flame,* Vol. 6 pp. 137–145, 1962.

[152] Sampara C.S., Bissett E.J., Chmielewski M., Assanis D. "Global kinetics for platinum diesel oxidation catalysts". *Industrial and Engineering Chemistry Research,* Vol. 46, pp. 7993–8003, 2007.

[153] Sampara C.S., Bissett E.J., Chmielewski M. "Global kinetics for a commercial diesel oxidation catalyst with two exhaust hydrocarbons". *Industrial and Engineering Chemistry Research,* Vol 47, pp. 311–322, 2008.

[154] Polifke W., Geng W., Döbbeling K. "Optimization of rate coefficients for simplified reaction mechanisms with genetic algorithms". *Combustion and Flame*, Vol. 113, pp. 119–134, 1998.

[155] Yang S., Deng C., Gao Y., He Y. "Diesel particulate filter design simulation: A review". *Advances in Mechanical Engineering,* Vol. 8, pp. 1–14, 2016.

[156] Serrano J.R., Climent H., Piqueras P., Angiolini E. "Filtration modelling in wall-flow particulate filters of low soot penetration thickness". *Energy,* Vol. 112, pp. 883–898, 2016.

[157] Payri F., Broatch A., Serrano J.R., Piqueras P. "Experimental-theoretical methodology for determination of inertial pressure drop

distribution and pore structure properties in wall-flow diesel particulate filters (DPFs)". *Energy*, Vol. 36 pp. 6731–6744, 2011.

[158] Bermúdez V., Serrano J.R., Piqueras P., Sanchis E.J. "On the impact of particulate matter distribution on pressure drop of wall-flow particulate filters". *Applied Sciences,* Vol. 7, 2017.

[159] American Standards. Standard Test Method for Motor Octane Number of Spark-Ignition Engine *Fuel*. pp. 1–68, 2003.

[160] Szybist J.P., Splitter D.A. "Pressure and temperature effects on fuels with varying octane sensitivity at high load in SI engines". *Combustion and Flame*, Vol. 177, pp. 49–66, 2017.

[161] Leppard W.R. "The Chemical Origin of Fuel Octane Sensitivity". *SAE Technical Papers*, n° 902137, 1990.

[162] Leppard W.R. "The Autoignition Chemistries of Primary Reference Fuels, Olefin/Paraffin Binary Mixtures, and Non-Linear Octane Blending". *SAE Technical Papers*, n° 922325, 1992.

[163] Mittal V., Heywoodv, Green W.H. "The underlying physics and chemistry behind fuel sensitivity". *SAE Technical Papers*, n° 2010-01-0617, 2010.

[164] Javed T., Lee C., AlAbbad M., Djebbi K., Beshir M., Badra J., H. Curran, A. Farooq. "Ignition studies of n-heptane/iso-octane/toluene blends". *Combustion and Flame*, Vol. 171, pp. 223–233, 2016.

[165] Prakash A., Wang C., Janssen A., Aradi A., Cracknell R., Impact of Fuel Sensitivity (RON-MON) on Engine Efficiency". *SAE International Journal of Fuels and Lubricants*, Vol. 10, 2017.

[166] Curran H.J., Gaffuri P., Pitz W.J., Westbrook C.K. "A comprehensive modeling study of n-heptane oxidation". *Combustion and Flame*, Vol. 114, pp. 149–177, 1988.

[167] Herzler J., Jerig L., Roth P. "Shock tube study of the ignition of lean n-heptane/air mixtures at intermediate temperatures and high

pressures". *Proceedings of Combustion Institute*, Vol. 30, pp. 1147–1153, 2005.

[168] Vandersickel A., Hartmann M., Vogel K., Wright Y.M., Fikri M., Starke R., Schulz C., Boulouchos K. "The autoignition of practical fuels at HCCI conditions: High-pressure shock tube experiments and phenomenological modeling". *Fuel*, Vol. 93, pp. 492–501, 2012.

[169] Lawler B., Lacey J., Dronniou N., Dernotte J., Dec J., Guralp O., Najt P., Filipi Z. "Refinement and validation of the thermal stratification analysis: A post-processing methodology for determining temperature distributions in an experimental HCCI engine". *SAE Technical Papers*, n° 2014-01-1276, 2014.

[170] Zhou Y., Gainey B., Hariharan D., Lawler B., Mamalis S. "Understanding HCCI combustion in a free piston engine with a multi-zone, control-mass model with thermal stratification and chemical kinetics". *SAE Technical Papers*, n° 2019-01-0958, 2019.

[171] Hao H., Liu F., Liu Z., Zhao F. "Compression ignition of low-octane gasoline: Life cycle energy consumption and greenhouse gas emissions, Applied Energy, Vol. 181, pp. 391–398, 2016.

[172] Badra J., Viollet Y., Elwardany A., Im H.G., Chang J. "Physical and chemical effects of low octane gasoline fuels on compression ignition combustion". *Applied Energy*, Vol. 183, pp. 1197–1208, 2016.

[173] García A., Monsalve-Serrano J., Martínez-Boggio S., Rückert Roso V., Duarte N. "Potential of bio-ethanol in different advanced combustion modes for hybrid passenger vehicles". *Renewable Energy*, Vol. 150, pp. 58–77, 2020.

[174] Hank C., Lazar L., Mantei F., Ouda M., White R.J., Smolinka T., Schaadt A., Hebling C., Henning H.M. "Comparative well-to-wheel life cycle assessment of OME3-5 synfuel production via the power-to-liquid pathway". *Sustainable Energy Fuels*, Vol. 3, pp. 3219–3233. 2019.

[175] Toyir J., Miloua R., Elkadri N.E., Nawdali M., Toufik H., Miloua F., Saito M. "Sustainable process for the production of methanol from CO2 and H2 using Cu/ZnO-based multicomponent catalyst". *Physics Procedia*, Vol. 2, pp. 1075–1079, 2009

[176] Pastor J. V., García A., Micó C., Lewiski F., An optical investigation of Fischer-Tropsch diesel and Oxymethylene dimethyl ether impact on combustion process for CI engines, *Applied Energy*, Vol. 260, 2020.

[177] Alleman T.L., McCormick R.L., Fischer-tropsch diesel fuels - Properties and exhaust emissions: A literature review, *SAE Technical Papers*, n° 2003-01-0763, 2003.

[178] Dworschak P., Berger V., Härtl M., Wachtmeister G., Neat Oxymethylene Ethers: Combustion Performance and Emissions of OME2, OME3, OME4 and OME5 in a Single-Cylinder Diesel Engine, *SAE Technical Papers*, n° 2020-01-0805, 2020.

[179] DeWitt M.J., Corporan E., Graham J., Minus D. "Effects of aromatic type and concentration in Fischer-Tropsch fuel on emissions production and material compatibility". *Energy and Fuels*. Vol. 22 pp. 2411–2418, 2008.

[180] Kim Y.D., Yang C.W., Kim B.J., Moon J.H., Jeong J.Y., Jeong S.H., Lee S.H., Kim J.H., Seo M.W., Lee S.B., Kim J.K., Do Lee U. "Fischer–tropsch diesel production and evaluation as alternative automotive fuel in pilot-scale integrated biomass-to-liquid process". *Applied Energy*, Vol.180, pp. 301–312, 2016.

[181] Van Vliet O.P.R., Faaij A.P.C., Turkenburg W.C. "Fischer-Tropsch diesel production in a well-to-wheel perspective: A carbon, energy flow and cost analysis". *Energy Conversion and Management*, Vol. 50 pp. 855–876, 2009.

[182] Deutz S., Bongartz D., Heuser B., Kätelhön A., Schulze L., Omari A., Walters M., Klankermayer J., Leitner W., Mitsos A., Pischinger S., Bardow A. "Cleaner production of cleaner fuels: Wind-to-wheel-

environmental assessment of CO2-based oxymethylene ether as a drop-in fuel". *Energy and Environmental Sciences*, Vol. 11, pp. 331–343, 2018.

[183] Bongartz D., Burre J., Mitsos A. "Production of Oxymethylene Dimethyl Ethers from Hydrogen and Carbon Dioxide - Part I: Modeling and Analysis for OME1". *Ind. Engineering and Chemical Research*, Vol. 58 pp. 4881–4889, 2019.

[184] Oestreich D., Lautenschütz L., Arnold U., Sauer J. "Production of oxymethylene dimethyl ether (OME)-hydrocarbon fuel blends in a one-step synthesis/extraction procedure". *Fuel*, Vol. 214, pp. 2018.

[185] García A., Monsalve-Serrano J., José Sanchís E., Fogué-Robles Á. "Exploration of suitable injector configuration for dual-mode dual-fuel engine with diesel and OMEx as high reactivity fuels". *Fuel*, Vol. 280, 2020.

[186] García A., Monsalve-Serrano J., Villalta D., Lago Sari R., Gordillo V., Gaillard P. "Potential of e-Fischer Tropsch diesel and oxymethyl-ether (OMEx) as fuels for the dual-mode dual-fuel concept". *Applied Energy*, Vol. 253, 2019.

[187] Benajes J., García A., Monsalve-Serrano J., Martínez-Boggio S. "Potential of using OMEx as substitute of diesel in the dual-fuel combustion mode to reduce the global CO2 emissions". *Transportation in Engineering*, Vol. 1, 2020.